The Formation and Characterisation of a Polypyrrole Based Sensor for the Detection of Urea

NUI MAYNOOTH

Ollscoil na hÉireann Má Nuad

Anita Hamilton BSc. (Hons)

Department of Chemistry

National University of Ireland Maynooth

July 2012

Thesis Submitted to the National University of Ireland in Fulfilment of the Requirements for the Degree of Doctor of Philosophy

Supervisor: Professor Carmel Breslin

Head of Department: Dr. John Stephens

Table of Contents

Title Page *i*

Table of Contents *ii*

Declaration *ix*

Acknowledgements *xi*

Dedication *xii*

Abstract *xiv*

Chapter 1: Introduction and Literature Review

1.1 Introduction 2

1.2 Conducting Polymers 3

1.2.1 What is a Conducting Polymer? 3

1.2.2 Formation of Conducting Polymers 8

1.2.3 Applications of Conducting Polymers 9

1.3 Polypyrrole 10

1.3.1 Synthesis of Polypyrrole 11

1.3.2 Factors Affecting Electropolymerisation 14

1.3.3 Redox Properties of Polypyrrole 18

1.4 Supramolecular Systems 20

1.4.1 Cyclodextrins 20

1.4.2 Structural Features of Cyclodextrins 22

1.4.3 Inclusion Complexation 25

1.4.4 Applications of Cyclodextrins 29

1.4.5 Methods for Determining Inclusion Complex Association Constant 30

1.5 Serum Albumins 31

1.5.1 Binding Interactions of BSA 34

1.5.2 Applications of BSA 35

1.6 Urea 37

1.7 Urea Sensors 38

1.7.1 Polymer Modified Electrodes 39

1.7.1.1 Urea Biosensors based on Non-conducting Polymer Matrices 39

1.7.1.2 Urea Biosensors based on Conducting Polymer Matrices 40

1.7.1.3 Urea Biosensors based on Sol-Gel Matrices 41

1.7.2 Urea Biosensors based on Langmuir-Blodgett Films 42

1.7.3 Urea Biosensors based on Nanomaterials 42

1.8 References 43

Chapter 2: Experimental

2.1 Introduction 62

2.2 Experimental Techniques 62

2.2.1 Cyclic Voltammetry 62

2.2.2 Potentiostatic Measurements 63

2.2.3 Impedance Measurements 65

2.2.4 Ultraviolet-Visible Spectroscopy 69

2.2.5 Differential Scanning Calorimetry 69

2.2.6 Scanning Electron Microscopy and EDX Analysis 70

2.3 Instrumentation, Software and Ancillary Equipment 72

2.4 Chemicals and Solutions 73

2.5 The Electrochemical Cell Setup 73

2.6 Fabrication and Characterisation of the Polypyrrole Films 76

2.7 Kinetic Analysis 76

2.8 Complexation Studies 79

2.8.1 Job's Method 79

2.8.2 Formation Constants 81

2.9 References 83

Chapter 3: Formation and Characterisation of PPy-BSA and its Interactions with Tryptophan and Ascorbic Acid

3.1 Introduction 86

3.2 Experimental 86

3.3 Results and Discussion 87

3.3.1 Factors Affecting the Growth of PPy-Cl and PPy-BSA 88

3.3.1.1 Influence of the Concentration of Pyrrole 88

3.3.1.2 Influence of the Concentration of BSA 91

3.3.1.3 Influence of the Applied Potential 95

3.3.1.4 Rate of Electropolymerisation 97

3.3.2 Characteristics and Properties of PPy-BSA 100

3.3.2.1 Morphology and Surface Characterisation 100

3.3.2.2 Electroactivity of PPy-Cl and PPy-BSA 104

3.3.2.3 Capacitance Measurements 107

3.3.2.4 Electrochemical Window 109

3.3.2.5 Effect of pH on the PPy-Cl and PPy-BSA Polymers 111

3.3.2.6 Overoxidation of the PPy-BSA Polymer Films 116

3.3.2.7 Temperature Analysis of the Polymers using DSC 117

3.3.2.8 Impedance Analysis of the Polymers 118

3.3.3 Favourable Conditions for the Formation of PPy-BSA 122

3.3.4 Interactions of PPy-BSA with Tryptophan 123

3.3.5 Interactions of PPy-BSA with Ascorbic Acid 129

3.4 Conclusions 132

3.5 References 133

Chapter 4: The Development of a Polypyrrole Modified Electrode for the Enhanced Detection of Urea

4.1 Introduction 141

4.2 Experimental 142

4.3 Results and Discussion 142

4.3.1 Formation of the PPy-Urs-Cl 143

4.3.2 Characteristics and Properties of the PPy-Cl and PPy-Urs-Cl Films 145

4.3.2.1 SEM and EDX Analysis 145

4.3.2.2 Electroactivity of the PPy-Cl and PPy-Urs-Cl Polymers 147

4.3.2.3 Capacitance Measurements 152

4.3.3 Detection of Urea using the PPy-Cl and PPy-Urs-Cl Films 155

4.3.4 Formation of the PPy-Urs-SCD and PPy-SCD Polymer Films 158

4.3.5 Characteristics and Properties of PPy-SCD and PPy-Urs-SCD 161

4.3.5.1 SEM and EDX Analysis 161

4.3.5.2 Electroactivity of the PPy-SCD and PPy-Urs-SCD Polymer Films 163

4.3.6 Stability of the PPy-Urs-SCD Polymer Films 168

4.3.6.1 Thickness of the PPy-Urs-SCD Polymer Films 169

4.3.6.2 Reusability of the PPy-Urs-SCD Polymer Films 170

4.3.6.3 Reproducibility of the PPy-Urs-SCD Polymer Films 171

4.3.6.4 Shelf-life of the PPy-Urs-SCD Polymer Films 172

4.3.6.5 Storage Conditions of the PPy-Urs-SCD Polymer Films 173

4.3.7 Urea Detection using the PPy-SCD and PPy-Urs-SCD Polymers 175

4.4 Conclusions 178

4.5 References 179

Chapter 5: An Investigation into the Effects of Interfering Compounds on the Detection of Urea

5.1 Introduction 185

5.2 Experimental 186

5.3 Results and Discussion 186

5.3.1 Ascorbic Acid as an Interfering Species 187

5.3.2 Uric Acid 193

5.3.3 Thiourea 199

5.3.4 Hydroxyurea 202

5.3.5 Creatinine 204

5.3.6 Ammonium Chloride 207

5.4 Conclusions 209

5.5 References 210

Chapter 6: Complexation Studies

6.1 Introduction 215

6.2 Experimental 216

6.3 Results and Discussion 216

6.3.1 Urea 217

6.3.1.1 Urea with SCD 217

6.3.1.2 Urea with α-SCD 225

6.3.2 Ascorbic Acid 228

6.3.3 Uric Acid 229

6.3.4 Hydroxyurea 230

6.3.5 Thiourea 231

6.3.6 Creatinine 232

6.4 Conclusions 234

6.5 References 234

Chapter 7: Conclusions

7.1 General Conclusions 239

7.2 Future Work/Potential Applications 241

7.3 Conference Presentations 242

7.4 Papers in Preparation/Submitted 243

7.5 References 244

Declaration

I hereby certify that this thesis, which I now submit for assessment on the programme of study leading to the award of PhD, has not been submitted, in whole or in part, to this or any other University for any degree, and is, except where otherwise stated, the original work of the author.

Signed: _____ Date: _____

“To laugh often and much; to win the respect of intelligent people and the affection of children; to earn the appreciation of honest critics and to endure the betrayal of false friends. To appreciate beauty; to find the best in others; to leave the world a bit better whether by a healthy child, a garden patch, or a redeemed social condition; to know that even one life has breathed easier because you have lived. This is to have succeeded.” - *Ralph Waldo Emerson*

“Finish each day and be done with it. You have done what you could. Some blunders and absurdities no doubt crept in; forget them as soon as you can. Tomorrow is a new day. You shall begin it serenely and with too high a spirit to be encumbered with your old nonsense.” - *Ralph Waldo Emerson*

Acknowledgements

First and foremost, I would like to thank my supervisor, Professor Carmel Breslin, for her continued support during my PhD. Carmel's door was always open and, for that, I am eternally grateful. Carmel gave me support and encouragement and a belief in myself and my accomplishments. Without her support and guidance, I would not have completed my PhD.

During my PhD I was supported by the Irish Research Council for Science and Engineering Technology (IRCSET), Intel and the Leitrim County Council.

I would like to thank Dr. John Colleran, for always being there to answer any questions, no matter how trivial, and for bringing the banter and a sense of belonging to the lab group. His wealth of knowledge and expertise is inspiring and I am indebted to him for sharing some of that with me. Also, a big thank you to all the staff of the chemistry department, particularly to Ken, Ria, Ann, Ollie and Barbara. A special thank you to Noel, we would all be lost without him.

Ursula, we started together and now we're finishing together four years on – thank you for the memories and the chats, and I wish you all the best in your future; what ever you decide to do I'm sure you will be great at it. A special mention to Paul – thank you for being there for me and being my friend, I will never forget you. To the rest of the lab group, Orla, Emer and Dave – I wish you all the success in the future also. To all of the postgrads and postdocs, it was great working with you and thank you for keeping me sane. To all my friends outside of the lab, a special thanks to John for the visits and the tea. And Ciaran, I could not have completed this without your technical expertise; for that, and everything else, I thank you.

Last, but by no means least, I would like to thank my family. To my mum, Bernadette, thank you for teaching me to stand on my own two feet and aim for the sky. To my dad, Bernard, you have always stood by me and believed in me, even when I doubted myself. To Belinda and Alan, thank you for being there for me and keeping me going through it all. Thank you all for your unconditional love and support. Finally, to Iain – it hasn't been easy but you have always been there for me; for that and so much more than I can say, I thank you from the bottom of my heart.

This thesis is dedicated to my family, with love. Thank you for all your support.

"A PhD is obtained by one who knows more and more about less and less, until eventually one knows everything about nothing." - *Anon*.

Abstract

This thesis originates with the development and characterisation of polypyrrole (PPy), formed in the presence of a large protein, bovine serum albumin (BSA). The BSA was incorporated into the polymer film during electropolymerisation from an aqueous solution of pyrrole monomer, BSA and NaCl as a supporting electrolyte. The presence of the BSA within the polymer film was confirmed using cyclic voltammetry, electrochemical impedance spectroscopy and scanning electron microscopy (SEM) coupled with electron dispersive X-Ray analysis (EDX). Optimum conditions for the growth of the polypyrrole-bovine serum albumin film (PPy-BSA) were obtained by varying the concentration of the monomer and BSA, the applied potential and the polymerisation charge. Highly adherent polymers were formed at 0.70 V vs. SCE in a 0.10 mol dm^{-3} NaCl supporting electrolyte with high concentrations of pyrrole (0.5 mol dm^{-3}) and low concentrations of BSA (< 200 µL). The presence of the BSA within the polymer film greatly reduced the electroactivity of the film.

The urease enzyme was also immobilised in the polypyrrole film. The modified polypyrrole film was formed at 0.70 V vs. SCE from an aqueous solution of pyrrole and urease (4000 mg dm^{-3}) in the presence of 0.10 mol dm^{-3} NaCl as a supporting electrolyte. The presence of urease within the polypyrrole-urease (PPy-Urs-Cl) film was confirmed using SEM and EDX and the PPy-Urs-Cl was then investigated as a sensing material for urea. The PPy-Urs-Cl film exhibited a reasonable sensitivity towards urea of 5.41 µC μM^{-1} in the 1.0 x 10^{-5} to 1.0 x 10^{-3} mol dm^{-3} urea concentration range. Sulphonated-β-cyclodextrin (SCD) was then incorporated into the polymer to give a PPy-Urs-SCD film. This PPy-Urs-SCD polymer film was investigated as a sensing material for urea in a phosphate buffer solution. It was found that the SCD dopant greatly enhanced the detection of urea, with detection of urea in the 1.0 x 10^{-10} mol dm^{-3} region and a sensitivity of 46.09 µC μM^{-1}.

A wide variety of interfering compounds was examined to establish their effect, if any, on the detection of urea using the modified PPy-Urs-SCD. The interference from the common biological interfering compound, ascorbic acid, was effectively blocked and no interference was observed in the presence of common salts, such as ammonium chloride. Interference was observed in the presence of uric acid,

hydroxyurea, thiourea and creatinine. The urease enzyme and the SCD are large, giving rise to porous PPy-Urs-SCD films and this allows access of the interfering compounds to the electrode surface. However, this interference was reduced by depositing a layer of the more compact PPy-Urs-Cl followed by the PPy-Urs-SCD film.

A detailed investigation into the host-guest complexation properties of SCD with urea, and the interfering compounds, was performed using cyclic voltammetry. Clear evidence for complexation between SCD as the host molecule and urea as the guest molecule was obtained, which accounts for the high sensitivity in the detection of urea. No inclusion complex was formed between urea and the α-SCD or between SCD and the interfering compounds.

Chapter 1

Introduction and Literature Review

"The whole problem with the world is that fools and fanatics are always so certain of themselves, but wiser people so full of doubts."
- *Bertrand Russell*

1.1 Introduction

The objective of this thesis is to develop a polypyrrole based sensor for the detection of urea. Urea is an important molecule in both the medical and agricultural industries, and enhanced levels of urea in the body can be an indication of renal failure, hence, it is important to be able to monitor urea concentrations simply and readily.

In this chapter, an introduction to conducting polymers, primarily polypyrrole, and their uses is given. This is followed by an introduction to supramolecular systems with a particular emphasis on cyclodextrins and their inclusion complexation. Finally, an overview of serum albumins and a detailed introduction to urea and the sensing devices used to detect urea is supplied. The second chapter details the relevant experimental techniques and apparatus employed, along with an overview of the theories and related equations used in this thesis.

The results and main findings are presented and discussed in Chapters 3 – 6. In Chapter 3, the formation and characterisation of a polypyrrole modified film doped with a large protein, bovine serum albumin (BSA), is investigated. The PPy-BSA film is successfully formed and the optimum parameters are obtained by varying the polymerisation potential, concentration of pyrrole and concentration of BSA. The PPy-BSA film is then examined as a sensor for the amino acid tryptophan and, additionally, for ascorbic acid.

In Chapter 4, results are presented on the incorporation of the urease enzyme into the polymer matrix during electropolymerisation in a chloride-containing solution, forming PPy-Urs-Cl. This was then investigated as a sensor for urea, giving reasonable detection limits in the 5.0×10^{-5} mol dm^{-3} region. In order to investigate the effects of the dopant anion on urea detection, the dopant was altered from a simple chloride anion to a sulphonated-β-cyclodextrin (SCD), forming PPy-Urs-SCD. The SCD is a large anionic species which contains between 7-11 sulphonated (SO_3^-) groups. The SCD dopant greatly enhances the detection of urea, with detection of urea in the 1.0×10^{-10} mol dm^{-3} region.

In Chapter 5, an investigation into the effects of interfering compounds on the detection of urea using the PPy-Urs-SCD polymer film is carried out. Two common

interfering compounds in biological systems are ascorbic acid (AA) and uric acid (UA); these are investigated along with the biological molecule, creatinine. Additionally, the effects of two compounds that are structurally similar to urea, i.e., hydroxyurea and thiourea, are investigated. The PPy-Urs-SCD polymer film successfully repels the anionic ascorbic acid; hence, no interference occurs in the presence of AA. However, the other interfering compounds cause an increase in the oxidation charge arising from the detection of urea, which is surprising as most interfering compounds tend to foul or block the electrode surface, thus diminishing the obtained currents and oxidation charges.

Finally, in Chapter 6, results are presented and discussed on the formation of a 1:1 inclusion complex between urea and the sulphonated-β-cyclodextrin. The formation of an inclusion complex between urea and the sulphonated-α-cyclodextrin is also investigated. Additionally, the formation of inclusion complexes between sulphonated-β-cyclodextrin and each of the interfering compounds is examined. An inclusion complex only appears to form between urea and the sulphonated-β-cyclodextrin and, not with the sulphonated-α-cyclodextrin. This indicates that the cavity diameter is very important in the formation of inclusion complexes. No inclusion complex is formed between the sulphonated-β-cyclodextrin and the interfering compounds.

1.2 Conducting Polymers

1.2.1 What is a Conducting Polymer?

Everyday polymers, which are more commonly known as plastics, are composed of simple repeating molecule units called monomers. These names come from the Greek words ‘poly’ meaning ‘many’, ‘mono’ meaning ‘single’ and ‘mer’ meaning ‘part’. Polymers are well known for their insulating properties, indeed it is this characteristic that has led to their wide usage in the electronics and packaging industries[1].

Conducting polymers, on the other hand, differ greatly from these insulating polymers because, as their name suggests, they are intrinsically conducting[2]. The development of these polymers is largely due to the work of three scientists: A. J.

Heeger, A. G. MacDiarmid and H. Shirakawa, who received the Nobel Prize in Chemistry in 2000 for their work on polyacetylene, Figure 1.1, and other conducting polymers. Conducting polymers date back to the early 1900s with reports on 'aniline black' and 'pyrrole black'. However, at this time the synthetic routes only produced black powders and much of this early work was discarded[3]. Significant developments came about in 1977 when MacDiarmid *et al.*[4] reported a 10^6-fold increase in the conductivity of polyacetylene doped with iodine. Although the first polymerisation of acetylene was performed earlier in 1958 by Natta and co-workers[5], this material had poor processability and attracted little interest, until the work of MacDiarmid and co-workers[4]. Despite the metal-like conductivity of polyacetylene, it has poor thermal stability and accordingly other conducting polymers with better stability and processability have received more attention.

Conducting polymers are made up of carbon and hydrogen, along with heteroatoms such as nitrogen or sulphur. All conducting polymers have π-conjugation across the polymer backbone; typical conducting polymers include polyaniline (PANi), polypyrrole (PPy), polythiophene and polyacetylene. These are shown in Figure 1.1.

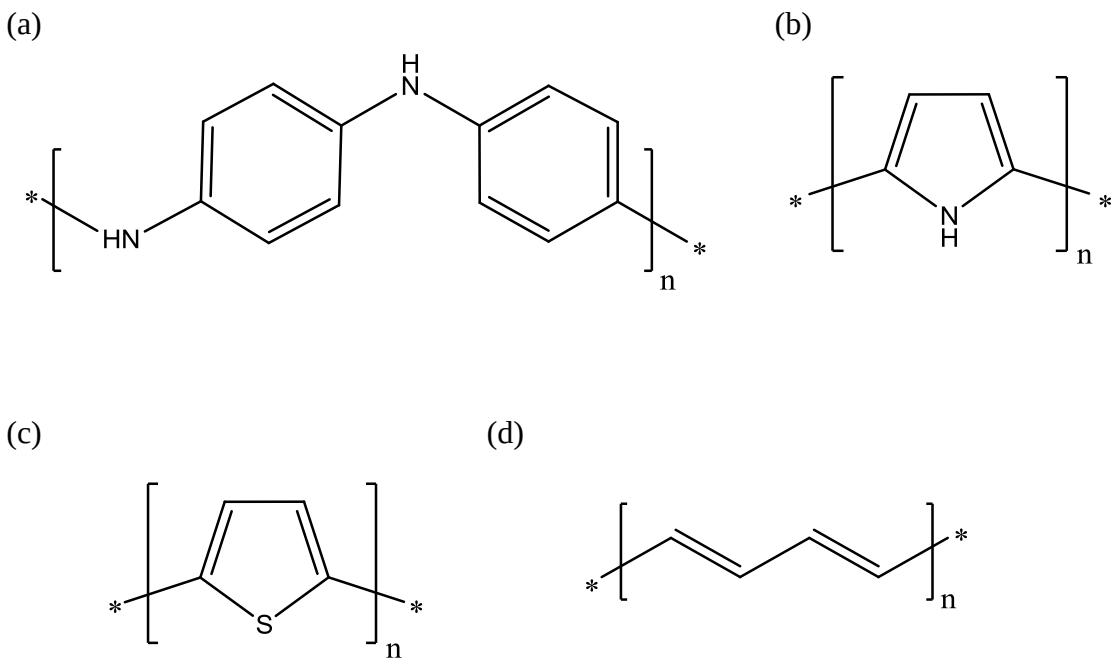

Figure 1.1: Structures of (a) polyaniline, (b) polypyrrole, (c) polythiophene and (d) polyacetylene all in their dedoped states.

A number of approaches have been used to explain the origin of the conductivity in conducting polymers. Bredas and Street[6] used the band theory of solids to initially determine the conductivity classification of conducting polymers back in 1985. In general, materials can be classified into three categories depending on their electrical conductivity: non-conductors/insulators, semi-conductors and conductors, based on the band gap energy model. In this analysis there are two energy bands, a valence band and a conductance band. A valence band corresponds to the occupied electronic energy levels and a conductance band is equivalent to the unoccupied energy levels. The difference in energy between the top of the outermost valence band and the bottom of the conduction band is referred to as the band gap, E_g, as shown in Figure 1.2.

Conductivity arises due to the transition of electrons from the valence band to the conductance band. For conductors, the valence band overlaps with the conduction band, i.e., $E_g \approx 0$ eV, and so the conduction band is now partially filled with electrons. For semi-conductors there is a small gap between the valence and conduction bands, where $E_g \approx 1.0$ eV; as a result the electrons can be excited from the valence band into the conduction band at room temperature. However, for insulators, the electrons in the valence band are separated from the conduction band by a large band gap, where $E_g \geq 10$ eV, and consequently it is difficult to excite the electrons from the valence band into the conduction band. Bredas and Street[6] established that the band gap, E_g, for conducting polymers was in the region of 1.0 eV, and as such, conducting polymers were classified as semi-conductors. However, the conductivity associated with conducting polymers cannot be explained entirely using this band theory model.

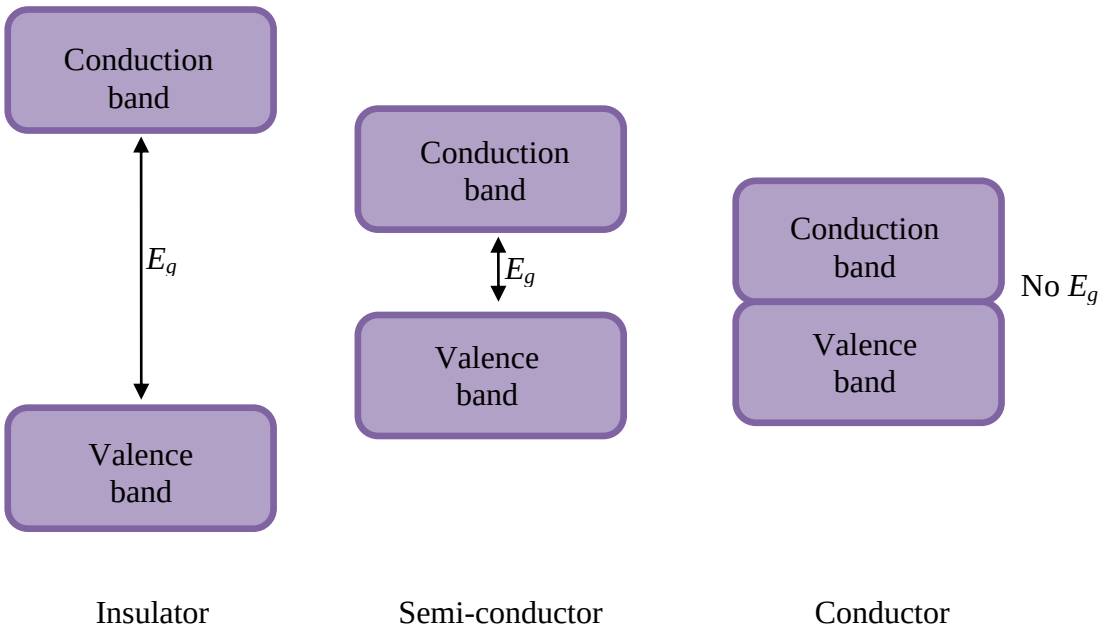

Figure 1.2: A schematic illustrating the band gap energy model, showing the band gap energy, E_g, for insulators, semi-conductors and conductors.

It is now generally accepted that the conducting nature of the polymers arises from the formation of various redox states upon oxidation of the conjugated backbone. This is due to the formation of mobile charge carriers, which are termed polarons and bipolarons[6,7,8]. In the case of polypyrrole, a polaron is formed upon removal of an electron from the conducting polymer chain. This occurs as the polymer is oxidised giving a free radical and a positive charge, which are coupled together *via* local resonance of the charge. The combination of the radical and the charged site is known as a polaron. These charges are further stabilised and localised on the chain by interacting with an added dopant, a charged species of opposite sign that interacts electrostatically with the polaron. In this way, the polymer oxidation can be viewed as *p*-doping, giving a radical cation and a negatively charged dopant. As the oxidation continues, bipolarons are formed, which are lower in energy than two separate polarons[9]. The formation of a bipolaron is possible because the stabilisation energy gained by the interaction with the distorted lattice is larger than the Coulomb repulsion between the two polarons. These polarons and bipolarons are mobile due to the conjugated polymer backbone, and it is the movement of these charges along the backbone that gives rise to the electrical conductivity of the polymer. In particular, the polarons and bipolarons can move along the polymer chains (*intrachain transfer*) if surrounded by an electrostatic field of closely distributed

ionic dopants. However, *interchain transfer* is also possible where the charge carriers transfer from chain to chain in order to cover distances longer than an average molecular bond length[9].

In terms of the band gap energy model, the polaron is equivalent to the generation of localised energy states in the forbidden energy gap, with the lower energy state being occupied by single unpaired electrons. When a bipolaron is generated this gives rise to more electronic energy states and, as more of these are generated, the upper and lower bipolaron bands eventually merge with the conductance band and valence band to produce partially filled bands that are approaching metallic-like conductivity. As a result, the smaller the energy gap is, the more conducting the polymer becomes.

As already stated, in order to maintain polymer neutrality, the charges generated along the polymer backbone during the oxidation or reduction of the polymer are compensated for by the incorporation of anionic or cationic species into the polymer matrix, as shown in Equations 1.1 and 1.2. Here P represents the polymer in its neutral state, P^{n+} is the polymer in the oxidised state, P^{n-} is the polymer in the reduced state, X^{+} is any cation, F^{-} is any anion, and n is the number of moles of the salt. The anionic and cationic species that are incorporated into the polymer are referred to as dopants.

Anionic Doping $$P + nXF \rightarrow P^{n+}nF^{-} + nX^{+} \quad (1.1)$$

Cationic Doping $$P + nXF \rightarrow nX^{+}P^{n-} + nF^{-} \quad (1.2)$$

Both the anionic and cationic doping processes enhance the conducting properties of the polymer since the conductivity increases with the doping level due to the creation of more mobile charges along the polymer backbone3. However, there is a maximum doping level that varies for the different conducting polymers, and also with different dopants. For example, the dopant may contribute to 20% to 60% by mass in polypyrrole, depending on the dopant used[10]. As a result, the conductivity of the polymer is not only dependent on the redox state of the polymer but also on the degree of doping.

1.2.2 Formation of Conducting Polymers

The synthesis of conducting polymers can be carried out in two main ways, using either chemical synthesis or electrochemical methods[9,11]. In either case, the initial step of the polymerisation involves the oxidation of the monomer to generate a radical cation. These highly reactive radical cations then react with each other, or with a neutral monomer, to form a radical dimer, which in turn is transformed to a trimer and longer chain lengths.

Chemical synthesis is achieved when the monomer is exposed to a relatively strong oxidising agent such as ammonium peroxydisulphate, permanganate or dichromate anions, ferric ions or hydrogen peroxide[12]. This is typically carried out in solution, although it can also be carried out directly onto a surface, using a technique known as vapour phase polymerisation[13]. This involves coating the desired surface with the oxidising agent and then subsequently treating the surface with the vapour of the monomer, which results in the deposition of the polymer film exclusively at the surface of preference. The chemical synthesis of a polymer in solution requires the polymer to be precipitated from a monomer solution upon the addition of an oxidising agent. This typically results in bulk polymerisation. The rate of polymerisation can be controlled by varying the reaction conditions, for example, varying the concentration of oxidant and monomer, varying the reaction temperature, and appropriately treating the surface to be coated by the polymer[14].

Electrochemical polymerisation differs from chemical polymerisation, in that following radical generation upon oxidising the monomer, propagation occurs by radical-radical recombination, which causes the loss of two electrons and hence the formation of a dimer. Oxidation of this dimer then generates an oligomeric radical which combines with other oligomeric radicals to generate a polymeric structure. Electrochemical polymerisation occurs when a suitable anodic potential or current is applied to a conducting substrate that has been immersed in a monomer electrolyte. A schematic representation of the electrochemical cell set up required for electropolymerisation is given is Section 2.5. A wide range of electrochemical techniques can be used for electropolymerisation, but galvanostatic (constant current), potentiostatic (constant potential) and potential sweeping techniques, such as cyclic voltammetry, are the methods that are generally employed[15]. Depending on

the technique used, a range of polymer morphologies can be achieved.

Electrochemical polymerisation, particularly potentiostatic and galvanostatic modes, has several advantages over chemical polymerisation because the precipitated polymer is deposited onto a conducting surface. Hence, an adherent polymer can be grafted directly onto an electrode surface in one simple step. The film thickness can be controlled by monitoring the charge passed during deposition, resulting in more reproducible films[16], and the films formed have fewer impurities as harsh oxidising agents are not used. In addition to this, it is also possible to perform *in situ* characterisation of the polymer while it is growing[17]. However, electrochemical polymerisation is limited to monomers which can be oxidised on the application of a potential to form the radical ion intermediates for polymerisation[18], whereas all polymers can be prepared using chemical synthesis.

1.2.3 Applications of Conducting Polymers

There has been a growing interest in conducting polymers in the last number of years due to their wide range of potential applications in areas such as rechargeable batteries[19,20], electronics, electrochromic displays[21] and optics, to name just a few. More recently, the ion exchange properties of conducting polymers have been utilised to develop sensors. Conducting polymers doped with small mobile anions are known to have anion exchange properties, whereas conducting polymers doped with large immobile anions have cation exchange properties. This has resulted in the formation of not only sensors, but actuators[22,23,24,25], drug delivery systems[26] and metal ion transporters[27]. In addition to this, conducting polymers have also been used as sensors in environmental applications, in both aqueous and gaseous based systems, and they are also known for their use in amperometric sensing to detect hazardous gases and vapours. Conducting polymers have also been used extensively for various electrochromic and optoelectronic devices. This is due to the optical properties of the polymer changing in the ultraviolet-visible (UV-Vis) and the near infrared (NIR) regions upon the introduction of dopants into the polymer. In addition to this the electrical properties of the polymer are also increased[28].

1.3 Polypyrrole

Polypyrrole (PPy), Figure 1.3, is synthesised from the pyrrole monomer, which consists of a 5-membered ring, containing a nitrogen (N) heteroatom. As with other organic molecules, pyrrole polymerisation occurs upon oxidation of the monomer, which forms a conjugated polymer chain with overlapping π-orbitals and a positive charge along the polymer backbone[29]. PPy was first synthesised chemically in 1916 by the oxidation of the pyrrole monomer using hydrogen peroxide[30], which yielded an amorphous black powder known as 'pyrrole black'. It wasn't until many years later that the first electrochemical synthesis of polypyrrole was reported by Dall'Ollio *et al.* [31] in 1968. Dall'Ollio *et al.*[31] used an aqueous solution of pyrrole and sulphuric acid to electrosynthesise a layer of PPy on a platinum electrode. Since then, a wide variety of substrates and solutions have been used to deposit polypyrrole electrochemically[32,33,34].

There have been a lot of investigations into polypyrrole as it has a large surface area owing to its fibrous structure and it is a high capacity electrode material[33]. Its ease of preparation, inherent electrical conductivity and high stability in both aqueous systems and in air make PPy a promising interfacial material[33,34]. As a result, it is one of the most intensively used and studied polymers and accordingly it is an ideal candidate for a number of advanced technologies such as sensors[35,36]. An additional feature of PPy is that it forms a biologically compatible polymer matrix[37], which has led to its use in a broad number of biomedical fields including biosensors[38,39], tissue engineering[40,41] and implantable biodevices[42]. Another interesting and prominent property of PPy is its ability to switch its redox behaviour. This has resulted in the design of ion-selective electrodes, electrochromic displays, solar cells, drug delivery systems and actuators[43,44,45,46,47,48,49].

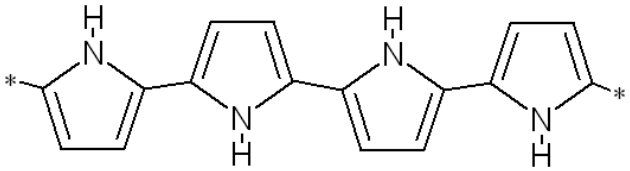

Figure 1.3: Structure of PPy in the neutral state.

1.3.1 Synthesis of Polypyrrole

Like all conducting polymers, polypyrrole can be synthesised by either chemical or electrochemical methods. One of the easiest and most common ways of chemically synthesising PPy in large quantities is in solution. This involves exposing the pyrrole monomer to a strong oxidising agent, which yields a black precipitate. In chemical polymerisation, the propagation step is controlled by the fact that the monomer is in large excess of the radical cation that is formed upon oxidation, which then attacks another monomer molecule generating a dimer radical cation which becomes further oxidised. Because of this, and coupled with the loss of hydrogen, the polymer chain grows until termination, Figure 1.4.

Common oxidants that have been used for pyrrole polymerisation include ferric chloride, ferric perchlorate and ammonium peroxydisulphate[12]. Several other oxidising agents, including organic acids, have been employed; however, films generated from these oxidants tend to exhibit lower conductivity[50] and as such, the salts of transition metal ions are generally used instead. A major disadvantage of polymerising pyrrole in this way is that the PPy is produced in the bulk of the solution and hence, only some of the PPy will cover the surface of any material that is introduced into the solution.

Another way of chemically synthesising PPy is by directly depositing the polymer film onto a surface. This can be achieved using a process known as vapour phase polymerisation. This involves applying the oxidant to the surface using a solvent coating process, then exposing the coated surface to the vapour of the monomer. This vapour phase polymerisation was initially described by Mohammadi *et al.*[51], where the authors used $FeCl_3$ or H_2O_2 as oxidants in order to form PPy films. Since then the method has been altered slightly, with Fe(III) *p*-toluenesulphonic acid and a range of other Fe(III) sulphonates now generally being used as the oxidising agents[52,53].

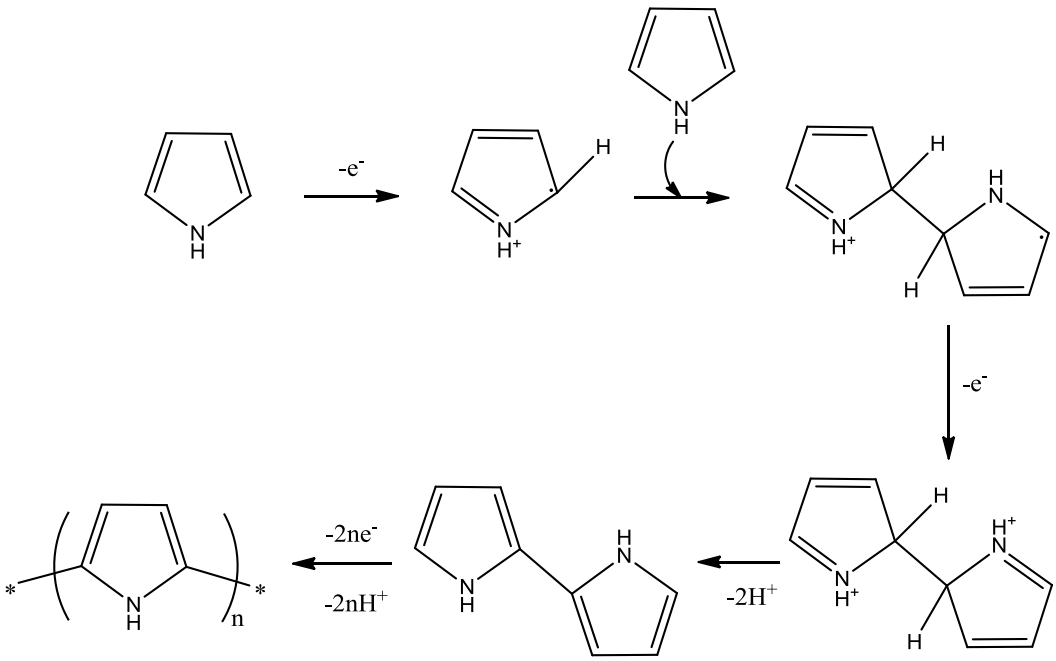

Figure 1.4: The mechanism for the chemical synthesis of polypyrrole.

The electrochemical polymerisation of pyrrole occurs on the application of an anodic potential or current to a conducting substrate that has been immersed in a suitable electrolyte containing the monomer and the desired doping salt. This can be achieved using various electrochemical methods, e.g., potentiostatic[54], potentiodynamic[55] or galvanostatic[56] methods.

There is still some debate on the exact mechanism of electropolymerisation[57,58,59], but the mechanism proposed initially by Diaz and Castillo[60] and later explained by Henry *et al.*[61] is generally taken to be the accepted mechanism, and is the most commonly encountered mechanism in the literature. This mechanism is summarised in Figure 1.5. This process involves the one-electron oxidation of the pyrrole monomer (1a), by which a radical cation is generated. This takes place at the electrode or substrate surface. The oxidation of pyrrole at the electrode surface is considered to be faster than the diffusion of the monomer from the bulk of the solution to the interface. In this way the monomer at the interface is predominantly present as a radical cation formed at potential E_1. This high concentration of radical cations gives rise to radical-radical coupling. This occurs at the α-position of each radical, forming a radical dication (1b), which subsequently loses two protons to generate a neutral dimer (1c). This dimer becomes further oxidised to generate another radical species (2a), which then couples with another radical monomer to

form a trimer (2b and 2c). The propagation (ia, ib and ic) is continued via this sequence until the final polymer product is obtained. The chain growth is terminated either by reaction (t1) of the macromolecular radical cation with water or hydroxide anions, or by lack of reactivity of the radical cation (t2) due to delocalisation over a greater length as the polymer chain grows.

The preferred bond formation is between the rings at the carbons in position 2 and 5 (α-coupling); however bonding at positions 3 and 4 (β-coupling) is also possible[62,63]. When β-coupling occurs, it gives rise to a widening of the band gap and a decrease in the conductivity of the polymer through the formation of branches that break the planarity and linearity of the PPy chains[64].

It is important to note that the final electrosynthesised polymer is oxidised. Intrinsic conductivity results from the formation of charge carriers upon oxidising the conjugated backbone, as discussed previously. Indeed, the final PPy chain is in an oxidised/doped state due to the incorporation of dopants that are present in order to maintain charge balance within the polymer[65]. The number of electrons taken from each monomer is equal to $2+p$, two electrons for the polymerisation and p electrons for the oxidation of the polymer chain. For PPy the value of p is usually 0.25 to 0.33 corresponding to one positive charge delocalised over every 3 to 4 monomeric units and accordingly one anionic dopant for every 3 to 4 monomeric units[66]. The overall stoichiometry for the electropolymerisation of the pyrrole monomer is depicted in Figure 1.6.

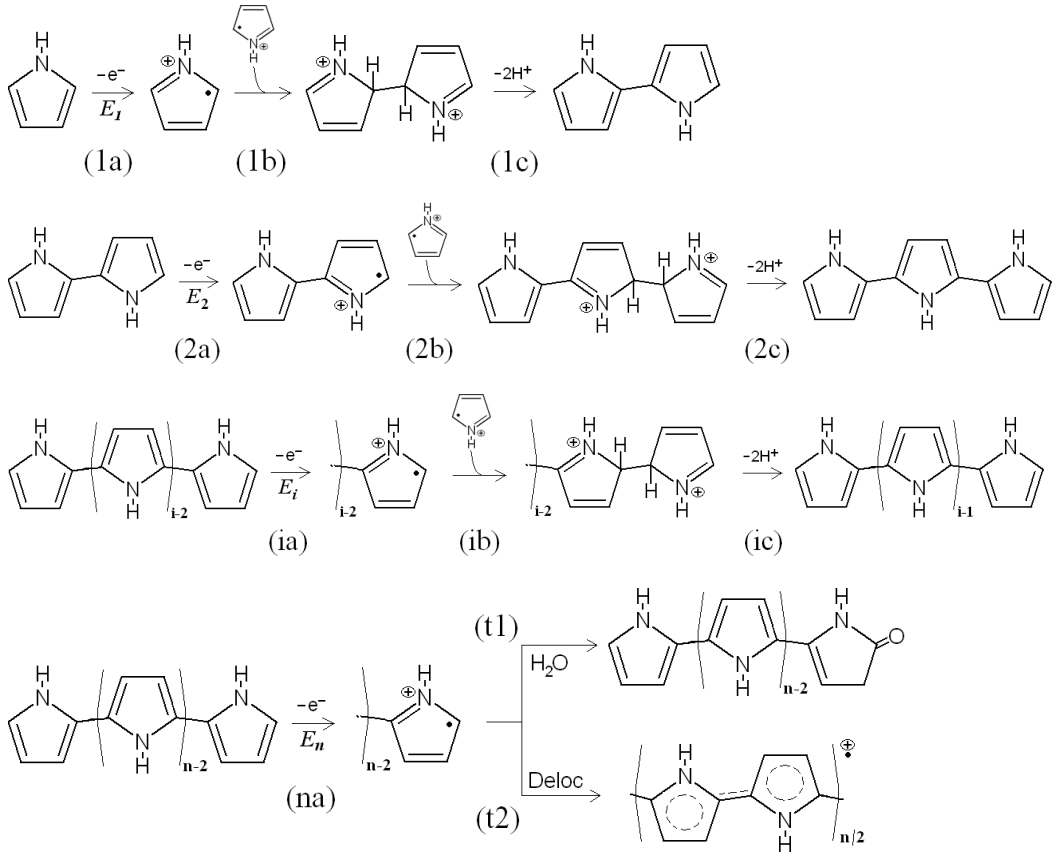

Figure 1.5 Electropolymerisation mechanism of pyrrole as proposed by Diaz[60].

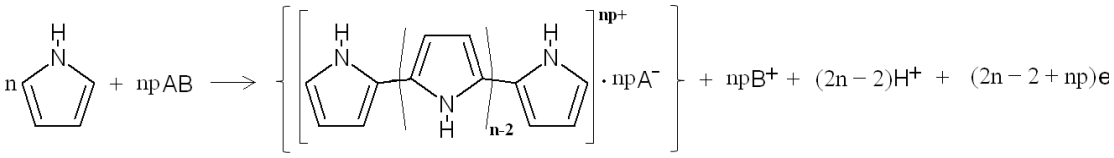

Figure 1.6: Stoichiometry of the electropolymerisation of pyrrole, where A^- and B^+ are the anion and cation from a simple AB salt dissolved in a suitable solvent with the monomer, pyrrole.

1.3.2 Factors Affecting Electropolymerisation

The electrochemical polymerisation of pyrrole is affected by a number of parameters used in the synthesis. These parameters can include, but are not limited to, the nature of the electrode[67], the concentration and nature of the electrolyte[65], the solvent[68,69,70,71], the applied potential or current density[72], the reaction temperature[73]

and pH and the mode of electropolymerisation. These will all have a strong effect on the rate of electropolymerisation and on the properties of the resulting polymer.

The electrode surface at which electrodeposition of polypyrrole occurs must not be oxidisable as this would compete with the oxidation of the pyrrole monomer. If this were to happen the oxidation and polymerisation of pyrrole would be severely hindered; because of this most studies have focused on using inert anodes such as platinum, gold or glassy carbon[74,75,76]. Apart from these metals, pyrrole has also been electropolymerised on a wide range of other substrates, which include silicon[77] and the transparent indium tin oxide glass (ITO)[78], which is useful for spectroscopic applications.

The nature of the supporting electrolyte plays an important role in the electropolymerisation process. This is because the chosen electrolyte determines the type of dopants that will be incorporated into the polymer during electropolymerisation. The size of the anion will influence various characteristics of the polymer film, including the redox properties and the porosity of the film[65]. The concentration of the electrolyte is also important as the doping degree increases with increasing electrolyte concentration, which produces different induction times, mechanisms of nucleation and polymer growth[79] and as such, the electropolymerisation rate varies with each dopant. In addition to this, the higher the concentration of the electrolyte, the greater the conductivity and tensile strength of the polymer film, as shown by Li and Yang[80]. A PPy film that has initially high conductivity is less prone to attack by oxygen[69] thus, the polymer matrix is increasingly stable with increasing doping levels and increasing conjugation.

Another parameter that has a very strong influence on the electrochemical polymerisation of pyrrole is the nature of the chosen solvent. The main requirement of the solvent is that it has good ionic conductivity and a good electrochemical resistance against decomposition at the potentials at which the monomer becomes oxidised[81]. PPy films have been prepared using aqueous, organic and ionic liquid solutions[82,83,84]. Aqueous solutions generally require a reasonably high concentration of supporting electrolyte to achieve the desired conductivity, whereas organic solutions usually require a suitable organic salt. Carquigny *et al.*[85] have investigated the characteristics of PPy grown from aqueous, non-aqueous and mixed solutions

and the authors found that thinner films were deposited from the pure acetonitrile/$LiClO_4$ solutions in contrast to the thicker PPy films formed from the water/$LiClO_4$ solutions and the mixed water/acetonitrile/$LiClO_4$ solutions. Similarly, Sutton and Vaughan reported that the addition of methanol into water leads to a drop in the conductivity of PPy films[86]. In addition to this, the films formed from the water/$LiClO_4$ and the mixed water/acetonitrile/$LiClO_4$ solutions were more porous, which is consistent with Ko *et al*.[87] who also found that PPy films prepared in acetonitrile/tetraethylammonium perchlorate had superior electron transfer characteristics and conductivities to those prepared in the aqueous medium.

The applied potential is also very significant in the electropolymerisation of pyrrole. Electropolymerisation can be carried out using cyclic voltammetry, potentiostatic or galvanostatic methods[15]. It is well known that the electrochemical method controls the structural form of the electrodeposited polypyrrole films[74,88,89]. Polymer films that are prepared using potentiostatic or cyclic voltammetry methods are usually smooth and compact. Hernandez-Perez *et al*.[89] showed that potentiostatic methods give rise to smooth surfaces. The authors used atomic force microscopy (AFM) to investigate the surface morphology of PPy films prepared at platinum electrodes by potentiostatic and voltammetric methods. They concluded that the potentiostatic mode of growth was better for obtaining thin films with a smooth surface morphology. Furthermore, the PPy film growth was easier to control using this method, whereas galvanostatically prepared polymer films are more rough and porous[89]. Li *et al*.[67] investigated the effect of using various electrochemical techniques for the formation of PPy on the redox properties of PPy, and found that the galvanostatic deposition of PPy produced polymer films of higher electrochemical reactivity in comparison to those prepared using either potentiostatic or cyclic voltammetry methods.

In addition to this, the applied potential can be used to overoxidise the polymer and decrease the polymer conductivity. Asavapiryanont *et al*.[58] showed that pyrrole oxidises between 0.65 V and 0.90 V vs. SCE, but oxidation at potentials higher than this leads to overoxidation of the deposited PPy film which is an irreversible process that occurs gradually with increasing potential[90]. To date, the mechanism for overoxidation is still unclear, but the most commonly accepted mechanism is the nucleophillic attack of PPy by strong aqueous nucleophiles such as OH^-, Br^- and

H_2O[90] which in turn causes the formation of carbonyl groups on the α-carbons of the pyrrole ring which breaks the conjugation of the polymeric chain[91]. Overoxidation of PPy can also occur with increased oxygen content within the polymer, which disturbs the conjugation and lowers the conductivity. Diaz and Clarke[92] reported that the oxidation potential for the oxidation reaction of PPy shifts towards more negative values as PPy growth proceeds from the initial stages. This is related to the reactivity of each species with air, which increases as the oxidation potential becomes more positive and the corresponding conjugation length becomes shorter. However, as reported by Thieblemont *et al.*[93], PPy shows good stability and undergoes only slow degradation in ambient atmosphere.

The electropolymerisation temperature has a considerable influence on the kinetics of the polymerisation, as well as on the conductivity, redox properties and mechanical characteristics of the polymer films[65]. In general, as the temperature increases the rate of polymerisation will also increase, but there is a decrease in the conductivity and redox properties of the polymer. As a result, the higher conductivities are obtained at lower temperatures[94]; however, the films produced at these low temperatures are generally of a lower quality[65].

The pH of the monomer solution also has a significant influence on the conductivity and electropolymerisation of pyrrole. Asavapiryanont *et al.*[58] investigated the electrodeposition of PPy onto platinum electrodes from acidic, neutral and basic aqueous solutions and found that polymerisation favours a neutral or weakly acidic pH. This is in close agreement with the work of Zhou and Heinze[95], who also found this to be the case when they investigated the effect of pH on the electropolymerisation of pyrrole from an acetonitrile solution. At high pH values, i.e., pH values greater than 7.0, the electropolymerisation of pyrrole is hindered due to the cation radicals being deprotonated to form neutral radicals; this interferes with radical-radical coupling and hence, the conductivity of the polymer film drops significantly[58,95,96,97]. On the other hand, the electropolymerisation of pyrrole prepared in a highly acidic/low pH solution produces polymers with weak conductivity due to the acid catalysed formation of non conjugated trimers which react further to form a partly conjugated polypyrrole film[65].

1.3.3 Redox Properties of Polypyrrole

The most important electrochemical property of polypyrrole is its ability to be electrochemically switched between its conducting and insulating states, as shown in Figure 1.7. In its reduced state, PPy is insulating and maintains a neutral state, but in its oxidised form the polymer is highly conducting and positively charged. This is due to the neutral form of PPy being oxidised whereby an electron is removed from the polymer backbone. It is at this stage that the polymer is said to be in its oxidised state, Figure 1.7(b). In order to counterbalance the formation of these positive charges on the polymer backbone, anions are incorporated into the polymer from the solution, Figure 1.8(a). These anions are referred to as dopants, as they literally dope the polymer with negative charges.

(a)

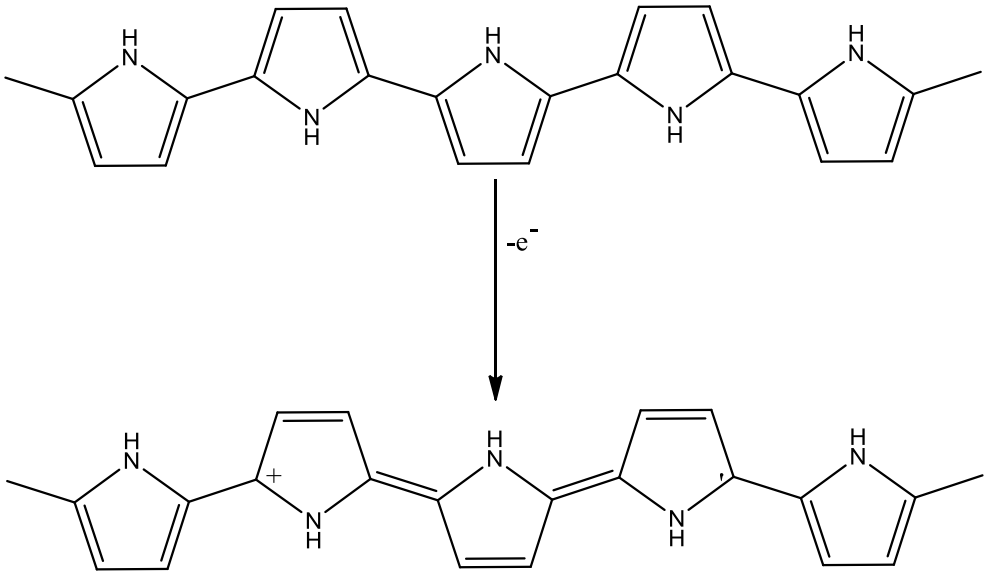

(b)

Figure 1.7: The insulating and conducting forms of PPy where (a) is the neutral PPy and (b) is the oxidised PPy.

On the reduction of the polymer back to its neutral state, the dopant anions are subsequently expelled from the polymer again, Figure 1.8(b). However, this scenario only works with small mobile dopants such as chlorides[98]. When larger anions are used to dope the polymer, they become permanently anchored into the polymer matrix. These anions include large sulphonate groups, such as polyvinylsulphonate, *p*-dodecylbenzene sulphonate[99] and polystyrenesulphonate[100], and the reduction of the polymer doped with these will not result in the release of these dopants[101]. Instead, in this situation, the electroneutrality of the polymer is maintained by the influx of mobile cations from the electrolyte solution into the polymer. This cation exchange must take place in order to counterbalance the now overall negatively charged PPy matrix, Figure 1.9(b). In the case of medium sized anions, such as *p*-toluene sulphonate and dodecyl sulphate, these can exhibit both anionic and cationic exchange, as reported by Wallace and co-workers[99]. It is important to note that the ion-exchange properties of PPy are dependent on both the dopant present in the polymer and the ionic nature of the electrolyte in solution. PPy can also exchange OH^- ions when electrochemically switched in basic solutions. However, the hydroxyl anions have a deactivating effect on the conductivity of the polymer. This is due to the N-H···OH hydrogen bonding which inhibits the generation of polaronic positive charges on the nitrogen sites. This is the origin of the observed dramatic decrease in the conductivity of PPy after treatment in base[102]. In general, the rate-determining step in the doping/dedoping process in PPy is the ion migration. The rate of the electron transfer is usually much faster during the redox switching[103].

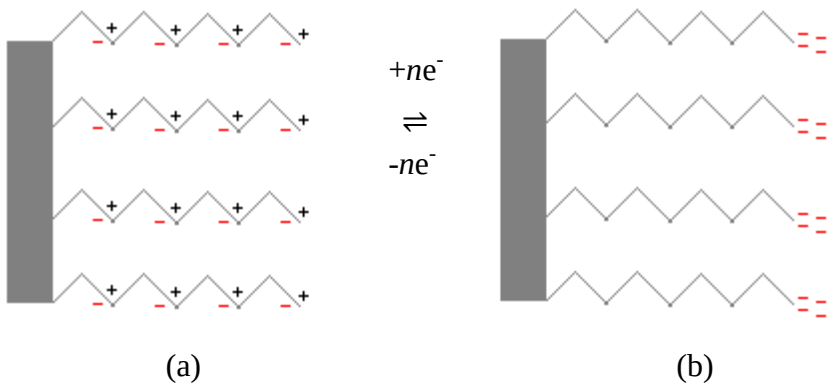

Figure 1.8: (a) The incorporation of anions into the PPy film and (b) the release of anions from the PPy film.

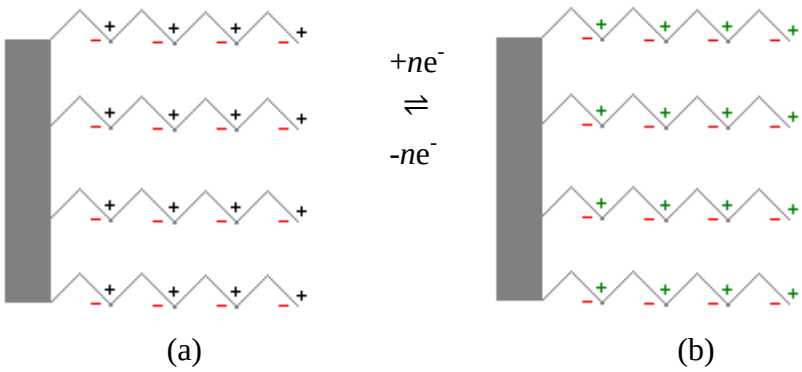

Figure 1.9: (a) The incorporation of immobile anions into the PPy film and (b) the cation incorporation into the PPy film where + is the charge on the PPy, - is the anions and + is the cations.

1.4 Supramolecular Systems

While traditional chemistry focuses on the covalent bond, supramolecular chemistry examines the weaker and reversible non covalent interactions between molecules. As such, a supramolecular system consists of two or more molecular entities held together and organised by means of inter-molecular, non covalent binding interactions[104,105]. One such system is a host-guest interaction, whereby an inclusion complex is formed. Generally, host molecules are cyclic structures and the guest molecules are favourably inserted into the ring structure as a result of a particular driving force. These forces can include hydrogen bonding, metal coordination, hydrophobic forces, Van der Waals forces, π-π interactions and electrostatic effects[106]. Examples of well known host molecules in supramolecular chemistry are cryptates, crown ethers, calixarenes and cyclodextrins (CD)[107].

1.4.1 Cyclodextrins

Cyclodextrins (CD) are a series of naturally occurring macrocyclic oligosaccharides formed from α-1,4-linked-$_D$-glucopyranose units[108] as shown in Figure 1.10. They can consist of six, seven and eight glucopyranose units, which correspond to α-, β- and γ-cyclodextrins, respectively, as shown in Figure 1.11.

The earliest discovery of cyclodextrins was by Villiers, in 1891[109], when a small amount of crystalline material was obtained in addition to reducing dextrins during the starch digest of *Bacilus amylobacter*. Research continued to isolate and identify the macrocylic structures[110,111]; and the α- and β- cyclodextrins were determined by X-Ray crystallography in 1942[112]. It was some years later, in 1948, that the γ-cyclodextrin structure was determined[108].

Bender and Komiyama showed that cyclodextrins can be produced *via* a relatively simple enzymatic conversion, whereby the addition of the enzyme to an aqueous solution of starch causes the linkages of the starch to split forming maltodextrinyl radicals[113]. These radicals then react with their own non-reducing end to produce a crude mixture of the α-, β- and γ-cyclodextrins, along with a small amount of cyclodextrins with more than eight glucopyranose units[114]. Due to advances in technology, the cyclodextrins can be readily isolated and purified in large amounts[115]. The cyclodextrins with more than eight glucopyranose units have been purified and characterised from enzymes[116]. However, their low solubility implies that they are not suitable for important applications such as solubilisers for drugs[117]; whereas CD containing less than six glucopyranose units have been synthesised chemically as it is not possible to produce these enzymatically[118].

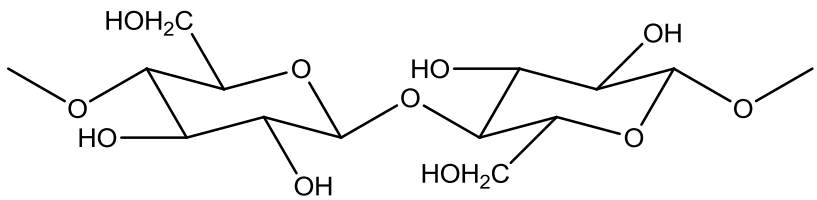

Figure 1.10: The 1,4 link that joins the D-glucopyranose units to form the macrocyclic oligosaccharides.

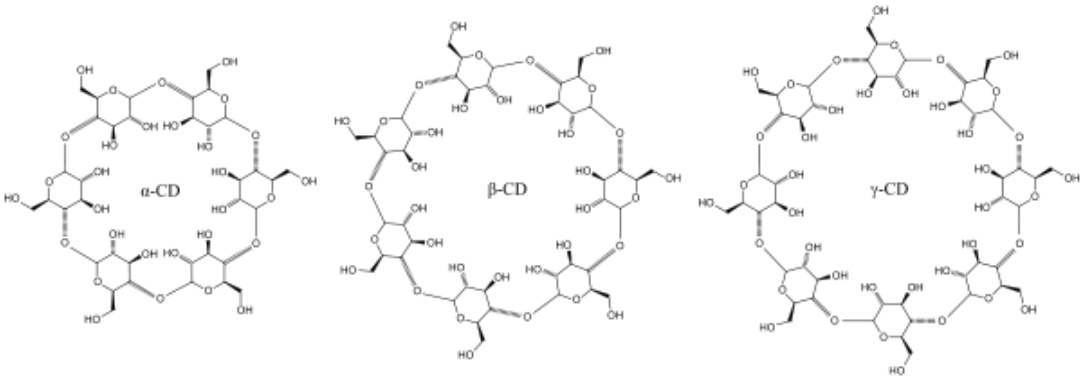

Figure 1.11: Molecular structures of (a) α-cyclodextrin, (b) β-cyclodextrin and (c) γ-cyclodextrin.

1.4.2 Structural Features of Cyclodextrins

Although all the cyclodextrins have an identical height of 7.9 Å, the variation in the number of linked glucopyranose units determines the size of their interior cavity[110]. Del Valle[108] stated that the cavity diameters are 4.7, 6.0 and 7.5 Å for α-, β- and γ-cyclodextrins, respectively. On the basis of the X-Ray crystal structures it was deduced that cyclodextrins adopt a hollow truncated cone structure with all glucopyranose units in the $^4C_1$ chair conformation, as depicted in Figure 1.12[119]. Song *et al.*[107] stated that the secondary hydroxyl groups (C_2 and C_3) are located on the wide edge of the cyclodextrin ring, which is termed the secondary rim, while the primary hydroxyl groups (C_6) are found on the other edge of the ring, known as the primary rim, of the cyclodextrin. The cavity of the cyclodextrin is then lined with C_3 and C_5 hydrogens and ether-like oxygens[108]. The primary and secondary hydroxyl groups on the exterior of the cyclodextrin are polar, while the hydrogens inside of the cyclodextrin are apolar. As a result, the cyclodextrins are soluble in water whilst retaining the hydrophilic exterior, and their hydrophobic interior cavity matrix[120]. It is this distinctive property of cyclodextrins that gives rise to their exceptional complexation ability in aqueous media. This is discussed further in Section 1.4.3.

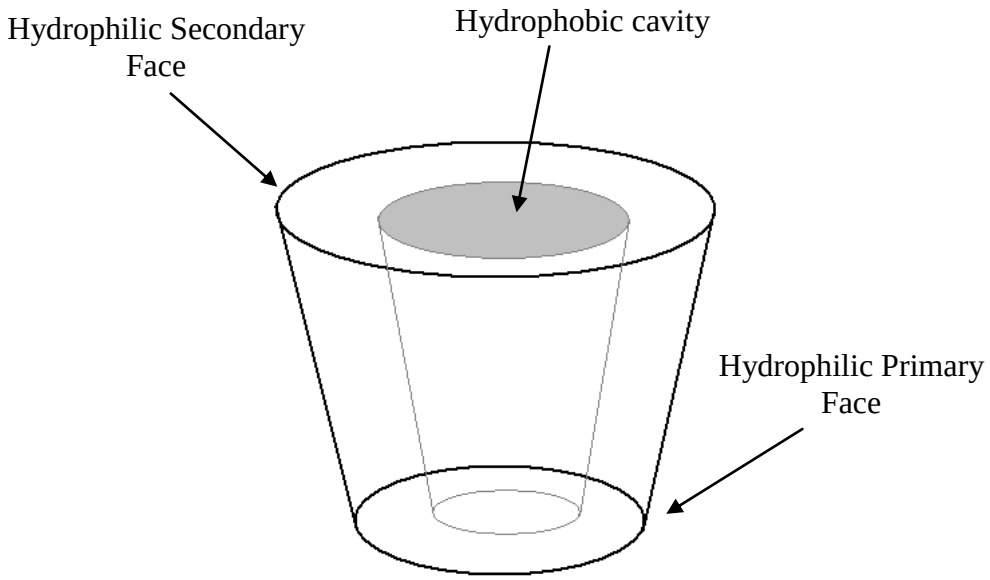

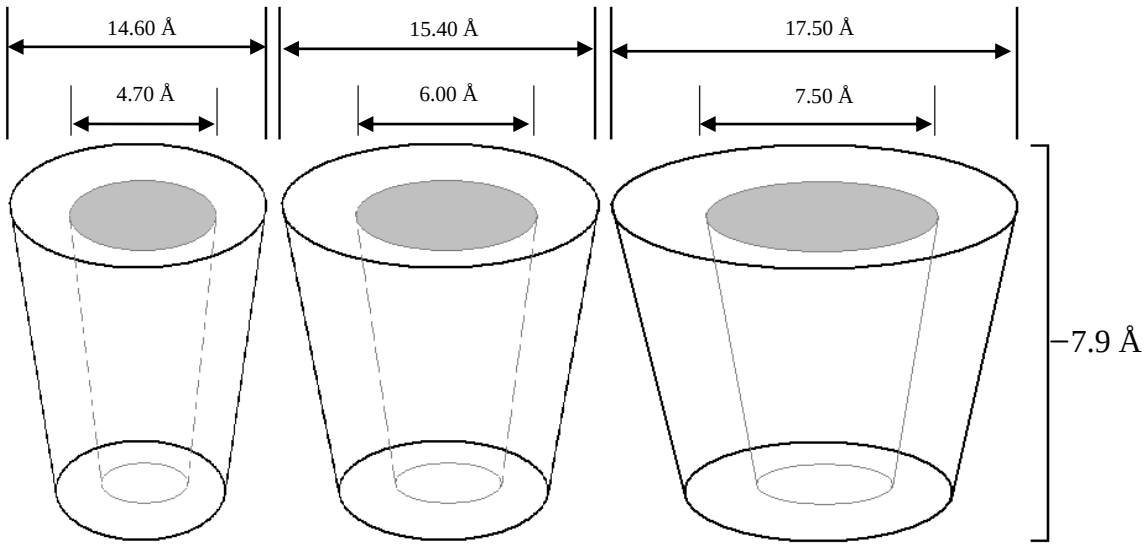

Figure 1.12: (a) The hollow truncated cone structure and (b) geometric dimensions of the α-, β- and γ-cyclodextrins.

A wide variety of cyclodextrin derivatives can be prepared from the α-, β- and γ-cyclodextrins, but the most derivatives arise from the β-cyclodextrin. A total of 21 hydroxyl groups on the β-cyclodextrin can be substituted by replacing the hydrogen or the hydroxyl groups with appropriate substituting groups such as alkyls or thio groups[111]. β-cyclodextrin contains 21 hydroxyl groups, seven on the primary face and 14 on the secondary face. Many of these 21 hydroxyl groups can be chemically modified in order to enhance the solubility of the cyclodextrin and the hydrophobic properties of the interior cavity matrix. In addition to this, substituting the hydroxyl

groups on the cyclodextrin can either improve or inhibit the binding affinity of the complexation, depending on the substitute groups that are used[121].

For the purpose of this study, the cyclodextrin that was chosen was a commercially available sulphonated-β-cyclodextrin, which has between 7 and 11 sulphonated (SO_3^-) groups per cyclodextrin. The structure of this sulphonated cyclodextrin, SCD, is shown in Figure 1.13. Amini *et al.*[122] and Chen *et al.*[123] investigated the structure of SCD; both authors found that complete sulphonation occurs at the C_6 position, with the C_2 secondary hydroxyls becoming partially sulphonated, and no sulphonation occurring at the C_3 position. This gives rise to the primary face being fully sulphonated, with seven SO_3^- groups on the primary face. This preferential sulphonation at the C_6 position over the C_2 position is expected due to the higher reactivity of the primary alcohol at the C_6 position[123]. Along with this, the higher acidity of the hydroxyl groups in the C_2 position mean that the C_2 position is preferentially sulphonated over the C_3 position[124], but the preferential sulphonation of the C_6 position may stereochemically prevent or reduce the accessibility of the C_3 hydroxyl.

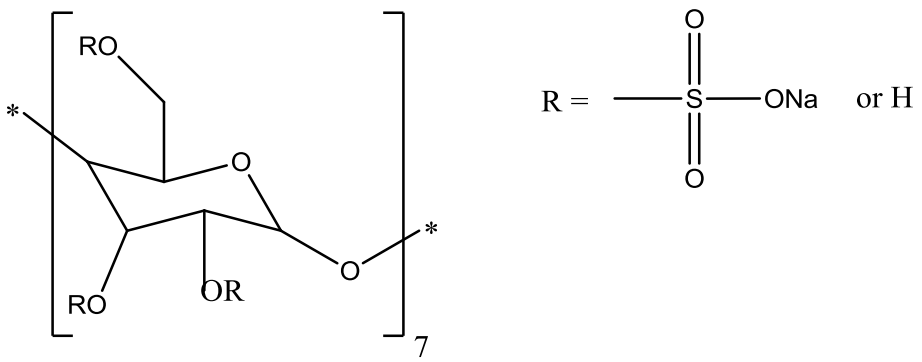

Figure 1.13: The chemical structural representation of the sulphonated-β-cyclodextrin, SCD.

Sulphonated-β-cyclodextrins have been used in a wide variety of applications, including the biomedical industry, due to the non toxicity of the complex[125] and in capillary electrophoresis as chiral separating agents[122,123,126]. One important feature of cyclodextrins is their ability to form inclusion complexes with a wide range of compounds in the solid, liquid or gaseous phases[127]. This feature makes them very useful in the area of sensing, whereby the cyclodextrin can bind to a suitable guest molecule to form inclusion complexes, whilst the negatively charged sulphonated

groups can repel any anionic interferants, thus enhancing the sensitivity of the sensor. This is discussed in greater detail in Section 1.4.3.

1.4.3 Inclusion Complexation

The inclusion chemistry of cyclodextrins can be broken down into two categories. These categories are aqueous complexation and solid state complexation. The former, aqueous inclusion complexation, is prominent given the unique hydrophobic and hydrophilic properties of cyclodextrins. It is generally accepted that cyclodextrins bind with suitable guest molecules in an aqueous medium to form inclusion complexes[115]. The formation of such inclusion complexes occurs without the formation or breaking of any covalent bonds[108,116]. The complex formed between a cyclodextrin (CD) and a guest molecule (G) is typically a 1:1 association, which is the simplest scenario, but other more complicated associations are also known to exist[128]. The inclusion complex formed for the 1:1 complexation is governed by a dynamic equilibrium process with a complex formation constant, *K*, as depicted in Equations 1.3 and 1.4, whereby CD is the host molecule and G is the guest molecule. The complex formation constant, *K*, describes the stability of the inclusion complex, which is governed by a thermodynamic equilibrium as illustrated in Equation 1.4[110,119]. As a result, large guest molecules give rise to a slower formation and dissociation of the inclusion complex. This process is energetically favoured by the interaction of the guest molecule with the hydrophobic cavity of the host[119].

$$CD + G \rightleftharpoons CD.G \qquad 1.3$$

$$K = \frac{[CD.G]}{[CD][G]} \qquad 1.4$$

The formation of cyclodextrin complexes in aqueous solutions has been studied using a wide variety of both electrochemical and spectroscopic methods. The most common techniques used include nuclear magnetic resonance (NMR)[129,130], UV-Vis[131,132] and fluorescence spectroscopy[133,134], cyclic voltammetry[135,136] and rotating

disc voltammetry[137,138]. Because cyclodextrins alter the electrochemical and spectral behaviour of the guest molecule on the formation of an inclusion complex, the easiest and most straightforward way of determining complexation is to carry out a titration[106]. This involves varying the concentration of the cyclodextrin while keeping the concentration of the guest molecule constant, which can also be used in order to determine the value of the complex formation constant, *K*. When an inclusion complex is formed there will be a significant and easily measurable difference in the behaviour of the guest molecule, which becomes more evident as the concentration of the cyclodextrin is increased.

There are two main factors which can affect the formation and stability of complexation in aqueous solutions: steric factors and thermodynamic factors. It is well known that the relative size of the cavity to the size of the guest molecule is a key factor in the complexation process; however, the manner in which thermodynamic factors influence complexation is still a matter of debate. As such, several hypotheses have been put forward in order to explain the driving force for the formation of cyclodextrin inclusion complexes[116]. These include electrostatic interactions, hydrogen bonding interactions, Van der Waals forces and hydrophobic interactions[139,140,141,142,143]. However, the formation of the inclusion complex cannot be explained by any one of these factors alone, as several of these are evident in the inclusion complex[128,140].

The influence of electrostatic interactions on the formation of inclusion complexes has been studied by Liu and Guo[144], who described an electrostatic interaction as the energy of interaction between the undistorted charge distribution of two molecules. There are three important types of electrostatic interactions: ion-ion interactions, ion-dipole interactions and dipole-dipole interactions.

Ion-ion interactions occur only when the cyclodextrin has been appropriately substituted and both the host and guest are charged[145]. Okimoto and Matsui[145] have shown that the binding between a neutral or positively charged guest molecule and an anionically charged cyclodextrin is superior to the binding of the same neutral or positively charged guest molecule with a neutral cyclodextrin, whereas the neutral cyclodextrin exhibits enhanced binding with the anionically charged guest molecules.

The second electrostatic interaction that could take place is the ion-dipole interaction. This is the interaction of an ion with a polar molecule and would be expected to occur because neutral cyclodextrins are naturally polar molecules. In general, the ion-dipole interaction increases with the size of the ion, hence complexation should increase with increasing ion size. However, this can be very difficult to observe in aqueous solutions because there is also a strong interaction between the guest molecules and the water molecules. As a result, ion-dipole interactions are not significant in complexation[144].

The final electrostatic interaction is the dipole-dipole interaction; this occurs between molecules that have a dipole moment. In contrast to the ion-dipole interactions, this interaction has a significant influence on both the stability and the orientation of the complex that is formed[144]. This is due to the dipoles of the guest molecules always being antiparallel to that of the host molecules. In addition to this, as the magnitude of the guest dipole increases, so does the value of the cyclodextrin dipole but in the opposite direction, as demonstrated by Chujo *et al.*[146] in 1988.

Another factor which may influence the stability and formation of the inclusion complex is hydrogen bonding. A hydrogen bond may also be regarded as a type of dipole-dipole interaction, whereby a hydrogen atom attached to an electronegative atom would be attracted to a neighbouring dipole on an adjacent molecule[147]. In aqueous systems in particular, there is some controversy as to the contribution that this would have on complexation. However, as hydrogen bonds can form with the guest and water molecules they would inhibit the formation of an inclusion complex[148]. Therefore, it has been proposed that it is the hydrogen at the C_6 position that would be involved in hydrogen bonding as it is flexible and can also rotate around the C_5 bond[144].

The factor that plays a more important role in the binding of cyclodextrins and guest molecules is Van der Waals forces. Van der Waals interactions describe induction (dipole induced dipole interaction) and dispersion forces[128]. The involvement of these forces in cyclodextrin complexes is unsurprising due to the relatively large dipole moment that cyclodextrins have. A vast majority of these claims are based on the fact that a negative enthalpy change in complexation is observed, which verifies the theoretical calculations stating that Van der Waals forces are indeed the main

driving force in the formation of cyclodextrin complexes. However, these calculations were mainly carried out in the gas phase and did not take into account actual solvent effects[144].

The induction and dispersion forces depend on polarisability, which is related to the molecular size and electron density[147]. Hence, these forces can result in weak electrostatic interactions as, in an aqueous environment, both the cyclodextrin and the water molecules are polar. However, the polarisability of the water is much lower than that of the organic components within the cyclodextrin cavity, thus it is expected that the Van der Waals forces should be stronger between the cyclodextrin and the guest in contrast to the water molecules and the guest. Casu and Rava reported experimental evidence that has shown that the stability of complexation increases as the factors which contribute to polarisability are increased[149].

The final factor that has been put forward in order to explain the driving force for the formation of cyclodextrin inclusion complexes is the role of hydrophobic effects. Hydrophobic effects relate to the association of non-polar molecules in water; however, the thermodynamics that give rise to this association are complex and are not fully understood. Consequently, the influence of hydrophobic effects on cyclodextrin complexation is debatable. This interaction is usually associated with a positive enthalpy and positive entropy due to the association of the non-polar molecules in the water but, according to Equation 1.5, the inclusion complex will only be formed if there is a net driving force, i.e., $\Delta G < 0$. The association is said to be 'entropy driven' and this entropic hydrophobic effect arises because the hydration shells of the two molecules are destroyed when they combine. The structured hydration water is then released and stabilised by other water molecules.

$$\Delta G = \Delta H - T\Delta S \qquad 1.5$$

The experimental observation in most cases for cyclodextrin complexation is that the entropy and enthalpy changes are negative[150]. This implies that the hydrophobic effect has little or no impact on the inclusion complex. However, several other methods have shown that the hydrophobic interactions play a significant role. It is widely stated in the literature that the strength of the inclusion complex will also

increase as the hydrophobicity of the guest molecule is increased[151,152,153]. Indeed, Alvira *et al*.[153] reported that the interaction energy between the β-cyclodextrin and an acrylic ester increased as the hydrophobicity of the alkyl group in the ester was increased.

In addition to this, the complex formed is usually weakened upon the addition of an organic co-solvent and strengthened when an inorganic co-solvent is added[144]. This further supports the evidence of hydrophobic effects since the addition of an inorganic salt to the solvent makes the bulk solution more polar, thus strengthening the binding. On the other hand, the addition of an organic salt will decrease the binding as the organic salt will be in competition with the guest molecule. Viernstein *et al*.[154] studied the equilibrium constant of a triflumizole β-cyclodextrin complex during the addition of a number of alcohols to the solvent. The authors found that the equilibrium constant decreases as the number of co-solvents and the apolar nature of the alcohol increase. This further highlights the importance of the hydrophobic effect in cyclodextrin complexation.

1.4.4 Applications of Cyclodextrins

Cyclodextrins have been applied to a wide variety of products and processes due to their ability to encapsulate guest molecules[115] and also due to their excellent biocompatibility. Cyclodextrins have been used extensively in the pharmaceutical industry due to their ability to form inclusion complexes with active ingredients, i.e., drugs. This gives rise to enhanced stabilisation and solubility of the drug and as a result, cyclodextrins are very popular ingredients in the area of drug formulations[155]. In addition, cyclodextrins are potential drug delivery candidates in many applications because of their ability to alter the physical, chemical and biological properties of guest molecules through the formation of inclusion complexes[156].

Cyclodextrins are also used in the food industry, particularly as food stabilisers. Cyclodextrins act as molecular encapsulants[115] and can protect the flavour of the food throughout food-processing methods such as freezing and thawing. This allows the quality of the food to be preserved and thus provides longevity to the food. In addition to this, cyclodextrins are known for their ability to reduce unpleasant odour and taste by capturing malodorous molecules within their cavities[115]. It is this

technique that was employed by Febreeze®, a commercially successful household odour eliminator, which contains a modified β-cyclodextrin as its active ingredient. Because the malodorous molecule is encapsulated within the cyclodextrin cavity, it can no longer be detected. Cyclodextrins have also found applications in cosmetic, chemical, agricultural[157], coatings, adhesives, plastics and photographic industries[108,110,111,114].

1.4.5 Methods for Determining Inclusion Complex Association Constant

As previously mentioned in Section 1.3.3, the simplest scenario for the complex formed between a host molecule and a guest molecule is a 1:1 association, however, some inclusion complexes that are formed have a more complex association. The inclusion complex formed for the 1:1 complexation is governed by a dynamic equilibrium process, which involves an inclusion complex association constant, *K*, as stated in Equations 1.3 and 1.4. There are many methods that have been employed in order to evaluate this *K* value, which yield important information regarding the type of binding interaction that is taking place.

In order to quantify the association constant value, the stoichiometry of the interaction is firstly required. This can be obtained using the Job's method, which is a continuous variation method[158,159]. Job's method involves the preparation of a series of solutions of host and guest molecules, whereby the sum of the total host and guest concentration remains constant while changing the mole fraction[160]. This is achieved by mixing different volumes of the two components such that the overall volume remains the same. A variety of methods can be used in order to obtain a Job's plot, these include both spectroscopic methods and electrochemical methods.

Spectroscopic techniques are used based on the changes in fluorescence[161,162,163,164], absorbance[161,165,166,167] and chemical shifts as acquired from NMR spectroscopy[168,169,170,171]. Electrochemical techniques such as cyclic voltammetry[135] and rotational disc voltammetry[172] can also be used, providing that some measurable property value changes during the formation of the host-guest complex. The maximum of this property is related to the stoichiometric ratio[160], hence the value of *K* can easily be determined from the data obtained by carrying out a host-guest titration. This involves keeping the concentration of one of the species (usually the

guest) constant, while varying the concentration of the other species (generally the host). Upon addition of increasing amounts of host concentration, there will be a significant and easily measurable difference in the behaviour of the guest molecule. These changes arise as the inclusion complex is formed due to the shift in equilibrium from uncomplexed to complexed species, as depicted in Equation 1.3, and this becomes more evident as the concentration of the host molecule is increased.

1.5 Serum Albumins

Bovine serum albumin, commonly referred to as BSA, is a large (66.4 kDa) globular protein derived from the albumin of bovine animals. Albumin is generally regarded as the serum albumin or plasma albumin, which differs from albumen, which refers to egg white. The word albumin is used to describe a protein or a group of proteins defined by their solubility in water. It is the most abundant protein in the circulatory system and contributes to over 80% of the colloidal osmotic blood pressure[173]. It has been determined that serum albumin is chiefly responsible for the maintenance of the blood pH[174]. Because of this, a lot of research has been carried out in order to identify the structure and properties of serum albumin and, to investigate the effect serum albumin has on the functionality of foods in which it is included, as well as other novel applications. Albumin is synthesised initially as preproalbumin by the liver of mammals. After the cleavage of the signal peptide, the resultant proalbumin is further processed by the removal of the six-residue propeptide from the new N-terminus, Figure 1.14. The albumin released into circulation possesses a half-life of 19 days[175].

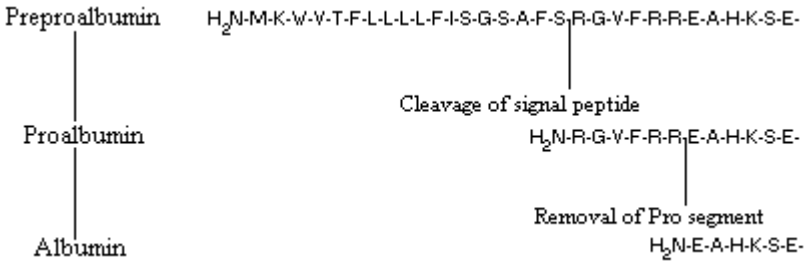

Figure 1.14: A schematic of the synthesis of albumin from preproalbumin in the liver.

Serum albumin is comprised of a single peptide chain containing approximately 600 amino acid residues, which is held in three homologous domains (I, II, III) and divided into nine loops (L1-L9) by 17 disulphide bonds as shown in Figure 1.15. The loops in each domain are made up of a sequence of long-short-long loops forming a triplet. Each domain in turn is the product of two sub-domains. The disulphide (S-S) bonds provide stability while the intervening peptide strands allow for flexibility, Figure 1.16.

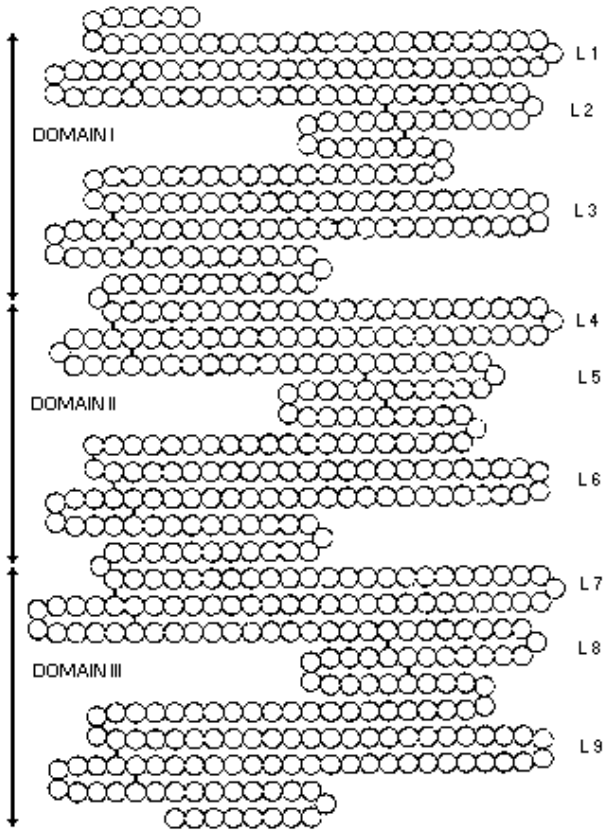

Figure 1.15: A schematic of the amino acid sequence in serum albumins showing the three homologous domains and the 9 loops that are held in place by 17 disulphide bonds.

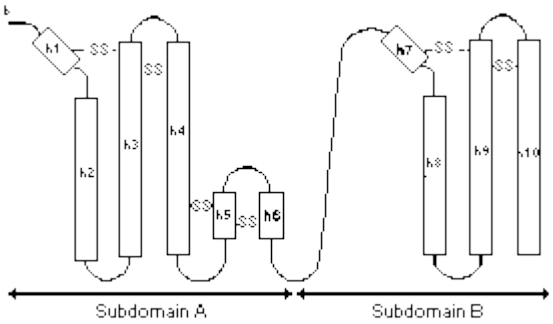

Figure 1.16: A schematic of serum albumin showing the locations of the disulphide bonds.

The albumin is not uniformly charged within the primary structure. Peters and co-workers[176] calculated a net charge of -10, -8, and 0 for domains I, II, and III of bovine serum albumin, respectively, at a neutral pH. The surface charge distribution of the frontal view of the BSA is shown in Figure 1.17.

Serum albumins are amphoteric[177] due to the charge distribution; hence, serum albumin can act either as an acid or as a base at varied pHs. In addition to this, serum albumins can form negatively charged nanospheres. The cross-linking rate of protein particles can be determined by a measurement of turbidity, in which the transmitted light, after a beam of incident light of a certain wavelength passing through the solution of light path length, *l*, is measured.

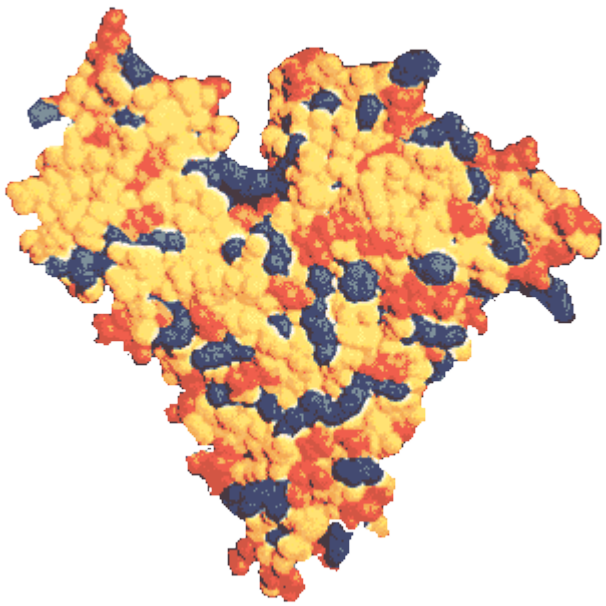

Figure 1.17: The surface charge distribution of the bovine serum albumin with the basic residues coloured in blue, the acidic residues in red, and the neutral areas in yellow.

Although human serum albumin (HSA) and BSA share 80% of their sequence homology, have identical isoelectric points of 4.77[177] and their molecular weights differ by less than 1%[178], HSA has a unique tryptophan at position 132, whereas BSA contains two tryptophan moieties at positions 134 and 212 as well as tyrosine and phenylalanine[179]. Because of this, and due to its water-soluble nature, BSA is used as a model protein for interaction studies.

Serum albumins are the principal carriers of fatty acids that are otherwise insoluble in circulating plasma. They also perform many other functions in the plasma, such as, sequestering oxygen free radicals and inactivating various toxic lipophilic metabolites such as bilirubin[180]. Albumin has a high affinity for fatty acids, bilirubin and hematin and a broad affinity for small negatively charged aromatic compounds.

Fasano *et al*.[181] have shown how albumin acts as a sponge in ligand binding, whereby numerous ligands can bind at different sites in the three domains. As a result, albumin can provide a depot for ligands, while holding toxins in strained orientations leading to metabolic charges along the molecule. In addition, albumins have a high affinity for Cu(II) whereby they bind Cu(II) at the N-terminal Asp-X-His site. Rozga *et al*.[182] have measured this affinity as 1 pM. The interactions between serum albumin and Zn(II) have also been studied[183].

1.5.1 Binding Interactions of BSA

The binding of several different categories of small molecules to BSA has been studied for many years to elucidate details of the protein structure and binding mechanism. Included in these categories are ionic surfactants such as sodium dodecyl sulphate (SDS), cethyltrimethylammonium chloride (CTAC) and N-hexadecyl-N,N-dimethyl-3-ammonium-1-propanesulphonate (HPS). Indeed, Gelamo *et al*.[184] and, more recently, Tabak and co-workers[185] have modelled the interaction of ionic surfactants with BSA using fluorescence and electron paramagnetic resonance (EPR) spectroscopy.

In addition, the effect of protein adsorption onto various hydrophobic and hydrophilic surfaces has been extensively studied using BSA. BSA has been

considered as a soft protein, as it has a high potential to undergo structural rearrangements upon adsorption onto surfaces[186]. Tantipolphan and co-workers[186] used ATR-FTIR spectroscopy to investigate the adsorption of BSA to lecithin and Larsericsdotter *et al*.[187] investigated the structure, stability and orientation of BSA adsorbed onto silica particles using DSC and limited proteolysis in combination with mass spectrometry. This gave a fundamental insight into the process of adsorption-induced structural changes in proteins.

1.5.2 Applications of BSA

Because of its abundance and functional properties, along with its ability to reversibly bind to a wide variety of ligands and other proteins[178], BSA has numerous biochemical applications. It has been used as a blocking agent during western blotting to reduce background and non-specific binding and immunohistochemistry[188]. It has also found applications in protein microarray technology, lysate microarray technology, ELISA, enzymatic reactions and as a carrier protein in many vaccines and medicines. Given its immunogenicity and ability to bind to other proteins, it has been used as an adjuvant to enhance the immune response to other proteins and carbohydrates. In addition, BSA is also used as a nutrient in cell and microbial cultures and it has been demonstrated to be useful in separating the optical isomers of drugs, small molecules and especially amino acids[189].

It is these unique binding properties of BSA that make it promising in the area of sensors and biosensors. The first crucial issue for BSA sensors is the attachment or immobilisation of the BSA onto the electrode[189]. The most commonly used method of immobilisation is the covalent binding technique as it can artificially bind the target which forms an ordered and dense monolayer[189]. In recent years however, sol-gel chemistry has been used as a more effective method for the immobilisation of proteins due to the low temperature mechanism required for immobilisation in contrast to the traditional covalent binding mechanism, which can often denature the proteins. The covalent immobilisation of functional, biological species such as BSA into a sol-gel matrix or onto a suitable surface such as titanium dioxide provides numerous applications for in vitro studies on the behaviour of biological structures

and biosensors[190]. Along with this, BSA can be incorporated into hydrogels[191] and nano-composites[192,193], which has led to numerous applications in both drug delivery systems and in the area of biosensors.

Other immobilisation methods that have been used to immobilise BSA have been investigated by Soldatkin *et al.*[194] whereby a biologically active membrane on the transducer surface was formed by protein cross-linking in saturated glutaraldehyde vapour. Similarly, Im and co-workers[195] electrodeposited a mixture of glucose oxidase and BSA onto a Pt electrode and subsequently cross-linked with glutaraldehyde to form a glucose amperometric biosensor with good sensing behaviour. Another method of immobilising BSA is to incorporate it into self-assembled monolayers (SAMs)[188]. Ignat *et al.*[188] have investigated the organisation of SAMs of functionalised thiols and the incorporation of various proteins onto gold and silicon substrates for their potential integration in nanoscale sensors/biosensors and optical devices. The authors claim that the biomolecule immobilisation of the proteins by covalent chemistry allows for the fabrication of reproducible, protein-modified surfaces, which is in good agreement with the literature[189].

Amperometric immunosensors have become one of the most powerful methods for the quantification of immunological moieties in clinical samples due to the employment of the innate amplification properties of enzymes[196]. However, the conventional methods used in the fabrication of enzyme amperometric immunosensors usually involve enzyme labelling, which is relatively expensive and time consuming as it requires sample pre-treatment. Because of this, the immobilisation of enzymes and the entrapment of mediators (electrochemically active compounds) onto the electrode surfaces have attracted great interest, since most immune protein analytes are not intrinsically able to act as redox partners in an electrochemical reaction[196]. BSA has free NH_2 groups that are capable of enhancing the immobilisation of an enzyme[197]. The NH_2 groups provide stability to and thus decrease the denaturation of the enzyme.

Because of their unique binding properties, albumins have proven to be very useful in the area of sensors and biosensors; however, they are also used in a variety of other applications. One of the major biological functions of albumins is their ability to carry drugs as well as endogenous and exogenous substances[179]. BSA is widely

used for the preparation of proteinaceous microspheres due to its availability in a pure form and its biodegradability, non-toxicity, and non-immunogenicity[198]. In addition to its functionality for transporting different macromolecules in the bloodstream to target organs, it was also found that albumin accumulates in solid tumours, making it a potential macromolecular carrier for the site-directed delivery of anti-tumour drugs[198].

Another application of BSA is in chiral recognition. Chirality is a determinative property of most biological molecules and, as a result, the development of techniques for the precise determination of bioactive chiral molecules is of great interest. The interactions between BSA and other molecules such as tryptophan have been studied in order to investigate the chiral recognition properties of BSA[189].

1.6 Urea

Urea, also known as carbamide, is a relatively small nitrogen-containing compound that serves a vital role in the metabolism of nitrogen-containing compounds by animals. The structure of urea is given in Figure 1.18. Its primary function in the body is nitrogen excretion, whereby it is dissolved in the blood and then excreted by the kidneys as a component of urine. A small amount of urea is also excreted from the body *via* perspiration, along with water and salts.

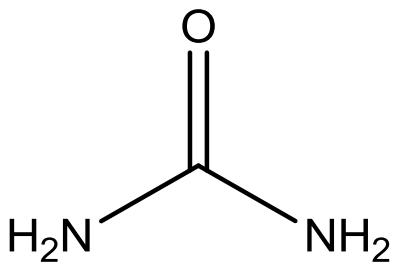

Figure 1.18: The chemical structure of Urea.

Urea is a colourless, odourless solid which is primarily neutral and highly soluble in water[199]. When dissolved in water, urea can break down to form ammonia, which has a strong odour. Ammonia is more mobile due to its smaller size and, if allowed

to accumulate, ammonia can raise the pH in cells to toxic levels. For this reason, the majority of organisms convert ammonia to urea, even though this synthesis has a net energy cost. However, urea is practically a neutral compound, thus it is a safe vehicle for the body to transport and excrete excess nitrogen.

Urea also plays an important role in the agricultural industry[200,201]. Because of its ability to release ammonia and therefore nitrogen, it has a vital role in the fertiliser industry. Annual world production of urea exceeds 100 million metric tonnes, the majority of which is produced as fertiliser. Since excessive nitrogen fertiliser applications can lead to pest problems by increasing the birth rate and overall longevity of certain pests, urea estimation is extremely important during environmental monitoring.

Many methods are already available for urea estimation; these include calorimetry[202], fluorimetry[203] and gas chromatography[204] to name but a few. However, these methods are unsuitable for on-site monitoring as they suffer from complicated sample pretreatment steps and, as such, sensors have been developed to overcome these difficulties.

1.7 Urea Sensors

Urea is one of the most extensively studied and analysed compounds due to its wide distribution in nature and its impact in clinical and agricultural chemistry as described in Section 1.6. Urea is known to be an important marker for the evaluation of uremic toxin levels. The normal blood level of urea is from 2.5 to 7.5 mmol dm^{-3}. However, in patients suffering from renal insufficiency, the urea concentrations in serum vary from 25 to 70 mmol dm^{-3}. At these high levels, i.e., above 25 mmol dm^{-3}, hemodialysis is required in order to reduce the build up of ammonia in the body, which would lead to cell toxicity and eventually to death.

As previously mentioned in Section 1.6, many techniques for urea estimation are available; however, this section will focus only on the biosensors that have been designed and developed in order to estimate the amount of urea in the blood serum. Enzymatic biosensors utilise the biospecificity of an enzymatic reaction; hence, in

the fabrication of urea biosensors, the enzyme urease is commonly chosen as the biosensing element. The urea and urease enzyme bind together in an enzyme-substrate complex which produces the ammonium ion as a product, as shown in Equation 1.6. The ammonium ion can be readily detected and quantified using a transducer. The transducer can be optical/thermal/piezoelectric/amperometric or potentiometric. Many matrices have been used to provide support and stability to the biomolecules that make up the biosensors; these include polymers, sol-gels, Langmuir-Blodgett films, nanomaterials and self-assembled monolayers[205].

$$NH_2CONH_2 + 3H_2O \xrightarrow{Urease} 2NH_4^+ + HCO_3^- + OH^- \qquad 1.6$$

1.7.1 Polymer Modified Electrodes

The development of urea sensors based on electrodes modified with polymeric films has been widely investigated due to the polymers ability to have their chemical and physical properties tailored[205]. The polymer films used can be either conducting or non-conducting, as both are found to be biocompatible, flexible and cost-effective. In addition, they can be obtained in the form of free-standing films for the fabrication of biosensors.

1.7.1.1 Urea Biosensors based on Non-conducting Polymer Matrices

Multiple efforts have been made in order to fabricate urea biosensors from various polymer matrices including polyurethane-acrylate[206], polyvinyl alcohol (PVA)[207], polyvinyl chloride (PVC)[208,209,210] and chitosan[211]. These materials provide mechanical strength and long-term stability as supports for the immobilisation of the enzymes. There are a variety of methods by which enzymes can be immobilised, ranging from covalent chemical bonding to physical entrapment.

Natural polymers, for example, the polysaccharides chitin and cellulose, are biocompatible and non-toxic and, as such, they have become the materials of choice for recent technological advances in biosensor fabrication[212,213]. Enzymatic sensors

with chitin and its deacetylated product, chitosan, supports have been reported for the determination of glucose, lactate, ethanol and urea. Most research papers reported in the literature toward urease immobilisation on chitosan are dominated by the use of beads[211]; however, a lot more work must be done in this field to obtain a commercial urea biosensor based on natural polymers.

In addition to the natural polymers, there has been a lot of research into utilising PVC polymers for the development of potentiometric urea biosensors. These biosensors are based on the principle of being able to detect slight changes in pH due to the formation of hydrogen or ammonium ions during an enzymatic reaction[214,215,216,217,218,219]. However, these also suffer from having a narrow dynamic range and fast loss in sensitivity[214]. More recently, functionalised PVC polymers have been investigated for use as electrode membrane materials to facilitate efficient enzyme immobilisation[216,220]. In addition, suitable ionophores have been utilised with PVC ion electrodes to enhance response characteristics including response time and reproducibility of the biosensor[221,222]. However, more efforts must be made in order to minimise the influence of interferants and, as such, the idea of using conducting polymer matrices as biosensors has gained more interest in recent years.

1.7.1.2 Urea Biosensors based on Conducting Polymer Matrices

Various conducting polymers have been used for the fabrication of urea biosensors[223,224,225,226]. These matrices are biocompatible and, they are ideal supports for biomolecules, resulting in biosensors that have enhanced sensitivity and versatility. The greatest advantage of conducting polymers over non-conducting polymers is that conducting polymers can be synthesised both chemically and electrochemically. Electrochemical deposition can be used to deposit uniform polymer films at electrodes of any shape and size[227,228]. In addition to this, biological entities, such as enzymes, can be trapped during electropolymerisation in one simple step into the polymer matrix. Also, the interactions of analytes and analyte recognition sites can be readily transduced into electrical signals that can be easily monitored.

The conducting polymers used in the fabrication of biosensors include polyaniline (PANi), polypyrrole (PPy) and polythiophene[229]. Polyaniline is often used as an immobilising substrate for biomolecules and as an efficient catalyst. However, the necessity to detect bioanalytes in neutral pH ranges leads to electro-inactivity of the deposited polymer film, hence polypyrrole is the most extensively used conducting polymer in the preparation of urea biosensors[230,231].

Amperometric, flow injection urea biosensors have been developed by the entrapment of the urease enzyme during the polymerisation of pyrrole and the influence of flow rate, applied potential and polymerisation time has been investigated[231]. The sensitivity and detection range were further improved by increasing the enzyme loading and utilising pulsed amperometric detection. However, these sensors suffer from the necessity of pretreatment steps. Osaka *et al.*[232] developed a potentiometric urea sensor using composite films with polyion complexes. The sensitivity of these biosensors was found to be significantly enhanced due to the effective immobilisation of high amounts of urease by treatment of the electrode with a pre-coated polyion complex, but reproducibility studies of this sensor were not reported.

Various approaches and immobilisation methods have been investigated in order to improve the stability, sensitivity and reproducibility of conducting polymer based biosensors. These approaches include using copolymers and composites, for example, polyaniline-nafion composites have been used to develop amperometric urea biosensors[231,233], and different immobilisation methods including inclusion during electropolymerisation and casting methods. However, obtaining good sensitivity, reproducibility and long-term stability of the conducting polymer urea biosensors is still a significant challenge.

1.7.1.3 Urea Biosensors based on Sol-Gel Matrices

Sol-gel matrices have been used in the fabrication of chemical opto-electronic sensors due to their chemical inertness, thermal and photochemical stability and optical transparency[234]. More recently, they have also been investigated as biosensors owing to the attractive low temperature process of immobilisation for

various biomolecules such as enzymes and antibodies, which tend to lose activity at higher temperatures[234].

Another advantage of using sol-gel matrices as biosensors is that the fabrication of multi-analyte detection electrodes is quite simple; which leads to shorter response times. In addition, the biological species can be easily entrapped into the matrix without leaching, leading to longer biomolecule stability and an enhanced life-time of the biosensor. Disadvantages, as with other biosensors, include loss in sensitivity and poor reproducibility. Also, sol-gel matrices have diffusional limitations and unknown catalyst-matrix interactions and kinetics, which pose a challenge to researchers as these are difficult to overcome[235].

1.7.2 Urea Biosensors based on Langmuir-Blodgett Films

Langmuir-Blodgett films have also been used as a means of sensing urea. Langmuir-Blodgett technology is a tool for designing artificial systems with biological functions, such as biosensors. The Langmuir-Blodgett films are ultra-thin, thus preserving high enzymatic activity of the incorporated biomolecules, hence, various biosensors have been designed using Langmuir-Blodgett films as the biosensitive part[236,237].

Urea biosensors based on Langmuir-Blodgett films have been developed by immobilising highly stable urease monolayers onto a substrate using the Langmuir-Blodgett deposition technique[238,239]. These biosensors were found to have a relatively good sensitivity; however, the detection limit of these sensors does not cover the physiological range of urea. In addition to this, the influence of interferants on the biosensor was not investigated.

1.7.3 Urea Biosensors based on Nanomaterials

Nanostructured materials are found in a large variety of applications such as catalytic reactions, fluorescent tags and smoke/fog screens, owing to their characteristic properties including high surface areas, good optical properties and light scattering effects. Nanomaterials have also found applications in the areas of drug delivery, pesticide delivery and, more recently, in the area of biosensors[240,241,242,243].

Biological species can retain their activity when adsorbed onto nanomaterials, such as gold nanoparticles[244]. Gold nanoparticles can also be used to immobilise enzymes based on chemical adsorption onto self-assembled monolayers[245,246]. Biological sensors have also been produced from nanostructured metal oxides, which enable higher catalytic activity, faster responses and possibly longer life-times[247].

1.8 References

1 A. Azapagic, A. Emsley and I. Hamerton, *Polymers: the environment and sustainable development*, John Wiley and Sons, 219, (2003)

2 S. Brady, D. Diamond and K.-T. Lau, *Sensors and Actuators A*, **119**, 398, (2005)

3 P. Chandrasekhar, *Conducting Polymers, Fundamentals and Applications: A Practical Approach*, Kluwer Academic Publishers, 718, (1999)

4 A. G. MacDiarmid and A. J. Heeger, *Synthetic Metals*, **1**, (2), 101 (1980)

5 G. Natta, G. Mazzanti and P. Corradini, *Atti della Accademia Nazionale dei Lincei, Classe di Scienze Fisiche, Matematiche e Naturali, Rendiconti Lincei*, **25**, 3, (1958)

6 J. L. Bredas and G. B. Street, *Accounts of Chemical Research*, **18**, 309, (1985)

7 B. Scrosati, *Applications of Electroactive Polymers*, Springer, 354, (1993)

8 J. van Haare, E. E. Havinga, J. L. J. van Dongen, R. A. J. Janssen, J. Cornil and J. L. Bredas, *Chemistry-a European Journal*, **4**, 1509, (1998)

9 N. K. Guimard, N. Gomez and C. E. Schmidt, *Progress in Polymer Science*, **32**, 876, (2007)

10 A. L. Briseno, A. Baca, Q. Z. Zhou, R. Lai and F. M. Zhou, *Analytica Chimica Acta*, **441**, 123, (2001)

11 J. M. Pringlea, O. Ngamnac, J. Chenc, G. G. Wallace, M. Forsyth and D. R. MacFarlane, *Synthetic Metals*, **156**, (14-15), 979, (2006)

12 H. S. Nalwa, *Advanced Functional Molecules and Polymers: Volume 3: Electronic and Photonic Properties*, Taylor and Francis, 386, (2001)

13 B. Winther-Jensen and K. West, *Macromolecules*, **37**, (12), 4538, (2004)

14 A. Malinauskas, *Polymer*, **42**, 3957, (2001)

15 W. Schuhmann, C. Kranz, H. Wohlschlager and J. Strohmeier, *Biosensors and Bioelectronics*, **12**, 1157, (1997)

16 M. Gerard, A. Chaubey and B. D. Malhotra, *Biosensors and Bioelectronics*, **17**, 345, (2002)

17 M. Nuñez, *Progress in Electrochemistry Research*, Nova Publishers, 190, (2005)

18 N. K. Guimard, N. Gomez and C. E. Schmidt, *Progress in Polymer Science*, **32**, 876, (2007)

19 K. A. Mauritz, I.D. Stefanithis, S. V. Davis, R. W. Scheetz, R. K. Pope, G. L. Wilkes and H. H. Huang, *Journal of Applied Polymer Science*, **55**, 181, (1995)

20 R. C. D. Peres, M. A. Depaoli, S. Panero and B. Scrosati, *Journal of Power Sources*, **40**, 299, (1992)

21 G. A. Sotzing, J. R. Reynolds and P. J. Steel, *Chemistry of Materials*, **8**, 882, (1996)

22 S. Ramirez-Garcia and D. Diamond, *Sensors and Actuators A*, **135**, 229, (2007)

23 G. Han and G. Shi, *Sensors and Actuators B: Chemical*, **99**, 525, (2004)

24 M. S. Cho, H. J. Seo, J. D. Nam, H. R. Choi, J. C. Koo and Y. Lee, *Smart Materials and Structures*, **16**, S237, (2007)

25 P. A. Anquetil, H. H. Yu, J. D. Madden, P. G. Madden, T. M. Swager and I. W. Hunter, *Smart Structures and Materials 2002: Electroactive Polymer Actuators and Devices (Eapad)*, **4695**, 424, (2002)

26 P. M. George, D. A. LaVan, J. A. Burdick, C. Y. Chen, E. Liang and R. Langer, *Advanced Materials*, **18**, 577, (2006)

27 D. A. Reece, S. F. Ralph and G. G. Wallace, *Journal of Membrane Science*, **249**, 9, (2005)

28 U. Lange, N. V. Roznyatovskaya and V. M. Mirsky, *Analytica Chimica Acta*, **614**, 1, (2008)

29 A. J. Heeger, *Synthetic Metals*, **125**, 23, (2001)

30 A. Angeli, *Gazzetta Chimica Italiana*, **46**, 279, (1916)

31 A. Dall'Ollio, G. Dascola, V. Varacca and V. Bocchi, *Comptes rendus hebdomadaires Des Seances De L Academie des Sciences Serie C*, **267**, 433, (1968)

32 K. Keiji Kanazawa, A. F. Diaz, W. D. Gill, P. M. Grant, G. B. Street, G. Piero Gardini and J. F. Kwak, *Synthetic Metals*, **1**, 329, (1980)

33 M. Nishizawa, H. Nozaki, H. Kaji, T. Kitazume, N. Kobayashi, T. Ishibashi and T. Abe, *Biomaterials*, **28**, 1480, (2007)

34 S. Carquigny, O. Segut, B. Lakard, F. Lallemand and P. Fievet, *Synthetic Metals*, **20**, 365, (1987)

35 S. Carquigny, J.-B. Sanchez, F. Berger, B. Lakard and F. Lallemand, *Talanta*, **78**, 199, (2009)

36 S. A. Waghuley, S. M. Yenorkar, S. S. Yawale and S. P. Yawale, *Sensors and Actuators B: Chemical*, **128**, 366, (2008)

37 S. Geetha, C. R. K. Rao, M. Vijayan and D. C. Trivedi, *Analytica Chimica Acta*, **568**, 119, (2006)

38 J. Wang and M. Musameh, *Analytica Chimica Acta*, **539**, 209, (2005)

39 K. Ghanbari, S. Z. Bathaie and M. F. Mousavi, *Biosensors and Bioelectronics*, **23**, 1825, (2008)

40 J. H. Collier, J. P. Camp, T. W. Hudson and C. E. Schmidt, *Journal of Biomedical Materials Research*, **50**, 574, (2000)

41 M. Martina and D. W. Hutmacher, *Polymer International*, **56**, 145, (2007)

42 P. M. George, A. W. Lyckman, D. A. LaVan, A. Hegde, Y. Leung, R. Avasare, C. Testa, P. M. Alexander, R. Langer and M. Sur, *Biomaterials*, **26**, 3511, (2005)

43 J.-D. Kwon, P.-H. Kim, J.-H. Keum and J. S. Kim, *Solar Energy Materials and Solar Cells*, **83**, 311, (2004)

44 S. Anastasova-Ivanova, U. Mattinen, A. Radu, J. Bobacka, A. Lewenstam, J. Migdalski, M. Danielewski and D. Diamond, *Sensors and Actuators B*, **146**, 199, (2010)

45 R. T. Richardson, B. Thompson, S. Moulton, C. Newbold, M. G. Lum, A. Cameron, G. Wallace, R. Kapsa, G. Clark and S. O'Leary, *Biomaterials*, **28**, 513, (2007)

46 S. Ramirez-Garcia, M. Baeza, M. O'Toole, Y. Wu, J. Lalor, G. G. Wallace and D. Diamond, *Talanta*, **77**, 463, (2008)

47 A. M. Rocco, M.-A. De Paoli, A. Zanelli and M. Mastragostino, *Electrochimica Acta*, **41**, 2805, (1996)

48 G. M. Spinks, B. Xi, D. Zhou, V.-T. Truong and G. G. Wallace, *Synthetic Metals*, **140**, 273, (2004)

49 J. Migdalski, T. Blaz and A. Lewenstam, *Analytica Chimica Acta*, **322**, 141, (1996)

50 S. K. Ghosh, *Functional Coatings By Polymer Microencapsulation*, Wiley-VCH, 371, (2006)

51 A. Mohammadi, M. A. Hasan, B. Liedberg, I. Lundstrom and W. R. Salaneck, *Synthetic Metals*, **14**, 189, (1986)

52 P. Subramanian, N. B. Clark, L. Spiccia, D. R. MacFarlane, B. Winther-Jensen and C. Forsyth, *Synthetic Metals*, **158**, 704, (2008)

53 B. Winther-Jensen, J. Chen, K. West and G. Wallace, *Macromolecules*, **37**, 5930, (2004)

54 W. Prissanaroon-Ouajai, P. J. Pigram, R. Jones and A. Sirivat, *Sensors and Actuators B: Chemical*, **135**, 366, (2008)

55 J. Tietje-Girault, C. Ponce de León and F. C. Walsh, *Surface and Coatings Technology*, **201**, 6025, (2007)

56 A. S. Liu and M. A. S. Oliveira, *Materials Research*, **10**, 205, (2007)

57 K. J. Kim, H. S. Song, J. D. Kim and J. K. Chon, *Bulletin of the Korean Chemical Society*, **9**, 248, (1988)

58 S. Asavapiriyanont, G. K. Chandler, G. A. Gunawardena and D. Pletcher, *Journal of Electroanalytical Chemistry*, **177**, 229, (1984)

59 Y. J. Qiu and J. R. Reynolds, *Journal of Polymer Science Part a-Polymer Chemistry*, **30**, 1315, (1992)

60 A. F. Diaz and J. I. Castillo, *Journal of the Chemical Society-Chemical Communications*, 397, (1980)

61 M. C. Henry, C. C. Hsueh, B. P. Timko and M. S. Freund, *Journal of the Electrochemical Society*, **148**, D155, (2001)

62 S. A. Shaffer, J. K. Wolken and F. Tureček, *Journal of the American Society for Mass Spectrometry*, **8**, (11), 1111-1123, (1997)

63 V.Q. Nguyen and F. Turecek, *Journal of Mass Spectrometry*, **31**, (10), 1173, (1996)

64 J. Jang, J. Hak Oh and X. Li Li, *Journal of Materials Chemistry*, **14**, 2872, (2004)

65 S. Sadki, P. Schottland, N. Brodie and G. Sabouraud, *Chemical Society Reviews*, **29**, 283, (2000)

66 I. Dodouche and F. Epron, *Applied Catalysis B: Environmental*, **76**, 291, (2007)

67 C. M. Li, C. Q. Sun, W. Chen and L. Pan, *Surface and Coatings Technology*, **198**, 474, (2005)

68 K. Imanishi, M. Satoh, Y. Yasuda, R. Tsushima and S. Aoki, *Journal of Electroanalytical Chemistry*, **260**, 469, (1989)

69 R. Cervini, R. J. Fleming, B. J. Kennedy and K. S. Murray, *Journal of Materials Chemistry*, **4**, 87, (1994)

70 J. Ouyang and Y. F. Li, *Polymer*, **38**, 1971, (1997)

71 J. Tietje-Girault, C. Ponce de Leon and F. C. Walsh, *Surface and Coatings Technology*, **201**, 6025, (2007)

72 D. S. Maddison and J. Unsworth, *Synthetic Metals*, **52**, 227, (1992)

73 W. B. Liang, J. T. Lei and C. R. Martin, *Synthetic Metals*, **30**, 47, (1989)

74 M. Zhou and J. Heinze, *Electrochimica Acta*, **44**, 1733, (1999)

75 H. Korri-Youssoufi, N. Desbenoit, R. Ricoux, J. P. Mahy and S. Lecomte, *Materials Science and Engineering: C*, **28**, 855, (2008)

76 H. B. Fredj, S. Helali, C. Esseghaier, L. Vonna, L. Vidal and A. Abdelghani, *Talanta*, **75**, 740, (2008)

77 R. K. Sharma, A. C. Rastogi and S. B. Desu, *Physica B: Condensed Matter*, **388**, 344, (2007)

78 L. Tian, Y. Qi and B. Wang, *Journal of Colloid and Interface Science*, **333**, 249, (2009)

79 A. A. A. Almario and R. L. T. Cacers, *Journal of the Chilean Chemical Society*, **54**, 971, (2006)

80 Y. F. Li and J. Yang, *Journal of Applied Polymer Science*, **65**, 2739, (1997)

81 H. S. Nalwa, *Handbook of Advanced Electronic and Photonic Materials and Devices*, Academic Press, 3366, (2000)

82 E. De Giglio, M. R. Guascito, L. Sabbatini and G. Zambonin, *Biomaterials*, **22**, 2609, (2001)

83 J. C. Wu, X. M. Yu, H. Lord and J. Pawliszyn, *Analyst*, **125**, 391, (2000)

84 Deepa and S. Ahmad, *European Polymer Journal*, **44**, 3288, (2008)

85 S. Carquigny, O. Segut, B. Lakard, F. Lallemand and P. Fievet, *Synthetic Metals*, **158**, 453, (2008)

86 S. J. Sutton and A. S. Vaughan, *Synthetic Metals*, **58**, 391, (1993)

87 J. M. Ko, H. W. Rhee, S. M. Park and C. Y. Kim, *Journal of the Electrochemical Society*, **137**, 905, (1990)

88 T. F. Otero and E. Delarreta, *Synthetic Metals*, **26**, 79, (1988)

89 T. Hernandez-Perez, M. Morales, N. Batina and M. Salmon, *Journal of the Electrochemical Society*, **148**, C369-375, (2001)

90 F. Beck, P. Braun and M. Oberst, *Berichte Der Bunsen-Gesellschaft-Physical Chemistry Chemical Physics*, **91**, 967, (1987)

91 H. L. Ge, G. J. Qi, E. T. Kang and K. G. Neoh, *Polymer*, **35**, 504, (1994)

92 A. F. Diaz and T. C. Clarke, *Journal of Electroanalytical Chemistry*, **111**, 115, (1980)

93 J. C. Thieblemont, A. Brun, J. Marty, M. F. Planche and P. Calo, *Polymer*, **36**, 1605, (1995)

94 M. Satoh, K. Kaneto and K. Yoshino, *Synthetic Metals*, **14**, 289, (1986)

95 M. Zhou and J. Heinze, *Journal of Physical Chemistry B*, **103**, 8443, (1999)

96 S. Kuwabata, J. Nakamura and H. Yoneyama, *Journal of the Chemical Society-Chemical Communications*, 779, (1988)

97 S. Shimoda and E. Smela, *Electrochimica Acta*, **44**, 219, (1998)

98 M. Karthikeyan, K. K. Satheeshkumar and K. P. Elango, *Journal of Hazardous Materials*, **167**, 300, (2009)

99 R. Ansari Khalkhali, W. E. Price and G. G. Wallace, *Reactive and Functional Polymers*, **56**, 141, (2003)

100 C. K. Baker, Y. J. Qiu and J. R. Reynolds, *Journal of Physical Chemistry*, **95**, 4446, (1991)

101 C. Weidlich, K. M. Mangold and K. Juttner, *Electrochimica Acta*, **47**, 741, (2001)

102 M. Forsyth, *Polymer*, **36**, (4), 725, (1995)

103 A. Malinauskas, *Synthetic Metals*, **107**, 75, (1999)

104 J. M. Lehn, *Angewandte Chemie-International Edition in English*, **27**, 89, (1988)

105 F. Diedrich, *Journal of Chemical Education*, **67**, 813, (1990)

106 H. Dodziuk, *Cyclodextrins and their Complexes: Chemistry, Analytical Methods, Applications*, Wiley-VCH, 489, (2006)

107 L. X. Song, L. Bai, X. M. Xu, J. He and S. Z. Pan, *Coordination Chemistry Reviews*, **253**, 1276, (2009)

108 E. M. M. Del Valle, *Process Biochemistry*, **39**, 1033, (2004)

109 A. Villiers, *Comptes Rendus de l'Academie des sciences*, **112**, 536, (1891)

110 J. Szejtli, *Chemical Reviews*, **98**, 1743, (1998)

111 J. Szejtli, *Pure and Applied Chemistry*, **76**, 1825, (2004)

112 H. J. Buschmann and E. Schollmeyer, *Journal of Cosmetic Science*, **53**, 185, (2002)

113 M. L. Bender and M. Komiyama, *Cyclodextrin Chemistry*, Springer-Verlag, Berlin, (1978)

114 J. Szejtli, *Journal of Materials Chemistry*, **7**, 575, (1997)

115 T. Loftsson and D. Duchene, *International Journal of Pharmaceutics*, **329**, 1, (2007)

116 K. L. Larsen and W. Zimmermann, *Journal of Chromatography A*, **836**, 3, (1999)

117 M. E. Brewster and T. Loftsmann, *Advanced Drug Delivery Reviews*, **59**, 645, (2007)

118 T. Nakagawa, K. Ueno, M. Kashiwa and J. Watanabe, *Tetrahedron Letters*, **35**, 1921, (1994)

119 G. Astray, C. Gonzalez-Barreiro, J. C. Mejuto, R. Rial-Otero and J. Simal-Gandara, *Food Hydrocolloids*, **23**, 1631, (2009)

120 J. Szejtli, *Trends in Biotechnology*, **7**, 170, (1989)

121 S. Hbaieb, R. Kalfat, Y. Chevalier, N. Amdouni and H. Parrot-Lopez, *Materials Sciences and Engineering. C-Biomimetic Supramolecular Systems.*, **28**, 697, (2008)

122 A. Amini, T. Rundlof, M. B. G. Rydberg and T. Arvidsson, *Journal of Separation Science*, **27**, 1102, (2004)

123 F. T. A. Chen, G. Shen and R. A. Evangelista, *Journal of Chromotography A*, **924**, 523, (2001)

124 A. Ueno and R. Breslow, *Tetrahedron Letters*, **23**, 3451, (1982)

125 T. Loftsson and T. Järvinen, *Advanced Drug Delivery Reviews*, **36**, 59, (1999)

126 A. M. Stalcup and K. H. Gahm, *Analytical Chemistry*, **68**, 1360, (1996)

127 S. D. Eastburn and B. Y. Tao, *Biotechnology Advances*, **12**, 325, (1994)

128 K. A. Connors, *Chemical Reviews*, **97**, 1325, (1997)

129 K. J. Liao, X. H. Yan, D. Y. Zhao and X. Y. Ma, *Chinese Chemical Letters*, **13**, 227, (2002)

130 A. Bernini, O. Spiga, A. Ciutti, M. Scarselli, G. Bottoni, P. Mascagni and N. Niccolai, *European Journal of Pharmaceutical Sciences*, **22**, 445, (2004)

131 X.-J. Dang, M.-Y. Nie, T. Jian and H.-L. Li, *Journal of Electroanalytical Chemistry*, **448**, 61, (1998)

132 C. Yáñez, R. Salazar, L. J. Núñez-Vergara and J. A. Squella, *Journal of Pharmaceutical and Biomedical Analysis*, **35**, 51, (2004)

133 Y. Y. Zhou, C. Liu, H. P. Yu, H. W. Xu, Q. Lu and L. Wang, *Spectroscopy Letters*, **39**, 409, (2006)

134 D. K. Roy, N. Deb, B. C. Ghosh and A. K. Mukherjee, *Spectrochimica Acta Part A: Molecular and Biomolecular Spectroscopy*, **73**, 201, (2009)

135 G.-C. Zhao, J.-J. Zhu, J.-J. Zhang and H.-Y. Chen, *Analytica Chimica Acta*, **394**, 337, (1999)

136 M. S. Ibrahim, I. S. Shehatta and A. A. Al-Nayeli, *Journal of Pharmaceutical and Biomedical Analysis*, **28**, 217, (2002)

137 E. Coutouli-Argyropoulou, A. Kelaidopoulou, C. Sideris and G. Kokkinidis, *Journal of Electroanalytical Chemistry*, **477**, 130, (1999)

138 J.-F. Bergamini, M. Belabbas, M. Jouini, S. Aeiyach, J.-C. Lacroix, K. I. Chane-Ching and P.-C. Lacaze, *Journal of Electroanalytical Chemistry*, **482**, 156, (2000)

139 J. Szejtli, *Cyclodextrin Technology*, Kluwer Academic Publisher, Dordrecht, (1988)

140 K.-H. Fromming and J. Szejtli, *Cyclodextrins in Pharmacy*, Kluwer, Dordrecht, (1994)

141 J. F. Wojcik, *Bioorganic Chemistry*, **12**, 130, (1984)

142 Y. Matsur, T. Nishioka and T. Fujita, *Topics in Current Chemistry*, **128**, 61, (1985)

143 R. J. Clarke, J. H. Coates and S. F. Lincoln, *Advances in Carbohydrate Chemistry and Biochemistry*, **46**, 205, (1988)

144 L. Liu and Q. X. Guo, *Journal of Inclusion Phenomena and Macrocyclic Chemistry*, **42**, 1, (2002)

145 A. Okimoto and Y. Matsui, *Bulletin of the Chemical Society of Japan*, **51**, 3030, (1978)

146 R. Chujo, M. Kitagawa, H. Hoshi, M. Sakurai and Y. Inoue, *Bulletin of the Chemical Society of Japan*, **61**, 4225, (1988)

147 J. W. Steed and J. L. Atwood, *Supramolecular Chemistry*, John Wiley and Sons, Ltd., Chichester, New York, Weinheim, Brisbane, Singapore and Toronto, (2000)

148 D. W. Griffiths and M. L. Bender, In: D. D. Eley, H. Pines and P. B. Weisz (Eds), *Advances in Catalysis*, Academic Press, **23**, 209, (1973)

149 B. Casu and L. Rava, *Ricerca Scientifica*, **36**, 733, (1966)

150 M. V. Rekharsky and Y. Inoue, *Chemical Reviews*, **98**, 1875, (1998)

151 M. Zhang, J. Li, L. Zhang and J. Chao, *Spectrochimica Acta Part A-Molecular and Biomolecular Spectroscopy*, **71**, 1891, (2009)

152 C. Yãnez, L. J. Nunez-Vergara and J. A. Squella, *Electroanalysis*, **15**, 1771, (2003)

153 E. Alvira, J. A. Mayoral and J. I. García, *Chemical Physics Letters*, **245**, 335, (1995)

154 H. Viernstein, P. Weiss-Greiler and P. Wolschann, *International Journal of Pharmaceutics*, **256**, 85, (2003)

155 V. J. Stella and R. A. Rajewski, *Pharmaceutical Research*, **14**, 556, (1997)

156 K. Uekama, F. Hirayama and T. Irie, *Chemical Reviews*, **98**, 2045, (1998)

157 S. M. Han, *Biomedical Chromatography*, **11**, 259, (1997)

158 A. Dimitrovska, B. Andonovski and K. Stojanoski, *International Journal of Pharmaceutics*, **134**, 213, (1996)

159 C. Y. Huang, R. X. Zhou, D. C. H. Yang and P. B. Chock, *Biophysical Chemistry*, **100**, 143, (2003)

160 A. Sayago, M. Boccio and A. G. Asuero, *International Journal of Pharmaceutics*, **295**, 29, (2005)

161 S. Letellier, B. Maupas, J. P. Gramond, F. Guyon and P. Gareil, *Analytica Chimica Acta*, **315**, 357, (1995)

162 S. Ishiwata and M. Kamiya, *Chemosphere*, **34**, 783, (1997)

163 I. DuranMeras, A. M. DelaPena, F. Salinas and I. R. Caceres, *Applied Spectroscopy*, **51**, 684, (1997)

164 Y. L. Loukas, V. Vraka and G. Gregoriadis, *Journal of Pharmacy and Pharmacology*, **49**, 127, (1997)

165 K. Kitamura and N. Imayoshi, *Analytical Sciences*, **8**, 497, (1992)

166 S. E. Brown, J. H. Coates, C. J. Easton, S. F. Lincoln, Y. Liu and A. K. W. Stephens, *Australian Journal of Chemistry*, **44**, 855, (1991)

167 R. Deponti, C. Torricelli, A. Motta and M. Crivellente, *European Journal of Pharmaceutics and Biopharmaceutics*, **37**, 106, (1991)

168 G. Endresz, B. Chankvetadze, D. Bergenthal and G. Blaschke, *Journal of Chromatography A*, **732**, 133, (1996)

169 B. Chankvetadze, G. Endresz, G. Schulte, D. Bergenthal and G. Blaschke, *Journal of Chromatography A*, **732**, 143, (1996)

170 Y. L. Loukas, *Journal of Pharmacy and Pharmacology*, **49**, 944, (1997)

171 S. Takhashi, E. Suzuki and N. Nagashima, *Bulletin of the Chemical Society of Japan*, **59**, 1129, (1986)

172 E. Coutouli-Argyropoulou, A. Kelaidopoulou, C. Sideris and G. Kokkinidis, *Journal of Electroanalytical Chemistry*, **477**, 130, (1999)

173 D. C. Carter and J. X. Ho, Structure of Serum Albumin. *Advanced Protein Chemistry*, **45**, 153-203, (1994)

174 J. Figge, T. H. Rossing, and V. Fencl, The Role of serum-proteins in Acid-Base Equilibria, *Journal of Laboratory and Clinical Medicine*, **117**, 453 (1991)

175 T. A. Waldmann, In: Albumin Structure, Function and Uses, V. M. Rosenoer, M. Oratz, and M. A. Rothschild (Eds), Pergamon, Oxford, 255, (1977)

176 T. Peters, Jr., Serum Albumin. *Adv. Protein Chem.*, **37**, 161, (1985)

177 B. Lu, S.-B. Xiong, H. Yang, X.-D. Yin and R.-B. Zhao, *International Journal of Pharmaceutics*, **307**, 168, (2006)

178 T. Mogues, J. Li, J. Coburn and D. J. Kuter, *Journal of Immunological Methods*, **300**, 1, (2005)

179 A. Ravindran, A. Singh, A. M. Raichur, N. Chandrasekaran and A. Mukherjee, *Colloids and Surfaces B: Biointerfaces*, **76**, 32, (2010)

180 T. E. Emerson, Jr., Unique features of albumin: A brief review. *CRC Critical Care Medicine*, **17**, 690, (1989)

181 M. Fasano, S. Curry, E. Terreno, M. Galliano, G. Fanali, P. Narciso, S. Notari and P. Ascenzi, *IUBMB Life*, **57**, (12), 787, (2005)

182 M. Rozga, A. M. Sokolowska, W. B. Protas, *Journal of Biology and Inorganic Chemistry*, **12**, (6), 913, (2007)

183 E. Ohyoshi, Y. Hamada, K. Nakata and S. Kohata, *Journal of Inorganic Biochemistry*, **75**, 213, (1999)

184 E. L. Gelamo, C. H. P. T. Silva, H. Imasato and M. Tabak, *Biochimica et Biophysica Acta*, **1594**, 84, (2002)

185 D. de Sousa Neto, C. E. G. Salmon, A. Alonso and M. Tabak, *Colloids and Surfaces B: Biointerfaces*, **70**, 147, (2009)

186 R. Tantipolphan, T. Rades, A. J. McQuillan and N. J. Medlicott, *International Journal of Pharmaceutics*, **337**, 40, (2007)

187 H. Larsericsdotter, S. Oscarsson and J. Buijs, *Journal of Colloid and Interface Science*, **289**, 26, (2005)

188 T. Ignat, M. Miu, I. Klepa, A. Bragaru, M. Simion and M. Danila, *Materials Science and Engineering B*, **169**, 55, (2010)

189 Y. Wang, X. Yin, M. Shi, W. Li, L. Zhang and J. Kong, *Talanta*, **69**, 1240, (2006)

190 C. K. Simi and T. E. Abraham, *Colloids and Surfaces B: Biointerfaces*, **71**, 319, (2009)

191 J.-C. Gayet and G. Fortier, *Journal of Controlled Release*, **38**, 177, (1996)

192 J. Liang, X. Ai, Z. He, H. Xie and D. Pang, *Materials Letters*, **59**, 2778, (2005)

193 C. K. Simi and T. E. Abraham, *Colloids and Surfaces B: Biointerfaces*, **71**, 319, (2009)

194 A. P. Soldatkin, J. Montoriol, W. Sant, C. Martelet, N. Jaffrezic-Renault, *Talanta*, **58**, (2), 351, (2002)

195 D. M. Im, D. H. Jang, S. M. Oh, Ch. Striebel, H.-D. Wiemhöfer, G. Gauglitz and W. Göpel, *Sensors and Actuators B*, **24-25**, 149, (1995)

196 Y. Zhuo, R. Yuan, Y. Chai, A. Sun, Y. Zhang and J. Yang, *Biomaterials*, **27**, 5420, (2006)

197 T. Ahuja, I. A. Mir, D. Kumar and Rajesh, *Sensors and Actuators B*, **134**, 140, (2008)

198 O. Grinberg, M. Hayun, B. Sredni and A. Gedanken, *Ultrasonics Sonochemistry*, **14**, 661, (2007)

199 K. C. Nicolaou and T. Montagnon, *Molecules That Changed The World*, Wiley-VCH, 11, (2008)

200 A. J. Taylor and P. Vadgama, *Analytical Reviews in Clinical Biochemistry*, **29**, 245, (1992)

201 L. Della Diana and G. Caputo, *Clinical Chemistry*, **42**, 1079, (1996)

202 A. Ramsing, J. Ruzicka and E. H. Hensen, *Analytica Chimica Acta*., **114**, 165, (1980)

203 F. Roch-Ramel, *Analytical Biochemistry*, **21**, 372, (1967)

204 C. J. Patton and S. R. Crouch, *Analytical Chemistry*, **49**, 464, (1977)

205 B. Adhikari and S. Majumdar, *Progress in Polymer Science*, **29**, 699, (2004)

206 Puig-Lleixa, C. Jimenez, J. Alonso and J. Bartroli, *Analytica Chimica Acta*, **389**, 179, (1999)

207 A. Sehitogullari and A. H. Uslan, *Talanta*, **57**, 1039, (2002)

208 M. Gutierrez, S. Algert and M. D. Valle, *Biosensors and Bioelectronics*, **22**, 2171, (2007)

209 K. S. Pekyardymcy and E. Kylyc, *Artificial Cells, Blood Substitutes and Biotechnology*, **33**, 329, (2005)

210 N. Tinkilic, O. Cubuck and I. Isildak, *Analytica Chimica Acta.*, **452**, 29, (2002)

211 J. M. C. S. Magalhães and A. A. S. C. Machado, *Talanta*, **47**, 183, (1998)

212 S. Hirano, Production and application of chitin and chitosan in Japan, in: G. Skja-Braek, T. Anthonsen, P. Sandford (Eds.), Chitin and Chitosan, Sources, Chemistry, Biochemistry, Physical Properties and Applications, Elsevier, Amsterdam, **37**, (1988)

213 M. Nakajuma, K. Atsumi and K. Kifune, Development of absorbable sutures from chitin, in: J. P. Zikakis (Ed.), Chitin, Chitosan and Related Enzymes, Academic Press, New York, 407, (1984)

214 J. Ruzicka, E. H. Hansen, A. K. Ghose and H. A. Mottola, *Analytical Chemistry*, **51**, 199-203, (1979)

215 P. M. Vadgama, K. G. M. M. Alberti and A. K. Covington, *Analytica Chimica Acta.*, **136**, 403, (1982)

216 I. Karube, E. Tamiya and J. M. Dicks, *Analytica Chimica Acta.*, **185**, 195, (1986)

217 G. G. Guilbault and J. G. Montalvo, *Journal of the American Chemical Society*, **91**, 2164, (1969)

218 L. Campanella, F. Mazzei, M. P. Sammartino and M. Tomassetti, *Bioelectrochemistry and Bioenergetics.*, **23**, 195, (1990)

219 C. Eggenstein, M. Borchardt, D. Christoph, B. Gründig, C. Dumschat, K. Cammann, M. Knoll and F. Spener, *Biosensors and Bioelectronics*, **14**, 33, (1999)

220 M. Holmberg, M. Eriksson, C. Krantz-Rülcker, T. Artursson, F. Winquist, A. Lloyd-Spetz and I. Lundström, *Sensors and Actuators B*, **101**, 213, (2004)

221 S. A. Rosario, G. S. Cha, M. E. Meyerhoff and M. Trojanowicz, *Analytical Chemistry*, **62**, 2418, (1990)

222 S. Glab, R. Koncki, E. Kopczewska, I. Walcerz and A. Hulanicki, *Talanta*, **41**, 1201-1205, (1994)

223 N. C. Foulds and C. R. Lowe, *Journal of the Chemical Society, Faraday Transactions*, **182**, 1259, (1986)

224 G. Fortier, E. Brassard and D. Belanger, *Biosensors and Bioelectron*ics, **5**, 473, (1990)

225 S. E. Wolowacz, B. F. Y. Y-Hin and C. R. Lowe, *Analytical Chemistry*, **64**, 1541, (1992)

226 B. F. Y. Y-Hin, M. Smolander, T. Cromptan and C. R. Lowe, *Analytical Chemistry*, **65**, 2067, (1993)

227 T. Kaku, H. I. Karan and Y. Okamoto, *Analytical Chemistry*, **66**, 1231, (1994)

228 L. C-Guerente, S. Cosnier, C. Innocent and P. Mailley, *Analytica Chimica Acta.*, **311**, 23, (1995)

229 S. de Marcos, R. Hortiguiela, J. Galbfin, J. R. Castillo and O. S. Wolfbeis, *Mikrochimica Acta*., **130**, 267, (1999)

230 S. Komaba, M. Seyama, T. Momma and T. Osaka, *Electrochimica Acta*, **42**, 383, (1997)

231 S. B. Adeloju, S. J. Shaw and G. G. Wallace, *Analytica Chimica Acta*, **341**, 155, (1997)

232 T. Osaka, S. Komaba, M. Seyama and K. Tanabe, *Sensors and Actuators B*, **35–36**, 463, (1996)

233 W. J. Cho and H. J. Huang, *Analytical Chemistry*, **70**, 3946–3951, (1998)

234 R. Gupta and N. K. Chaudhury, *Defence Science Journal*, **57**, (3), 241-253, (2007)

235 R. Sahney, S. Ananda, B. K. Puri and A. K. Srivastava, *Analytica Chimica Acta*, **578**, 156, (2006)

236 R. Singhal, A. Gambhir, M. K. Pandey, S. Annapoorni and B. D. Malhotra, *Biosensors and Bioelectronics*, **17**, 697, (2002)

237 A. P. Girard-Egrod, R. M. Morelis and P. R. Coulet, *Thin Solid Films*, **292**, 282, (1997)

238 A. Zhang, Y. Hou, N. Jaffrezic-Renault, J. Wan, A. Soldatkin and J.-M. Chovelon, *Bioelectrochemistry*, **56**, 157, (2002)

239 Y. Hou, N. J. Renault, A. Zhang, J. Wan, A. Errachid and J.-M. Chovelon, *Sensors and Actuators B*, **86**, 143, (2002)

240 P. Pandey, S. P. Singh, S. K. Arya, V. Gupta, M. Datta, S. Singh and B. D. Malhotra, *Langmuir*, **23**, 3333, (2007)

241 K. Sawicka, P. Gouma, S. Simon, *Sensors and Actuators B*, **108**, 585, (2005)

242 S. K. Arya, P. R. Solanki, S. P. Singh, K. Kaneto, M. K. Pandey, M. Datta and B. D. Malhotra, *Biosensors and Bioelectronics*, **22**, 2516, (2007)

243 Ó. A. Loaiza, S. Campuzano, M. Pedrero, M. José and Pingarrón, *Talanta*, **73**, 838-844, (2007)

244 K. C. Grabar, R. G. Freeman, M. B. Hommer and M. J. Natan, *Analytical Chemistry*, **67**, 735, (1995)

245 M.-C. Daniel and D. Astruc, *Chemical Reviews*, **104**, 293, (2004)

246 A. L. Crumbliss, S. C. Perine, J. Stonehuerner, K. R. Tubergen, J. Zhao, R. W. Henkens and J. P. O'Daly, *Biotechnology and Bioengineering*, **40**, 483, (1992)

247 Y. Yang, Z. Wang, M. Yang, M. Guoa, Z. Wu, G. Shen and R. Yu, *Sensors and Actuators B*, **114**, 1, (2006)

Chapter 2

Experimental

"Insanity is doing the same thing, over and over again, but expecting different results." - *Albert Einstein*

2.1 Introduction

In this chapter the experimental techniques and apparatus employed during the course of this research are outlined. The procedures for the experiments undertaken are also detailed. In addition, an overview of the theories and related equations are described.

2.2 Experimental Techniques

The electrochemical and analytical techniques employed throughout this study were cyclic voltammetry, potentiostatic measurements, impedance measurements, ultraviolet-visible spectroscopy (UV-Vis), differential scanning calorimetry (DSC) and scanning electron microscopy (SEM) coupled with energy dispersive X-Ray analysis (EDX). A brief overview of each technique is given in this chapter.

2.2.1 Cyclic Voltammetry

Cyclic voltammetry (CV) is a very useful electroanalytical technique that can be used to obtain information about both simple and complicated electrode reactions. It is often one of the first experiments that is performed in an electroanalytical study and it is one of the most useful and widely applied techniques[1]. Cyclic voltammetry is performed by applying a sweeping potential to the working electrode between two chosen potential limits. This is done at a constant rate known as the scan rate, and the change in current is recorded. The initial applied potential, E_i, is swept to a vertex potential, E_v, then the scan is reversed and swept back to a final potential, E_f, which generally equates with the original (initial) potential, E_i. This process creates a cyclic effect and is usually repeated multiple times.

For a simple redox reaction, Equation 2.1, where only *R* is present, the current response of the forward scan is the linear potential sweep voltammogram as *R* is oxidised to *O* which produces an anodic peak. On the reverse scan, the reduction of *O* to *R* occurs, resulting in a cathodic peak. A plot of applied potential versus current is used to depict such generated cyclic voltammograms, Figure 2.1.

$$O + ne^- \rightleftharpoons R \qquad 2.1$$

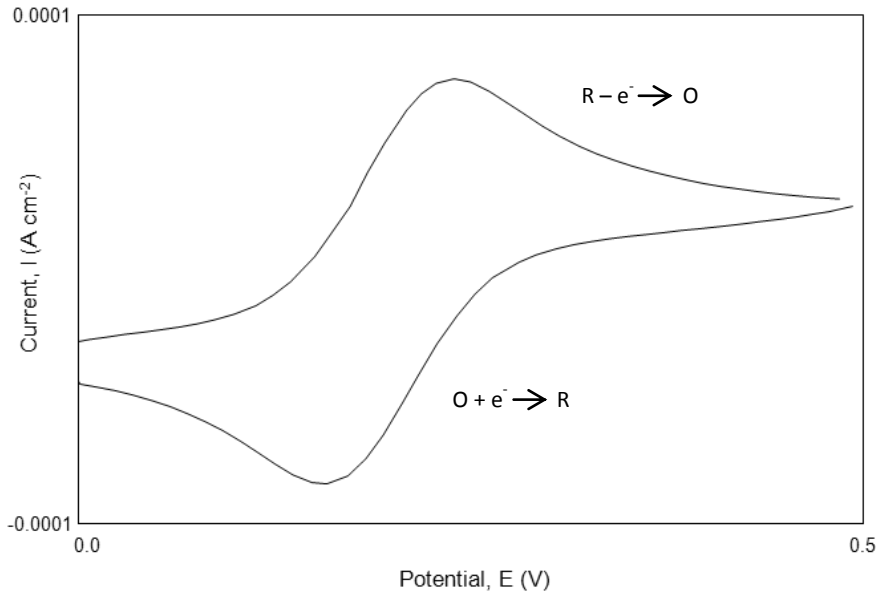

Figure 2.1: Typical current-potential profile for a cyclic voltammogram of a reversible redox species.

Cyclic voltammetry was used primarily in the study of the electrochemical behaviour of the polymers under various conditions, i.e., thickness and pH, in order to investigate the stability of the polymers under these parameters. The scan rate was varied from 5 to 300 mV s^{-1}, and the electrochemical window was generally in the range of -0.60 to 0.80 V vs. SCE. Further details on the kinetic information provided by the CV technique are provided in Section 2.7.

2.2.2 Potentiostatic Measurements

Potentiostatic measurements were utilised for a variety of different processes in this study. A potentiostatic mode was employed in order to grow the polypyrrole films doped with chloride anions (PPy-Cl), the polypyrrole films with bovine serum albumin (PPy-BSA) and the polymer films with the incorporated urease enzyme and the sulphonated-β-cyclodextrin (PPy-Urs-Cl, PPy-Urs-SCD and PPy-SCD). This was carried out by applying a constant potential to the working electrode in the monomer-containing electrolyte, initially for a fixed period of time, and then until a

desired charge/thickness of the polymer film was reached. The polymer was adherent to the electrode until a film thickness greater than 30 μm was reached. The growth of the polymer films was recorded by monitoring the current response (A cm^{-2}) as a function of time (s).

Both CV and potentiostatic techniques are routinely used in depositing polymer films and it is generally stated in the literature that the CV technique forms smoother polymer films[2]. However, in this experiment it was found that potentiostatic measurements were better for growing the polymers. By employing the potentiostatic mode, the polymers formed were smooth and the films were much more adherent to the working electrode in comparison to the films grown using the cyclic voltammetry method. The electrodeposition of polypyrrole using a potential step technique gives a well-defined chronoamperometric response, with a rising current-time transient during the initial stage, followed by decay in the current, to a near constant value[3]. These transients have been explained in terms of the nucleation of the polymer at the surface followed by three-dimensional growth[3]. It has also been shown that the initial polypyrrole nodules deposited at the electrode are isolated and randomly dispersed[3]. With continued time, the nodules grow in a three-dimensional manner to give an increasing number of grains on the surface. Depending on the potential applied a large number of nucleation sites can be generated to give a highly adherent polymer film.

In contrast, with cyclic voltammetry, the potential is swept across a large window, and the monomer becomes oxidised over a range of potentials to form the polymer. Hernandez-Perez *et al*.[4] followed, using AFM measurements, the formation of nano-sized polypyrrole nodules and their transformation into larger surface aggregates during CV measurements. This forms a rough surface and the polymer is less adherent to the electrode as it is being repeatedly oxidised and reduced. Indeed, Hernandez-Perez *et al*.[4] concluded that the potentiostatic method allows better control over the polymer growth giving a well-defined smooth surface.

2.2.3 Impedance Measurements

Electrochemical Impedance Spectroscopy (EIS) is a very useful method used to examine multiple factors at the surface of the working electrode. These factors can include the stability, kinetics and double layer capacitance of the working electrode, to name but a few[5]. Impedance measurements involve the application of a small perturbing sinusoidal voltage of 1 to 10 mV, which is superimposed on the fixed baseline potential or versus the open-circuit potential. Any shift that may occur in the phase and amplitude of this sinusoidal voltage will result in an AC current, which is as a result of variations occurring within the electrochemical cell.

The various components of the electrochemical cell are the determining factors in the overall impedance of a system. These components can include diffusion, passivating layers, electron-transfer kinetics and the solution resistance[5]. The relative contributions of these components tend to exhibit a variation with frequency; for example, diffusion may dominate at lower frequencies whereas electron-transfer kinetics can dominate at higher frequencies[5]. Electrochemical impedance spectroscopy is extremely useful as it allows measurements to be recorded over a wide frequency range, thus allowing multiple processes with varying time scales to be detected within the same experiment.

EIS results are expressed in two parts, real and imaginary, resulting from the shift in phase that arises as a result of the phase shift that occurs between the applied AC potential and the AC current response on the application of an AC potential to the electrochemical cell. These components are plotted on a vector diagram known as a Complex Plane or "Nyquist" plot, with the real component (Z') on the x-axis and the imaginary component (Z'') on the y-axis, as depicted in Figure 2.2 (a)[5].

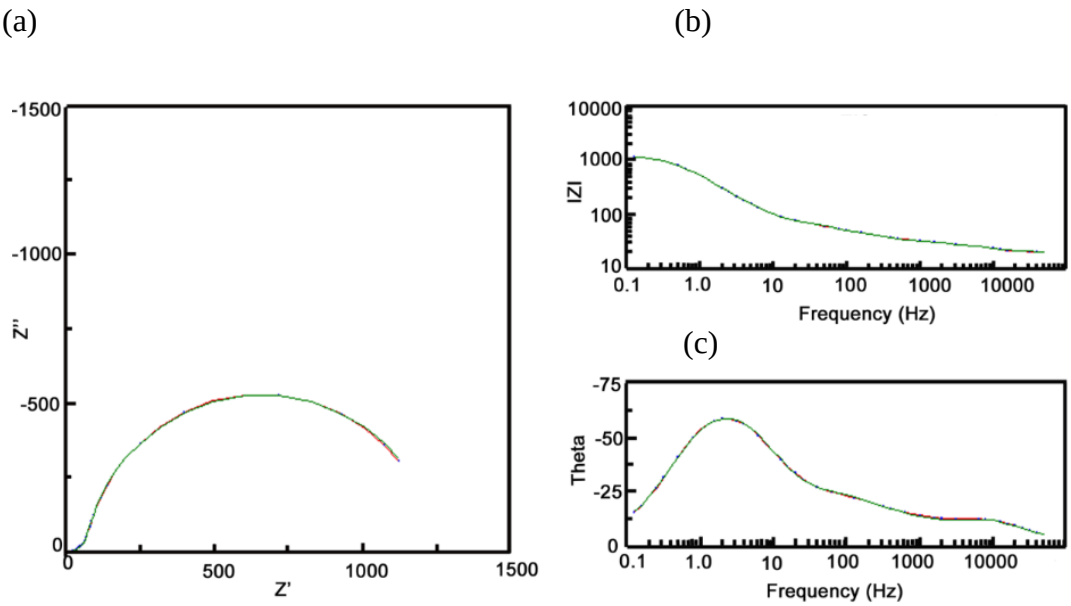

Figure 2.2: Example of a typical Complex Plane (or Nyquist) plot (a), Bode plot (b) and (c) with Z in units of Ω cm^2.

The experimental data may also be presented in the form of a Bode plot, as illustrated in Figure 2.2 (b) and (c). This displays the total impedance of the system, $|Z|$, on a logarithmic scale, typically in units of Ω and the phase angle, θ, as a function of the logarithmic of frequency. The total impedance, $|Z|$, is related to the real and imaginary components through Equation 2.2.

$$|Z| = \sqrt{Z_{real}^{\ 2} + Z_{imag}^{\ 2}} \qquad 2.2$$

For the purpose of this work, EIS measurements were carried out in order to obtain information on the capacitance and charge transfer resistance of the polymer films. The exact experimental conditions are described in detail in Section 3.3.2.8. However, in general, the polymer was conditioned for 30 min either at the open-circuit potential (OCP) or at a fixed applied potential, to ensure that a steady state was reached before measurements were performed. This was tested further by recording the impedance data from high to low frequencies, then reversing the sweep and recording the data from low to high frequencies. If no hysteresis was observed it was then concluded that steady-state conditions had been attained. A potential perturbation of 5 mV was used to ensure a pseudo-linear response of the system, while the frequency was varied from 65 kHz to 100 mHz.

The impedance response was modeled using Zview, a data modeling software package that is capable of modeling the data to appropriate equivalent electrical circuits using a non linear least squares fitting routine that considers both the real and the imaginary components of the data. The purpose of fitting the data to these equivalent circuit models is to mimic the actual impedance measurements with an equivalent electrical circuit which consists of resistors, capacitors and constant phase elements (semi-capacitors). The Zview software is designed to accurately model impedance data, whereby each circuit element in the model is selected to correspond to a real physical component in the electrochemical cell. In this work, estimated initial values were generated and these were used to build an electrical circuit, then the Zview software was used to refine these estimates using an iterative process to select alternative values that best fitted the experimental data.

The main electrical circuit elements used to model data were constant phase elements (CPE) and resistors (R). A resistor has no imaginary component; hence its value is equal to the impedance for the real component. The total resistance value is a combination of the value for the resistance elements in the electrolyte solution, which usually includes the solution resistance, (R_S) and the charge transfer resistance (R_{CT}). Constant phase elements (CPE) were used to determine the capacitance and/or the diffusional processes at the interface. In particular, the CPE was used instead of a pure capacitor as this allows for the inhomogeneity of the surface of the electrode to be taken into account. Equation 2.3 defines the impedance of a constant phase element, where ω is the angular frequency ($2\pi f$). The CPE is defined using two parameters; a magnitude term (T) and an exponent value (p). The exponent gives information on the physical processes that are occurring within the electrochemical cell; if the exponent value is equal to 1.0, it is correct to assume that the CPE is behaving as an ideal capacitor, however, values of 0.9 and higher are also acceptable capacitance components. The higher exponent values, $n > 0.95$, point to a relatively high degree of surface homogeneity, while lower values, $0.85 < n < 0.95$, indicate poor surface homogeneity, which may be related to a porous surface structure. On the other hand, an exponent value of 0.5 is consistent with a diffusion process; this coincides with a phase angle of 45°.

$$Z_{CPE} = \frac{1}{T(j\omega)^p} \qquad 2.3$$

By using various components in series or in parallel it is possible to create an appropriate equivalent electrical circuit model based on the physical system. Figure 2.3 shows the models that were designed in order to evaluate the data presented in this thesis. When this approach is used, it is very important that each element in the equivalent circuit element corresponds to an actual component of the electrochemical cell; otherwise the equivalent circuit has little or no meaning.

For this analysis, the simulated impedance was calculated based on the initial circuit parameters and values. This fit was then compared to the experimental data and the values of the circuit parameters modified, then the fit between the experimental and simulated data was re-evaluated. This iterative process was continued until there was a minimum difference between the simulated and experimental data. The percentage errors shown in Figure 2.3 give the percentage by which the circuit element can be modified without any loss in fit between the simulated and the experimental data, which, in turn, gives the actual errors in the values of each circuit component. For simple circuits the error was maintained at 2% or lower. If higher errors were achieved, then an alternative circuit was considered. A higher percentage error of 5% was accepted for more complex models that contained a greater number of circuit elements.

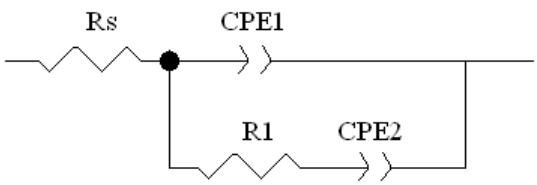

Element	Value	Error	Error %
Rs	192	1.70	0.88
CPE1-T	5.55×10^{-5}	5.12×10^{-6}	4.22
CPE1-P	0.585	0.014	2.10
R1	565	13.6	2.40
CPE2-T	7.66×10^{-4}	1.32×10^{-5}	1.73
CPE2-P	0.984	0.012	1.22

Figure 2.3: Typical equivalent circuit parameters and the data fitting routine, values and errors used to fit impedance data.

2.2.4 Ultraviolet-Visible Spectroscopy

Ultraviolet-visible (UV-Vis) spectroscopy is a very useful analytical technique as it can be used to determine the amount of substance present in a sample, and also to identify some chemical species. This is because the UV-Vis spectrometer measures the amount of ultraviolet and visible light that is transmitted or absorbed by a sample. The wavelength at which a chemical absorbs light is a function of its electronic structure and the intensity of this absorption is related to the amount of the sample between the light source and the detector. The measured absorbance is proportional to the concentration of the absorbing species given by the Beer-Lambert law, Equation 2.4; hence UV-Vis is also a well suited technique for the quantitative study of association constants.

$$A = \varepsilon bc \qquad 2.4$$

Here, A is the absorbance, ε is the molar absorbtivity, b is the path length and c is the concentration of the absorbing species. For the purpose of this study, UV-Vis spectroscopy was employed using a Varian Cary series spectrophotometer to investigate the stability of BSA in solution. For each measurement, a quartz crystal cuvette with a length of 1 cm, containing 3.0 mL of the sample solution, was used. The resolution of the spectrometer was 0.3 nm and the wavelength was scanned from 200 to 800 nm or from 200 to 400 nm at 300 nm min^{-1}.

2.2.5 Differential Scanning Calorimetry

Differential scanning calorimetry (DSC) is a very useful technique used to study the thermal properties and transitions of polymers. These transitions include the melting interval, decomposition, crystallisation and even the purity of the polymers[6]. The apparatus for DSC analysis is shown in Figure 2.4, whereby an aluminium pan containing the polymer is placed in the heating chamber close to an empty pan which acts as a reference. The furnace is set to increase or decrease the temperature at a fixed rate and the arrangement of the aluminium pans ensures that they are both at an identical temperature at all times. The DSC measures the energy that is required to

keep both aluminium pans at an identical temperature; hence the amount of heat absorbed or released by the polymer sample is recorded as the temperature is varied.

The measured data were recorded as the heat change expressed as heat flow (mW) as a function of the temperature (°C). For the purpose of these experiments, approximately 2.0 mg of polymer sample was heated from 25 °C up to 450 °C, at a constant rate of 10 °C min^{-1}, under an inert nitrogen atmosphere. The samples were then cooled from 450 °C back to 25 °C, again at a constant rate of 10 °C min^{-1}, using liquid nitrogen as the cooling agent, and a cyclic pattern was obtained. The instrument used was a Perkin Elmer Pyris 6.0 apparatus and the results were recorded and analysed using Pyris Data Analysis software; this depicts exothermic peaks as well shaped curves and endothermic peaks as bell shaped curves. This technique was utilised in order to investigate the thermal behaviour of the polymer doped with chloride anions and with the biological agents.

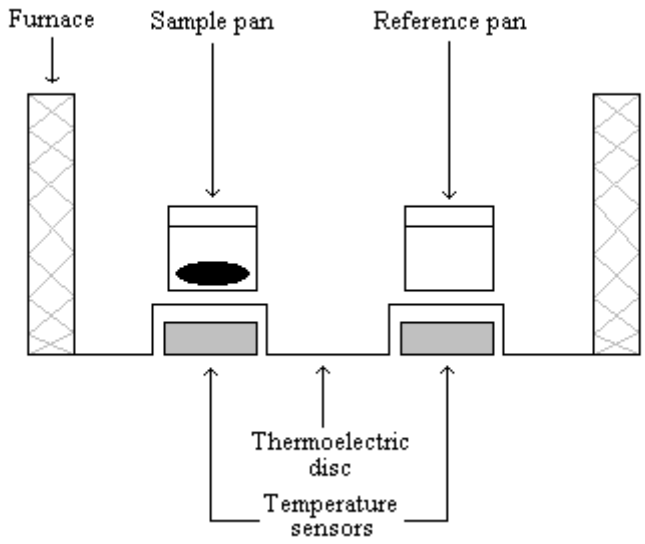

Figure 2.4: Schematic of the differential scanning calorimetry apparatus.

2.2.6 Scanning Electron Microscopy and Energy Dispersive X-Ray Analysis

The scanning electron microscope (SEM) is a microscope that uses electrons instead of light to form an image. It is generally used in order to generate high-resolution images of objects to reveal information about their surface morphology and

topography. These high-resolution images are generated by bombarding the surface of the sample under investigation with a high energy beam of primary electrons. This in turn causes the electrons from the sample to dislodge as secondary electrons. These secondary electrons are attracted to and detected by a positively charged detector and are then translated into signals which are amplified and analysed before being translated into understandable images. The sample preparation for SEM analysis is relatively easy as most SEM measurements only require the sample to be conductive, this can be done by coating the sample to be analysed with gold using a sputter coater[7]. The thickness is monitored using the principle of the quartz crystal microbalance; when sputtered material is deposited on an oscillating quartz crystal its frequency is decreased in relation to the mass of material deposited. In this way an exact thickness of material can be deposited onto the sample, which prevents the sample from becoming charged during SEM analysis.

The SEM is usually equipped with an energy dispersive X-Ray analysis (EDX) system in order to enable it to perform compositional analysis on specimens. This is done by measuring the omitted X-Rays from the sample when it is being bombarded with the primary electrons. The X-Ray energy is characteristic of the element from which it was emitted and as a result EDX analysis is very useful in identifying the chemical components of a sample[7]. The resolution of the EDX probe is given by the size of the volume of interaction between the electron beam and the sample. The size is usually a few microns. The EDX analysis can be affected by the surface roughness. The interaction of the electrons with the surrounding zones of the probed point can cause the emission of X-Rays that add to the signal belonging to the point of analysis. The extent of such interference is a major limitation that compromises the precision of any quantitative analysis. A quantitative EDX analysis is possible but only with high-quality flat-polished sample surfaces, and standards prepared and analysed in the exact same way. Semi-quantitative analysis is possible by comparing the relative peak heights from the sample and a standard of known composition measured under the same conditions.

For the purpose of this study, EDX was used to prove the presence of the BSA and urease in the PPy-BSA and PPy-Urs polymer films, respectively. The samples for SEM and EDX were prepared by growing the polymers onto a flat platinum electrode at varied potentials for different times, then dried in air overnight. The

non-conducting samples were sputter coated with gold using an Agar auto sputter coater until a layer of 50-100 nm in thickness was applied. The acceleration voltage applied during SEM and EDX analysis was 20 keV.

2.3 Instrumentation, Software and Ancillary Equipment

Potentiostatic and cyclic voltammetry experiments were carried out using a Solartron Potentiostat Model 1287. This used Scribner Associates CorrWare for Windows Version 3.0, and the resulting data were analysed using Scribner Associates CorrView for Windows Version 3.0. The impedance experiments were carried out using a Solartron Frequency Response Analyser Model 1255B, in conjunction with the Solartron Potentiostat Model 1287. The impedance data were recorded using Scribner Associates ZPlot for Windows Version 3.0 and analysed using Scribner Associates ZView for Windows Version 3.0. The remaining apparatus information is outlined in Table 2.1. General analysis of data and plotting of calibration curves were performed in Microsoft Excel 2007 and an overview of the ancillary equipment used throughout this study is given in Table 2.2.

Table 2.1: Analytical techniques used with model information.

Analytical Technique	Model
UV-Vis Spectroscopy	Varian Cary 50 UV-Vis Spectrometer
Differential Scanning Calorimetry	Perkin Elmer Pyris 6.0
SEM	Leica Stereoscan 440 / Joel 840 SEM / Hitachi S400
EDX	Tescan Mira XMU VPFE

Table 2.2: Ancillary equipment used with model information.

Equipment	Model
Sonicator	Branson 1510
Electronic Balance	Sartorius Models TE612 and TE124S
pH Meter	Orion Model 720A
Conductivity Meter	Jenway 4510
Gold Sputter Coater	Emitech K550x / Agar Scientific

2.4 Chemicals and Solutions

The chemicals used throughout this study were purchased from Sigma-Aldrich or its subsidiary company Fluka. All chemicals were used as supplied expect for pyrrole which was vacuum-distilled and stored in the dark at -20 °C prior to use, and the bovine serum albumin solution which came pre-prepared as a 30 % BSA in a saline solution. In order to use this BSA solution, all the experiments were recorded using a fixed volume of BSA solution (ranging from 25 μL to 200 μL) in a 10 mL monomer solution, unless otherwise stated. The concentration of the BSA is then expressed as a volume, being μL of BSA (30%)/10 mL of solution. This is kept constant for all the results that are presented, keeping in context with the literature[8] that presents the concentration of BSA as a volume and in a similar way. All other solutions were made from stock solutions of 0.10 mol dm^{-3} NaCl or 0.05 mol dm^{-3} phosphate buffer, pH 7.0, which were initially prepared using distilled water, as stated in the figure captions or the main text. All the amino acid and interfering compound solutions were prepared freshly before each experiment. Where necessary, the pH of the solutions was altered using concentrated HCl or NaOH. All experiments were performed at room temperature.

2.5 The Electrochemical Cell Setup

A standard three-electrode electrochemical cell configuration was employed for all electrochemical experiments. This consists of a working electrode (WE), a reference electrode (RE) and finally a counter/auxiliary electrode (CE), as shown in Figure 2.5.

The WE used was generally a commercial platinum (Pt) disc supported inside a Teflon® holder, the CE consisted of a high surface area Pt wire, and the RE was a saturated calomel electrode (SCE). This cell was then connected to a potentiostat and the results were recorded by a computer in the manner shown in Figure 2.6. In general, the potential is measured between the RE and the WE and the current is measured between the WE and the CE.

Care was taken to ensure that all electrodes were free from impurities and that all connections had negligible resistance. The working electrodes were prepared from a 1.5 cm length of the Pt rod (purity 99.99 %) obtained from Goodfellow Cambridge Ltd. This was set in a Teflon® holder with epoxy resin. The electrical contact was made with a copper wire attached using a highly conducting silver-loaded resin. The quality of the electrical contact was checked with a multimeter to ensure that the resistance between the surface of the electrodes and the connection to the potentiostat was lower than 1 Ω. Prior to each experiment, the working electrodes were polished to a mirror finish using 30, 15, 6 and 1 μm diamond suspensions on microcloth (Buehler), sonicated in distilled water and then in ethanol, and finally rinsed with distilled water. The reference electrodes were serviced regularly by changing the internal filling solution with a saturated solution of super-purum KCl (99.999+ %), and by checking the open-circuit potential against an unused SCE. Unless otherwise stated, all potentials in the figures are relative to the SCE reference electrode. The counter electrodes were brushed regularly with silicon carbide based abrasive paper (Buheler P2500), smoothed, cleaned and sonicated in distilled water.

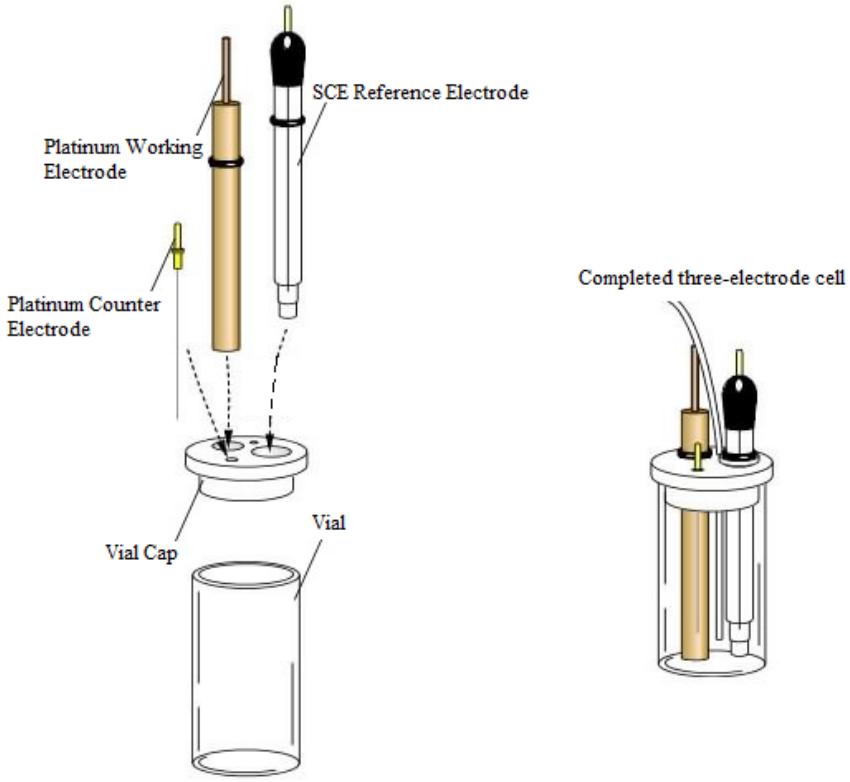

Figure 2.5: A schematic of the three-electrode cell used for electrochemical measurements.

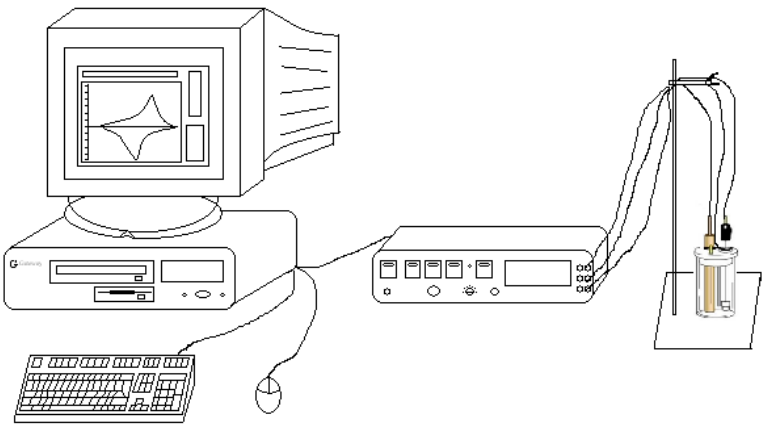

Figure 2.6: A schematic of the experimental setup used to record all electrochemical measurements.

2.6 Fabrication and Characterisation of the Polypyrrole Films

In general, the PPy films were electrosynthesised at the working electrode at 0.70 V vs. SCE from an aqueous solution of 0.50 mol dm^{-3} pyrrole monomer and 0.10 mol dm^{-3} NaCl or 0.02 mol dm^{-3} sulphonated-β-cyclodextrin, typically until a charge of 0.74 C cm^{-2} was reached. Any variation in the potentials, charge passed or polymer forming electrolyte is presented in the figure captions or corresponding text in the results section. The morphology and chemical composition of the PPy films were analysed using scanning electron microscopy (SEM) and energy dispersive X-Ray analysis (EDX). The samples were sputter-coated with gold prior to SEM imaging only where stated.

2.7 Kinetic Analysis

The cyclic voltammetry technique is a very useful tool as mentioned in Section 2.2; however, in addition to this it can also provide information on the kinetics of a system. The voltammogram response at varied scan rates can reveal kinetic information concerning the electrocatalytic process, including diffusion and adsorption effects, and it can also be used to determine the reversible behaviour of a system. For a reversible system, the factors that can influence the behaviour and magnitude of the peak current can be described by the Randles-Sevcik equation, Equation 2.5. A reversible cyclic voltammogram will only be observed when both the oxidation and reduction species are uniquely stable and if the electron-transfer occurs at a fast rate[9].

$$i_p = (2.69 \times 10^5) n^{3/2} D^{1/2} v^{1/2} c_o \qquad 2.5$$

Here, i_p is the peak current (A cm^{-2}), n is the electron stoichiometry, D is the diffusion coefficient (cm^2 s^{-1}), v is the scan rate (V s^{-1}) and c_o is the concentration (mol cm^{-3}).

It can be seen from the Randles-Sevcik equation that the peak current, i_p, is directly proportional to the concentration of the electroactive species in the system and also to the square root of the scan rate and diffusion coefficient. Therefore, a linear

relationship between the current and the square root of the scan rate is indicative that the redox reaction conforms to the Randles-Sevcik equation and hence is governed to some extent by a diffusion-controlled process. As a result, the redox reaction process is considered to be adsorption free. If a plot of the peak current against the square root of the scan rate yields a straight line, the diffusion coefficient can then be determined from the slope of this line when the electron stoichiometry, concentration and area of the electrode are known. This equation was used in Section 6.3.1 in order to determine the diffusion coefficient of urea at a glassy carbon electrode.

When a straight line is obtained from the Randles-Sevcik equation which correlates with a reversible system, it can then be assumed that the reversible system will follow other patterns also. Assuming that the system is reversible, there are tests that can be applied to the system that should be satisfied over a wide range of scan rates. For example, the ratio of the forward and reverse peak currents for a reversible system should be equal to unity, i.e., 1, Equation 2.6, and they are independent of scan rate. The peak separations should comply with Equation 2.7 and the difference in the peak potentials and the half-wave peak potentials should satisfy Equation 2.8. If any of these equations are not satisfied, this means that the electron transfer is not reversible under the conditions of the experiment and that the process is more complex[9].

$$\frac{i_p^A}{i_p^C} = 1 \qquad 2.6$$

$$\Delta E_p = E_p^A - E_p^C = \frac{59}{n}\, mV \qquad 2.7$$

$$E_p - E_{p/2} = \frac{59}{n}\, mV \qquad 2.8$$

Here, i_p^A is the oxidation peak current, i_p^C is the reduction peak current, E_p^A is the peak potential of the oxidation peak, E_p^C is the peak potential of the reduction wave, $E_{p/2}$ is the half-wave potential and n is the number of electrons transferred[9]. If the electron transfer is not taking place within the timescale of the experiment, i.e., the

rate of electron transfer is too slow, the system can be said to be irreversible. The main characteristic of an irreversible system is the absence of a reverse peak in the cyclic voltammogram. The peak current of an irreversible system can be described by Equation 2.9, where n_α is the number of electrons transferred up to and including the rate-determining step and α_c is the charge-transfer coefficient of the reverse reaction.

$$i_p = (2.99 \times 10^5) n(\alpha_c n_\alpha)^{1/2} c_o D^{1/2} v^{1/2} \qquad 2.9$$

In addition to this, for an irreversible system, although the oxidation peak currents are proportional to the square root of the scan rate, the peak potentials shift by $30/\alpha_c n_\alpha$ mV for each decade change in v. Also, the difference in the peak potentials and the half wave peak potential comply with Equation 2.10[9].

$$E_p - E_{p/2} = \frac{48}{\alpha_c n_\alpha} mV \qquad 2.10$$

When the system is neither totally reversible nor irreversible, a quasi-reversible system can exist between these two extremes. The kinetics of a quasi-reversible system are not very fast or very slow and both the forward and reverse reactions make a contribution to the peak current, which increases with the square root of the scan rate, as shown in Equation 2.5. However, at high scan rates where the standard rate constant, k^θ, is slow, the peak current is no longer proportional to the square root of the scan rate.

Just as with a totally reversible system, the ratio of the peak oxidation and reduction currents of a quasi-reversible system should equate to unity, provided that α_C and α_A are both equal to 0.5. The anodic and cathodic peaks are separated by more than 59/n mV and this separation increases with increasing scan rate, as the peak potential shifts[9]. These characteristics are summarised in Table 2.3.

Table 2.3: Reversible and quasi-reversible systems.

Reversible	Quasi-reversible
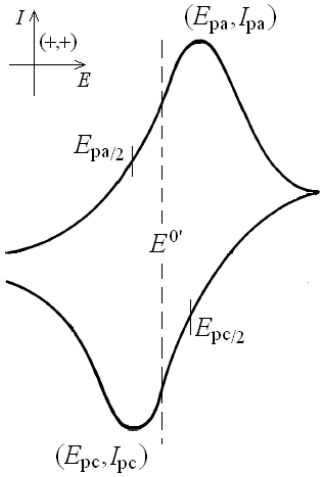	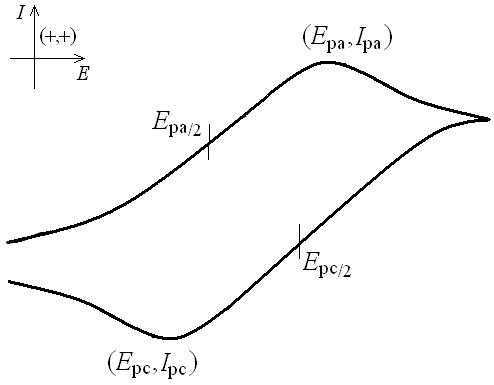
$I_p \propto \upsilon^{1/2}$	I_p not always proportional to $\upsilon^{1/2}$ as υ increases
E_p independent of υ	$\lvert E_p \rvert$ increases as υ increases
$\Delta E_p = 59/n$ mV	$\Delta E_p > 59/n$ mV

2.8 Complexation Studies

In order to evaluate complexation between the cyclodextrins and the urea and interfering compounds and to determine the stoichiometric values of these complexes, the formation constant and Job's method were employed using CV[10]. The related theory behind each of the equations used in this analysis is described in detail in this section.

2.8.1 Job's Method

It is imperative to determine the stoichiometry of the complex before any structural or associative measurements are performed on a host-guest interaction. A well known method of determining the stoichiometry of the complex is the commonly known continuous variation method or Job's method[11,12]. This is an experimental mixing technique widely used in the determination of stoichiometric ratios of each

constituent involved and can be applied to various techniques such as fluorescence, UV-Vis, NMR and electrochemical techniques, provided that either the guest or host molecule are electrochemically active[13,14,15].

The Job's plot method involves the preparation of a series of solutions whereby the sum of the guest and host concentrations is kept constant, but the mole fraction is changed[16]. This is achieved by mixing different volumes of equal concentrations of the guest and host molecules so that the overall volume remains the same, as shown in Table 2.4. The physicochemical parameter whose value changes when the guest and host molecules form a complex is measured in each solution. For example, the absorbance values may change for either the guest or host molecule when monitored using UV-Vis, there may be chemical shifts in the NMR spectra, or peak potential shifts in cyclic voltammetry.

Table 2.4: Solutions used in Job's analysis where the sum of the guest and host concentrations is kept constant, but the mole fraction is changed. Concentration of both the guest and host stock solution is 1.0 x 10^{-2} mol dm^{-3}.

Solution number	Volume of host molecule (mL)	Volume of guest molecule (mL)	Mole fraction of guest
1	10.0	0.0	0.0
2	9.0	1.0	0.1
3	8.0	2.0	0.2
4	7.0	3.0	0.3
5	6.0	4.0	0.4
6	5.0	5.0	0.5
7	4.0	6.0	0.6
8	3.0	7.0	0.7
9	2.0	8.0	0.8
10	1.0	9.0	0.9
11	0.0	10.0	1.0

For the purpose of this analysis, cyclic voltammetry was used to generate the Job's plots for urea in the presence of the sulphonated-β-cyclodextrin (SCD). The change of the property, i.e., the change in the electrochemical behaviour in the presence and absence of the sulphonated-β-cyclodextrin host, was calculated by subtracting the

currents recorded at a fixed potential from those of an equal concentration of free guest, Equation 2.11. This product is then plotted as a function of the mole fraction to generate the Job's plot. The stoichiometry of the complex is determined from the x-coordinate at the maximum value of the Job's curve[17].

$$\Delta I = I_{Guest} - I_{Guest+Host} \qquad 2.11$$

Cyclic voltammetry was also used to investigate the formation of an inclusion complex between urea and the sulphonated-α-cyclodextrin.

2.8.2 Formation Constants

Cyclodextrins are well known to form inclusion complexes in aqueous solutions[18,19,20]. The equilibrium that is established between the host and guest molecules is expressed as the complex formation, equilibrium, stability or binding constant and is denoted as K_f[21]. In complexation studies, the simplest method for the determination of the formation constant for a 1:1 inclusion complex is based on the equilibrium equation shown in Equation 2.12.

$$CD + G \rightleftharpoons CD.G \qquad 2.12$$

Here, *G* represents the guest molecule, *CD* represents the host molecule and *CD.G* represents the inclusion complex formed. From Equation 2.12, the formation constant can be defined as:

$$K_f = \frac{[CD.G]}{CD\ [G]} \qquad 2.13$$

where [*G*] and [*CD*] are the equilibrium concentrations of the guest and host molecules, respectively.

The formation of an inclusion complex between a guest and host molecule can be monitored electrochemically or spectroscopically, as the encapsulation of the guest inside the cyclodextrin cavity leads to alterations in the physical and chemical properties of the guest. Consequently, it is possible to calculate the formation constant by monitoring these changes. However, this depends on approximations; in this case, the two main approximations are that the host is always in excess of the guest and, that the stoichiometric value is a 1:1 ratio for the guest:host inclusion complex. The simplest way of calculating the formation constant is by keeping the concentration of the guest constant while changing the concentration of the host. This allows the host to be always in excess of the guest, and allows for this approximation to then be valid.

The formation of an inclusion complex between the cyclodextrin and a redox-active guest molecule can be monitored using an electrochemical approach such as CV or RDV. In this study, Chapter 6, the currents at a fixed potential were measured in the presence and absence of a large excess of the sulphonated-β-cyclodextrin (SCD). As the cyclodextrin is large in comparison to the guest, the included guest will diffuse more slowly than the free guest which, in turn, gives rise to a reduction in the currents at a fixed potential. The formation constant for the inclusion complex was calculated by monitoring the changes in the currents and then the data were fitted to Equation 2.14[10,14].

$$\frac{1}{[SCD]} = K_f \frac{(1 - A)}{(1 - \frac{i}{i_0})} - K_f \qquad 2.14$$

Here, [SCD] is the concentration of the sulphonated-β-cyclodextrin, i_0 and i are the currents recorded at a fixed potential in the absence and presence of SCD, respectively and A is a constant. Each experiment was performed a minimum of six times (n = 6).

2.9 References

1 J. Bard and L. R. Faulkner, *Electrochemical Methods: Fundamentals and Applications*, John Wiley & Sons, Inc., 833, (2001)

2 W.-S. Huang, B. D. Humphrey and A. G. MacDiarmid, *Journal of the Chemical Society, Faraday Transactions 1*, **82**, 2385, (1986)

3 T. de Lincona-Sanchez, G. A. Alvarez-Romero, L. H. Mendoza-Huizar and C. A. Galan-Vidal, *Journal of Physical Chemistry*, **114**, 9737, (2010)

4 T. Hernandez-Perez, M. Morales, N. Batina and M. Salmon, *Journal of the Electrochemical Society*, **148**, C369-375, (2001)

5 E. Barsoukov and J. E. Macdonald, *Impedance Spectroscopy. Theory, Experiment and Applications*, 2nd ed.; Wiley-Interscience, (2005)

6 G. W. H. Höhne., W. F. Hemminger and H. J. Flammersheim, *Differential Scanning Calorimetry*, Springer, (2003)

7 J. Goldstein, D. E. Newbury, P. Echlin, C. E. Lyman, D. C. Joy, E. Lifshin, L. Sawyer and J. R. Michael, *Scanning Electron Microscopy and X-Ray Microanalysis*, Springer, 689, (2003)

8 J. Wang, J. Wu, Z. H. Zhang, X. D. Zhang, L. Wang, L. Xu, B. D. Guo, H. Li and J. Tong, *Chinese Chemical Letters*, **16**, (8), 1105, (2005)

9 R. Greef, R. Peat, L. M. Peter, D. Pletcher and J. Robinson, *Instrumental Methods in Electrochemistry*, T. J. Kemp, Ellis Horwood Limited, 443, (1985)

10 G.-C. Zhao, J.-J. Zhu, J.-J. Zhang and H.-Y. Chen, *Analytica Chimica Acta*, **394**, 337, (1999)

11 A. Dimitrovska, B. Andonovski and K. Stojanoski, *International Journal of Pharmaceutics*, **134**, 213, (1996)

12 C. Y. Huang, R. X. Zhou, D. C. H. Yang and P. B. Chock, *Biophysical Chemistry*, **100**, 143, (2003)

13 H. Dodziuk, *Cyclodextrins and their Complexes: Chemistry, Analytical Methods, Applications*, Wiley-VCH, 489, (2006)

14 M. S. Ibrahim, I. S. Shehatta and A. A. Al-Nayeli, *Journal of Pharmaceutical and Biomedical Analysis*, **28**, 217, (2002)

15 C. Yanez, L. J. Nunez-Vergara and J. A. Squella, *Electroanalytical Chemistry*, **15**, 1771, (2003)

16 A. Sayago, M. Boccio and A. G. Asuero, *International Journal of Pharmaceutics*, **295**, 29, (2005)

17 S. Letellier, B. Maupas, J. P. Gramond, F. Guyon and P. Gareil, *Analytica Chimica Acta*, **315**, 357, (1995)

18 J.-F. Bergamini, M. Belabbas, M. Jouini, S. Aeiyach, J.-C. Lacroix, K. I. Chane-Ching and P.-C. Lacaze, *Journal of Electroanalytical Chemistry*, **482**, 156, (2000)

19 A. Bernini, O. Spiga, A. Ciutti, M. Scarselli, G. Bottoni, P. Mascagni and N. Niccolai, *European Journal of Pharmaceutical Sciences*, **22**, 445, (2004)

20 X.-J. Dang, M.-Y. Nie, T. Jian and H.-L. Li, *Journal of Electroanalytical Chemistry*, **448**, 61, (1998)

21 K. Hirose, *Journal of Inclusion Phenomena and Macrocyclic Chemistry*, **39**, 193, (2001)

Chapter 3

Formation and Characterisation of PPy-BSA and its Interactions with Tryptophan and Ascorbic Acid

"Personally, I'm always ready to learn, although I do not always like being taught." - *Sir Winston Churchill*

3.1 Introduction

There is much interest in the use of conducting polymers, such as polyaniline and polypyrrole, as supporting matrices for biological species[1,2]. As the monomer that forms the conducting polymer is oxidised, a lattice type structure is created whereby the oxidised positively charged polymer incorporates a negative ion to counterbalance the charge produced upon oxidation. This continues as the monomer becomes further oxidised, forming layer upon layer of positively charged polymer and negative anions. This lattice type matrix is therefore highly suitable to the incorporation of other species, such as proteins and enzymes. This is important in the fabrication of biosensors as the biological recognition element can easily be incorporated into the conducting polymer matrix and then used as a biosensor[3,4,5].

In order to investigate the suitability of conducting polymers as supporting matrices towards a biological element, polypyrrole (PPy) was chosen as the conducting polymer. This chapter describes the growth of polypyrrole using a common dopant anion, Cl^-, which gives a polypyrrole film doped with chloride anions, PPy-Cl. In addition, the effect of introducing a biological element into the monomer solution was investigated. The protein, bovine serum albumin (BSA), was chosen for this investigation as BSA is a relatively large protein of 66,000 Da containing over 630 amino acid residues[6]. Furthermore, BSA contains disulphide bonds, which make detection of the protein relatively simple using energy dispersive X-Ray (EDX) analysis, as the presence or absence of sulphur in the polymer film can be used to provide direct evidence of the presence or absence of the BSA. Finally, BSA was chosen as it is used as a model protein and it is readily available and reasonably inexpensive[7,8].

3.2 Experimental

The instrumentation and software employed for the experiments detailed in this chapter and their analysis are described in Section 2.3. The chemicals used throughout this study were purchased from Sigma-Aldrich or its subsidiary company Fluka. All chemicals were used as supplied expect for pyrrole which was vacuum-distilled and stored in the dark at -20 °C prior to use. All other solutions were made

from a stock solution of 0.10 mol dm^{-3} NaCl, which was initially prepared using distilled water. The bovine serum albumin solution as provided was very viscous, as such, this was diluted down using a 0.10 mol dm^{-3} NaCl solution; all concentrations of BSA are hence given as the volume of BSA (in μL) in 10 mL of 0.10 mol dm^{-3} NaCl. All of the solutions were freshly prepared before each experiment. Where necessary, the pH of the solutions was altered using concentrated HCl or NaOH. All experiments were performed at room temperature. Electrochemical impedance spectroscopy (EIS) measurements were carried out in a solution of 0.10 mol dm^{-3} NaCl, whereby the polymer film was initially conditioned for 30 min either at the open-circuit potential (OCP) or at a fixed applied potential, to ensure that a steady state was reached before measurements were performed. The impedance data were then recorded, initially from high to low frequencies, then reversing the sweep and recording the data from low to high frequencies. A potential perturbation of 5 mV was used to ensure a pseudo-linear response of the system, while the frequency was varied from 65 kHz to 100 mHz. The data were finally fitted to equivalent circuit models to mimic the actual impedance measurements with an equivalent electrical circuit which consists of resistors, capacitors and constant phase elements.

3.3 Results and Discussion

Polypyrrole is used extensively in the development of sensors due to it being biocompatible, redox active, easy to form, readily available and inexpensive to manufacture [9,10,11,12,13]. Because of the unique properties of the polymer, it is possible to incorporate biological species, such as enzymes and proteins, into the polymer matrix[3,14]. The first biological species that was incorporated into the polypyrrole film was the protein, bovine serum albumin (BSA). For comparative purposes, polypyrrole-chloride (PPy-Cl) was also studied. Polypyrrole-chloride (PPy-Cl) and polypyrrole-bovine serum albumin (PPy-BSA) were grown in a typical three-electrode electrochemical cell, as shown in Chapter 2, Figure 2.6, using a platinum (Pt) working electrode, a Pt wire counter electrode and a saturated calomel reference electrode.

3.3.1 Factors Affecting the Growth of PPy-Cl and PPy-BSA

A number of parameters affect the growth of polypyrrole[15,16,17,18]. Consequently, various experiments were carried out to investigate the growth of the biological-modified polymer film, PPy-BSA. These experiments included varying the concentration of the pyrrole monomer in solution, the concentration of the biological species, the applied potential, and the electropolymerisation charge. The presence of a supporting electrolyte in the monomer solution was also explored to investigate what effect, if any, it had on the growth of the polymer films.

3.3.1.1 Influence of the Concentration of Pyrrole

As BSA is a large globular protein, the first set of experiments involved selecting the appropriate concentration of the pyrrole monomer. In the absence of BSA, it is well known that an increase in the pyrrole concentration gives rise to an increase in the rate of electropolymerisation[19]. This is clearly shown in Figure 3.1, where current-time plots, recorded at 0.70 V vs. SCE in a 0.10 mol dm^{-3} NaCl solution with pyrrole concentrations varying from 0.02 to 0.60 mol dm^{-3}, are presented and compared. It can be seen that the concentration of the pyrrole monomer has a significant influence on the growth of the polypyrrole (PPy) films in the presence of Cl^- ions. On application of the potential, there is an initial rapid decrease in the current, which arises from the charging of the double layer. This charging current decays rapidly, being governed by the RC time constant, which is related to the size of the electrode and the conductivity of the solution[20]. This is then followed by a slower rise, at about 2 - 5 s, as the polypyrrole film begins to nucleate and deposit at the surface of the working electrode. At longer times, greater than 250 s, the current reaches a steady state for the lower pyrrole concentrations. However, there is a further more gradual increase in the current as the polymer becomes deposited onto the working electrode, with pyrrole concentrations higher that 0.30 mol dm^{-3}. Furthermore, the rate of this increase and the measured currents are higher with higher concentrations of monomer, Figure 3.2, which is consistent with higher deposition rates and larger surface areas[8,21].

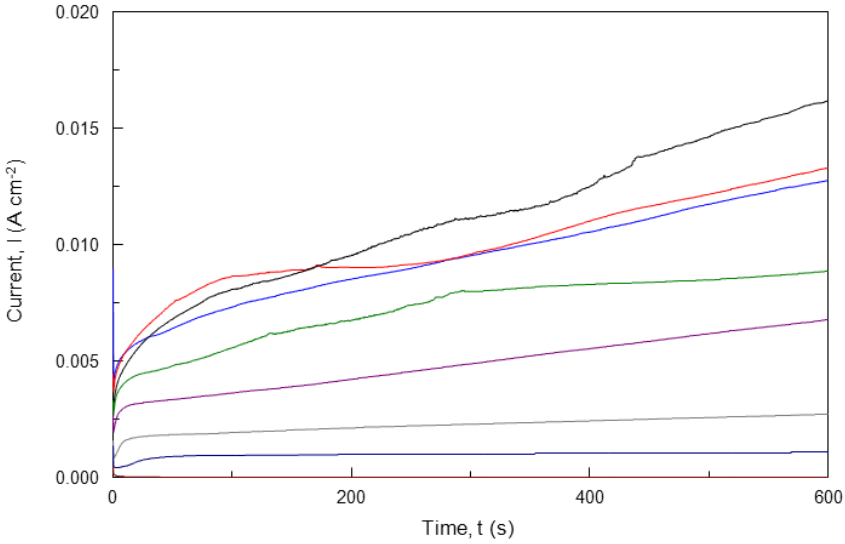

Figure 3.1: Current-time plots for the formation of PPy-Cl on a Pt electrode at 0.70 V vs. SCE from a solution containing 0.10 mol dm^{-3} NaCl, and — 0.60 mol dm^{-3} pyrrole — 0.50 mol dm^{-3} pyrrole — 0.40 mol dm^{-3} pyrrole — 0.30 mol dm^{-3} pyrrole — 0.20 mol dm^{-3} pyrrole — 0.10 mol dm^{-3} pyrrole — 0.05 mol dm^{-3} pyrrole and — 0.02 mol dm^{-3} pyrrole.

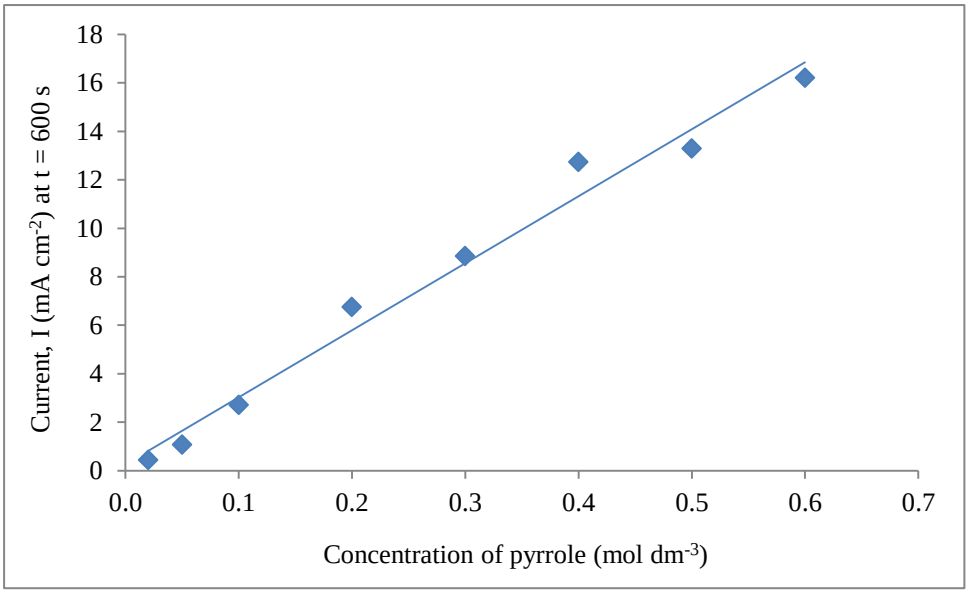

Figure 3.2: Current measured at 600 s plotted as a function of the concentration of pyrrole for the formation of PPy-Cl on a Pt electrode at an applied potential of 0.70 V vs. SCE.

This is clearly shown in Figure 3.2 and Table 3.1, where the current measured at 600 s, reaches 16.20 mA cm^{-2} with a pyrrole concentration of 0.60 mol dm^{-3}, but is lower for the lower pyrrole concentrations and continues to decrease as the pyrrole concentration is lowered. At the higher concentrations, the polymer forms rapidly and may contain multiple defects or deformities, leading to a loss in the sensing ability[21,22]. However, the currents recorded during the electropolymerisation in 0.02 mol dm^{-3} pyrrole are significantly lower, indicating inefficient formation of the polymer. This is probably connected with the formation of short chain oligomers, due to the low concentration of the monomer at the electrode surface. This, in turn, will give a polymer film with low conductivity. The formation of these short chain oligomers, resulting from an inadequate concentration of monomer in solution, has been well documented in the growth of conducting polymers, particularly in the case of polyaniline[8,22,23].

On addition of BSA to the electropolymerisation solution, the rate of electropolymerisation was altered, decreasing as the concentration of BSA was increased. Although these high pyrrole concentrations, > 0.30 mol dm^{-3}, are not suitable for the growth of PPy-Cl, giving very high rates of electropolymerisation, Figure 3.1, these concentrations were suitable in the presence of BSA, giving efficient and reproducible electropolymerisation conditions.

Table 3.1: Current at time, t = 600 s for the formation of PPy-Cl on a Pt electrode at 0.70 V vs. SCE as a function of the monomer concentration.

Concentration of pyrrole (mol dm^{-3})	**Current at time, t = 600 s (mA cm^{-2})**
0.60	16.20
0.50	13.29
0.40	12.74
0.30	8.85
0.20	6.75
0.10	2.71
0.05	1.08
0.02	0.44

3.3.1.2 Influence of the Concentration of BSA

The stability of BSA in the 0.10 mol dm^{-3} NaCl solution was explored prior to any electropolymerisation reactions. The concentrated BSA solution was diluted with 0.10 mol dm^{-3} NaCl to give 200 µL of BSA in 10 mL of 0.10 mol dm^{-3} NaCl and then the absorbance of the BSA-containing solution was monitored as a function of time, by recording a UV-Vis spectrum every 30 min for 13 h. The absorbance, recorded at 280 nm, was plotted against time, and is shown in Figure 3.3. The absorbance remains constant at 0.69 for about 4 h and then there is a slight increase for the remaining 9 h. However, this increase is small and there are no indications that the BSA is denatured during this 13 h period. It was not possible to monitor the absorbance of BSA in the presence of pyrrole, as the pyrrole monomer absorbs at similar wavelengths; however, it is clear that the BSA is stable for extended periods in the 0.10 mol dm^{-3} NaCl solution.

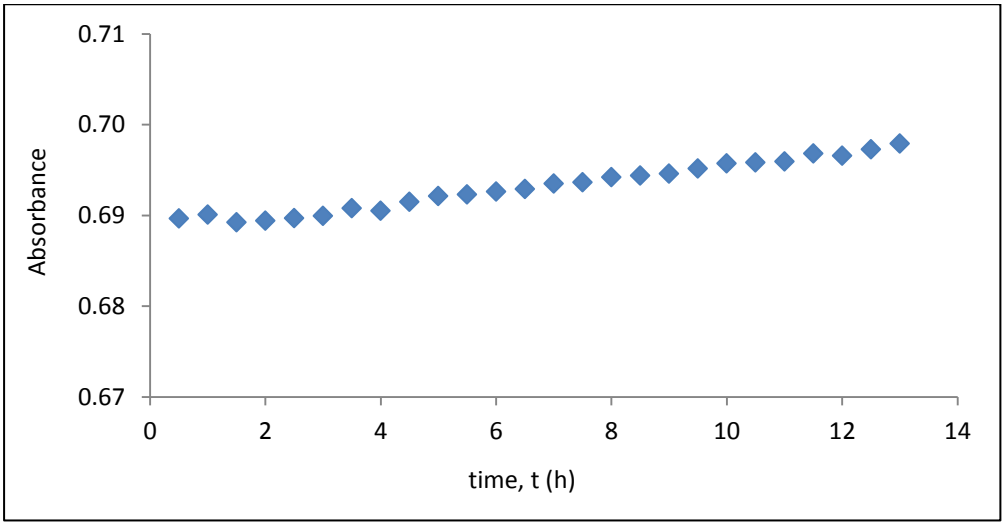

Figure 3.3: Absorbance of BSA, at 280 nm, dissolved in 0.10 mol dm^{-3} NaCl, plotted as a function of time.

The PPy-BSA films were electrosynthesised on a platinum working electrode by applying a constant potential of 0.70 V vs. SCE from monomer solutions where the concentration of pyrrole was kept constant at 0.50 mol dm^{-3} and the concentration of BSA was varied. In Figure 3.4, current-time plots are shown for increasing concentrations of BSA, while for comparative purposes, the plot recorded in the absence of BSA, is included. It can be seen from Figure 3.4 that as the BSA concentration is increased, the current density recorded during electropolymerisation

is reduced. This is due to the size and viscosity of the BSA. The BSA is a large globular protein that inhibits access of the monomer to the electrode surface[24]. This is very evident during the first few seconds of electropolymerisation, where the rate at which the current increases is considerably reduced in the presence of the BSA. Indeed, for the higher BSA concentrations, the current only increases after a considerable time period, typically 50 s, giving an induction period. This is consistent with a reduction in the concentration of the radical cations, dimers and other short chain oligomers that are generated during the oxidation of the pyrrole[24]. Longer time periods are required to generate a sufficient concentration of the cations and dimers and the deposition of the conducting polypyrrole film with increasing concentrations of BSA.

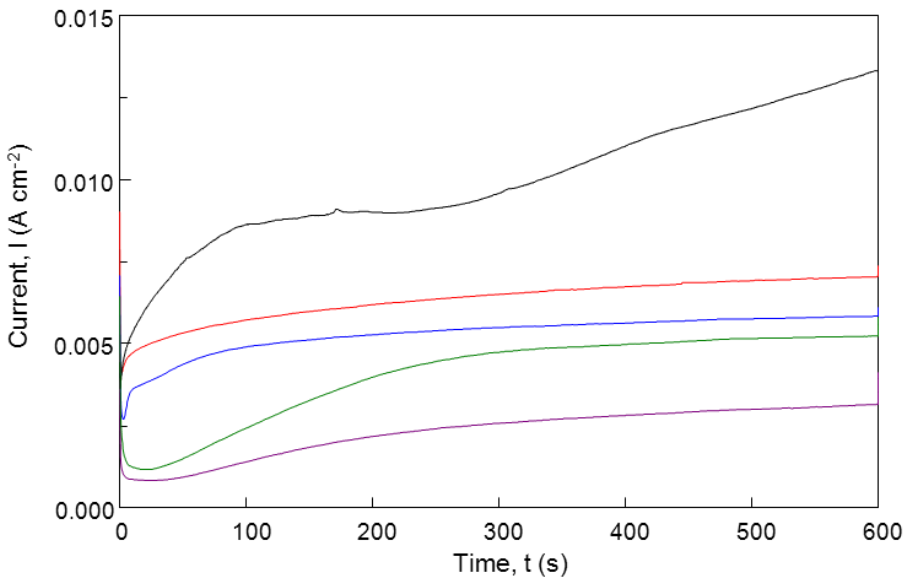

Figure 3.4: Current- time plots for the formation of PPy-Cl and PPy-BSA on a Pt electrode at 0.70 V vs. SCE from a solution containing 0.10 mol dm^{-3} NaCl and — 0.50 mol dm^{-3} pyrrole — 0.50 mol dm^{-3} pyrrole/25 µL BSA — 0.50 mol dm^{-3} pyrrole/50 µL BSA — 0.50 mol dm^{-3} pyrrole/100 µL BSA — 0.50 mol dm^{-3} pyrrole/200 µL BSA.

It is also evident from Figure 3.4 that the presence of the BSA in the monomer solution decreases the current density at longer times. This is shown in Table 3.2, where the current density measured at 600 s is reduced from 13.29 to 5.25 mA cm^{-2} with the presence of 100 µL/10 mL BSA, this corresponds to a significant reduction in the rate of electropolymerisation.

The charge-time plots recorded with different concentrations of BSA are shown in Figure 3.5. Linear plots were observed with the BSA-containing solutions. However, the rate of electropolymerisation is very high in the 0.50 mol dm^{-3} pyrrole solution with chloride anions as the dopant, giving different rates of electropolymerisation during the 600 s period. The slopes of the linear plots were calculated and plotted as a function of BSA concentration, as shown in Figure 3.6. There is a clear reduction in the rate of electropolymerisation with increasing concentrations of BSA. For example, the rate of electropolymerisation of pyrrole in the presence of 100 µL BSA is found to be 0.004 C cm^{-2} s^{-1}, compared to a rate of approximately 0.006 C cm^{-2} s^{-1} with 25 µL BSA.

Table 3.2: Current at time, t = 600 s for the formation of PPy-Cl and PPy-BSA on a Pt electrode as a function of the BSA concentration.

Concentration of BSA (µL/10 mL)	**Current at time, t = 600 s** (mA cm^{-2})
0	13.29
25	7.05
50	5.83
100	5.25
200	3.16

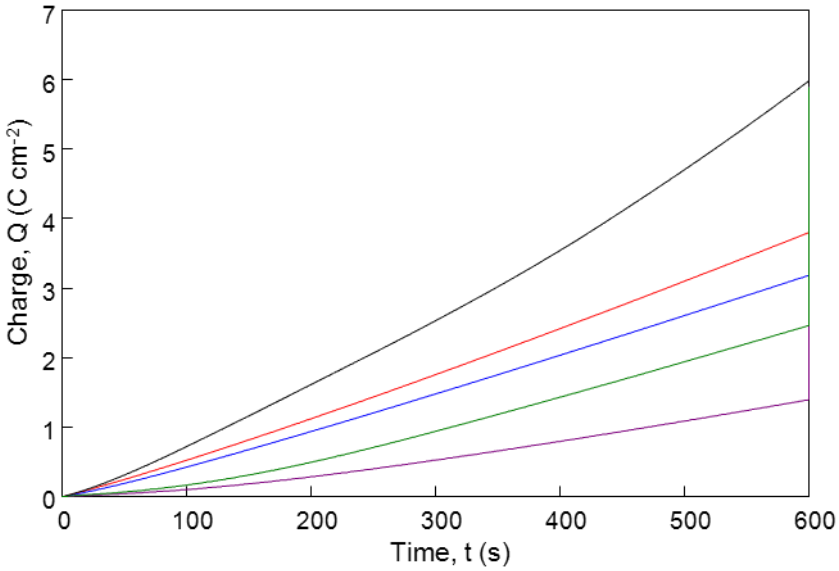

Figure 3.5: Charge plotted as a function of time for the formation of PPy-Cl and PPy-BSA on a Pt electrode at 0.70 V vs. SCE from a solution containing 0.10 mol dm^{-3} NaCl and ▬ 0.50 mol dm^{-3} pyrrole, ▬ 0.50 mol dm^{-3} pyrrole/25 µL BSA, ▬ 0.50 mol dm^{-3} pyrrole/50 µL BSA, ▬ 0.50 mol dm^{-3} pyrrole/100 µL BSA and ▬ 0.50 mol dm^{-3} pyrrole/200 µL BSA.

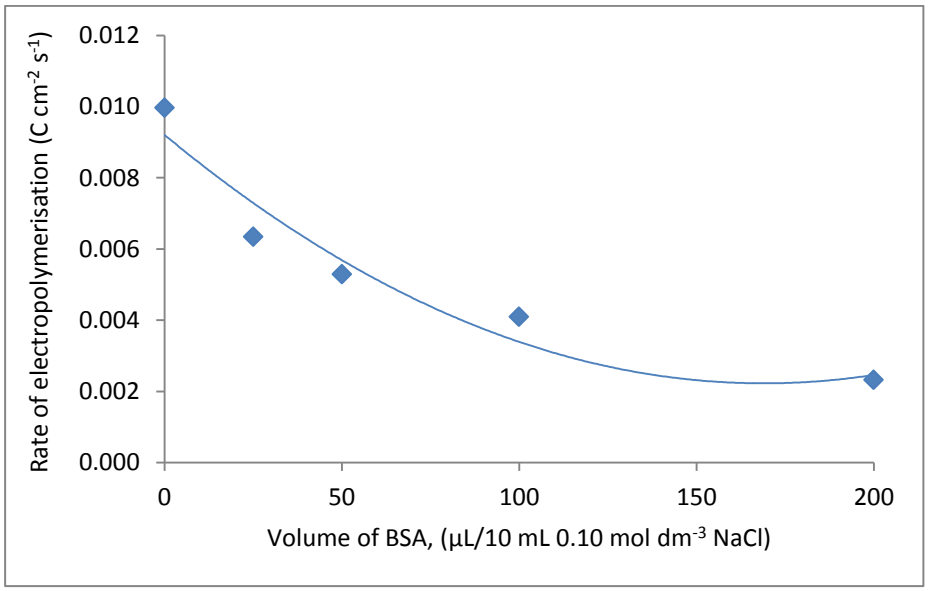

Figure 3.6: The rate of electropolymerisation obtained from the charge-time plots recorded with different concentrations of BSA as a function of BSA concentration.

3.3.1.3 Influence of the Applied Potential

In order to investigate the effect of the applied potential on the growth of the polymer films, the polymers were electrosynthesised at potentials ranging from 0.70 V to 0.90 V vs. SCE. This potential range was chosen as only potentials above 0.52 V vs. SCE will achieve adequate synthesis of the polymer. At lower potentials, pyrrole is not oxidised, or the rate of oxidation is too low, to generate the insoluble PPy. Instead, only the soluble oligomers are formed during the oxidation process[25]. Potentials higher than 0.90 V vs. SCE lead to overoxidation of the polypyrrole film and a considerable loss in the conductivity of the film[26].

Typical data are shown in Figure 3.7 with a fixed concentration of pyrrole at 0.50 mol dm^{-3}, and BSA, 50 µL/10 mL. The transients have similar characteristics, an initial drop in the current, followed by a gradual rise and finally a very slow increase in the current with increasing surface area as higher amounts of conducting polypyrrole is deposited. It is clear that the rate of polymer growth increases rapidly with increasing applied potential, reaching a current density of 1.98 mA cm^{-2} at 0.90 V vs. SCE, as shown in Table 3.3. Under these conditions reproducible current densities were difficult to obtain, while highly reproducible plots were obtained at the lower potential of 0.70 V vs. SCE. This potential was selected as the best applied potential for polymer growth giving consistent and reproducible data, and the final polymer was very smooth and stable which is consistent with reports in the literature[25].

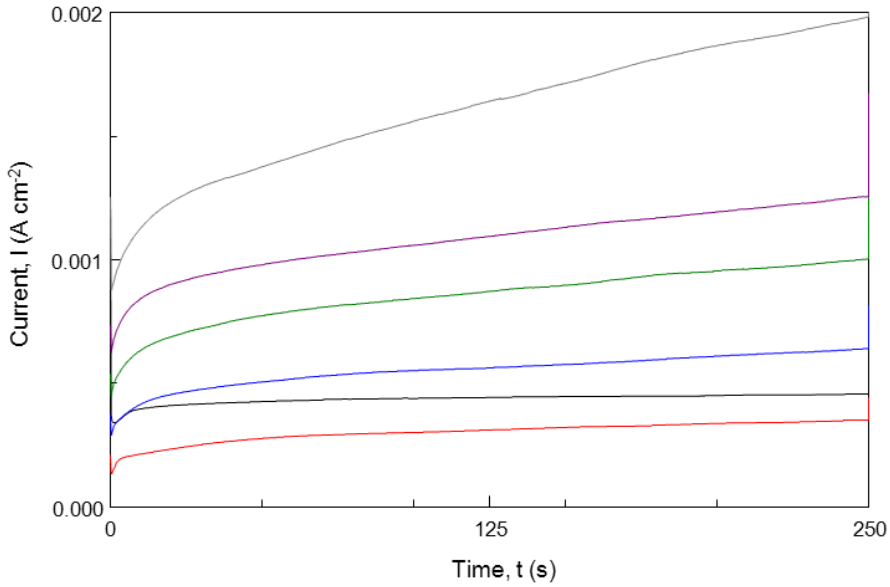

Figure 3.7: Current plotted as a function of time for the formation of PPy-Cl and PPy-BSA on a Pt electrode from a solution containing 0.50 mol dm^{-3} pyrrole/0.10 mol dm^{-3} NaCl ▬ at 0.70 V vs. SCE and 0.50 mol dm^{-3} pyrrole/50 µL BSA/0.10 mol dm^{-3} NaCl at ▬ 0.70 V, ▬ 0.75 V, ▬ 0.80 V, ▬ 0.85 V, and ▬ 0.90 V vs. SCE.

Table 3.3: Current recorded at time, t = 250 s for the formation PPy-BSA on a Pt electrode from a solution containing 0.50 mol dm^{-3} pyrrole/50 µL BSA/0.10 mol dm^{-3} NaCl.

Applied potential (V vs. SCE)	**Current at time, t = 250 s** (mA cm^{-2})
0.70	0.35
0.75	0.64
0.80	1.00
0.85	1.26
0.90	1.98

3.3.1.4 Rate of Electropolymerisation

The rate of electropolymerisation at a constant applied potential can be related to the monomer and dopant concentrations by using the rate law given in Equation 3.1. For this analysis, R represents the rate of the electropolymerisation reaction, [Py] represents the pyrrole monomer concentration, [BSA] represents the BSA concentration, k represents the rate constant, and α and β are the partial orders of the reaction.

$$R = k[\mathrm{Py}]^{\alpha}[\mathrm{BSA}]^{\beta} \qquad 3.1$$

The charge consumed during the growth of the polymer, Q, can be related to the amount of polymer deposited and accordingly, the rate of the electropolymerisation reaction can be given in terms of dQ/dt. Thus, Equation 3.1 can be expressed in terms of Equation 3.2 and modified to give Equation 3.3.

$$dQ/dt = k[\mathrm{Py}]^{\alpha}[\mathrm{BSA}]^{\beta} \qquad 3.2$$

$$\log (dQ/dt) = \log k + \alpha \log[\mathrm{Py}] + \beta \log [\mathrm{BSA}] \qquad 3.3$$

In these experiments, the applied potential was fixed at 0.70 V vs. SCE, and the concentration of pyrrole monomer, in both the presence and absence of BSA, was varied. The rate of electropolymerisation, dQ/dt, was found by plotting the electropolymerisation charge as a function of time. These values were then plotted as a function of the logarithm of the pyrrole concentration (in the presence and absence of BSA) to obtain α, while β was obtained from the slope of the logarithm of the rate as a function of the logarithm of the BSA concentration. The resulting plots are given in Figures 3.8, 3.9 and 3.10, respectively.

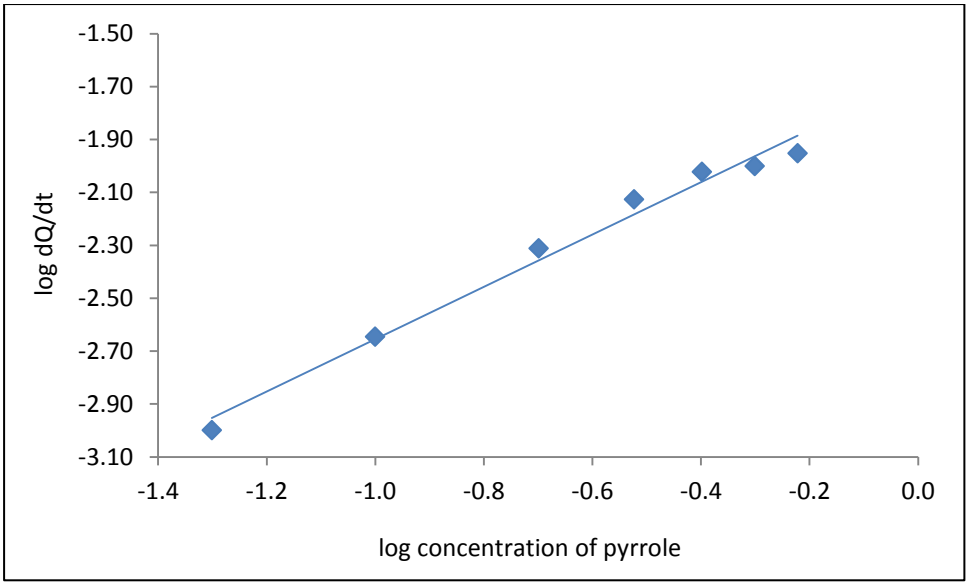

Figure 3.8: A plot of the logarithm of the rate of electropolymerisation, d*Q*/d*t*, as a function of the logarithm of the concentration of the pyrrole monomer in the absence of BSA.

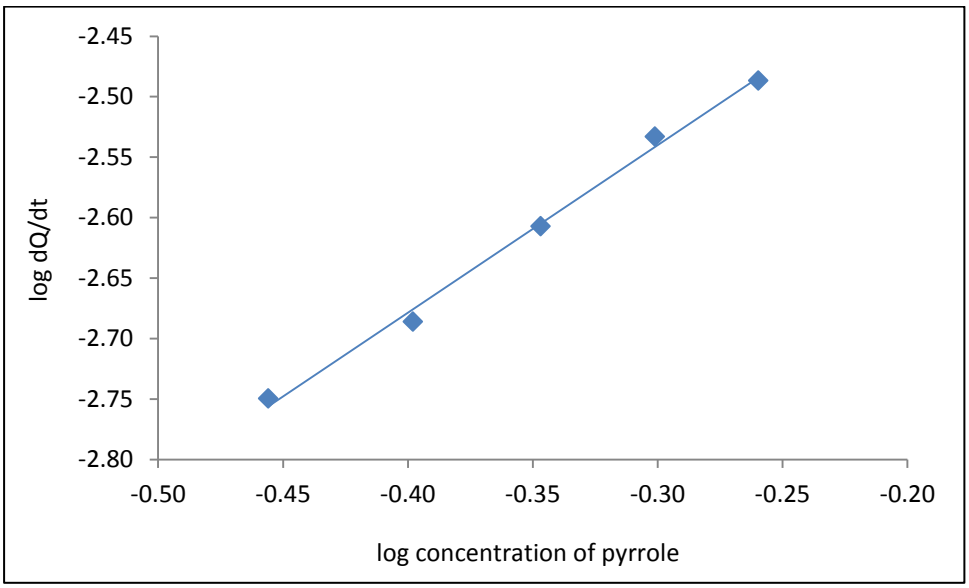

Figure 3.9: A plot of the logarithm of the rate of electropolymerisation, d*Q*/d*t*, as a function of the logarithm of the concentration of the pyrrole monomer in the presence of 100 µL BSA.

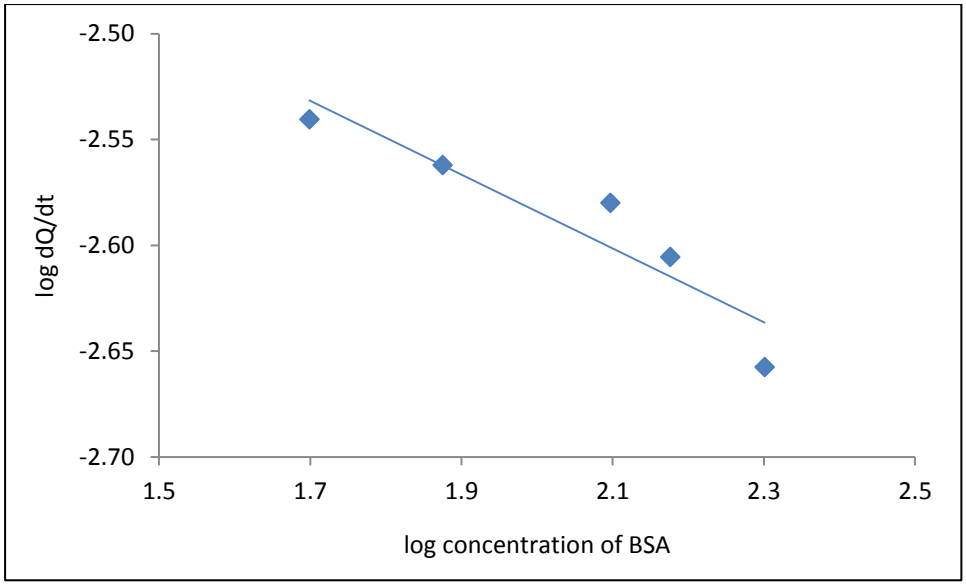

Figure 3.10: A plot of the logarithm of the rate of electropolymerisation, d*Q*/d*t*, as a function of the logarithm of the concentration of the BSA.

The partial order of the reaction with respect to the monomer concentration, α_1, was found to be 0.99 in the absence of BSA, while a somewhat higher value of 1.38 was obtained for the partial order of the reaction for the monomer concentration, α_2, in the presence of BSA. The partial order close to unity calculated for the growth of the film in the absence of BSA is in good agreement with previous literature values[27]. For example, Iroh and Wood[27], obtained partial orders close to 1.0 on studying the kinetics of electropolymerisation in simple sulphate solutions. The higher value of 1.38 computed in the presence of BSA shows that the addition of BSA to the electropolymerisation solution has a significant influence on the rate-determining step, giving a higher dependence on the pyrrole concentration. Furthermore, the value of the partial order of the reaction with respect to the BSA concentration was found to be negative, indicating a complex electropolymerisation process whereby the BSA inhibits the electropolymerisation process and decreases the rate of electropolymerisation.

The partial order of the reaction with respect to the BSA, β, has an extremely low value of -0.17. Negative values have not been reported in the literature for any dopant species in the electropolymerisation of pyrrole. Generally, the ratio of the partial orders with respect to the monomer and the dopant is close to 1:1[28]. The ratio between the partial orders in the presence of BSA is 1.38:0.17 giving an approximate ratio of 8:1. Ratios this high have not been reported for the electropolymerisation of

pyrrole. This low and negative partial order with respect to BSA is consistent with the decrease in the rate of electropolymerisation with increasing concentrations of BSA, as clearly evident in Figure 3.10 and also indicates that BSA has little influence in the rate-determining step.

3.3.2 Characteristics and Properties of PPy-BSA

3.3.2.1 Morphology and Surface Characterisation

Optical microscopy measurements were carried out to examine the surface morphology of the PPy-Cl polymer, Figure 3.11, and the PPy-BSA polymer, Figure 3.12. From these it can be seen that the PPy-Cl polymer film is very smooth in comparison to the PPy-BSA polymer which is much rougher, and contains globular entities on its surface. These globular entities are due to the viscosity of the bovine serum albumin solution[24].

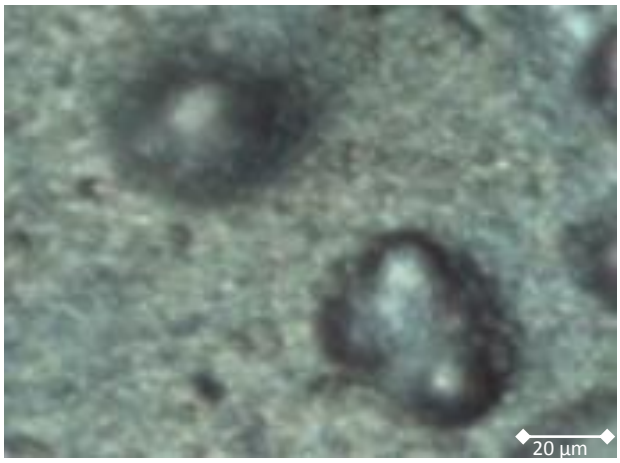

Figure 3.11: Optical micrograph of a PPy-Cl film electrosynthesised at 0.70 V vs. SCE from a solution containing 0.50 mol dm^{-3} pyrrole and 0.10 mol dm^{-3} NaCl until a charge of 10.48 C cm^{-2} was reached (magnification x 50).

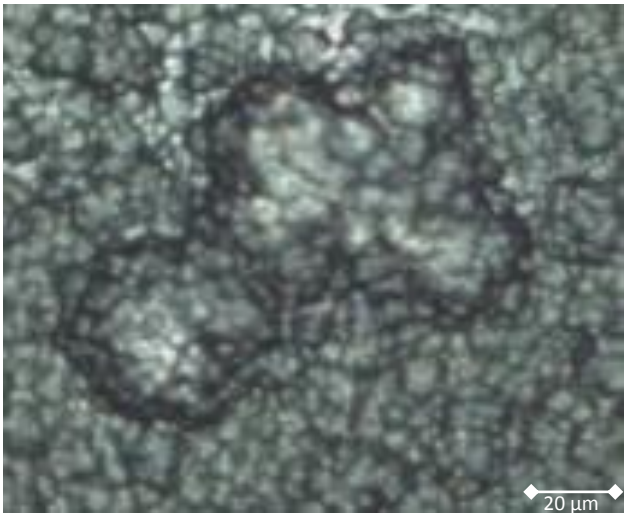

Figure 3.12: Optical micrograph of a PPy-BSA film electrosynthesised at 0.70 V vs. SCE from a solution containing 0.50 mol dm^{-3} pyrrole, 50 µL BSA and 0.10 mol dm^{-3} NaCl until a charge of 10.48 C cm^{-2} was reached (magnification x 50).

SEM measurements were also carried out on the PPy-Cl polymer, Figure 3.13, and the PPy-BSA polymer, Figure 3.14, to further investigate the surface morphology of the films. From these it can be seen that the PPy-Cl polymer film is much more structured and smooth with the typical cauliflower morphology of polypyrrole[29]. Even though the pyrrole concentration is much higher than that normally used to form PPy-Cl films[30], the cauliflower morphology is maintained. In comparison, the surface morphology of the PPy-BSA polymer is very different; the morphology is rough with multiple globular entities on the surface. In addition, the PPy-BSA contains fibrous structures throughout the film, which are consistent with a protein incorporated into the polymer structure[24].

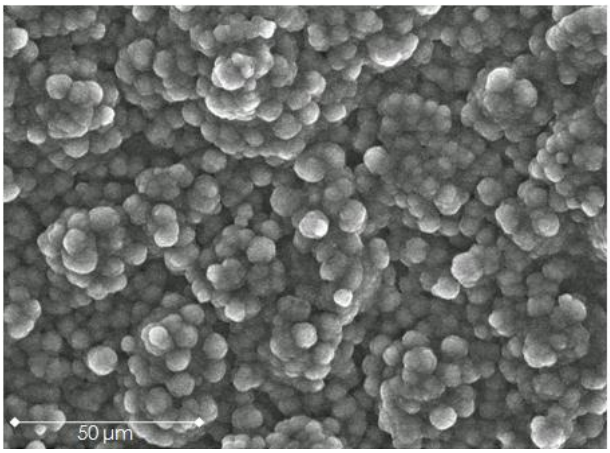

Figure 3.13: Scanning electron micrograph of a PPy-Cl film electrosynthesised at 0.70 V vs. SCE from a solution containing 0.50 mol dm^{-3} pyrrole and 0.10 mol dm^{-3} NaCl until a charge of 10.48 C cm^{-2} was reached.

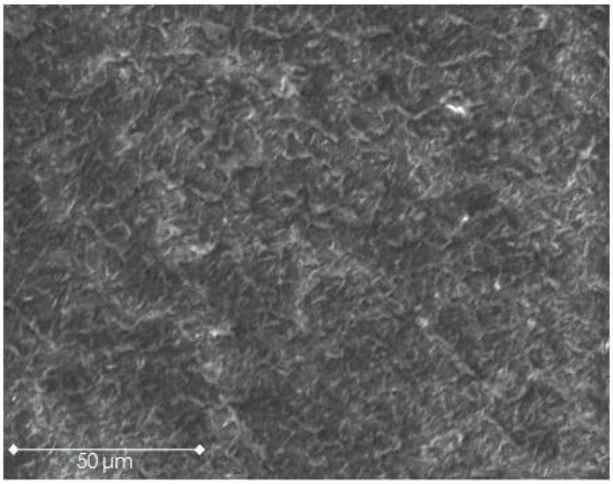

Figure 3.14: Scanning electron micrograph of a PPy-BSA film electrosynthesised at 0.70 V vs. SCE from a solution containing 0.50 mol dm^{-3} pyrrole, 50 µL BSA and 0.10 mol dm^{-3} NaCl until a charge of 10.48 C cm^{-2} was reached.

EDX measurements were also performed on the PPy-Cl and PPy-BSA films. The EDX spectrum of the PPy-Cl polymer, Figure 3.15, shows the presence of a large quantity of chloride anions at ~ 2.85 keV in the polymer film. The absence of a sodium signal shows that the chloride anions are present as dopants. The EDX spectrum of the PPy-BSA film, Figure 3.16, shows that although some chloride is present in the polymer film, sulphur is also present at ~ 2.35 keV. Again, no sodium is observed and this provides direct evidence for the incorporation of the BSA as the signal is due to the presence of disulphide bonds in the BSA[31,32]. The oxygen signal, which arises from the amino acids, is also consistent with the incorporation of BSA

within the polymer matrix. The presence of the chloride in the PPy-BSA film proves that the chloride ions from the 0.10 mol dm^{-3} NaCl used as the supporting electrolyte are incorporated into the polymer film as dopants during polymerisation to counteract the positive charge that is generated on the oxidised polypyrrole backbone[33,34].

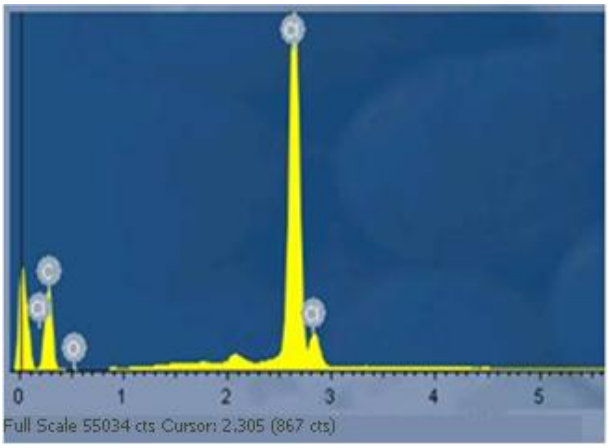

Figure 3.15: Energy-dispersive X-Ray spectrum of a PPy-Cl film electrodeposited from a solution containing 0.50 mol dm^{-3} pyrrole and 0.10 mol dm^{-3} NaCl with an applied potential of 0.70 V vs. SCE until a charge of 10.48 C cm^{-2} was reached. Cl is observed at ~ 2.85 keV.

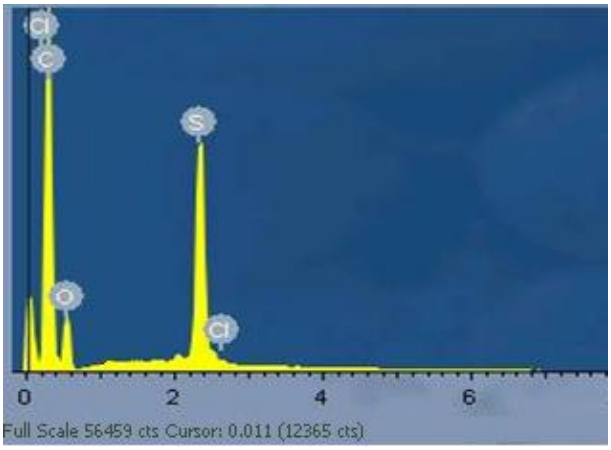

Figure 3.16: Energy-dispersive X-Ray spectrum of a PPy-BSA film electrodeposited from a solution containing 0.50 mol dm^{-3} pyrrole, 50 μL BSA and 0.10 mol dm^{-3} NaCl with an applied potential of 0.70 V vs. SCE until a charge of 10.48 C cm^{-2} was reached. Cl is observed at ~ 2.85 keV and S is observed at ~ 2.35 keV

3.3.2.2 Electroactivity of PPy-Cl and PPy-BSA

The electroactivity of the PPy-Cl and PPy-BSA films was studied using cyclic voltammetry in a 0.10 mol dm^{-3} NaCl solution. The PPy-Cl and PPy-BSA films were deposited at 0.70 V vs. SCE in solutions containing 0.50 mol dm^{-3} pyrrole/0.10 mol dm^{-3} NaCl and 0.50 mol dm^{-3} pyrrole/25 µL of BSA/0.10 mol dm^{-3} NaCl for the PPy-Cl and PPy-BSA polymer films, respectively. The polymer films were deposited to different charges ranging from 0.01 to 0.74 C. The films were then rinsed with distilled water and transferred to the chloride-containing electrolyte. The voltammograms were recorded at different scan rates, ranging from 100 to 5 mV s^{-1}. The polymer films were initially cycled at the higher scan rates in order to eliminate or reduce any effects arising with cycling the electrode repeatedly in the electrolyte solution. The cyclic voltammograms recorded for the PPy-BSA film are shown in Figure 3.17, where it is clear that the scan rate has a prominent influence on both the anodic and cathodic currents. There is a clear increase in the current as the scan rate is increased, in agreement with previous studies[35].

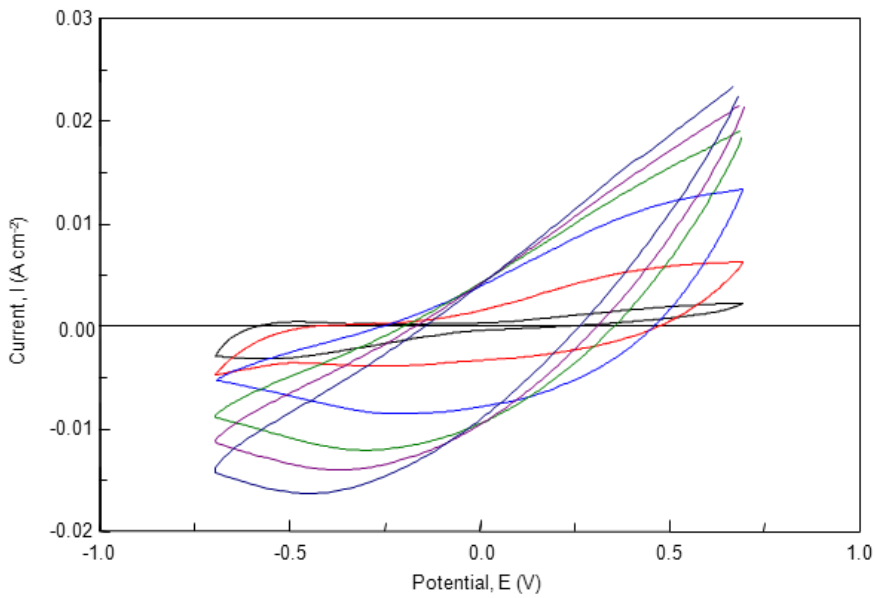

Figure 3.17: Cyclic voltammograms recorded for PPy-BSA (0.74 C) grown at a constant potential of 0.70 V vs. SCE in 0.50 mol dm^{-3} pyrrole/25 µL BSA/0.10 mol dm^{-3} NaCl showing the 20th cycle for — 100 mV s^{-1}, — 70 mV s^{-1}, — 50 mV s^{-1}, — 25 mV s^{-1}, — 10 mV s^{-1} and — 5 mV s^{-1}.

Although it is difficult to identify the oxidation peak, particularly at the higher scan rates, where the oxidation peak is centred at potentials higher than the vertex potential, a broad, but well defined, reduction peak is observed at all scan rates. This peak corresponds to reduction of the PPy-BSA film and the expulsion of chloride anions from the polymer film. The broad reduction peak indicates a slow conversion of the PPy-BSA film from the oxidised to the reduced state. This is consistent with literature reports on the redox properties of polypyrrole[36] and can be explained by the fact that the polymer layers adjacent to the electrode surface are reduced first to give an insulating interface, making the overall reduction process more difficult and slower. During the oxidation reaction, the layers next to the electrode surface are oxidised first, giving a conducting layer which facilitates oxidation of the adjacent layers until the conducting zone reaches the solution. At the slower scan rates, where the oxidation wave is observed, it is indeed clear that the oxidation wave is not as broad as the corresponding reduction wave.

In order to further investigate the electroactivity of the polymers, the PPy-BSA and PPy-Cl films were freshly electrodeposited onto a platinum working electrode and immediately placed into an electrolyte solution of 0.10 mol dm^{-3} NaCl. Cyclic voltammetry measurements were then recorded, from a high scan rate of 300 mV s^{-1} to a relatively slow scan rate of 5 mV s^{-1}, as shown in Figure 3.18. These voltammograms have lower currents than those shown in Figure 3.17 due to the different thicknesses of the polymer films. Again, lower currents are observed at the slower scan rates. On comparing the cyclic voltammograms recorded for the PPy-BSA and PPy-Cl films, it is clear that the PPy-Cl films are more electroactive with higher currents and more pronounced oxidation and reduction waves. Lower currents are recorded for the PPy-BSA film. This is probably connected with the fact that the large globular BSA inhibits the incorporation and expulsion of the chloride anion from the polypyrrole matrix, hence, the electroactivity of the PPy-BSA polymer film differs from that of the PPy-Cl polymer film[24]. In addition, the presence of the BSA within the polymer matrix may block any pores within the polypyrrole matrix, thus increasing the resistance of any solution trapped within the porous network. In the PPy-Cl film the open porous network provides easy access to solution species, giving a highly electroactive film, however, transport of the solution species is significantly inhibited if these pores are blocked with BSA[37].

The current obtained at a fixed potential of 0.50 V vs. SCE was plotted as a function of the scan rate, for both the PPy-Cl and PPy-BSA films and these data are compared in Figure 3.19. The slopes of the linear regions were calculated as 2.81 x 10^{-2} and 2.23 x 10^{-2} A V^{-1} s for the PPy-Cl and PPy-BSA films, respectively. Although the higher slope for the PPy-Cl polymer is indicative of a more electroactive film, the presence of the BSA within the polymer does not have much effect on the electroactivity of the polymer films.

(a)

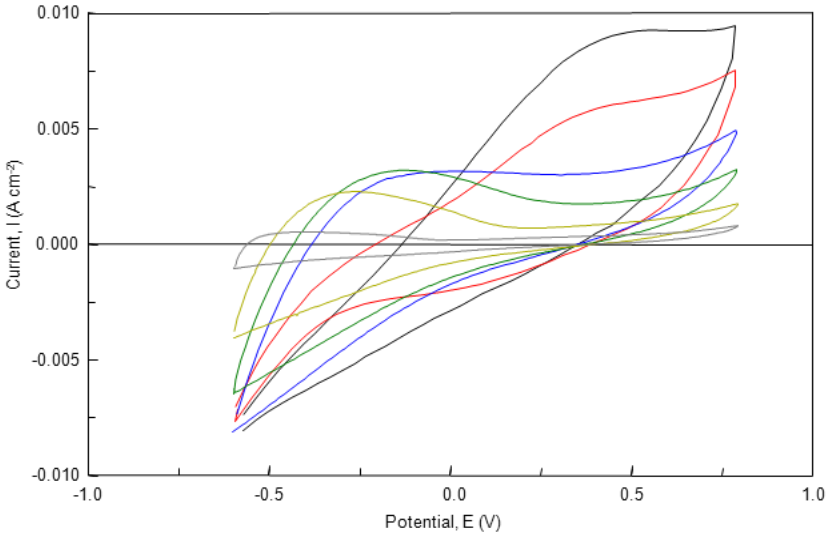

(b)

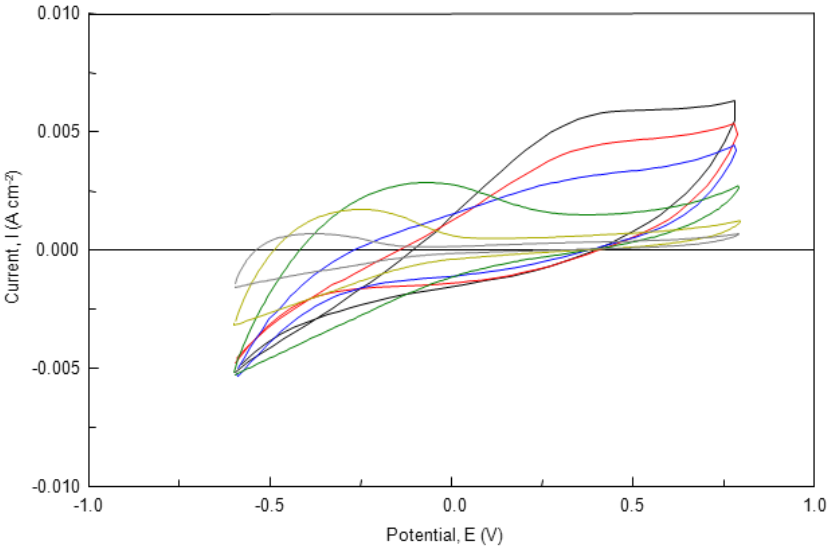

Figure 3.18: Cyclic voltammograms of the (a) PPy-Cl (0.017 C) and (b) PPy-BSA (0.017 C) polymer films at different scan rates: — 300 mV s^{-1}, — 200 mV s^{-1}, — 150 mV s^{-1}, — 100 mV s^{-1}, — 50 mV s^{-1}, — 25 mV s^{-1} and — 10 mV s^{-1}.

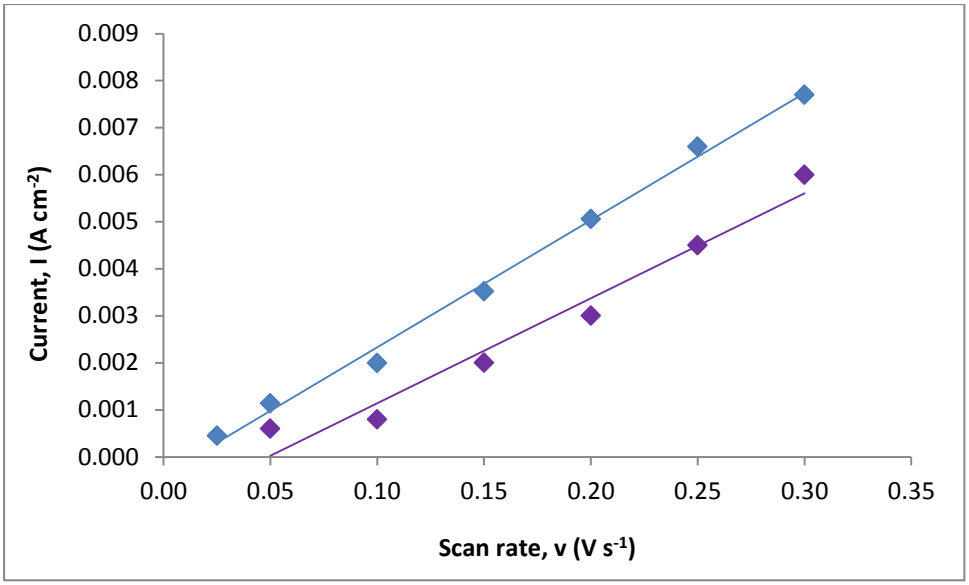

Figure 3.19: Current recorded at a fixed potential of 0.50 V vs. SCE as a function of the scan rate for both the — PPy-Cl (0.017 C) and — PPy-BSA (0.017 C) films.

3.3.2.3 Capacitance Measurements

The capacitance of both the PPy-Cl and PPy-BSA films was calculated using Equation 3.4, where C is the capacitance, I is the current density (A cm^{-2}) and dV/dt is the scan rate (Vs^{-1})[37].

$$C = \frac{I}{\frac{dV}{dt}} \qquad 3.4$$

To obtain a more realistic and correct capacitance, the PPy-Cl and PPy-BSA films were cycled in 0.10 mol dm^{-3} NaCl solution at various scan rates, but with a small electrochemical window. The electrochemical window was reduced to a lower potential limit of 0.10 V vs. SCE and an upper potential limit of 0.20 V vs. SCE, in order to avoid the effects of any faradic currents, and the current was obtained at a fixed potential of 0.17 V vs. SCE. The resulting cyclic voltammograms, shown in Figure 3.20, have a completely different profile from those recorded in a larger potential window. The currents are considerably lower as the faradic currents have been reduced dramatically[26], Figure 3.20.

(a)

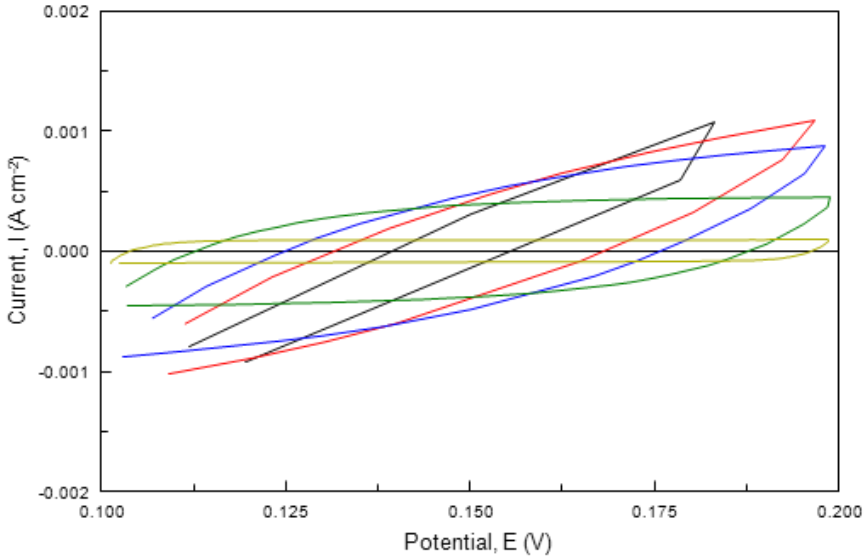

(b)

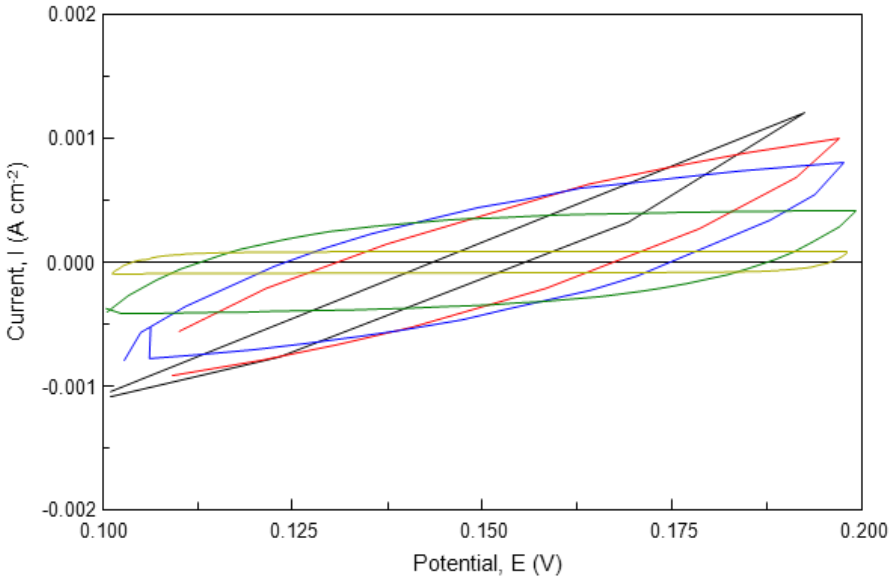

Figure 3.20: Cyclic voltammograms of the (a) PPy-Cl (0.017 C) and (b) PPy-BSA (0.017 C) polymer films at varied scan rates: ▬ 200 mV s^{-1}, ▬ 150 mV s^{-1}, ▬ 100 mV s^{-1}, ▬ 50 mV s^{-1} and ▬ 25 mV s^{-1}.

A plot of the current, *I*, versus the scan rate, *dV/dt* yields a straight line as shown in Figure 3.21 and correlation coefficients of 0.999 and 0.998 were obtained for the PPy-Cl and PPy-BSA films, respecively, on fitting the data to Equation 3.4. The capacitance was found to be in the region of 2.25 x 10^{-3} and 1.47 x 10^{-3} F cm^{-2} for the PPy-Cl and PPy-BSA polymer films, respectively. This is typical of the high capacitance values recorded for conducting polymers[38], and is in good agreement with the values reported in the literature[26,35,37].

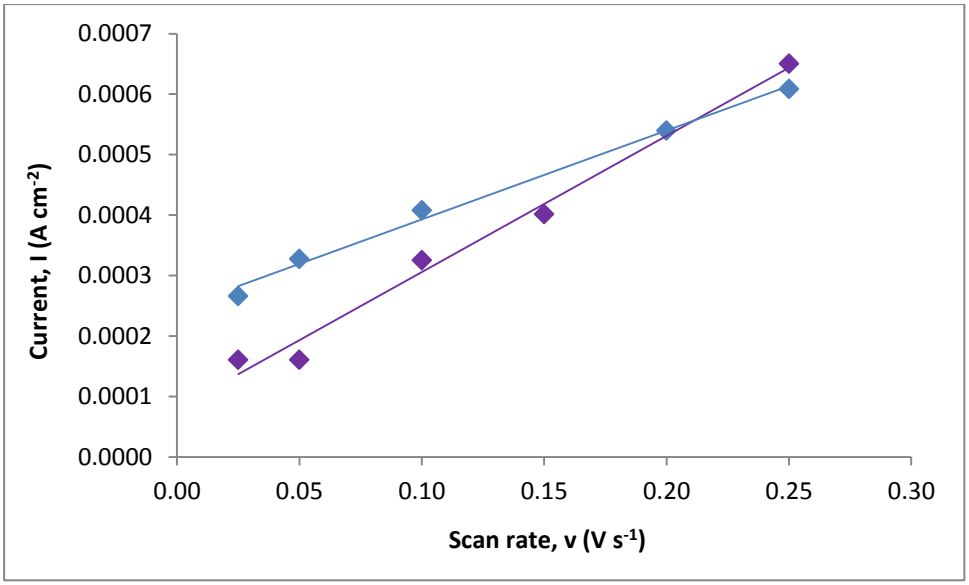

Figure 3.21: Current recorded at 0.17 V vs. SCE plotted as a function of the scan rate for the — PPy-Cl (0.017 C) and — PPy-BSA (0.017 C) films.

3.3.2.4 Electrochemical Window

The electrochemical window, i.e., the upper and lower potential limits chosen during cyclic voltammetry, also plays an important role in the oxidation and reduction of the polymer and, correspondingly, the currents measured[,39]. If a high upper potential limit is chosen, the polymer film may become overoxidised[40]. It is well known that overoxidation of polypyrrole results in a loss of conductivity and this gives rise to a sharp decrease in the corresponding current[40]. It is known that polypyrrole becomes overoxidised at potentials greater than 1.00 V vs. SCE[40]. As a result, the lower potential limit was fixed at -0.60 V vs. SCE and the upper potential limit was varied in order to investigate the effect of the electrochemical window on the polymer films.

It is apparent from Figure 3.22 that increasing the potential window has little or no effect on the observed oxidation current. A clear oxidation wave, corresponding to the oxidation of the PPy-BSA film and the incorporation of chloride anions as dopants, is seen, particularly in the electrochemical window extended up to 1.20 V vs. SCE. However, the stability of the polymer films is greatly affected by the more extended potential window. Figure 3.23 shows the oxidation charge plotted as a function of cycle number. At the higher potential window, i.e., up to 1.20 V vs.

SCE, the polymer degrades rapidly. After about 70 cycles, there is a 50% loss in the charge. This can be explained in terms of overoxidation of the PPy-BSA films at these high potentials, as it is well known that polypyrrole is overoxidised at potentials greater than 1.00 V vs. SCE and, as the polymer is repeatedly cycled to these high potentials, overoxidation occurs. Alternatively, good stability is observed in the smaller electrochemical window, there is no change in the measured charge for more than 160 cycles and then the loss in charge is only of the order of 2.5 % after 200 cycles. As a result, the smaller potential window was used for all subsequent cyclic voltammetry measurements.

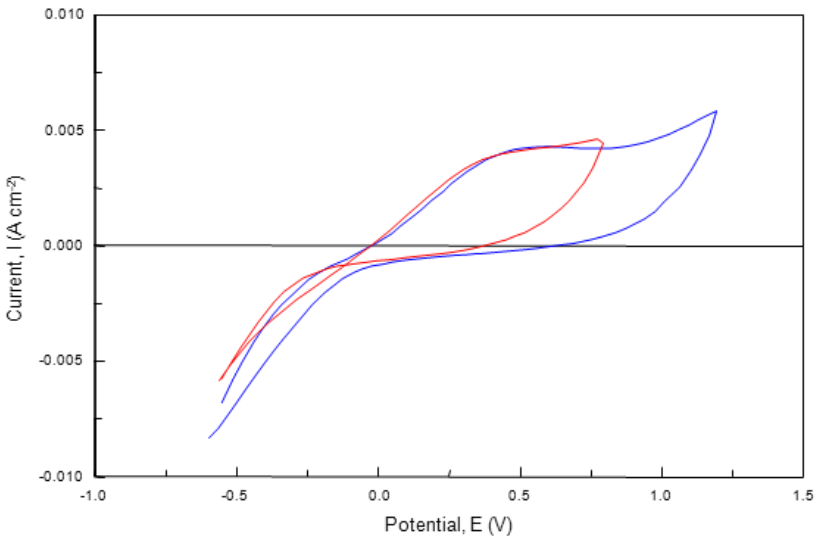

Figure 3.22: Cyclic voltammograms (5th cycle) recorded for the PPy-BSA (0.017 C) polymer film in a 0.10 mol dm^{-3} NaCl solution from — -0.60 to 1.20 V vs. SCE and — -0.60 to 0.80 V vs. SCE.

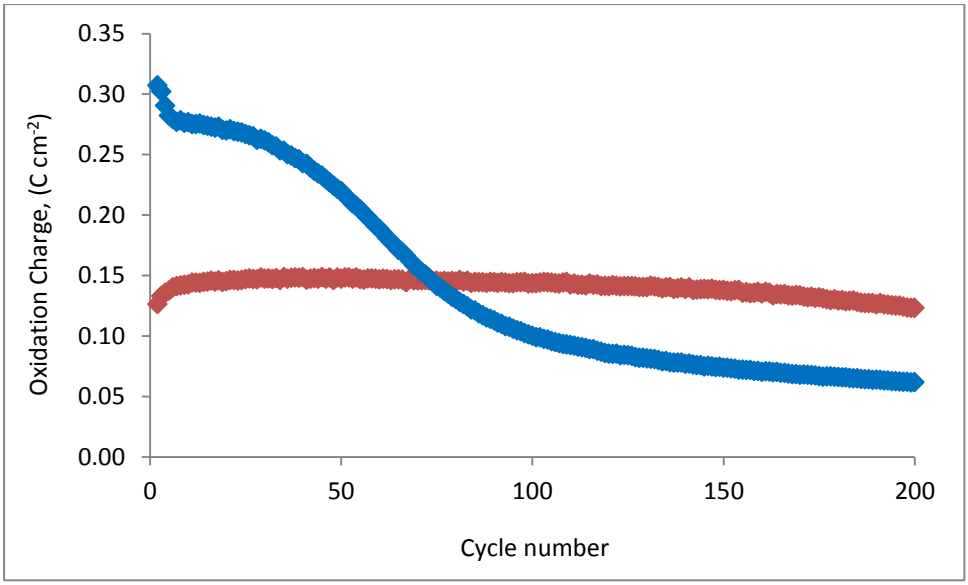

Figure 3.23: Oxidation charge recorded as a function of cycle number for PPy-BSA cycled in a 0.10 mol dm^{-3} NaCl solution, from — -0.60 to 1.20 V vs. SCE and — -0.60 to 0.80 V vs. SCE.

3.3.2.5 Effect of pH on the PPy-Cl and PPy-BSA Polymers

The effect of pH on the stability of both the PPy-Cl and PPy-BSA polymer films was investigated. The polymers were grown in the usual manner, at a constant potential of 0.70 V vs. SCE, then rinsed in distilled water and transferred to a solution of 0.10 mol dm^{-3} NaCl at pH values ranging from a pH of 2.0 to a pH of 12.0. The pH of the solutions was altered by adding, dropwise, a solution of HCl to make the solution more acidic, or NaOH to make the solution more alkaline. The final NaCl solutions were adjusted to pH values of 2.1, 4.0, 7.0, 9.0 and 12.0, enabling a full pH study to be undertaken for both the PPy-Cl and PPy-BSA films.

The cyclic voltammograms recorded at a pH of 7.0 are shown in Figure 3.24 for the PPy-Cl and PPy-BSA films formed from solutions containing 25 to 200 µL BSA. It is evident from Figure 3.24 that the PPy-Cl film has a higher current density than the PPy-BSA films at a neutral pH, which is in good agreement with the voltammetry shown in Section 3.3.2.2 and is consistent with the more insulating nature of the PPy-BSA[12]. Indeed, as the BSA concentration in the electropolymerisation solution is increased to give higher loadings of BSA within the polymer matrix, there is a further decrease in the measured currents. This is clearly evident in the vicinity of

the oxidation wave, where the peak oxidation currents decrease with an increase in the BSA concentration. This is also very apparent in Figure 3.25, where the oxidation current measured at a fixed potential of 0.60 V vs. SCE is plotted as a function of the cycle number for PPy-Cl and PPy-BSA prepared from 50 and 200 µL BSA. The current is significantly higher for the PPy-Cl film. It is also evident that the three polymer films are stable at this pH, there is no or little change in the current. The current increases slightly from the first to the third cycle, but then remains constant.

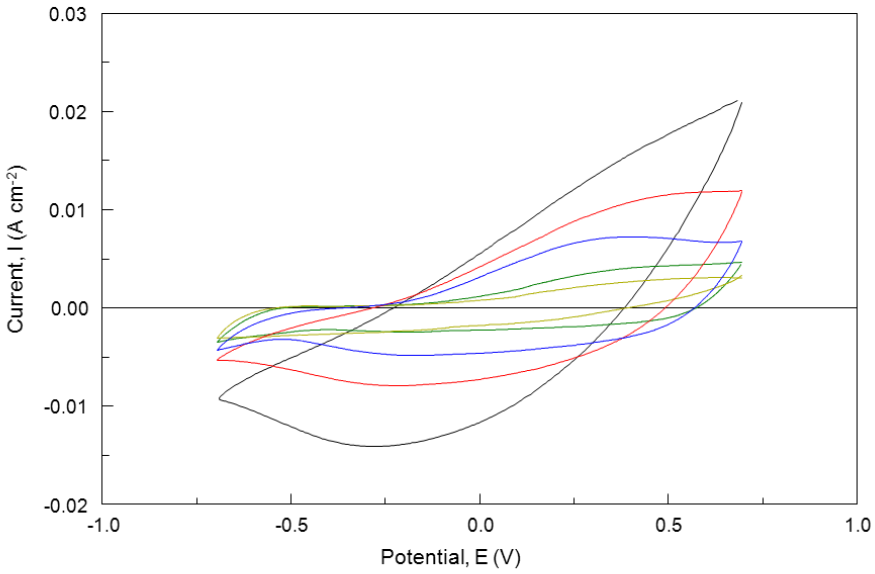

Figure 3.24: Cyclic voltammograms recorded in 0.10 mol dm^{-3} NaCl solution, pH 7.0, from -0.70 up to 0.70 V vs. SCE for the PPy-Cl (0.74 C) and PPy-BSA (0.74 C) films electropolymerised on a Pt electrode at 0.70 V vs. SCE from a solution containing 0.10 mol dm^{-3} NaCl and ▬ 0.50 mol dm^{-3} pyrrole, ▬ 0.50 mol dm^{-3} pyrrole/25 µL BSA, ▬ 0.50 mol dm^{-3} pyrrole/50 µL BSA, ▬ 0.50 mol dm^{-3} pyrrole/100 µL BSA and ▬ 0.50 mol dm^{-3} pyrrole/200 µL BSA.

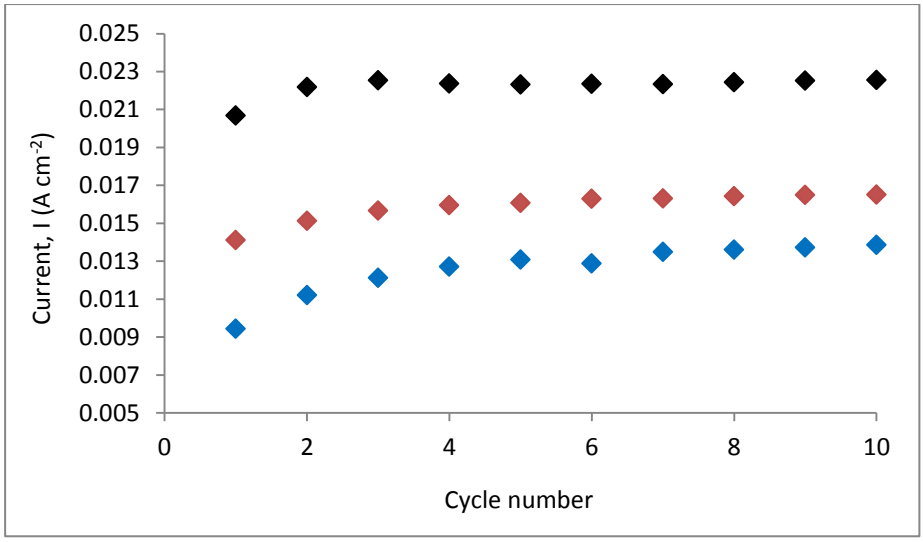

Figure 3.25: The current obtained at a fixed potential of 0.60 V vs. SCE plotted as a function of cycle number, for cycling the ▬ PPy-Cl (0.74 C), ▬ PPy-BSA (0.74 C, 50 µL BSA) and ▬ PPy-BSA (0.74 C, 200 µL BSA) polymer films in 0.10 mol dm^{-3} NaCl at a pH of 7.0.

In order to investigate the properties and stability of the polymer films across the entire pH range, the PPy-Cl and PPy-BSA (prepared from 50 and 200 µL BSA) films were electrodeposited as described previously, then cycled in 0.10 mol dm^{-3} NaCl at pH values ranging from 2.1 up to 12.0. The oxidation current measured at a fixed potential (0.60 V vs. SCE) was recorded and plotted as a function of the cycle number for each pH value. These plots are shown in Figures 3.26, 3.27, 3.28 and 3.29 for solutions of pH 2.1, 4.0, 9.0 and 12.0, respectively.

A similar trend is seen at all pH values, with higher currents observed for the PPy-Cl films. Again, good stability is observed at pH values of 2.0, 4.0 and 9.0 and the cyclic voltammograms and current densities are similar, with the pH having little influence from a pH of 2.0 to 9.0. However, at a pH of 12.0, the currents are considerably lower and after cycle 5 there is evidence of a further drop in the current indicating poor stability in this highly alkaline solution and a loss in conductivity[41,42], to give more insulating polymer films[43,44].

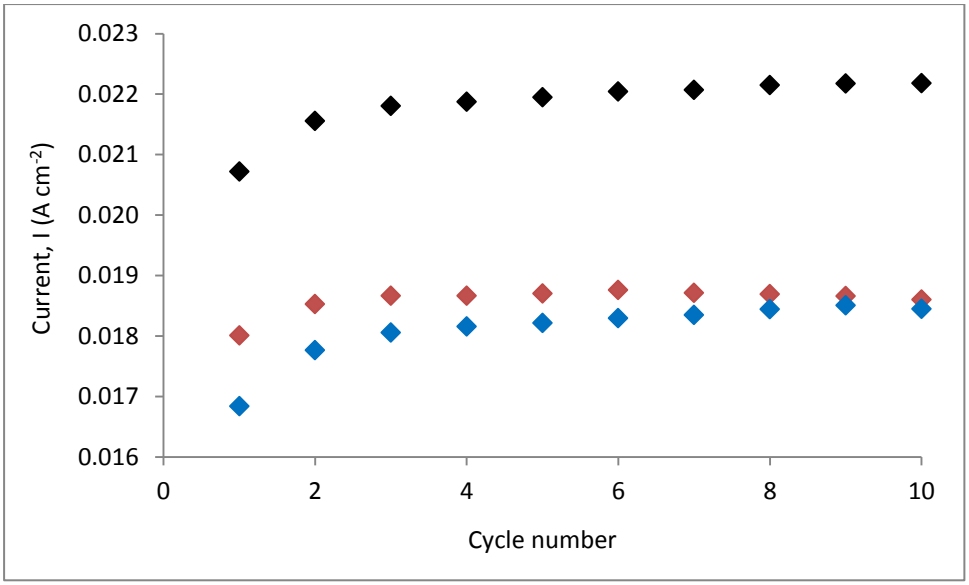

Figure 3.26: The current obtained at a fixed potential (0.60 V vs. SCE) plotted as a function of cycle number, by cycling the ▬ PPy-Cl (0.74 C), ▬ PPy-BSA (0.74 C, 50 µL BSA) and ▬ PPy-BSA (0.74 C, 200 µL BSA) polymer films in 0.10 mol dm^{-3} NaCl at a pH of 2.1.

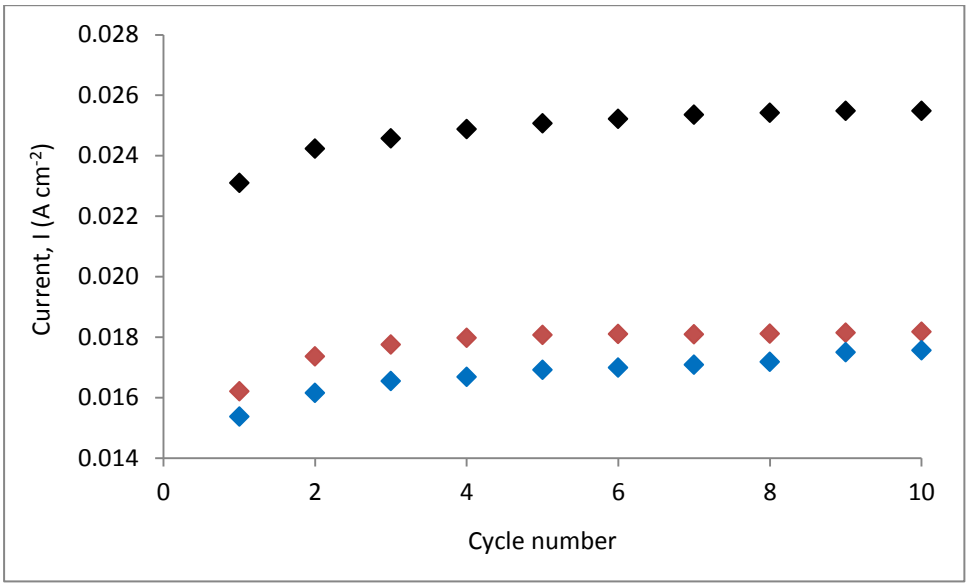

Figure 3.27: The current obtained at a fixed potential (0.60 V vs. SCE) plotted as a function of cycle number, by cycling the ▬ PPy-Cl (0.74 C), ▬ PPy-BSA (0.74 C, 50 µL BSA) and ▬ PPy-BSA (0.74 C, 200 µL BSA) polymer films in 0.10 mol dm^{-3} NaCl at a pH of 4.0.

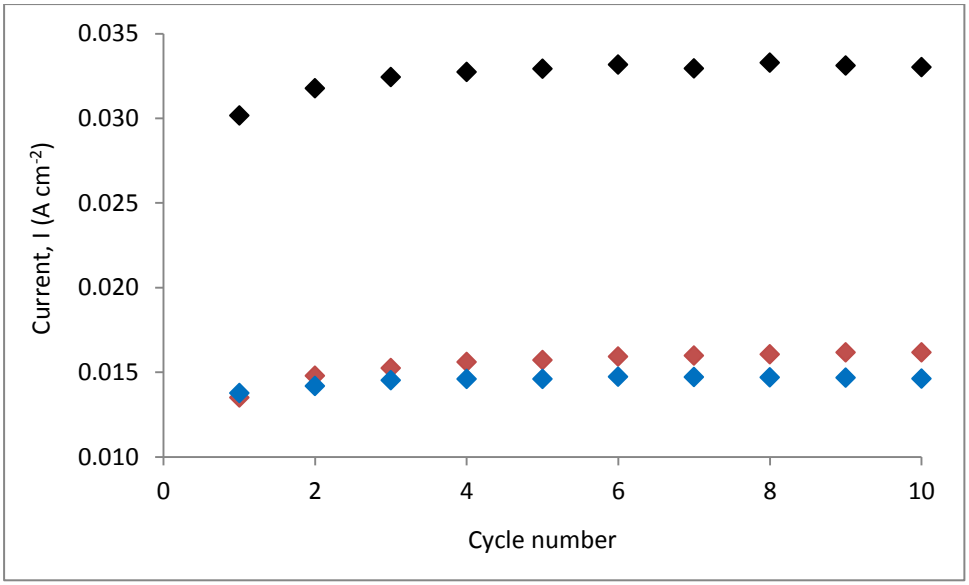

Figure 3.28: The current obtained at a fixed potential (0.60 V vs. SCE) plotted as a function of cycle number, by cycling — PPy-Cl (0.74 C), — PPy-BSA (0.74 C, 50 µL BSA) and — PPy-BSA (0.74 C, 200 µL BSA) polymer films in 0.10 mol dm^{-3} NaCl at a pH of 9.0.

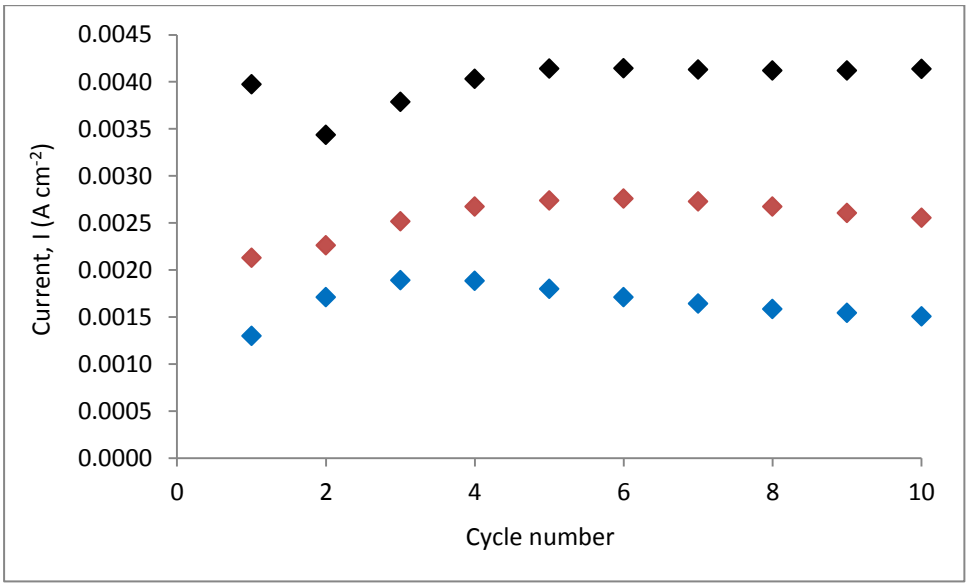

Figure 3.29: The current obtained at a fixed potential (0.60 V vs. SCE) plotted as a function of cycle number, by cycling — PPy-Cl (0.74 C), — PPy-BSA (0.74 C, 50 µL BSA) and — PPy-BSA (0.74 C, 200 µL BSA) polymer films in 0.10 mol dm^{-3} NaCl at a pH of 12.0.

3.3.2.6 Overoxidation of the PPy-BSA Polymer Films

It has already been observed in Section 3.3.2.4, that the electrochemical window plays an important role in the stability of the polymer films. However, a further investigation into the effects of overoxidation of the polymers was carried out. The PPy-BSA film was electropolymerised as before, by applying a constant potential of 0.70 V vs. SCE. The polymer was then cycled in a 0.10 mol dm^{-3} solution of NaOH, at a pH of 12.0 up to a vertex potential of 1.40 V vs. SCE, as polypyrrole is well known to overoxidise above 1.00 V vs. SCE and this is further facilitated in alkaline solutions[40]. It is evident from Figure 3.30 that, with continued cycling up to these high potentials, the PPy-BSA film becomes insulating and overoxidised. This is accompanied by a rapid decrease in the current density with repeated cycling in the NaOH solution. After only four cycles, highly insulating polymers are obtained and the currents are very low. Similar data were recorded with the PPy-Cl films.

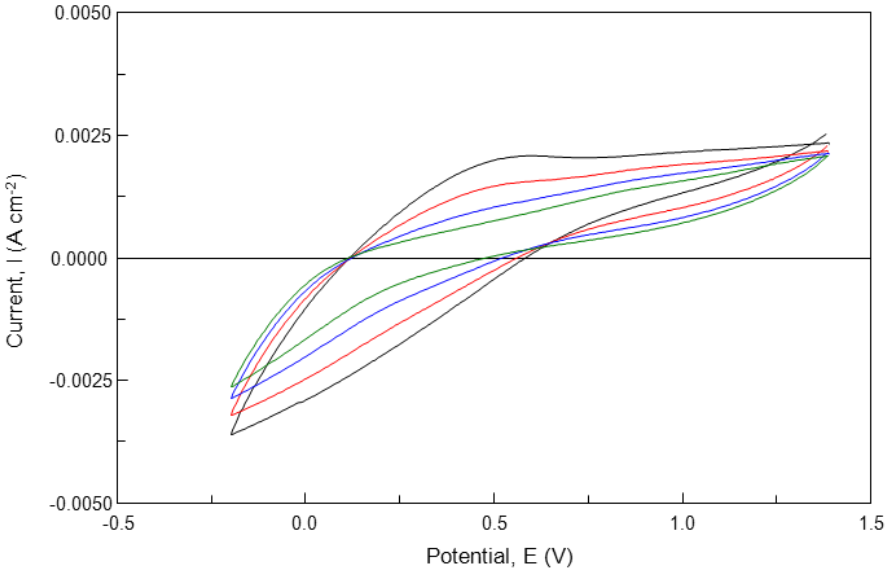

Figure 3.30: Cyclic voltammograms of the PPy-BSA (0.017 C) polymer film recorded in a 0.10 mol dm^{-3} NaOH solution: ▬ cycle 1, ▬ cycle 2, ▬ cycle 3 and ▬ cycle 4.

3.3.2.7 Temperature Analysis of the Polymers using DSC

The PPy-Cl and PPy-BSA polymer films were characterised using differential scanning calorimetry[45]. This involved investigating the thermal properties and the transitions of the polymer films by heating them in an aluminium pan along with an empty aluminium pan as a blank sample in a furnace and recording the energy that is required to keep the aluminium pans at an identical temperature[46]. This determines the amount of heat absorbed or released by the polymer sample as the temperature is varied, i.e., during heating or cooling. Consequently, the transitions of the polymer films that are recorded can include their melting interval, decomposition, crystallisation and even their purity[46]. For the purpose of these experiments, the PPy-Cl and PPy-BSA samples were heated from 25 °C up to 450 °C, then cooled from 450 °C back to 25 °C, creating a cyclic pattern as shown in Figure 3.31.

It is evident from Figure 3.31 that the same cyclic pattern is obtained for both the PPy-Cl and PPy-BSA films upon varying the temperature by heating and cooling the polymer films. It is also apparent that there are no endothermic or exothermic transitions indicating that both polymer samples are stable for temperatures lower than 450 ^{o}C. This is not surprising, as polypyrrole only starts to decompose above 650 °C[47,48]. Furthermore, there are no endothermic or exothermic transitions from the BSA incorporated within the polypyrrole matrix; however, the concentration of BSA may be too low in comparison to the large mass of polymer to observe the thermal properties of BSA. The thermal properties of BSA have been reported in several papers[49,50,51] and involve an irreversible denaturation, when the BSA is present in solution. As the BSA comprises of three different structural domains, three transitions in the thermal denaturation might be expected, however only one transition is normally observed and this occurs at about 57 – 60 ^{o}C with an enthalpy of 11 J g^{-1}. However, when the BSA is adsorbed at a surface this thermal transition is not observed[32]. This is more comparable to the BSA incorporated and trapped within the polymer matrix, suggesting that the BSA is stabilised when trapped within the polymer matrix.

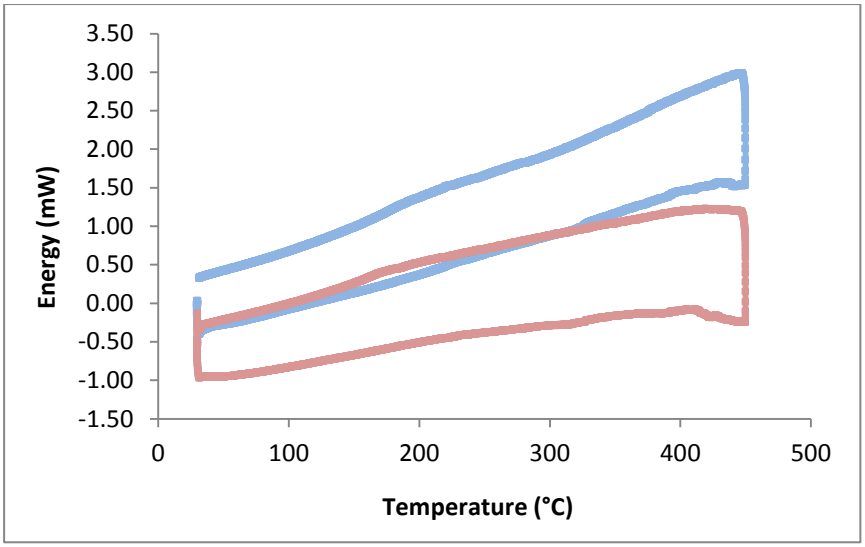

Figure 3.31: DSC thermograms of — PPy-Cl and — PPy-BSA. The temperature was scanned from 50 ^{o}C to 450 ^{o}C and back again at a rate of 10 ^{o}C min^{-1}.

3.3.2.8 Impedance Analysis of the Polymers

Electrochemical impedance spectroscopy, EIS, is a technique that is used to distinguish and describe the dominant processes that evolve with time in an electrochemical system. Fast processes are sampled only at high frequency, while slow processes dominate the response at low frequency[52]. EIS measurements were carried out on the PPy-Cl and PPy-BSA polymer films at applied potentials from -0.10 to 0.90 V vs. SCE. Prior to the measurements, the films were preconditioned for 30 min at the applied potential in the same solution. This conditioning period was sufficiently long to achieve steady-state conditions. The steady-state condition was verified by recording the impedance data from high to low frequencies and then from low to high frequencies. Although not shown here, identical impedance responses were observed during the forward and reverse scans, indicating steady-state conditions. Representative Nyquist and Bode plots are presented in Figure 3.32 (a) and (b) for the PPy-Cl and PPy-BSA films recorded in 0.10 mol dm^{-3} NaCl at 0.50 V vs. SCE. The modulus of the impedance, Z, and the phase angle, presented as a function of the frequency, gives the Bode plot, while the imaginary and real components of the impedance are plotted to give the Nyquist or complex plane. In all cases, the impedance data were recorded as a function of the immersion time at the fixed potential.

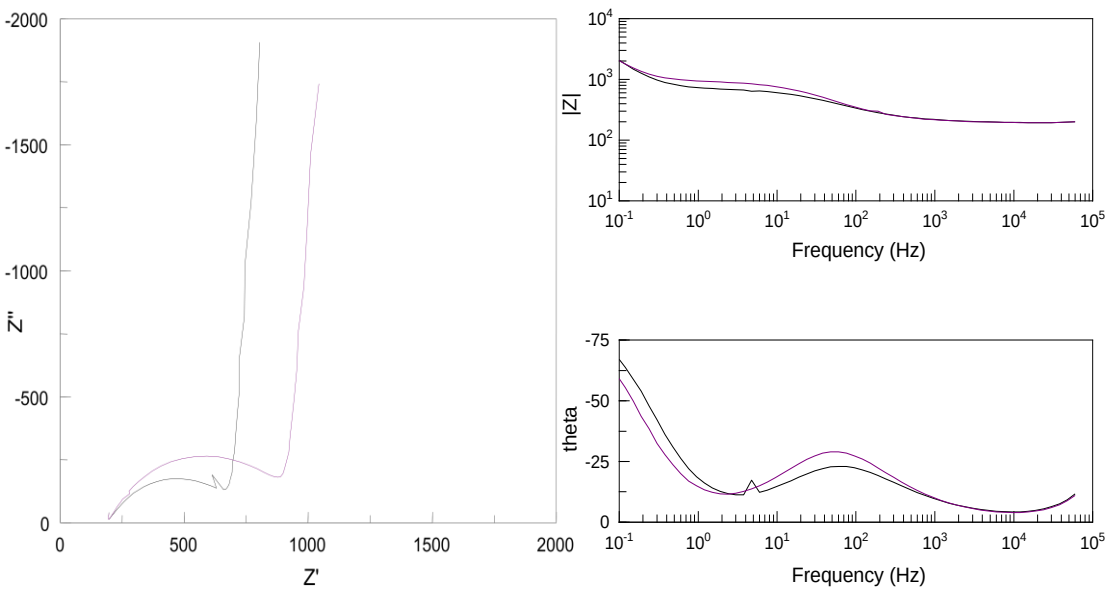

Figure 3.32: The Nyquist and Bode plots (with Z in units of Ω cm^2) recorded for the ▬ PPy-Cl (0.74 C) and ▬ PPy-BSA (0.74 C) films in 0.10 mol dm^{-3} NaCl at an applied potential of 0.50 V vs. SCE.

It is evident from Figure 3.32 that the PPy-Cl and PPy-BSA polymer films have similar impedance profiles, however the diameter of the depressed semicircle is higher for the PPy-BSA film, indicating a higher film resistance. At lower frequencies, a sharp increase in the imaginary impedance is observed, giving a diffusion-like tail. However, the phase angle approaches 90° indicating a process that is not purely diffusion controlled, but is more complex. The impedance data were fitted to the equivalent circuit depicted in Figure 3.33, which corresponds to a two-time constant model. The model contains the solution resistance, Rs, the charge-transfer resistance, R1, and two constant phase elements, CPE1 and CPE2. As described in Chapter 2, Section 2.2.3, the CPE has a magnitude and exponent term, where exponent values of 0.5 represent diffusional processes and values close to 1.0 represent an ideal capacitor. The exponent of the constant phase elements were higher than 0.98 for CPE2 and varied from 0.70 to 0.85 for CPE1, indicating that CPE2 corresponds to a pure capacitor and that CPE1 describes a distorted capacitance.

The impedance data were collected as a function of time and fitted to the circuit in Figure 3.33 to extract the charge-transfer resistance, R1, and the capacitance and distorted capacitance. These are plotted as a function of time for the PPy-Cl and PPy-BSA films in Figures 3.34, 3.35 and 3.36. The time-dependent behaviour of the

charge-transfer resistance is illustrated in Figure 3.34. Very good reproducibility was obtained for the PPy-Cl system, but there was some variation in the behaviour of the PPy-BSA films, although the resistance at short times is reproducible. At an applied potential of 0.50 V vs. SCE, the PPy-Cl and PPy-BSA films are oxidised. PPy is well known to have high electronic conductivity in the oxidised or even slightly oxidised states[37]. Accordingly, the electronic resistance is negligible under these conditions and the resistance denotes the resistance to ion transfer at the polymer boundary and the intrinsic charge transfer resistance. Interestingly, the resistance remains essentially constant for the PPy-Cl films; however, there is a significant increase in the resistance of the PPy-BSA with continued polarisation at 0.50 V vs. SCE in the chloride-containing electrolyte. These increasing resistance values may be related to conformational changes, solvent and electrolyte uptake within the film and indicate the evolution of the film to a more insulating state.

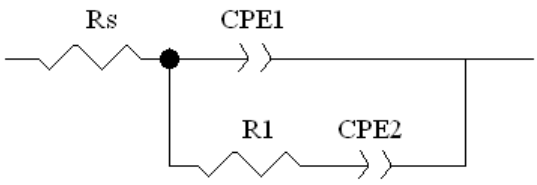

Figure 3.33: The equivalent electrochemical circuit used to fit impedance data for the PPy-Cl and PPy-BSA polymer films.

In Figure 3.35 the distorted capacitance, CPE1, is plotted as a function of time for the PPy-Cl and PPy-BSA films polarised at 0.50 V vs. SCE. A high capacitance of the order of 5 mF cm^{-2} is seen for the PPy-Cl film during the early stages of polarisation, but there is a significant decay in this capacitance with continued polarisation to reach values of the order of 0.50 mF cm^{-2} at 500 min. This high capacitance is in good agreement with the capacitance recorded for polypyrrole in the oxidised state[26,35,37]. A lower capacitance is observed for the PPy-BSA film and again this decays to values in the vicinity of 0.30 mF cm^{-2} after a 500 min polarisation period. The pure capacitance term, CPE2, is shown as a function of time for the PPy-Cl and PPy-BSA films polarised at 0.50 V vs. SCE in Figure 3.36. Again, higher values are observed for the PPy-Cl films consistent with the more conducting nature of the PPy-Cl films compared to the PPy-BSA films. In this case,

the capacitance remains essentially constant as a function of the polarisation period. Similar data were recorded at applied potentials from 0.20 to 0.80 V vs. SCE, while at an applied potential of 0.90 V vs. SCE overoxidation of the polymers was observed. In all cases, the PPy-Cl films were more conducting with lower charge-transfer resistance values and higher capacitance.

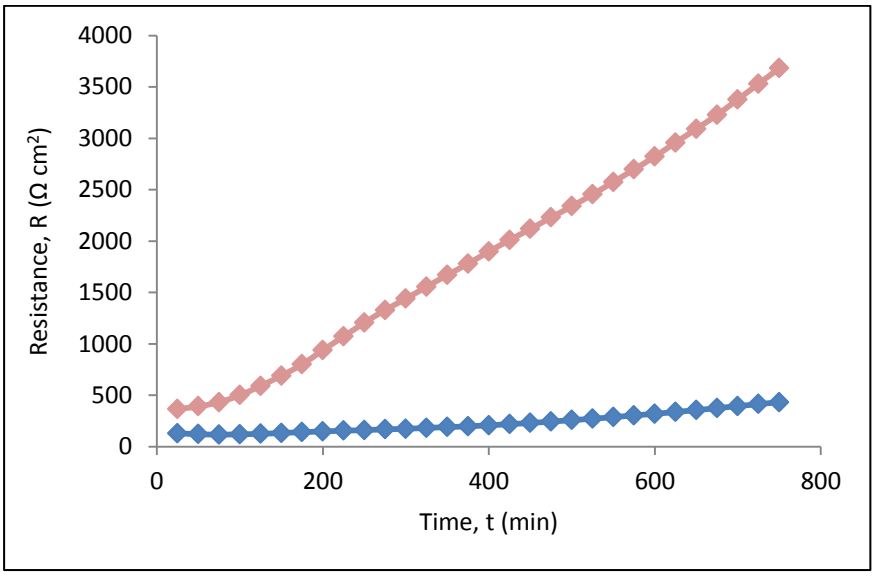

Figure 3.34: A plot of the charge transfer resistance recorded as a function of time at 0.50 V vs. SCE for the — PPy-Cl (0.74 C) and — PPy-BSA (0.74 C) polymer films.

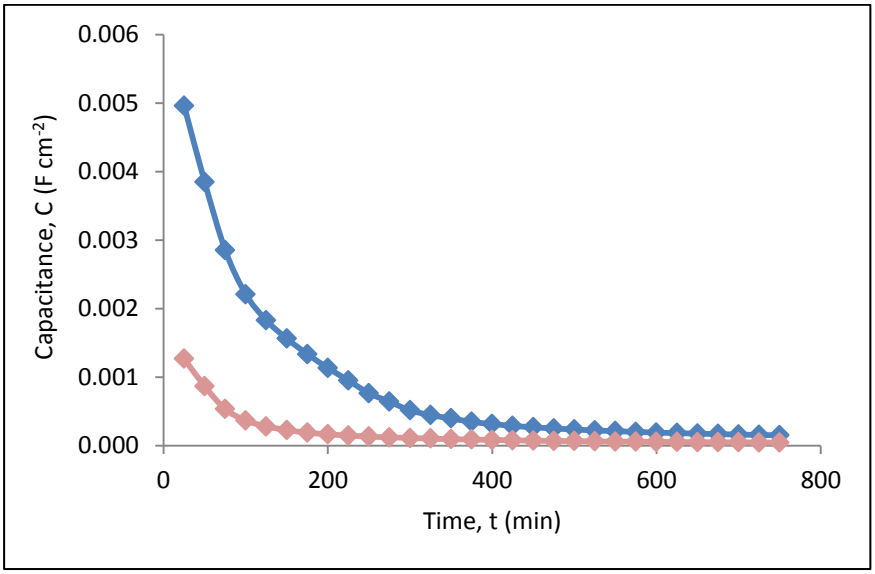

Figure 3.35: A plot of the capacitance, CPE1, recorded as a function of time at 0.50 V vs. SCE for the — PPy-Cl (0.74 C) and — PPy-BSA (0.74 C) polymer films.

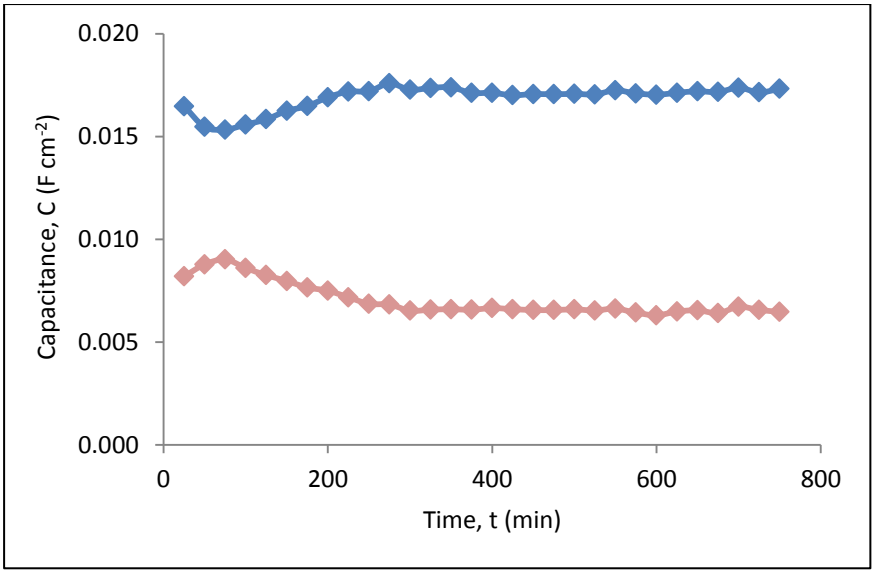

Figure 3.36: A plot of the capacitance, CPE2, recorded as a function of time at 0.50 V vs. SCE for the — PPy-Cl (0.74 C) and — PPy-BSA (0.74 C) polymer films.

3.3.3 Favourable Conditions for the Formation of PPy-BSA

Considering the parameters that may affect the growth of the PPy-BSA films, favourable conditions were obtained and these are summarised in Table 3.4. An applied potential of 0.70 V vs. SCE gave consistent current-time plots and highly reproducible conditions for the growth of PPy-BSA. A high monomer concentration was required and 50 µL of BSA dissolved in 10 mL NaCl gave a sufficient concentration of BSA and a solution that was not too viscous. The optimum electrochemical window for long-term stability of the PPy-BSA films was also determined and this is included in Table 3.4.

Once the favourable conditions for the growth of the PPy-BSA polymer film had been determined, and the polymer films characterised, the next step was to investigate the sensing ability of the BSA entrapped within the polymer matrix.

Table 3.4: The favourable conditions for the growth of the PPy-BSA polymer

Parameter	Favourable conditions
Applied potential	0.70 V vs. SCE
Volume of BSA	50 µL in 10 mL of 0.10 mol dm^{-3} NaCl
Pyrrole concentration	0.50 mol dm^{-3}
Electrochemical window	-0.60 V to 0.80 V vs. SCE

3.3.4 Interactions of PPy-BSA with Tryptophan

Tryptophan, (Trp) is a vital constituent of proteins and an essential amino acid for humans and animals due to its physiological roles[53,54]. Trp is indispensable in human nutrition for establishing and maintaining a positive nitrogen balance[55]. However, Trp cannot be synthesised directly in the human body and, consequently, it is often added to dietary, food products and pharmaceutical formulae as its presence in vegetables is scarce[56]. Tryptophan is a precursor for the neurotransmitter serotonin, the neuro-hormone melatonin, niacin and other relevant biomolecules[57] and has been implicated as a possible cause of schizophrenia in people who cannot metabolise it properly[58]. When Trp is improperly metabolised, a toxic waste product is created in the brain that can cause hallucinations and delusions[59,60]. In addition, the level of Trp in plasma is closely related with the extent of hepatic disease[61,62]. Consequently, a simple, sensitive and selective method of monitoring Trp is indeed necessary.

Bovine serum albumin is a well known complexing agent in the separation of chiral molecules such as racemic tryptophan[63], with different binding sites for the D- and L-enantiomers of Trp[64,65]. At a pH of 7.0, a hydrophobic interaction between Trp and BSA has been observed[66]. However, at higher pH values, the binding of L-Trp on BSA increases up to a maximum at a pH of 9.0[67]. At lower pH values, i.e., between pH 3.5 and 5.0, BSA undergoes conformational changes in which its three domains physically separate due to slight expansion of the BSA[68]. This is described in more detail in Chapter 1, Section 1.5.

Tryptophan is known to be electroactive at a variety of electrodes, including platinum[69], graphite[70] and glassy carbon[71]. Consequently, Trp was chosen and using cyclic voltammetry possible interactions between the Trp molecule and the BSA incorporated within the polypyrrole matrix were explored. The PPy-BSA films were deposited at 0.70 V vs. SCE to a fixed charge of 0.10 C cm^{-2} and cycled in 0.10 mol dm^{-3} NaCl to obtain a background current. Then, the PPy-BSA was transferred to a solution containing 0.10 mol dm^{-3} NaCl and 0.01 mol dm^{-3} Trp and the voltammograms were recorded. Both solutions were adjusted to a pH of 7.0, as the PPy-BSA film is stable at this pH and it is also close to the isoelectric point of Trp[72]. Similar studies were carried out with the PPy-Cl films. As the oxidation of Trp has been observed at potentials close to 0.70 V vs. SCE[73], the electrochemical window was extended to 0.90 V vs. SCE, and furthermore to -0.90 V vs. SCE in an attempt to lower the background current arising from the conducting properties of the polymers. These limits are somewhat different to those presented in Table 3.4, but nevertheless the PPy-Cl and PPy-BSA showed good stability under these conditions. Representative cyclic voltammograms are shown in Figure 3.37; these have much higher currents than those in Figure 3.24 that were recorded in the absence of tryptophan.

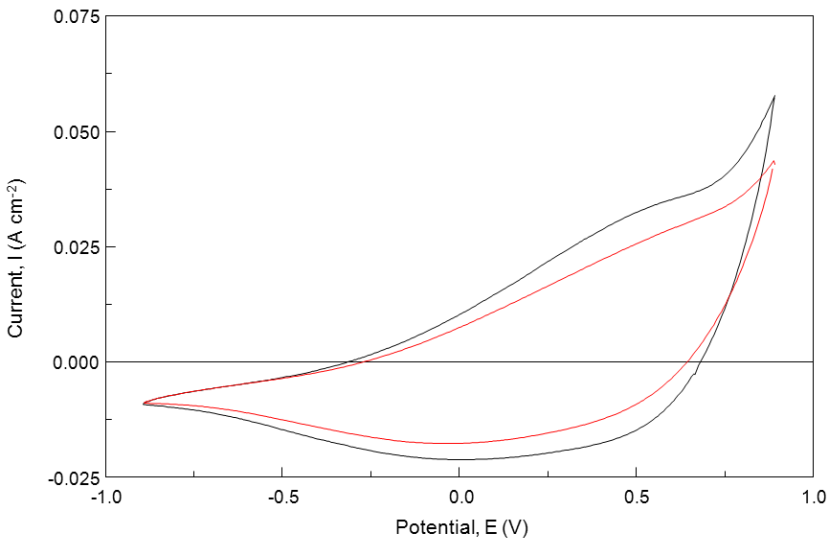

Figure 3.37: Cyclic voltammograms recorded for ▬ PPy-Cl and ▬ PPy-BSA polymer films in a 0.10 mol dm^{-3} NaCl solution containing 0.01 mol dm^{-3} Trp at a pH of 7.0.

There is no evidence of any peak arising from the oxidation of Trp. Slightly higher currents are recorded for the PPy-Cl films; however this is probably related to the higher conductivity of the PPy-Cl. As the pH of the solution may play an important role in the binding characteristics of BSA and Trp, the pH was varied from 2.1 to 12.0. In addition to the optimum BSA concentration, Table 3.4, the BSA concentration was increased to 200 μL to give PPy-BSA films with higher loadings of BSA. The PPy-Cl and PPy-BSA films were initially cycled in a background 0.10 mol dm^{-3} NaCl solution at the required pH and then cycled in 0.01 mol dm^{-3} Trp, 0.10 mol dm^{-3} NaCl at the same pH. Voltammograms similar to those presented in Figure 3.37 were obtained at pH 2.1, 4.0, 7.0 and 9.0 and only at a pH of 12.0 did the voltammograms differ, and this can be related to the loss in stability of the films in this highly alkaline solution, as shown earlier in Figure 3.29. The current observed at a fixed potential of 0.70 V vs. SCE, which is close to the potential where the oxidation of Trp has been reported[73], was recorded. In all cases, the background current was subtracted and this value was plotted as a function of the cycle number for the PPy-Cl, PPy-BSA (50 μL) and PPy-BSA (200 μL) films. These data are presented in Figure 3.38 (a) and (b), and Figure 3.39 (a) and (b) for pH values of 2.0, 4.0, 7.0 and 12.0, respectively.

It is clearly evident that higher currents are obtained with the PPy-Cl films regardless of the pH of the solutions. The concentration of BSA exerts a significant influence with lower currents been observed with the high loading of BSA (200 μL). For example, at a pH of 4.0 the current density is approximately 5 mA cm^{-2} for PPy-BSA (200 μL), 15 mA cm^{-2} for PPy-BSA (50 μL) and 20 mA cm^{-2} for PPy-Cl. A similar trend is seen at pH 7.0, with slightly lower currents recorded at pH 2.1 and 12.0. This is more clearly shown in Figure 3.40, where the background-corrected current at 0.70 V vs. SCE is plotted as a function of the pH for the PPy-Cl, PPy-BSA (50 μL) and PPy-BSA (200 μL) films. This suggests a clear interaction between the BSA incorporated within the polypyrrole matrix and the Trp in solution and this interaction appears to be stronger at pH 4.0 and 7.0.

(a)

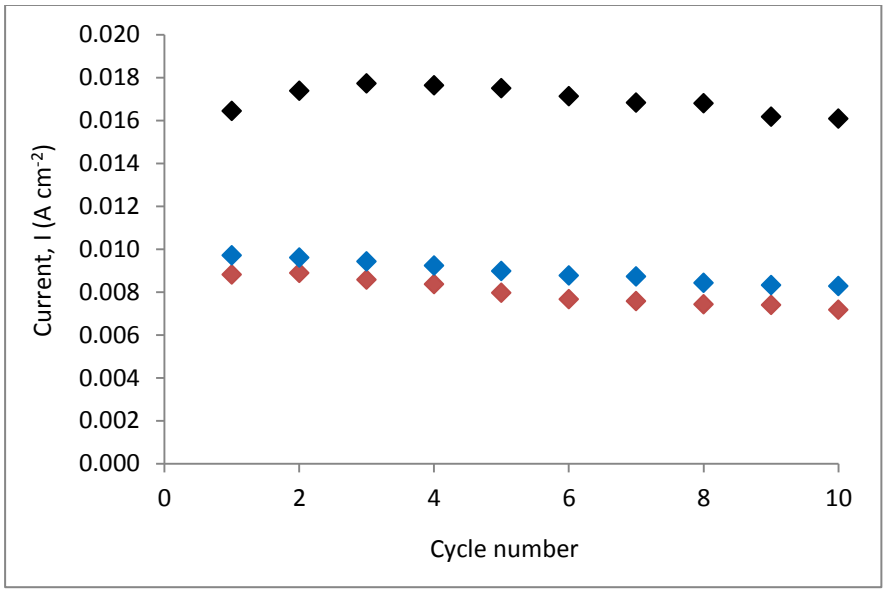

(b)

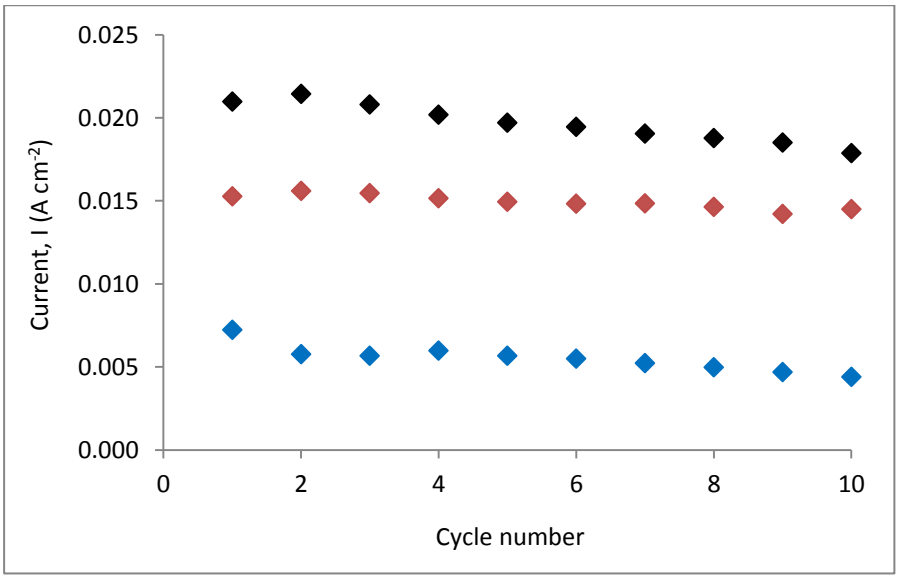

Figure 3.38: The current densities (obtained at a fixed potential of 0.60 V vs. SCE) less the background obtained from cycling the ▬ PPy-Cl (0.74 C), ▬ PPy-BSA (0.74 C, 50 µL) and ▬ PPy-BSA (0.74 C, 200 µL) polymer films from -0.90 V to 0.90 V vs. SCE in a 0.01 mol dm^{-3} Trp, 0.10 mol dm^{-3} NaCl solution at a pH of (a) 2.1 and (b) 4.0.

(a)

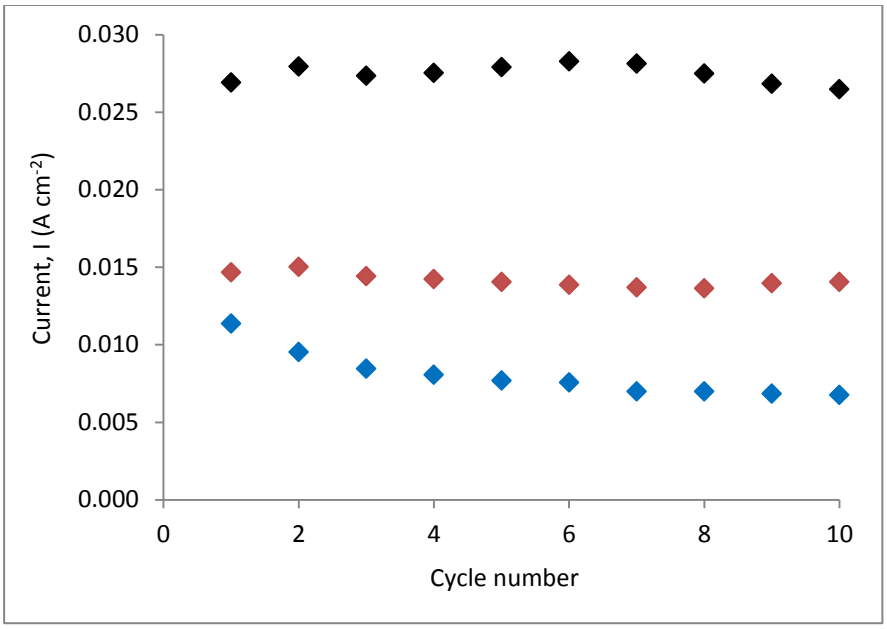

(b)

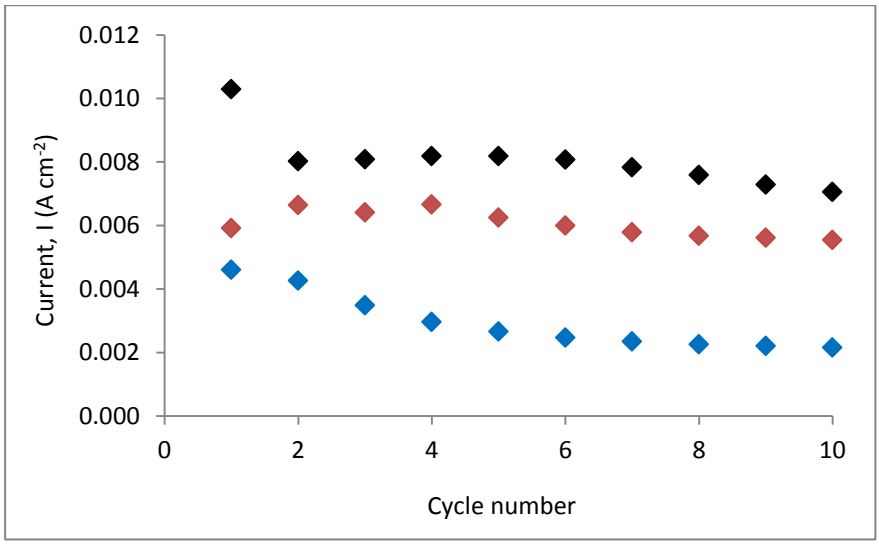

Figure 3.39: The current densities (obtained at a fixed potential of 0.60 V vs. SCE) less the background obtained from cycling the ▬ PPy-Cl (0.74 C), ▬ PPy-BSA (0.74 C, 50 µL) and ▬ PPy-BSA (0.74 C, 200 µL) polymer films from -0.90 V to 0.90 V vs. SCE in a 0.01 mol dm^{-3} Trp, 0.10 mol dm^{-3} NaCl solution at a pH of (a) 7.0 and (b) 12.0.

The percentage loss in the current density is summarised in Table 3.5. This was computed by calculating the difference in the currents of the PPy-Cl and PPy-BSA polymer films. This was then expressed as a percentage of the current measured for the PPy-Cl polymer film. This further highlights that the BSA is indeed binding to the tryptophan as the higher concentration of BSA yields a greater percentage loss in the signal and again this loss is more pronounced at pH 4.0 and 7.0.

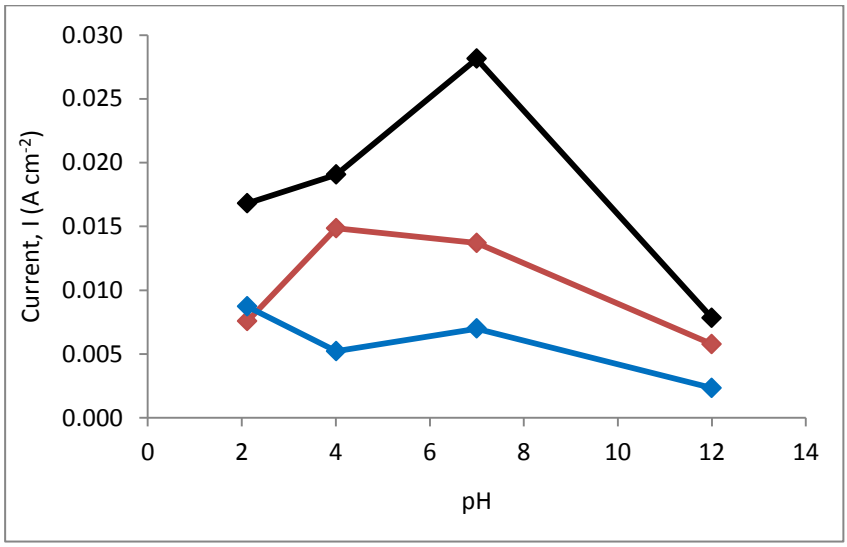

Figure 3.40: The current densities (obtained at a fixed potential of 0.70 V vs. SCE) of the fifth cycle of the ▬ PPy-Cl, ▬ PPy-BSA (50 µL) and ▬ PPy-BSA (200 µL) polymer films in a 0.01 mol dm^{-3} Trp, 0.10 mol dm^{-3} NaCl solution plotted as a function of pH.

Table 3.5: The percentage loss in the current recorded for the PPy-BSA films after cycling in 0.10 mol dm^{-3} NaCl and 0.01 mol dm^{-3} Trp.

pH	% loss in the current of PPy-BSA (50 µL)	% loss in the current of PPy-BSA (200 µL)
2.1	54.9 %	48.1 %
4.0	22.1%	72.6 %
7.0	51.3 %	75.2 %
12.0	26.9 %	70.1 %

3.3.5 Interactions of PPy-BSA with Ascorbic Acid

Ascorbic acid (AA), commonly known as Vitamin C, is an essential vitamin and thus a vital component in the diet of humans. Insufficient intake of AA leads to scurvy and AA is also used for the prevention and treatment of common colds, mental illness, infertility, cancer and AIDS[74,75]. Ascorbic acid is also a well known interfering compound in biological systems[76,77]. AA is a compound of significant biomedical interest because of its antioxidant properties and significant role in the functioning of the human metabolism, central nervous system and renal system[78]. Additionally, a number of studies have investigated the function of AA in gene expression and as a co-substrate of many important dioxygenases[75].

The structure of ascorbic acid is given in Figure 3.41. AA exists in the body at high concentrations[79,80] of up to 1.0 x 10^{-4} mol dm^{-3}. Due to its high concentration, AA often interferes with the detection of other important biological compounds such as dopamine, an important neurotransmitter[81], and uric acid, a primary end product of purine metabolism[82]. Consequently, many techniques have been developed in order to detect and eliminate ascorbic acid from interfering with the detection of other compounds[83]; these include electrochemical techniques as AA is electrochemically active and can be easily oxidised. The $E_{½}$ values of AA lie between -100 to 400 mV vs. SCE on most solid electrodes. However, the products of AA oxidation generally foul the electrode surface and cause a decrease in the peak currents[84].

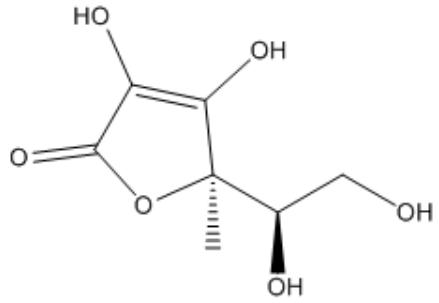

Figure 3.41: The structure of ascorbic acid.

The PPy-BSA polymer film and the PPy-Cl film as a comparison were grown as described previously, by applying a fixed potential of 0.70 V vs. SCE until the polymer reached a fixed charge of 0.10 C, i.e., approximately 3.55 µm in thickness. The polymer films were then cycled in a pH of 9.0, 0.10 mol dm^{-3} NaCl solution to obtain the background currents. The polymers were subsequently cycled in a

solution with a pH of 9.0, 0.01 mol dm^{-3} AA and 0.10 mol dm^{-3} NaCl. This was then repeated at a pH of 4.0 to investigate the effect of pH on AA detection; the resulting cyclic voltammograms are shown in Figure 3.42 and Figure 3.43 for the pH 9.0 and 4.0 solutions, respectively. These voltammograms are very different to those presented in Figure 3.37, which were recorded under similar conditions, but in the presence of Trp. In particular, a broad reduction wave is evident, extended from about -0.25 V to -0.90 V vs. SCE and an oxidation wave is also observed, centred at approximately -0.55 V vs. SCE. These waves were not present in the background voltammograms and can be related to the presence of AA. On reducing the concentration of AA, these waves decreased in magnitude. The oxidation current recorded at -0.55 V vs. SCE in the vicinity of the peak potential of the oxidation wave was recorded and plotted as a function of the cycle number. The resulting plots are shown in Figure 3.44 and Figure 3.45 for the pH 9.0 and 4.0 solutions, respectively.

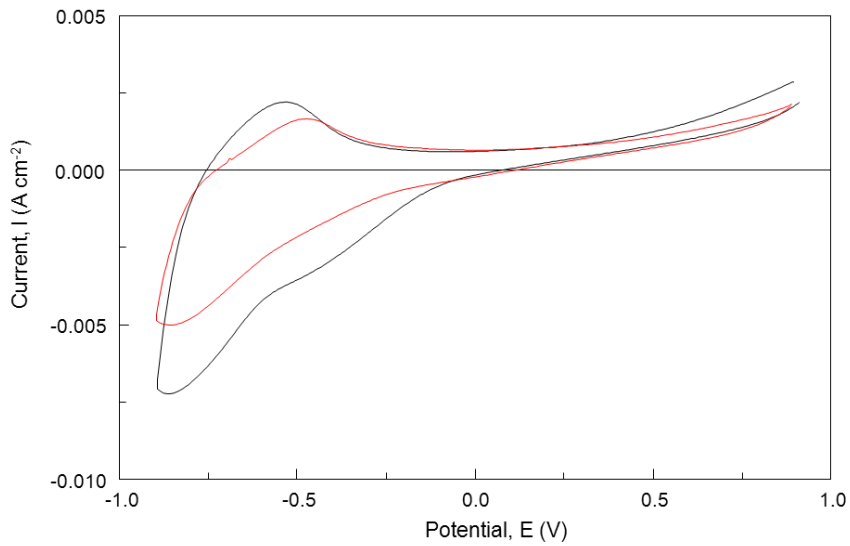

Figure 3.42: Cyclic voltammograms recorded for the ▬ PPy-Cl and ▬ PPy-BSA polymer films cycled in a 0.01 mol dm^{-3} ascorbic acid in 0.10 mol dm^{-3} NaCl solution at a pH of 9.0.

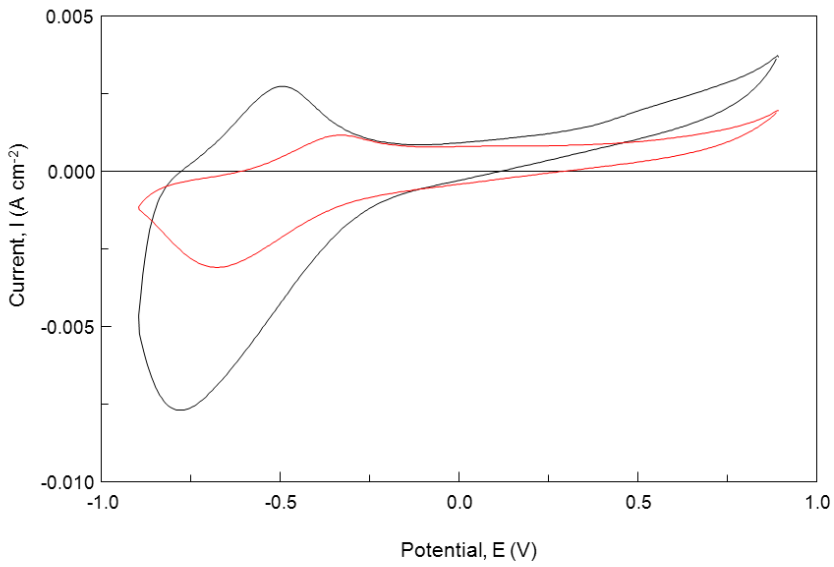

Figure 3.43: Cyclic voltammograms recorded for the ▬ PPy-Cl and ▬ PPy-BSA polymer films cycled in a 0.01 mol dm^{-3} ascorbic acid in 0.10 mol dm^{-3} NaCl solution at a pH of 4.0.

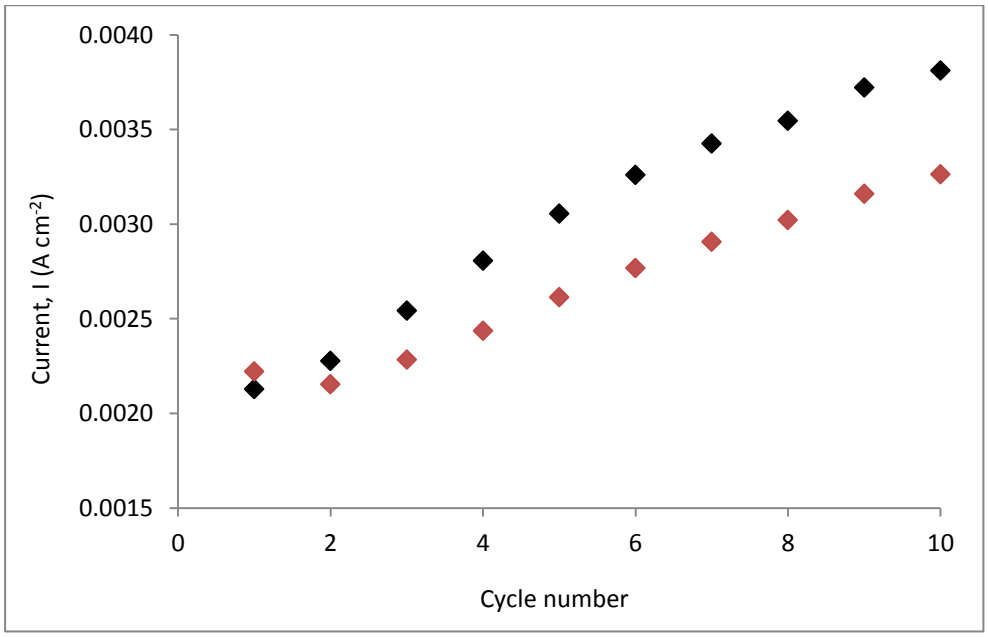

Figure 3.44: Oxidation current obtained at a fixed potential of -0.55 V vs. SCE (with subtraction of background current) plotted as a function of the cycle number for the ▬ PPy-Cl and ▬ PPy-BSA polymer films at a pH of 9.0.

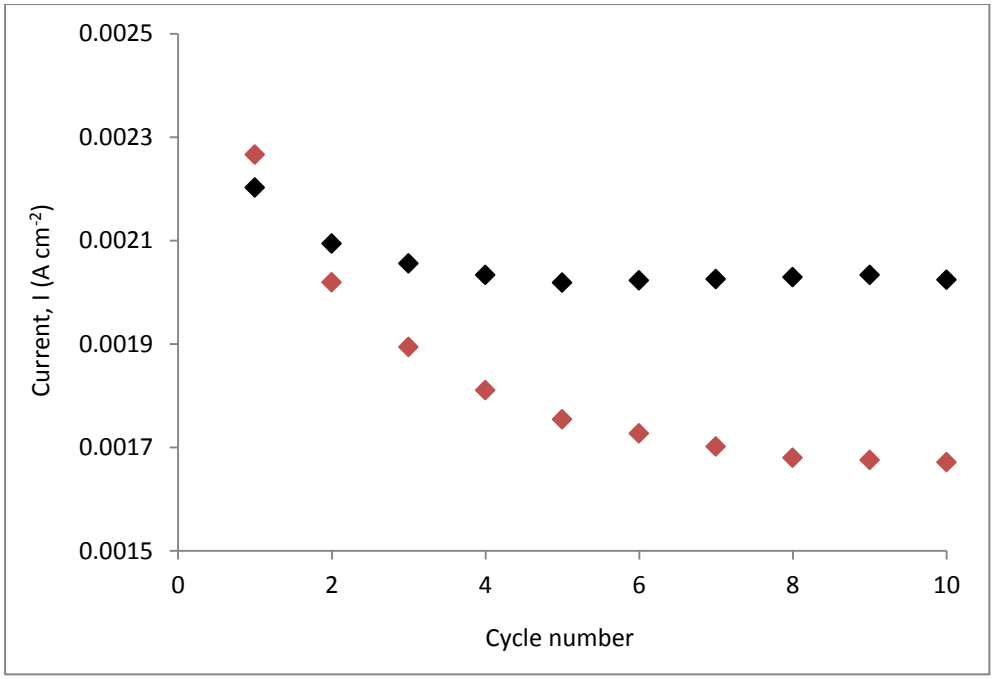

Figure 3.45: Oxidation current recorded at a fixed potential of -0.55 V vs. SCE (with subtraction of background current) plotted as a function of the cycle number for the ▬ PPy-Cl and ▬ PPy-BSA polymer films at a pH of 4.0.

With the exception of the first cycle, higher currents were observed for the PPy-Cl film. This is particularly evident in Figures 3.44 and 3.45, whereby the background currents were subtracted for each cycle. It is also apparent that the currents increase with increasing cycle number for both the PPy-Cl and PPy-BSA films at a pH of 9.0. However, at the more acidic pH of 4.0, the currents are observed to initially decrease with increasing cycle number, before a quasi-steady state is achieved, Figure 3.45. However, there is no clear evidence to suggest that the PPy-BSA film, or indeed the PPy-Cl film, can be used in the detection of AA.

3.4 Conclusions

In summary, the BSA protein was successfully incorporated into the polypyrrole matrix. The optimum conditions for PPy-BSA polymer growth were found to be a high concentration of pyrrole monomer, i.e., 0.50 mol dm^{-3} pyrrole, with low concentrations of BSA dissolved in a 0.10 mol dm^{-3} NaCl solution. The concentrations of BSA used were typically less than 200 µL in 10 mL of 0.10 mol dm^{-3} NaCl. The polymer was grown by applying a fixed potential of 0.70 V vs. SCE

and characterised using SEM and EDX analysis, cyclic voltammetry, differential scanning calorimetry and electrochemical impedance spectroscopy. The PPy-BSA polymer film was then investigated as a sensing material for the amino acid tryptophan over a pH range of 2.1 to 12.0; a clear interaction between the BSA incorporated within the polypyrrole matrix and the tryptophan in solution was observed. The polymer film was subsequently investigated as a sensor for ascorbic acid but there was no evidence found to suggest that it could be used in the detection of ascorbic acid.

3.5 References

1 S. Carquigny, J.-B. Sanchez, F. Berger, B. Lakard and F. Lallemand, *Talanta*, **78**, 199, (2009)

2 S. A. Waghuley, S. M. Yenorkar, S. S. Yawale and S. P. Yawale, *Sensors and Actuators B: Chemical*, **128**, 366, (2008)

3 S. Geetha, C. R. K. Rao, M. Vijayan and D. C. Trivedi, *Analytica Chimica Acta*, **568**, 119, (2006)

4 J. Wang and M. Musameh, *Analytica Chimica Acta*, **539**, 209, (2005)

5 K. Ghanbari, S. Z. Bathaie and M. F. Mousavi, *Biosensors and Bioelectronics*, **23**, 1825, (2008)

6 D. C. Carter and J. X. Ho, Structure of Serum Albumin. *Advanced Protein Chemistry*, **45**, 153, (1994)

7 T. Mogues, J. Li, J. Coburn and D. J. Kuter, *Journal of Immunological Methods*, **300**, 1, (2005)

8 T. Ignat, M. Miu, I. Klepa, A. Bragaru, M. Simion and M. Danila, *Materials Science and Engineering B*, **169**, 55, (2010)

9 A. J. Heeger, *Synthetic Metals*, **125**, 23, (2001)

10 M. Nishizawa, H. Nozaki, H. Kaji, T. Kitazume, N. Kobayashi, T. Ishibashi and T. Abe, *Biomaterials*, **28**, 1480, (2007)

11 S. Carquigny, O. Segut, B. Lakard, F. Lallemand and P. Fievet, *Synthetic Metals*, **20**, 365, (1987)

12 F.-W. Zeng, X.-X. Liu, D. Diamond and K. T. Lau, *Sensors and Actuators B: Chemical*, **143**, 530, (2010)

13 G. G. Wallace, P. C. Dastoor, D. L. Officer and C. O. Too, *Journal of the American Chemical Society*, **30**, (1), 14, (2000)

14 M.-J. Syu and Y.-S. Chang, *Biosensors and Bioelectronics*, **24**, 2671, (2009)

15 E. Garfias-Garcia, M. Romero-Roma, M. T. Ramirez-Silva, J. Morales and M. Palomar-Pardave, *International Journal of Electrochemical Science*, **5**, 763, (2010)

16 S. B. Adeloju, S. J. Shaw and G. G. Wallace, *Analytica Chimica Acta*, **341**, 155, (1997)

17 S. Komaba, M. Seyama, T. Momma and T. Osaka, *Electrochimica Acta*, **42**, (3), 383, (1997)

18 T. Momma, M. Yamamoto, S. Komaba and T. Osaka, *Journal of Electroanalytical Chemistry*, **407**, 91 (1996)

19 B. J. Hwang and K. L. Lee, *Thin Solid Films*, **279**, 236, (1996)

20 J. C. Myland and K. B. Oldham, *Journal of Electroanalytical Chemistry*, **575**, 81, (2005)

21 S. Sadki, P. Schottland, N. Brodie and G. Sabouraud, *Chemistry Society Reviews*, **29**, 283, (2000)

22 A. Ramanavicius, A. Ramanaviciene and A. Malinauskas, *Electrochimica Acta*, **51**, 6025, (2006)

23 T. Yuan, Y. Huang, S. Dong, T. Wang and M. Xie, *Polymer Testing*, **21**, 641, (2002)

24 T. Ahuja, I. A. Mir, D. Kumar and Rajesh, *Sensors and Actuators: B. Chemical*, **134** (1), 140, (2008)

25 T. *de* J. Licona-Sanchez, G, A. Alvarez-Romero, M. Palomar-Pardave, C. A. Galan-Videl, M. E. Paez-Hernandez, M. T. Ramirez Silva and M. Romero-Romo, *International Journal of Electrochemical Science*, **6**, 1537, (2011)

26 S. Suematsu, Y. Oura, H. Tsujimoto, H. Kanno and K. Naoi, *Electrochimica Acta*, **45**, 3813, (2000)

27 J. O. Iroh and G. A. Wood, *European Polymer Journal*, **33**, 107, (1997)

28 J. Serra Moreno, S. Panero and B. Scrosati, *Electrochimica Acta*, **53**, 2154, (2008)

29 G. G. Wallace, G. M. Spinks, L. A. P. Kane-Maguire and P. R. Teasdale, *Conductive Electroactive Polymers: Intelligent Materials Systems*, CRC Press, **237**, (2003)

30 A. M. Fenelon and C. B. Breslin, *Corrosion Science*, **45**, 2837, (2003)

31 R. Tantipolphan, T. Rades, A. J. McQuillan and N. J. Medlicott, *International Journal of Pharmaceutics*, **337**, 40, (2007)

32 H. Larsericsdotter, S. Oscarsson and J. Buijs, *Journal of Colloid and Interface Science*, **289**, 26, (2005)

33 A. L. Brisena, A. Baca, Q. Z. Zhou, R. Lai and F. M. Zhou, *Analytica Chimica Acta*, **441**, 123, (2001)

34 G. Maia, R. M. Torresi, E. A. Ticianelli and F. C. Nart, *Journal of Physical Chemistry*, **100**, 15910, (1996)

35 M. D. Ingram, H. Staesche and K. S. Ryder, *Solid State Ionics*, **169**, 51, (2004)

36 G. G. Wallace, P. C. Dastoor, D. L. Officer and C. O. Too; *Journal of the American Chemical Society*, **30**, (1), 14, (2000)

37 V. D. Patake, S. S. Joshi, C. D. Lokhande and O.-S, Joo, *Materials Chemistry and Physics*, **114**, 6, (2009)

38 B.-X. Zou, Y. Liang, X.-X. Liu, D. Diamond and K.-T. Lau, *Journal of Power Sources*, **196**, 4842, (2011)

39 J. Bard and L. R. Faulkner, *Electrochemical Methods: Fundamentals and Applications*, John Wiley and Sons, Inc., 833 (2001)

40 L. Ozcan, Y. Sahin and H. Turk, *Biosensors and Bioelectronics*, **24**, 512, (2008)

41 S. Asavapiriyanont, G. K. Chandler, G. A. Gunawardena and D. Pletcher, *Journal of Electroanalytical Chemistry*, **177**, 229, (1984)

42 M. Zhou and J. Heinze, *Journal of Physical Chemistry B*, **103**, 8443, (1999)

43 S. Shimoda and E. Smela, *Electrochimica Acta*, **44**, 219, (1998)

44 S. Kuwabata, J. Nakamura and H. Yoneyama, *Journal of the Chemical Society-Chemical Communications*, 779, (1988)

45 G. W. H. Höhne., W. F. Hemminger and H. J. Flammersheim, *Differential Scanning Calorimetry*, Springer, (2003)

46 G. Klancnid, J. Medved and P. Mrvar, *Materials and Geoenvironment*, **57**, (1), 127, (2010)

47 P. Mavinakuli, S. Wei, Q. Wang, A. B. Karki, S. Dhage, Z. Wang, D. P. Young and Z. Quo, *Journal of Physical Chemistry C*, **114**, 3874, (2010)

48 H.-J. Choi, Y.-M. Song, I. Chung, K.-S. Ryu and N.-J. Jo, *Smart Materials and Structures*, **18**, 1, (2009)

49 X. Cao, J. Li, X. Yang, Y. Duan, Y. Liu and C. Wang, *Thermochimica Acta*, **467**, (1-2), 99, (2008)

50 W. Norde and C. E. Giacomelli, *Macromolecular Symposia*, **145**, 125, (1999)

51 A. Michnik, *Journal of Thermal Analysis and Calorimetry*, **71**, 509, (2003)

52 J. R. Macdonald, *Annals of Biomedical Engineering*, **20**, 289, (1992)

53 S. Bihel and I. Birlouez-Aragon, *International Dairy Journal*, **8**, 637, (1998)

54 A. R. Fiorucci and E. T. G. Cavalheiro, *Journal of Pharmaceutical and Biomedical Analysis*, **28**, (5), 909, (2002)

55 B. Fang, Y. Wei, M. G. Li, G. F. Wang and W. Zhang, *Talanta*, **72**, 1302, (2007)

56 J.-B. Raoof, R. Ojani and M. Baghayeri, *Sensors and Actuators B*, **143**, 261, (2009)

57 X. Tang, Y. Liu, H. Hou and T. You, *Talanta*, **80**, 2182, (2010)

58 S. Shahrokhian and L. Fotouhi, *Sensors and Actuators B*, **123**, 942, (2007)

59 C. Li, Y. Ya and G. Zhan, *Colloids and Surfaces B: Biointerfaces*, **76**, 340, (2010)

60 K.-J. Huang, C.-X. Xu, W.-Z. Xie and W. Wang, *Colloids and Surfaces B: Biointerfaces*, **74**, 167, (2009)

61 A. Agazzi, F. De Ponti, R. De Giorgio, S. M. Candura, L. Anselmi, E. Cervio, A. Di Nucci and M. Tonini, *Digestive and Liver Disease*, **5**, 590, (2003)

62 J.-B. Raoof, R. Ojani and K. M. Hassan, *Electroanalysis*, **20**, 1259, (2008)

63 F. Garnier, J. Randon and J. L. Rocca, *Separation and Purification Technology*, **16**, 243, (1999)

64 S. Kiyohara, M. Nakamura, K. Saito, K. Sugita and T. Sugo, *Journal of Membrane Science*, **152**, 143, (1999)

65 H. Ito, M. Nakamura, K. Saito, K. Sugita and T. Sugo, *Journal of Chromatography A*, **925**, 41, (2001)

66 F. Garnier, J. Randon and J. L. Rocca, *Talanta*, **51**, 1001, (2000)

67 J. Hermansson, *Trends in Analytical Chemistry*, **8**, 251, (1989)

68 M. Kato, N. Matsumoto, K. Sakai-Kato and T. Toyo'oka, *Journal of Pharmaceutical and Biomedical Analysis*, **30**, (6), 1845, (2003)

69 S. M. MacDonald and S. G. Roscoe, *Electrochimica Acta*, **42**, 1189, (1997)

70 V. Brabec and V. Mornstein, *Biophysical Chemistry*, **12**, 159, (1980)

71 M. Masui, Y. Kamada, T. Iizuka and S. Ozaki, *Chemical and Pharmaceutical Bulletin*., **32**, 4740, (1984)

72 L.-F. Liu, L.-L. Yang, K.-Y. Jin, D.-Q. Xu and C.-J. Gao, *Separation and Purification Technology*, **66**, 443, (2009)

73 Y. Liu and L. Xu, *Sensors*, **7**, 2446, (2007)

74 A. A. Ensafi, M. Taei and T. Khayamian, *Journal of Electroanalytical Chemistry*, **633**, 212, (2009)

75 O. Arrigoni and M. C. De Tullio, *Biochimica et Biophysica Acta*, **1569** (1-3), 1, (2002)

76 G.-Z. Hu, D.-P. Zhang, W.-L. Wu and Z.-S. Yang, *Colloids and Surfaces B: Biointerfaces*, **62**, 199, (2008)

77 L. Zhang and X. Jiang, *Journal of Electroanalytical Chemistry*, **583**, 292, (2005)

78 H. R. Zare, N. Rajabzadeh, N. Nasirizadeh and M. M. Ardakani, *Journal of Electroanalytical Chemistry*, **589**, (1), 60, (2006)

79 G. Mihael and W. M. A. Damien, *Electrochimica Acta*, **49**, 4743, (2004)

80 J. Zheng and X. Zhou, *Bioelectrochemistry*, **70**, 408, (2007)

81 H. Zhao, Y. Zhang and Z. Yuan, *Analytica Chimica Acta*, **441**, 117, (2001)

82 S. Thiagarajan and S.-M. Chen, *Talanta*, **74**, 212, (2007)

83 J.-M. Zen, J.-J. Jou and G. Ilangovan, *Analyst*, **123**, 1345, (1998)

84 U. E. Majewska, K. Chmurski, K. Biesiada, A. R. Olszyna and R. Bilewicz, *Electroanalysis*, **18**, 1463, (2006)

Chapter 4

The Development of a Polypyrrole Modified Electrode for the Enhanced Detection of Urea

"The one important thing I have learned over the years is the difference between taking one's work seriously and taking one's self seriously. The first is imperative and the second is disastrous."
- *Margot Fonteyn*

4.1 Introduction

There is much interest in the development of urea sensors due to urea being such an important component in both the medical and agricultural industries[1,2]. This section focuses on the importance of urea in the medical sector. Urea is an important substance in both blood serum and urine[3]; in addition, urea is also a clinical variable that provides useful information of decompensated heart failure[4] and, abnormal urea concentrations are indicative of renal and hepatic failures[5].

Urea, also known as carbamide, is a nitrogen-containing compound with the chemical formula of NH_2CONH_2. It is a colourless, odourless solid with an overall neutral charge and is highly soluble in water, upon which it breaks down to form ammonia (NH_3). Ammonia is a much more mobile and volatile compound than urea[6] with a very strong odour.

Excess nitrogen in the form of urea is dissolved in the blood and then excreted by the kidneys as a component of urine. In addition, a small amount of urea is also excreted *via* sweat/perspiration, along with salts and water. If this excess nitrogen is not excreted, ammonia can build up in the body to high levels which leads to cell toxicity and eventually to death. Hence, urea is an important marker for the evaluation of uremic toxin levels[7]. As described in Chapter 1, Section 1.7, the normal blood levels of urea range from 2.5 to 7.5 mmol dm^{-3}, depending on the build and relative health of the body[7]. Above 7.5 mmol dm^{-3}, the patient is said to be suffering from renal deficiency, and the kidneys fail to excrete the excess nitrogen successfully. Hence, it is very important to monitor the level of urea to determine the health of the kidneys in the human body[8,9].

This chapter is focused on the development of a novel urea sensor formed by the entrapment of the urease enzyme within a polypyrrole matrix. This has been carried out previously[7,10], however, poor detection limits were obtained. To further enhance the detection of urea in solution, while repelling common interferants, such as uric acid and ascorbic acid, an anionic cyclodextrin was incorporated into the polypyrrole matrix together with the urease enzyme.

4.2 Experimental

The instrumentation and software employed for the experiments are detailed in Chapter 2 and their analysis are described in Section 2.3. The chemicals used throughout this study were purchased from Sigma-Aldrich or its subsidiary company, Fluka. All chemicals were used as supplied expect for pyrrole which was vacuum-distilled and stored in the dark at -20 °C prior to use. All solutions were made in distilled water. Most of the electrochemical characterisation experiments and calibration curves were carried out in a 0.05 mol dm^{-3} phosphate buffer, pH 7.0, while the sulphonated cyclodextrin-based polymers were formed in 0.02 mol dm^{-3} sulphonated-β-cyclodextrin and the chloride-doped polymers were prepared in 0.10 mol dm^{-3} NaCl. The urease enzyme was dissolved in the electropolymerisation solution to give a concentration of 4000 mg dm^{-3}. All the solutions were prepared freshly before each experiment. All experiments were performed at room temperature. The polymers were formed in the presence and absence of the urease enzyme, in order to test the characteristics and sensitivity of the films. The polymers were formed at a constant applied potential in a typical three-electrode electrochemical cell as shown in Figure 2.5, Chapter 2. The working electrode comprised of a platinum (Pt) disk encased in Teflon with a surface area of 0.0706 cm^{-2}; this was used in conjunction with a Pt wire counter electrode and a saturated calomel reference electrode. The electroactivity and redox properties of the PPy films were investigated using cyclic voltammetry, while scanning electron microscopy and energy dispersive X-Ray analysis was used to gain information on the surface morphology and composition of the polymer films.

4.3 Results and Discussion

Polypyrrole (PPy) is a common polymer used in the development of sensors. It is biocompatible, easy to form, readily available and inexpensive to manufacture. In addition, it is redox active and can be easily oxidised and reduced[11]. It is possible to incorporate biological species such as enzymes and proteins into the polymer by trapping the biological entities between the matrix structure of the polymer[8]. As a result, polypyrrole can be used in the formation of biosensors. After the successful incorporation of the biological entity, BSA, into PPy, which is described in detail in

Chapter 3, the next step was to incorporate the enzyme urease for the enhanced detection of urea[10]. Urease catalyses the conversion of urea to ammonia, as depicted in Equation 4.1. In addition, hydroxide and bicarbonate anions are formed as by-products of this reaction[10].

$$NH_2CONH_2 + 3H_2O \xrightarrow{Urease} 2NH_4^+ + HCO_3^- + OH^- \qquad 4.1$$

4.3.1 Formation of the PPy-Urs-Cl

As detailed in Chapter 3, a number of experimental parameters influence the electropolymerisation of pyrrole in the presence of a biological species[12]. These include the concentration of the pyrrole monomer in solution, the concentration of the biological species and the applied potential[13,14,15]. The concentration of the pyrrole monomer has a significant influence on the growth of the polypyrrole (PPy) film in the presence of Cl^- ions, as shown in Chapter 3. If there is not enough monomer in solution, then the film will not form. Alternatively, if there is an excess of monomer in the solution the polymer will form very quickly and may contain multiple defects or deformities, leading to a loss in sensing performance[16,17,18]. However, the addition of a biological entity, such as BSA, increases the viscosity of the monomer-containing solution. As a result, access of the monomer to the electrode interface is greatly inhibited[19]. In order to overcome this, high concentrations of pyrrole monomer were used in the growth of the PPy-BSA films, i.e., 0.50 mol dm^{-3} pyrrole. Again, this concentration was employed in the presence of 4000 mg L^{-1} urease and 0.10 mol dm^{-3} NaCl to form a polypyrrole film with incorporated urease, PPy-Urs-Cl. A constant applied potential of 0.70 V vs. SCE was used as this produced the most adherent PPy-BSA films, which is consistent with reports in the literature[20]. Figure 4.1 shows the growth profiles of both the PPy-Cl and PPy-Urs-Cl films.

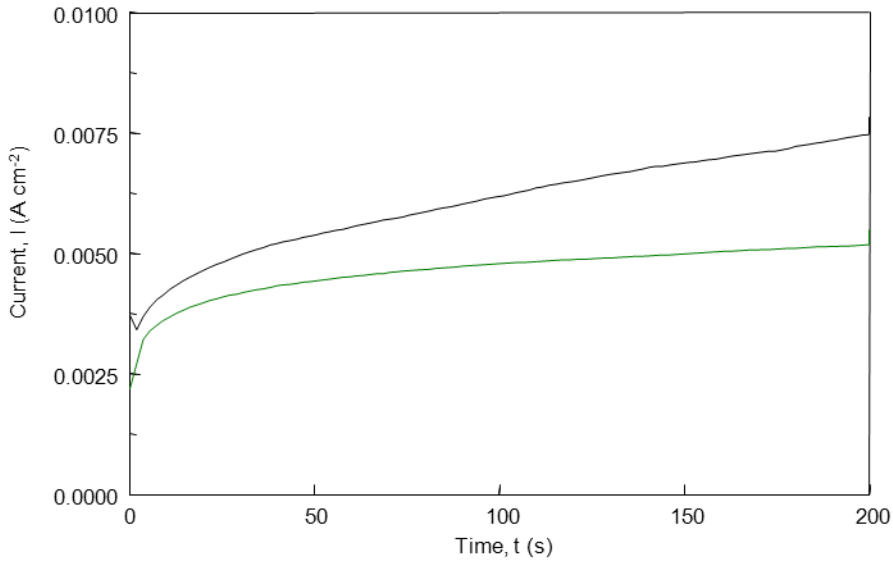

Figure 4.1: Current plotted as a function of time for the formation of PPy-Cl and PPy-Urs-Cl on a Pt electrode at 0.70 V vs. SCE from a solution containing ▬ 0.50 mol dm^{-3} pyrrole/0.10 mol dm^{-3} NaCl and ▬ 0.50 mol dm^{-3} pyrrole/4000 mg L^{-1} urease/0.10 mol dm^{-3} NaCl.

These current-time plots are similar to those shown for the PPy-BSA system in Figure 3.4. Initially, there is a rapid decrease in the current, which arises from the charging of the double layer. This is then followed by a fast rise in the current, which corresponds to the nucleation and growth of the polymer film[16]. There is a further more gradual increase in the current as the polymer is deposited onto the working electrode to give a higher surface area. It is evident from Figure 4.1 that the presence of the urease enzyme in the monomer solution decreases the current density and the rate of electropolymerisation. The urease blocks access of the pyrrole monomer to the electrode, which is evident in the first few seconds of the current-time plot, Figure 4.1, by the lower current density. Accordingly, it takes more time for the critical concentration of radical cations to develop, which in turn gives rise to the dimers and oligomers that are necessary in the deposition of the polymer[16].

4.3.2 Characteristics and Properties of the PPy-Cl and PPy-Urs-Cl Films

After electrochemical polymerisation, the PPy-Cl and PPy-Urs-Cl films were characterised using SEM and EDX and cyclic voltammetry.

4.3.2.1 SEM and EDX Analysis

The surface morphology of the PPy films was investigated using scanning electron microscopy (SEM), as described in Chapter 2, Section 2.2.7. The polymers were electrodeposited as described in Figure 4.1 at 0.70 V vs. SCE onto a flat platinum disc electrode encased in Teflon (0.1256 cm^2) to a charge of 10.48 C cm^{-2}. Typical SEM micrographs recorded for the PPy-Cl film are shown in Figure 4.2, while the micrographs obtained for the PPy-Urs-Cl film are presented in Figure 4.3. A clear difference in the surface morphology of the polymers is evident. The urease containing polymer film has a fibrous morphology due to the incorporated enzyme[8], whereas the PPy-Cl film without urease is very different and does not show any evidence of this fibrous morphology. In addition, the PPy-Cl has the typical cauliflower morphology of polypyrrole owing to the nuclei forming quickly in the presence of the small doping chloride ion and the bulk polymer subsequently growing preferentially around the nucleation sites[21].

EDX measurements were also carried out on the PPy-Cl and PPy-Urs-Cl polymer films, as shown in Figures 4.4 and 4.5, respectively. The EDX spectra of the two polymer films clearly show the presence of chloride at ~ 2.7 keV in both polymer films. This is due to the chloride being incorporated as a dopant anion during the electropolymerisation of pyrrole at 0.70 V vs. SCE, to generate the oxidised PPy which has a positive charge. The dopant anion is important in the growth of polypyrrole films as different sized ions lead to different dopant levels within the polypyrrole film[22,23]. The significant difference between the EDX spectra in the presence and absence of urease is the presence of the nickel at ~ 0.9 keV in the PPy-Urs-Cl film, which is absent in the PPy-Cl film. This nickel is contained in the active site of the Jack Bean urease enzyme[8], and its presence in the EDX spectrum of PPy-Urs-Cl is clear evidence and proof that the urease is indeed incorporated successfully.

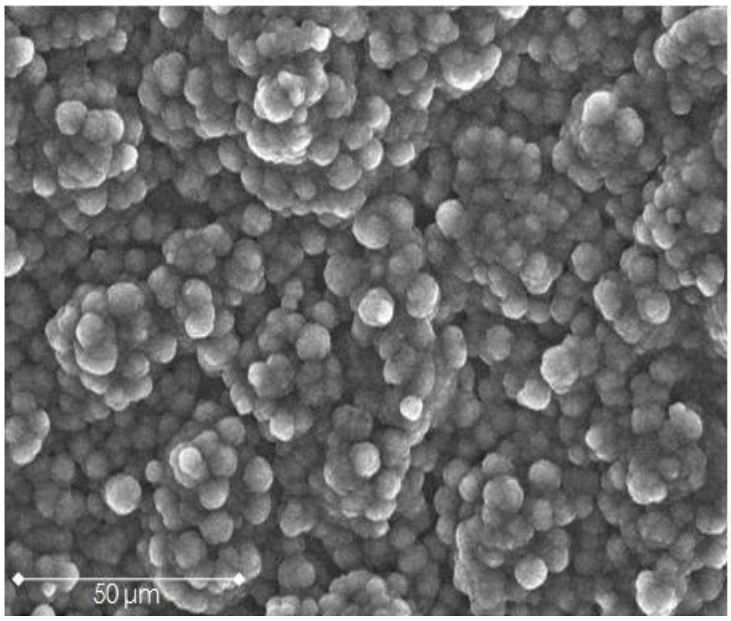

Figure 4.2: Scanning electron micrograph of PPy-Cl electrodeposited on a Pt electrode at 0.70 V vs. SCE from 0.50 mol dm^{-3} pyrrole/0.10 mol dm^{-3} NaCl to a charge of 10.48 C cm^{-2}.

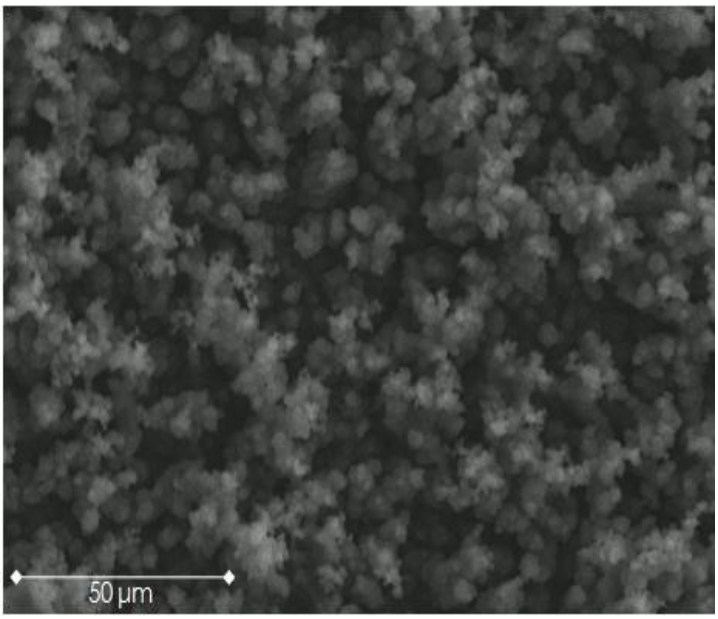

Figure 4.3: Scanning electron micrograph of PPy-Urs-Cl electrodeposited on a Pt electrode at 0.70 V vs. SCE from 0.50 mol dm^{-3} pyrrole/4000 mg L^{-1} urease/0.10 mol dm^{-3} NaCl to a charge of 10.48 C cm^{-2}.

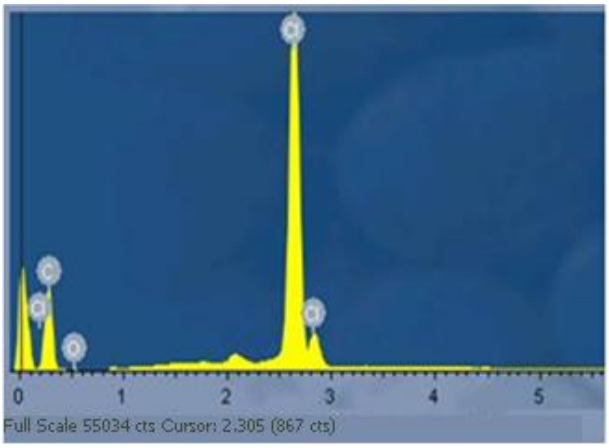

Figure 4.4: Energy-dispersive X-Ray (EDX) analysis of a PPy-Cl film electrodeposited from a solution containing 0.50 mol dm^{-3} pyrrole and 0.10 mol dm^{-3} NaCl with an applied potential of 0.70 V vs. SCE to a charge of 10.48 C cm^{-2}. Cl is observed at ~ 2.85 keV.

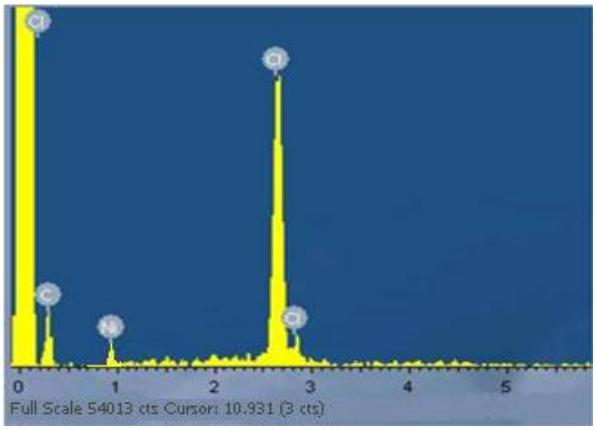

Figure 4.5: EDX analysis of a PPy-Urs-Cl film electrodeposited from a solution containing 0.50 mol dm^{-3} pyrrole, 4000 mg L^{-1} urease and 0.10 mol dm^{-3} NaCl with an applied potential of 0.70 V vs. SCE until a charge of 10.48 C cm^{-2} was reached. Cl is observed at ~ 2.85 keV and Ni is observed at ~ 0.90 keV.

4.3.2.2 Electroactivity of the PPy-Cl and PPy-Urs-Cl Polymers

As shown in Chapter 3, the electroactivity of the polymer films can be altered by changing different parameters such as the scan rate and electrochemical window. Both of these parameters were altered and the electroactivity of the polymers was investigated using cyclic voltammetry. The polymers were freshly electrodeposited onto a platinum working electrode and immediately placed into an electrolyte solution of a 0.05 mol dm^{-3} phosphate buffer solution at a pH of 7.0. Cyclic

voltammetry measurements were then recorded at various scan rates and in different electrochemical windows.

In order to investigate the effect of varying the scan rate on the polymer films, cyclic voltammetry measurements were performed at scan rates ranging from relatively high scan rates of 300 mV s^{-1} to quite slow scan rates of 5 mV s^{-1}. The resulting cyclic voltammograms are shown in Figure 4.6 for the PPy-Cl and PPy-Urs-Cl films. Similar voltammograms were obtained for the PPy-Cl and PPy-Urs-Cl films in this phosphate buffer solution.

It is evident from Figure 4.6 that on decreasing the scan rate lower currents arising from the polymer film, i.e., a decrease in the peak currents, are observed. This is in good agreement with previous studies[24]. With the higher scan rates a broad oxidation wave is observed from -0.10 V vs. SCE up to the upper potential limit of 0.80 V vs. SCE. This corresponds to oxidation of the polypyrrole backbone and the incorporation of anions from the electrolyte solutions. However, as the scan rate is decreased this oxidation wave shifts in potential in the negative direction and the wave is observed to begin at approximately -0.50 V vs. SCE at 10 mV s^{-1}. This behaviour is not connected to the presence of the urease, as similar variations in the potential were seen with the PPy-Cl films. The onset potential of this oxidation wave is shown as a function of the scan rate in Figure 4.7. There is a near linear increase in the onset potential of the oxidation wave with increasing scan rate from 5 to 100 mV s^{-1}, and then the position of the peak is nearly independent of scan rate from 100 to 300 mV s^{-1}. It is clear from Figures 4.6 and 4.7 that variations in the scan rate have a significant influence on both the electroactivity of the PPy-Cl and PPy-Urs-Cl films. These results are different to those shown for the PPy-BSA films, Figure 3.17, Chapter 3, and may be connected to the relatively low concentration of ions in the phosphate buffer solution and the neutral pH, in comparison to the 0.10 mol dm^{-3} NaCl solution used to record the cyclic voltammograms for the PPy-BSA films.

(a)

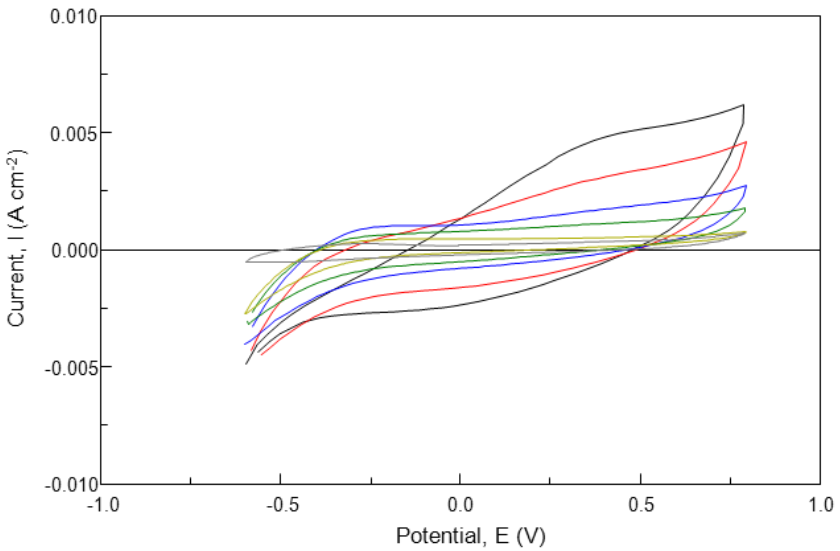

(b)

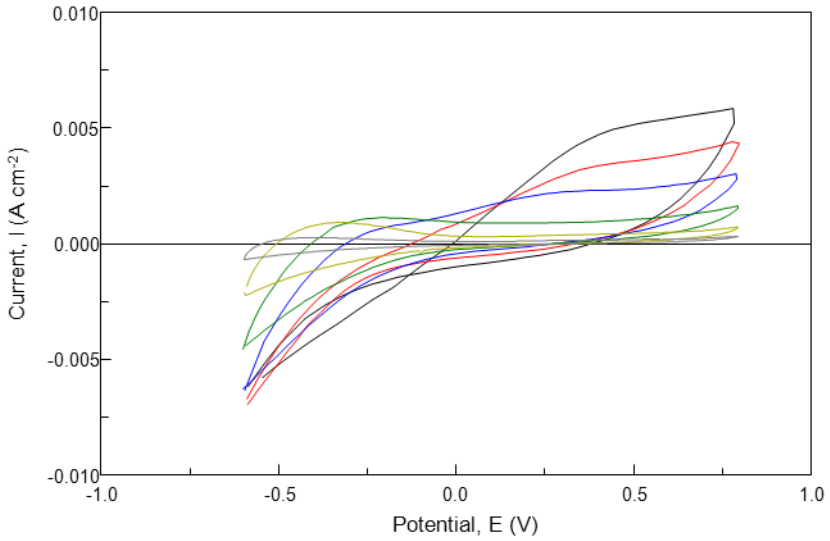

Figure 4.6: Cyclic voltammograms of (a) PPy-Cl and (b) PPy-Urs-Cl recorded in 0.05 mol dm^{-3} phosphate buffer solution, pH of 7.0, at scan rates of — 300 mV s^{-1}, — 200 mV s^{-1}, — 100 mV s^{-1}, — 50 mV s^{-1}, — 25 mV s^{-1} and — 10 mV s^{-1}.

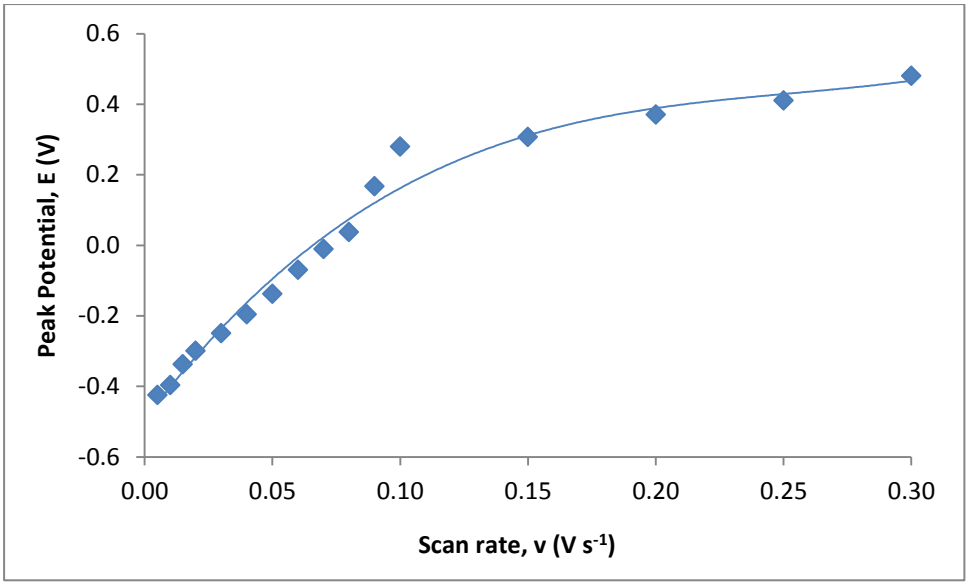

Figure 4.7: Onset potential of the oxidation wave plotted as a function of scan rate for the PPy-Urs-Cl films cycled in 0.05 mol dm^{-3} phosphate buffer, pH of 7.0 at 50 mV s^{-1}.

Typically in cyclic voltammetry an upper and lower potential limit is chosen and the potential is cycled between these two limits[25,26]. Selection of the upper limit is important with conducting polymers as the polymer may be subjected to overoxidation, which results in a considerable loss in conductivity[27]. In order to investigate the effect of the electrochemical window, the PPy-Cl and PPy-Urs-Cl films (0.10 C cm^{-2}) were cycled in a 0.05 mol dm^{-3} phosphate buffer solution, at a pH of 7.0 between -0.60 V vs. SCE and two upper potential limits of 0.80 and 1.20 V vs. SCE. Representative cyclic voltammograms recorded at 50 mV s^{-1} are shown in Figure 4.8.

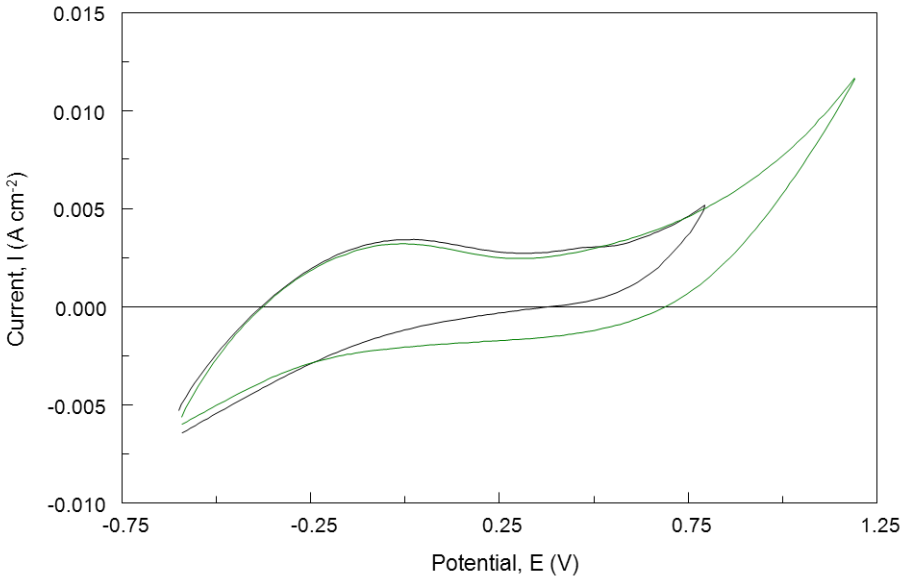

Figure 4.8: Cyclic voltammograms (5th cycle) recorded for PPy-Urs-Cl in a phosphate buffer solution, 0.05 mol dm^{-3}, pH 7.0, from ▬ -0.60 to 1.20 V vs. SCE and ▬ -0.60 to 0.80 V vs. SCE at 50 mV s^{-1}.

Although there is little difference in these voltammograms, except for the additional current with the extended window, repeated cycling between -0.60 and 1.20 V vs. SCE has a significant effect on the stability of the film as shown in Figure 4.9. In this plot the oxidation charge is plotted as a function of the cycle number. There is an initial decay in the oxidation charge over the first 10 to 30 cycles, but then the charge reaches a near steady-state value for the polymer cycled between -0.60 and 0.80 V vs. SCE. This indicates good stability as there is no change in the oxidation charge from 25 to 300 cycles. However, at the higher potential, i.e., up to 1.20 V vs. SCE, the polymer degrades rapidly. There is a sharp reduction in the charge after 150 cycles. This is consistent with overoxidation of the polymer at these high potentials, as it is well known that polypyrrole overoxidises at potentials greater than 1.00 V vs. SCE[27]. Accordingly, this smaller potential window was used for all subsequent cyclic voltammetry measurements.

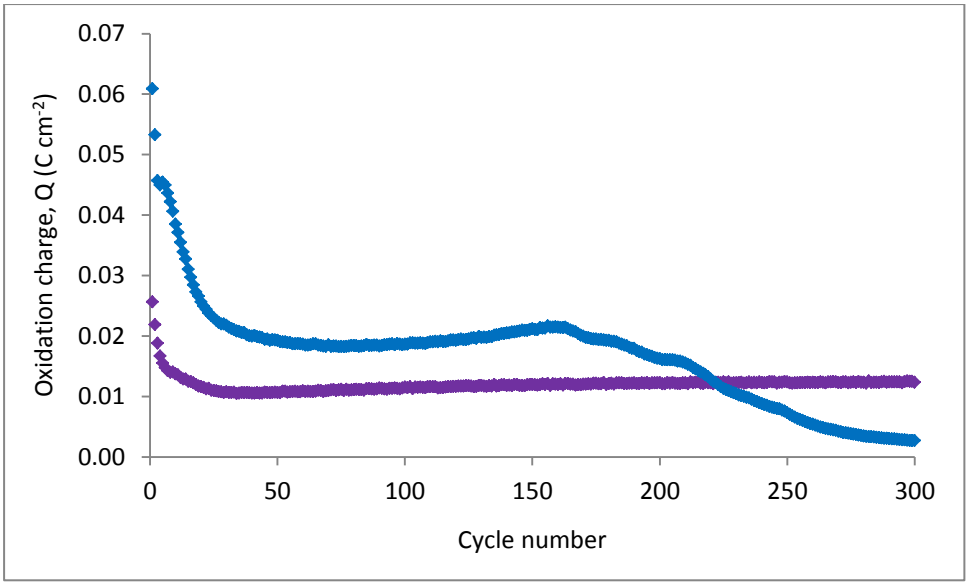

Figure 4.9: Oxidation charge plotted as a function of cycle number for PPy-Urs-Cl cycled in a phosphate buffer solution, 0.05 mol dm^{-3}, pH 7.0, from — -0.60 to 1.20 V vs. SCE and — -0.60 to 0.80 V vs. SCE at 50 mV s^{1}.

4.3.2.3 Capacitance Measurements

It is evident from Figures 4.6 and 4.8 that the PPy-Cl and PPy-Urs-Cl films have high background currents. This is typical of a conducting polymer system with a high capacitance[24,28]. In order to determine the capacitance, the PPy-Cl and PPy-Urs-Cl polymers were cycled in 0.05 mol dm^{-3} phosphate buffer solution, pH 7.0, at different scan rates, but in a small electrochemical window to avoid the effects of faradic currents[27]. The electrochemical window was reduced to 0.10 V up to 0.20 V vs. SCE, and the current was obtained at a fixed potential of 0.14 V vs. SCE. The resulting cyclic voltammograms have a completely different shape from those obtained in a larger potential window as the faradic currents have been reduced, Figure 4.10.

(a)

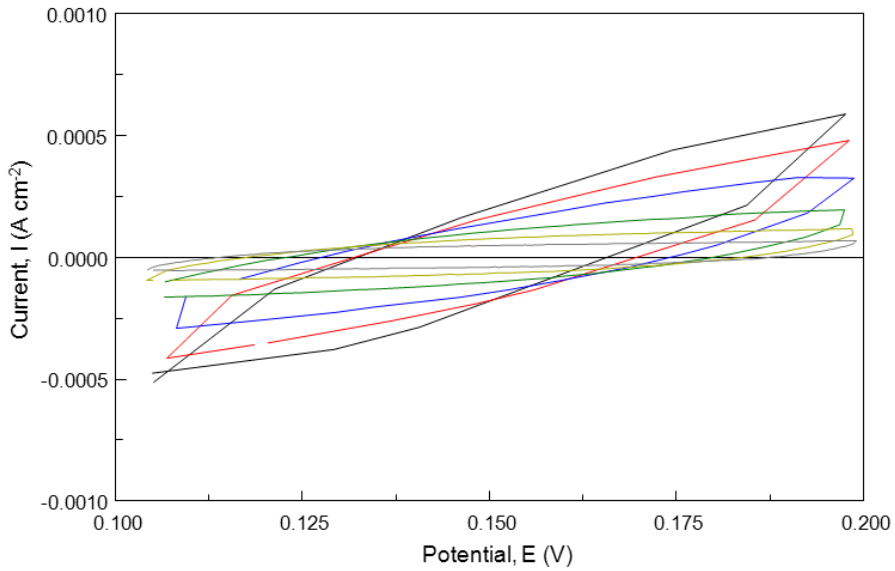

(b)

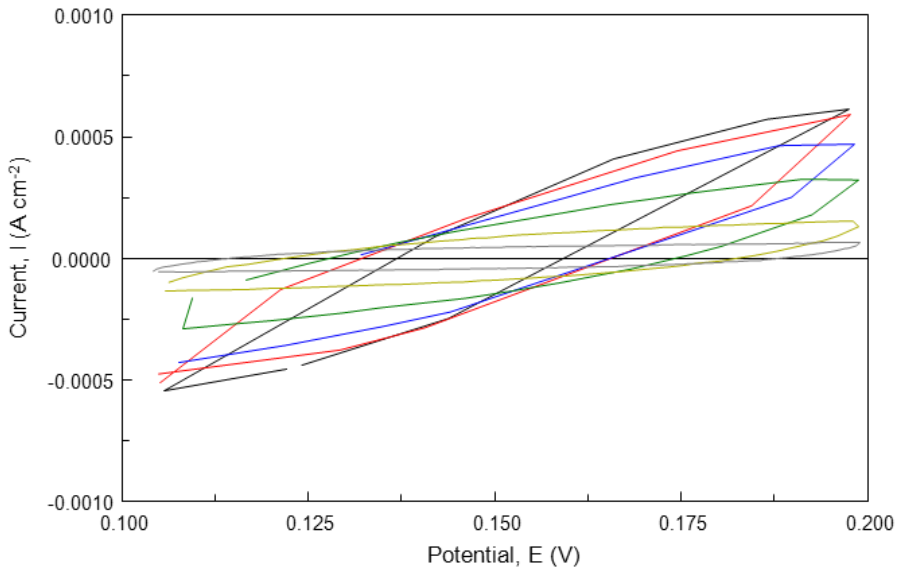

Figure 4.10: Cyclic voltammograms of (a) PPy-Cl and (b) PPy-Urs-Cl polymer films (0.017 C) cycled in 0.05 mol dm^{-3} phosphate buffer at scan rates of ▬ 300 mV s^{-1}, ▬ 200 mV s^{-1}, ▬ 100 mV s^{-1}, ▬ 50 mV s^{-1}, ▬ 25 mV s^{-1} and ▬ 10 mV s^{-1}.

The capacitance was calculated using Equation 4.2, where *C* represents the capacitance (F cm^{-2}), *I* is the current density (A cm^{-2}) and *dV/dt* is the scan rate (V s^{-1})[27,28].

$$C = \frac{I}{\frac{dV}{dt}} \qquad 4.2$$

A plot of the current, *I*, versus the scan rate, *dV/dt*, yields a straight line as shown in Figure 4.11. Correlation coefficients of 0.978 and 0.979 were obtained for the PPy-Cl and PPy-Urs-Cl polymers, respectively, on fitting the data to Equation 4.2, indicting very good linearity. The capacitance of the polymers was found to be in the region of 1.33 x 10^{-3} F cm^{-2}, and 6.70 x 10^{-4} F cm^{-2} for the PPy-Cl and PPy-Urs-Cl films, respectively. This high capacitance is typical of the capacitance recorded for conducting polymers, and is in good agreement with the values reported in the literature[27,29]. The PPy-Urs-Cl film has a slightly lower capacitance which is connected with the presence of the urease enzyme.

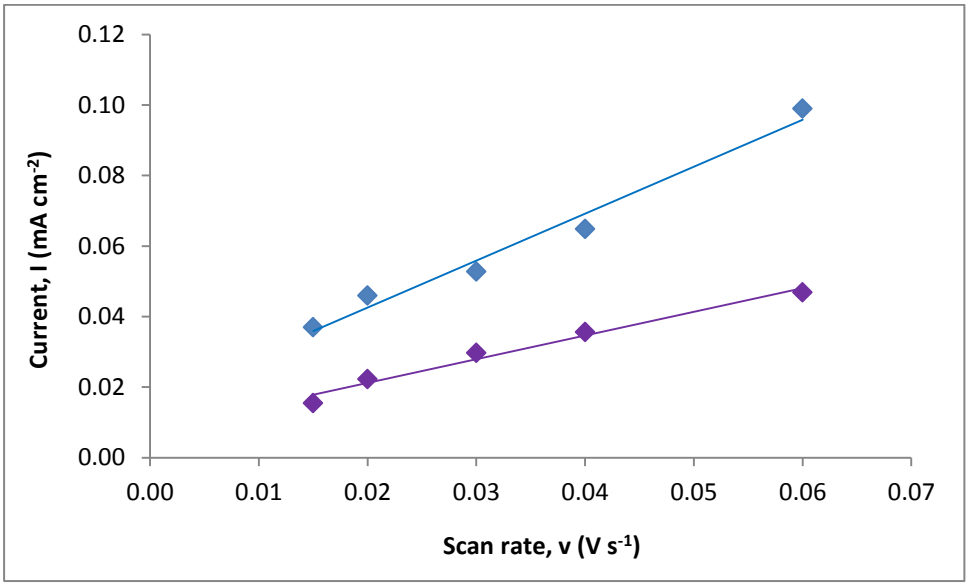

Figure 4.11: Current recorded at a fixed potential of 0.140 V vs. SCE plotted as a function of the scan rate for the — PPy-Cl and — PPy-Urs-Cl polymer films.

4.3.3 Detection of Urea Using the PPy-Cl and PPy-Urs-Cl Films

Once the growth of the PPy-Urs-Cl films was optimised and the presence of the urease enzyme in the film was confirmed, the next step was to investigate the sensing performance of the polymer and its sensitivity to urea. The PPy-Urs-Cl films were electrodeposited onto a Pt electrode, as detailed in Figure 4.1. The modified electrode was rinsed using distilled water to remove any monomer adhering to the surface of the electrode and then placed into a phosphate buffer solution. The film was then cycled between -0.60 and 0.80 V vs. SCE in the phosphate buffer until a steady state was reached. The electrode was removed and placed into a low concentration of urea in phosphate buffer. Again, the film was cycled for a fixed number of cycles (usually 10 cycles) and then placed into the next phosphate buffer solution with a slightly higher concentration of urea. This was repeated over a large concentration range, with rinsing of the modified electrode carried out between each solution in order to avoid transfer and contamination of the solutions. Similar experiments were carried out with the PPy-Cl films.

Although most sensors are amperometric[10], where the current at a fixed potential is monitored, or potentiometric[8], where the potential is recorded, a different approach was taken in this study. On examining the cyclic voltammograms of the modified electrode in the absence and presence of urea (Figure 4.12), it is evident that there is an increase in the current in the presence of urea but this extends over the entire electrochemical window, with no well-defined peak in the current. Accordingly, the entire potential range (-0.60 to 0.80 V vs. SCE) was used and the oxidation charge over this potential was computed, producing a coulombometric sensor. As the presence of urea significantly increases the oxidation charge, Figure 4.12, the charge arising in the absence of urea, from the background phosphate buffer, can be easily subtracted. Hence, all the results presented are given with the background charge subtracted, and thus represent the true charge arising from the urea.

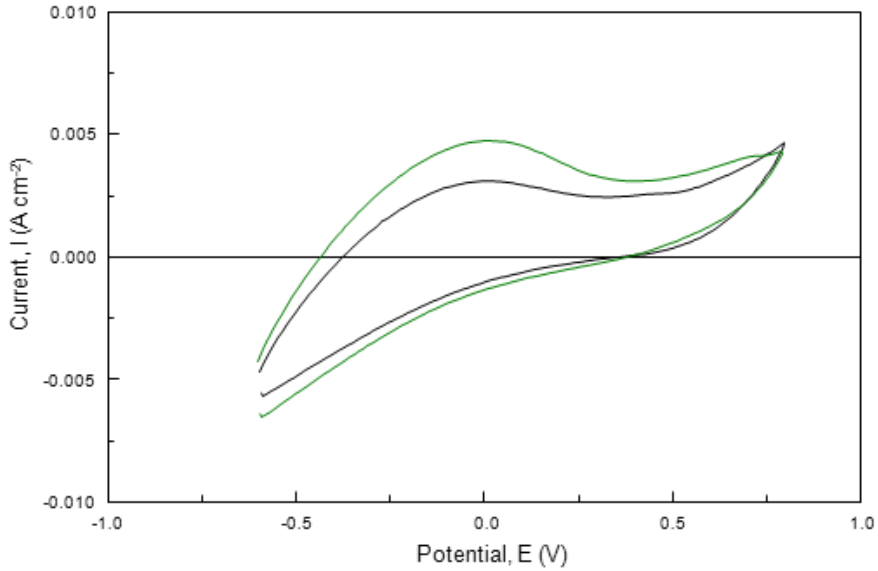

Figure 4.12: Cyclic voltammograms recorded for the PPy-Urs-Cl polymer film in the ▬ presence and ▬ absence of urea.

Typical calibration curves recorded for the PPy-Cl and PPy-Urs-Cl films with the oxidation charge plotted as a function of the urea concentration are presented in Figure 4.13. There is a considerable difference between the PPy-Cl and PPy-Urs-Cl films, with the PPy-Cl showing a poor response to the urea. It is evident from Figure 4.13 that the calibration curve has two linear regions. The slopes of these linear regions were obtained for both the PPy-Cl and PPy-Urs-Cl polymer films. The linear region corresponding to the lower urea levels for the PPy-Cl polymer film was found to have a slope of 2.68 C cm^{-2} mol^{-1} dm^3, whereas the same linear region for the PPy-Urs-Cl film has a slope of 5.41 C cm^{-2} mol^{-1} dm^3. This can be equated to the sensitivity of these films, giving the PPy-Cl film a sensitivity of 2.68 µC $µM^{-1}$ in this region and the PPy-Urs-Cl film a sensitivity of 5.41 µC $µM^{-1}$ in this same region. The same analyses were performed on the second linear regions; again, the PPy-Cl film was found to have a lower sensitivity to urea of 0.43 µC $µM^{-1}$, whereas the PPy-Urs-Cl film was found to have a good sensitivity of 0.76 µC $µM^{-1}$ in this higher urea concentration region.

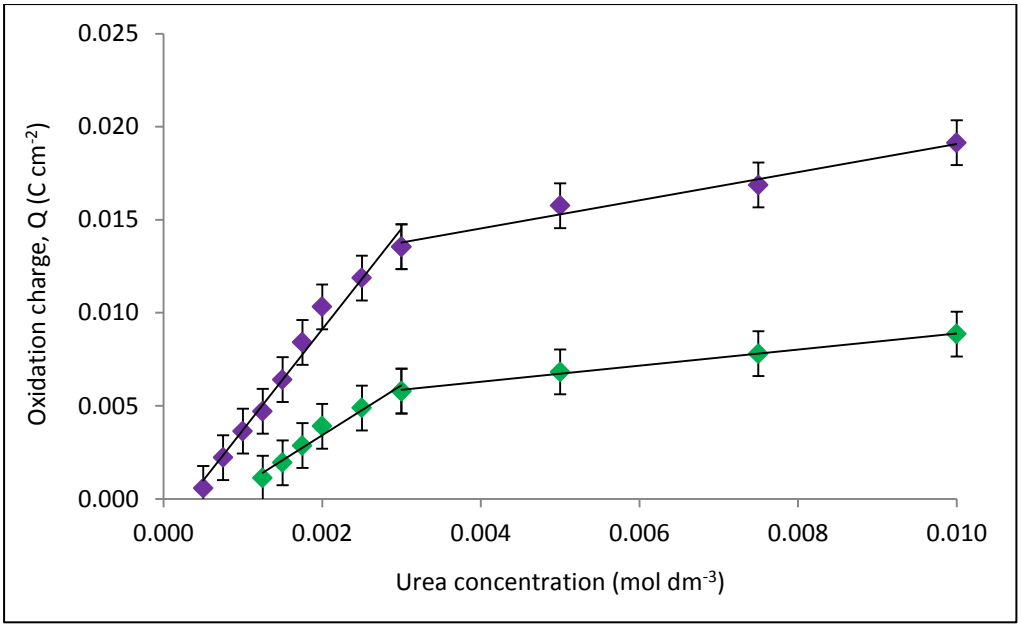

Figure 4.13: A calibration curve (n = 6) obtained from the oxidation charge plotted as a function of urea concentration for — the PPy-Urs-Cl and — the PPy-Cl films.

It is clearly evident that the addition of the urease to the polypyrrole film greatly enhances the sensitivity of the sensor. The limit of detection (LOD) was found to be 1.0 x 10^{-3} mol dm^{-3} urea for the PPy-Cl film, but for the PPy-Urs-Cl film it was measured as 5.0 x 10^{-4} mol dm^{-3} urea.

For the higher urea concentrations, the slope of the linear region is much lower compared to that computed at the lower concentrations, making it relatively straightforward to differentiate between low and elevated levels of urea. Although the PPy-Urs-Cl film exhibits reasonable sensitivity, especially at the lower urea concentrations, the limit of detection is poor when compared to other techniques, such as chromatography. For example, Clarke *et al*. found a limit of detection in the region of 5.0 x 10^{-8} mol dm^{-3} urea[30]. As no further modifications could be made to the PPy-Urs-Cl film, another dopant anion was considered with a view to enhancing the performance of the sensor in the detection of urea.

4.3.4 Formation of the PPy-Urs-SCD and PPy-SCD Polymer Films

As mentioned previously, the PPy-Urs-Cl film provides sufficient detection for urea in the 0.001 to 0.010 mol dm^{-3} urea concentration region. Although this complies with the normal and elevated blood urea levels, higher sensitivity and better detection limits can be reached using other techniques. Clarke *et al*.[30] describe a urea sensor using high performance liquid chromatography (HPLC) with a LOD of 5.0 x 10^{-8} mol dm^{-3} urea. Accordingly, further investigations into the modification of the sensor with an anionic species were carried out as the dopant anion plays an important role[31,32]. In addition, increasing the anionic charge on the polymer film may reduce the interference from common anionic interfering substances such as ascorbic acid (AA)[33,34], which exists in the body at high concentrations of up to 1.0 x 10^{-4} mol dm^{-3}, and uric acid (UA), which also exists at high concentrations[35,36].

The sulphonated-β-cyclodextrin (SCD) was chosen to provide the anionic charge, as each SCD has between 7 and 11 sulphonated (SO_3^-) groups[29]. As described in Chapter 1, the most common commercially available cyclodextrins include the α- β- and γ- cyclodextrins[37]. These differ due to the number of glucose units present, i.e., α-cyclodextrin has 6 glucose units, the β-cyclodextrin has 7 and γ-cyclodextrin has 8 glucose units[38]. As the cavity size is dependent on the number of glucose units, this leads to vast differences in the cavity sizes between the cyclodextrins[39]. The β-cyclodextrin was used as the α-cyclodextrin has a small diameter, and the γ-cyclodextrin is very expensive. In addition, there has been very little research reported on the electrochemical synthesis of polypyrrole doped with sulphonated-β-cyclodextrin[40,41] and, to the best of our knowledge, the literature reviewed shows that the formation of PPy-SCD films was attained in the presence of a supporting electrolyte, such as lithium perchlorate, as described by Temsamani and co-workers[42]. Furthermore, the polymer was cycled to very high potentials of 1.80 V vs. SCE[42] where polypyrrole films are well known to overoxidise[27.] This is an irreversible process which leads to the degradation of the polymer film, thus, the redox activity, conductivity and overall electroactivity of the polymer film is greatly reduced[27]. Also, at these high potentials, overoxidation of the polymer film leads to an increased porosity in the film. In analysing the data presented by Temsamani and co-workers[42], the cyclic voltammograms presented illustrate redox activity which could be attributed to the gold substrate used[12].

The PPy-Urs-SCD polymer films, and the PPy-SCD films as a comparison, were grown by applying a constant potential of 0.70 V vs. SCE to deposit the polymer film at the working electrode. The PPy-SCD films were prepared in 0.50 mol dm^{-3} pyrrole in the presence of 0.02 mol dm^{-3} SCD, while the PPy-Urs-SCD films were deposited from a solution containing 0.50 mol dm^{-3} pyrrole, 0.02 mol dm^{-3} SCD and 4000 mg L^{-1} urease. Figure 4.14 shows the growth profiles recorded for the PPy-SCD and PPy-Urs-SCD films at an applied potential of 0.70 V vs. SCE. These current-time transients are very different to those presented in Figure 4.1. The currents are slightly higher in the presence of the SCD anions; however, it is the shape of the current-time transients that is significantly different, showing the influence of the SCD anions on the rate of the electropolymerisation reactions.

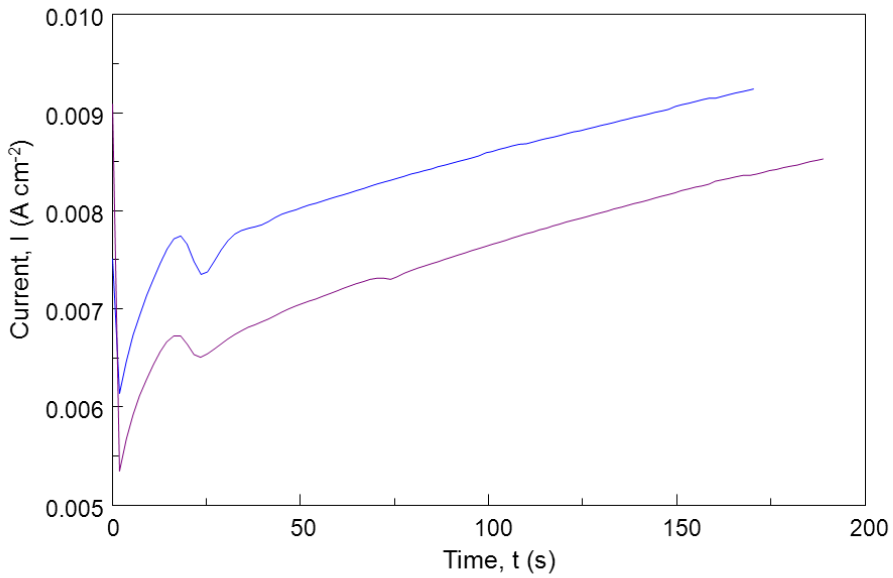

Figure 4.14: Current plotted as a function of time for the formation of PPy-SCD and PPy-Urs-SCD on a Pt electrode at 0.70 V vs. SCE from solutions containing — 0.50 mol dm^{-3} pyrrole/0.02 mol dm^{-3} SCD and — 0.50 mol dm^{-3} pyrrole/4000 mg L^{-1} urease/0.02 mol dm^{-3} SCD.

Again, on application of the potential, there is an initial decrease in the current as the charging of the double layer is achieved. This is followed by a relatively sharp increase in the current, which corresponds to the nucleation and growth of the polymer film. This current reaches a maximum value within a number of seconds, typically 20 s, which is characteristic of the SCD electrolyte[43], at which time the current begins to decrease again. This is then followed by a further more gradual increase in the current as the polymer becomes deposited onto the working electrode[20,43]. One possible explanation for these current-time transients may be the polyelectrolyte properties of the SCD[43]. As no other supporting electrolyte was used, these polyanions will migrate to the positively charged platinum surface on application of the potential. This gives rise to a high local concentration of the SCD anions during the initial stages of electropolymerisation. Once the monomer oxidation is initiated, the electropolymerisation reaction proceeds at a very high rate in the presence of the high concentration of SCD. However, as the electropolymerisation reaction proceeds, the concentration of the SCD anions is reduced as they are doped within the polypyrrole layers deposited onto the electrode, and the rate of the electropolymerisation reaction is now dominated by the transport and diffusion of the large SCD anions to the interface. The diffusion of the SCD anions is slow due to the size of the SCD with 7-11 sulphonate groups and this gives rise to a drop in the rate of electropolymerisation which is consistent with the slight dip in the current at approximately 20 s, Figure 4.14.

It is evident from Figure 4.14 that the presence of the urease enzyme in the monomer solution decreases the current density; this is similar to that observed with the formation of the PPy-Urs-Cl films and the PPy-BSA films. Again, the urease appears to block access of the pyrrole monomer to the electrode, this is similar to the results discussed in the literature[44]. It therefore takes more time for the radical cations created by the oxidation of pyrrole to form and generate the dimers and subsequently the oligomers and polymer films[43]. Nevertheless, the current-time transients have similar characteristics in the absence and presence of urease with the diffusion of the SCD anions giving rise to a dip in the current after about 20 s.

4.3.5 Characteristics and Properties of PPy-SCD and PPy-Urs-SCD

A combination of SEM, EDX and cyclic voltammetry was used to characterise the PPy-SCD and PPy-Urs-SCD films.

4.3.5.1 SEM and EDX Analysis

Micrographs were obtained for the PPy-SCD and PPy-Urs-SCD films using the scanning electron microscope (SEM) as described in Chapter 2, Section 2.2.6. The polymers were electrodeposited as described previously, onto a flat platinum disk electrode at 0.70 V vs. SCE, to a charge of 10.48 C cm^{-2} from an aqueous solution containing 0.50 mol dm^{-3} pyrrole and 0.02 mol dm^{-3} SCD in the presence and absence of the urease enzyme. SEM micrographs are shown for the PPy-SCD film in Figure 4.15, and the PPy-Urs-SCD film in Figure 4.16. From these it can be seen that the surface morphology is very different in the absence and presence of the urease. The PPy-SCD film has the typical cauliflower morphology of polypyrrole[21] and is much smoother than the PPy-Urs-SCD films. A much rougher surface morphology and evidence of fibrous regions are seen in the micrograph recorded for PPy-Urs-SCD. However, the surface morphology of the PPy-Urs-SCD film is very different to the morphology of the PPy-Urs-Cl film, Figure 4.3, indicating that the morphology is not entirely dominated by the urease enzyme, but also depends on the nature of the supporting electrolyte.

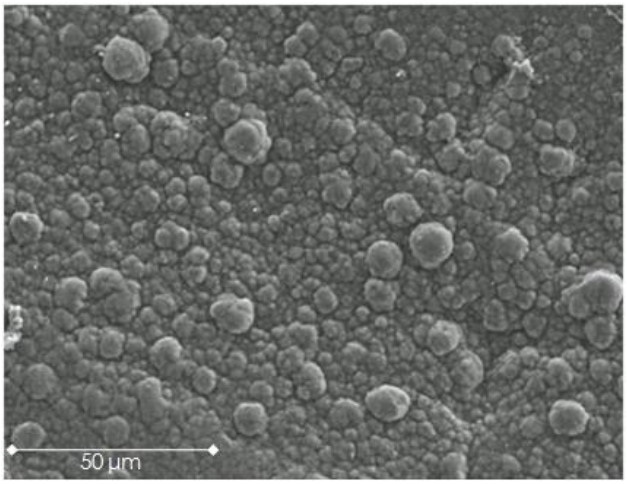

Figure 4.15: Scanning electron micrograph of PPy-SCD electrodeposited on a Pt electrode at 0.70 V vs. SCE from a solution containing 0.50 mol dm^{-3} pyrrole/0.02 mol dm^{-3} SCD.

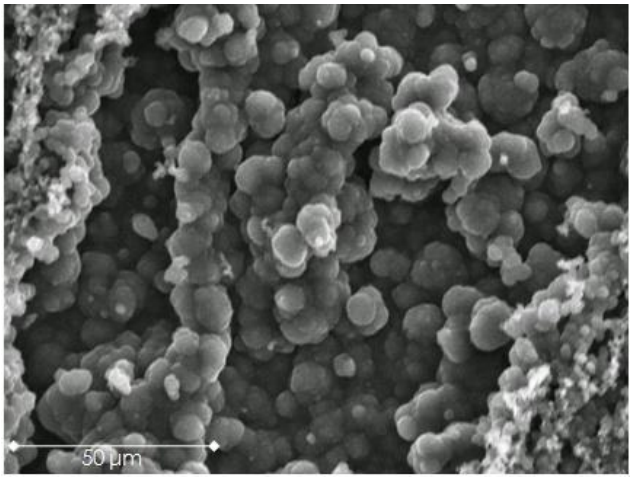

Figure 4.16: Scanning electron micrograph of PPy-Urs-SCD electrodeposited on a Pt electrode at 0.70 V vs. SCE from a solution containing 0.50 mol dm^{-3} pyrrole/4000 mg L^{-1} urease/0.02 mol dm^{-3} SCD.

Energy dispersive X-Ray (EDX) analysis was also carried out on the PPy-SCD and PPy-Urs-SCD polymers, as shown in Figures 4.17 and 4.18, respectively. Both of these EDX spectra show the presence of sulphur at 2.305 keV, which indicates the presence of the SCD anion as a dopant. However, only the urease-containing film shows evidence of nickel (Ni) at 0.851 keV; this is the nickel that is contained in the active site of the urease from Jack Bean enzyme[8] and provides clear evidence for the incorporation of the urease enzyme within the polymer matrix.

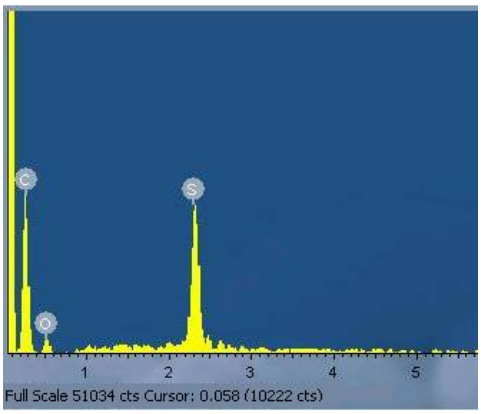

Figure 4.17: EDX analysis of a PPy-SCD film electrodeposited from a solution containing 0.50 mol dm^{-3} pyrrole and 0.02 mol dm^{-3} SCD at an applied potential of 0.70 V vs. SCE until a charge of 10.48 C cm^{-2} was reached. S is observed at ~ 2.30 keV.

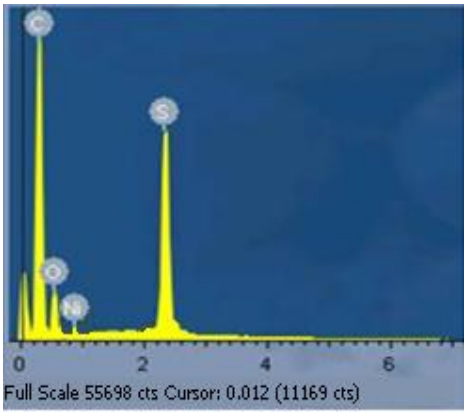

Figure 4.18: EDX analysis of a PPy-Urs-SCD film electrodeposited from a solution containing 0.50 mol dm^{-3} pyrrole, 4000 mg L^{-1} urease and 0.02 mol dm^{-3} SCD at an applied potential of 0.70 V vs. SCE until a charge of 10.48 C cm^{-2} was reached. S is observed at ~ 2.30 keV and Ni is observed at ~ 0.90 keV.

4.3.5.2 Electroactivity of the PPy-SCD and PPy-Urs-SCD Polymer Films

The electroactivity of the PPy-SCD and PPy-Urs-SCD films was studied and compared by cycling the polymers in two different electrochemical windows and by varying the scan rate. The influence of the upper potential limit is shown in Figure 4.19, where voltammograms are presented for the PPy-Urs-SCD film cycled repeatedly from -0.60 to 0.80 V vs. SCE, Figure 4.19 (a) and from -0.60 to 1.20 V vs. SCE, Figure 4.19 (b) in a phosphate buffer, at a pH of 7.0. Very good stability is observed when the polymer is cycled in the smaller electrochemical window, with

nearly identical voltammograms recorded for cycles 1, 20, 50, 100, 200 and 300. However, a significant decay in the electroactivity of the polymer, corresponding to overoxidation of the polymer film[27], is observed at the higher potential of 1.20 V vs. SCE.

(a)

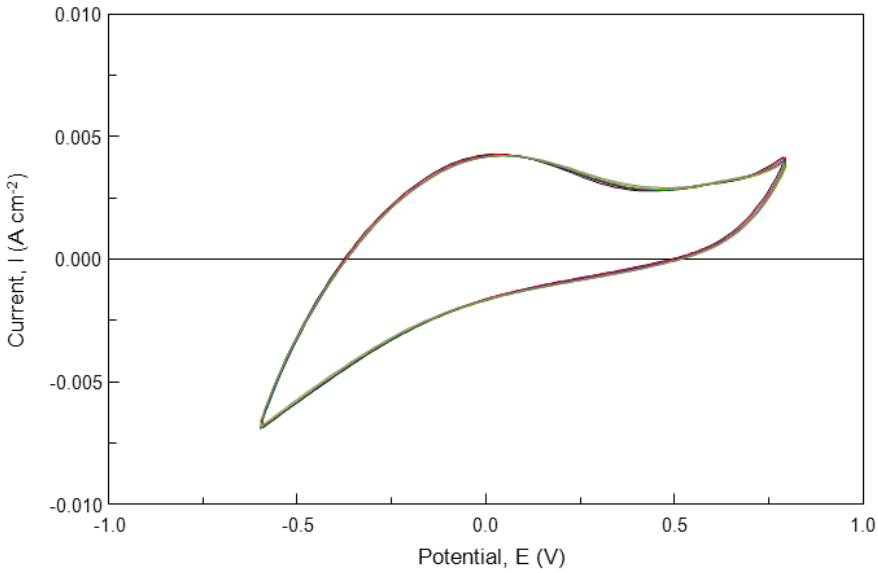

(b)

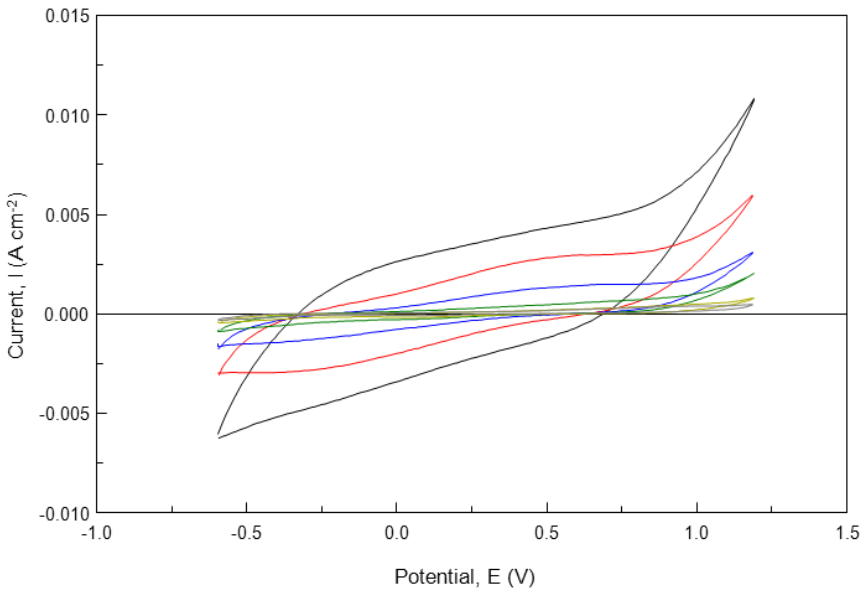

Figure 4.19: Cyclic voltammograms recorded for PPy-Urs-SCD in buffer solution at a pH of 7.0 ▬ cycle 1, ▬ cycle 20, ▬ cycle 50, ▬ cycle 100, ▬ cycle 200 and ▬ cycle 300 (a) cycled from -0.60 V to 0.80 V vs. SCE and (b) cycled from -0.60 V to 1.20 V vs. SCE.

In the larger electrochemical window, the faradic currents decrease rapidly with increasing cycle number, this is more clearly evident in Figure 4.20, where the charge, consumed during oxidation of the polymer, is presented as a function of the cycle number. Again, at the higher potential window, i.e., up to 1.20 V vs. SCE, the polymer degrades and the charge is negligible after 50 cycles; however, the charge increases slightly when the polymer is cycled in the smaller electrochemical window showing no evidence of overoxidation.

These results are similar to those presented in Figure 4.9 for the PPy-Urs-Cl films. On comparison of the charge-time plots presented in Figure 4.9 and the data recorded in Figure 4.20 for the PPy-Urs-SCD, it is evident that the PPy-Urs-SCD film is overoxidised at a faster rate when exposed to potentials in the vicinity of 1.20 V vs. SCE.

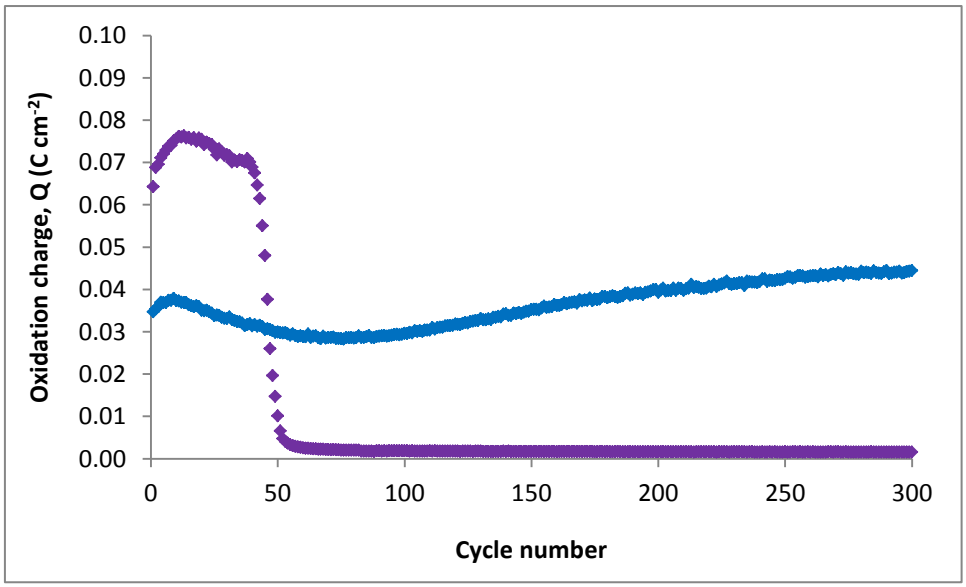

Figure 4.20: Oxidation charge recorded as a function of cycle number for PPy-Urs-SCD cycled in a phosphate buffer, 0.05 mol dm^{-3}, pH 7.0, from — -0.60 V to 1.20 V vs. SCE and — -0.60 V to 0.80 V vs. SCE.

The effect of scan rate on the polymer signal was also investigated. The PPy-SCD and PPy-Urs-SCD polymers were cycled in a 0.05 mol dm^{-3} phosphate buffer solution at a pH of 7.0, at scan rates from 300 mV s^{-1} to 5 mV s^{-1}. The resulting cyclic voltammograms are shown in Figure 4.21. Similar voltammograms were recorded for the PPy-SCD and PPy-Urs-SCD films and with an increase in the scan rate higher currents were recorded. It is also evident that the scan rate has a

significant influence on the electroactivity of the films[28]. At the higher scan rates an oxidation wave, which extends from about -0.30 V to 0.50 V vs. SCE, is clearly evident. This corresponds to oxidation of the film, while the reduction wave is at potentials below -0.60 V vs. SCE and is not visible in the figure. Indeed, when the electrochemical window was extended to -1.10 V vs. SCE, a broad reduction wave with a maximum current centred at about -0.65 V vs. SCE was observed. As the sulphonated cyclodextrin is large and immobile it is not lost during reduction of the polymer film. Instead, reduction of the polymer is accompanied by the ingress of Na^+ cations from the phosphate buffer. This potential is considerably lower than that observed for the reduction of PPy-Cl[11], where the expulsion of chloride anions occurs, and can be explained by the fact that the applied potential must be further lowered to facilitate the reduction of the polymer backbone and the ingress of Na^+. Interestingly, the presence of the urease enzyme exerts some influence on the oxidation of the polymer. Again, at the higher scan rates, where the oxidation waves are clearly visible, somewhat broader oxidation waves are seen in the presence of urease. For example, the peak potential of the oxidation wave is approximately 0.20 V vs. SCE for the PPy-SCD film and slightly higher at 0.40 V vs. SCE for the PPy-Urs-SCD films. Oxidation of the polymer is accompanied by the release of the Na^+ cations as the polypyrrole backbone is converted from a neutral to a positively charged structure. It appears that the release of the Na^+ ions is slightly inhibited by the incorporated urease.

(a)

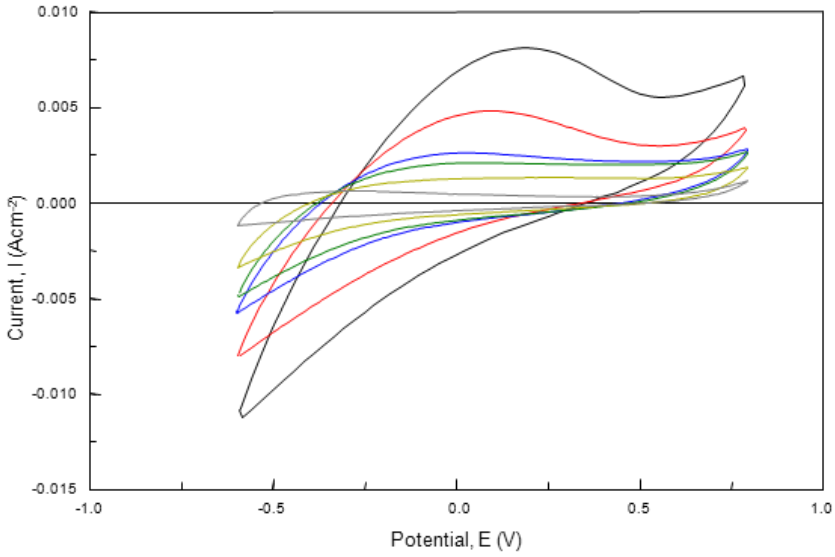

(b)

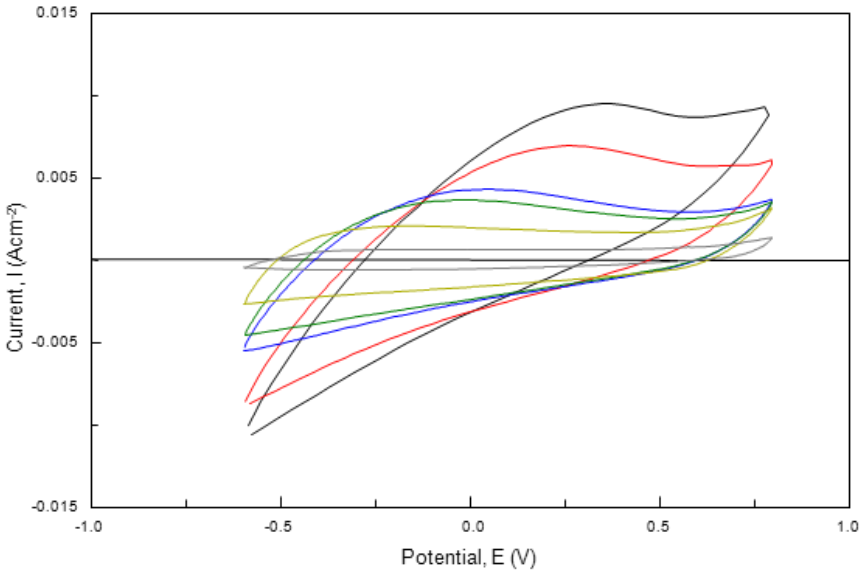

Figure 4.21: Cyclic voltammograms recorded in 0.05 mol dm^{-3} phosphate buffer solution, pH of 7.0, at scan rates ▬ 300 mV s^{-1}, ▬ 200 mV s^{-1}, ▬ 100 mV s^{-1}, ▬ 50 mV s^{-1}, ▬ 25 mV s^{-1} and ▬ 10 mV s^{-1} of (a) PPy-SCD and (b) PPy-Urs-SCD.

Finally, the capacitance of the PPy-Urs-SCD and PPy-SCD films was determined by cycling the polymer films in a pH 7.0, 0.05 mol dm^{-3} phosphate buffer solution between 0.10 V and 0.20 V vs SCE as a function of the scan rate, as detailed earlier in Section 4.3.2.3 for the PPy-Urs-Cl and PPy-Cl films. The current was plotted as a function of the scan rate in accordance with Equation 4.2, to give linear plots, with correlation coefficients greater than 0.98, as shown in Figure 4.22. From these data the capacitance of the polymer films was computed as 1.59 x 10^{-3} and 2.00 x 10^{-3} F cm^{-2} for the PPy-SCD and PPy-Urs-SCD polymer films, respectively. The presence of the urease enzyme has little influence on the capacitance of the films in the presence of the sulphonated-β-cyclodextrin.

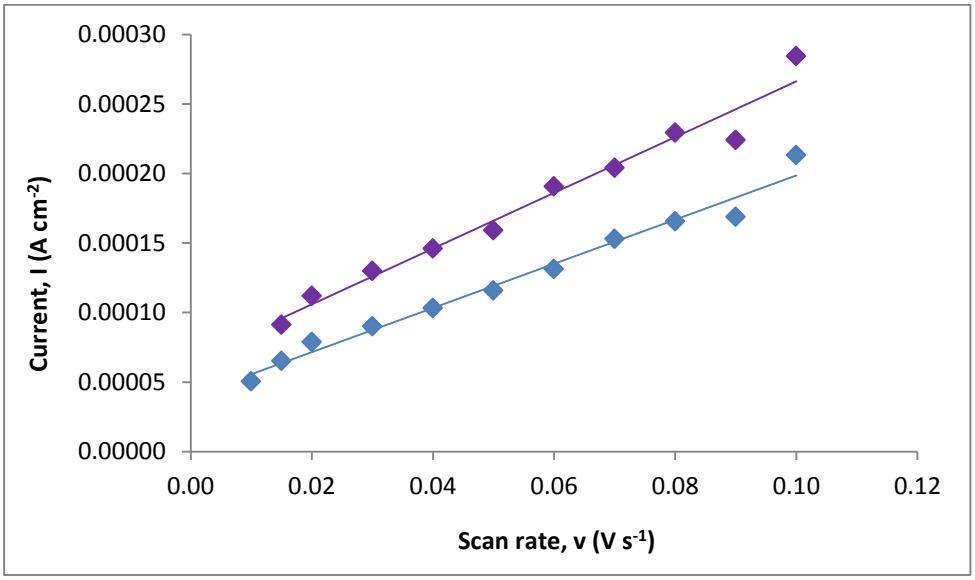

Figure 4.22: Current plotted as a function of the scan rate for the — PPy-SCD and — PPy-Urs-SCD polymer films.

4.3.6 Stability of the PPy-Urs-SCD Polymer Films

In order to further explore and probe the stability of the PPy-SCD and PPy-Urs-SCD polymer films, other parameters such as film thickness, reusability, reproducibility, shelf life and the storage conditions of the polymer film were investigated. These parameters are discussed in detail in the following sections, and are well known to be important in the development of a urea sensor [45].

4.3.6.1 Thickness of the PPy-Urs-SCD Polymer Films

The effect of varying the thickness of the polymer films on their stability was investigated using three different polymer thicknesses. The polymer films were grown to a fixed charge to keep the thicknesses relatively constant and the charges chosen were 0.24, 1.42 and 10.48 C cm^{-2} which correspond to an approximate polymer thickness of 0.60 µm, 3.55 µm and 26.20 µm, respectively. This thickness was theoretically calculated using the charge thickness ratio derived by Diaz *et al*.[46] for a simple chloride dopant. In this analysis it is assumed that 1 C cm^{-2} of charge passed is equivalent to 2.5 µm of polymer film. It is important to mention that the theoretical values of thickness obtained for the PPy-SCD and PPy-Urs-SCD films are only an approximation, as the films doped with the large anionic groups may not have the same charge to polymer thickness ratio as the PPy-Cl films[47]. Indeed, this has been confirmed by Schmidt and co-workers[48], who have shown that PPy-Cl forms thicker films than PPy doped with tosylate or polystyrene sulphonate.

In order to investigate the stability of the polymer films deposited to different thickness, the oxidation charge for the polymer films cycled in phosphate buffer solution from -0.60 V up to 0.80 V vs. SCE was plotted over 300 cycles, as shown in Figure 4.23. It is evident from this plot that the thinner polymer, with a thickness of approximately 0.60 µm, decays or decomposes rapidly and the charge drops to negligible values after 65 cycles. In contrast, the polymer films approximated as 3.55 µm and 26.20 µm appear considerably more stable. There is an initial decay in the charge during the first 50 cycles for the polymer deposited to 3.55 µm, but the charge then increases to reach a near constant value of about 0.04 C cm^{-2}. Likewise, the polymer with a thickness of about 26.20 µm appears to be reasonably stable, in this case the charge increases over the first 100 cycles, before a steady-state is reached. Accordingly, the medium thickness polymer film of 3.55 µm was chosen for all further measurements.

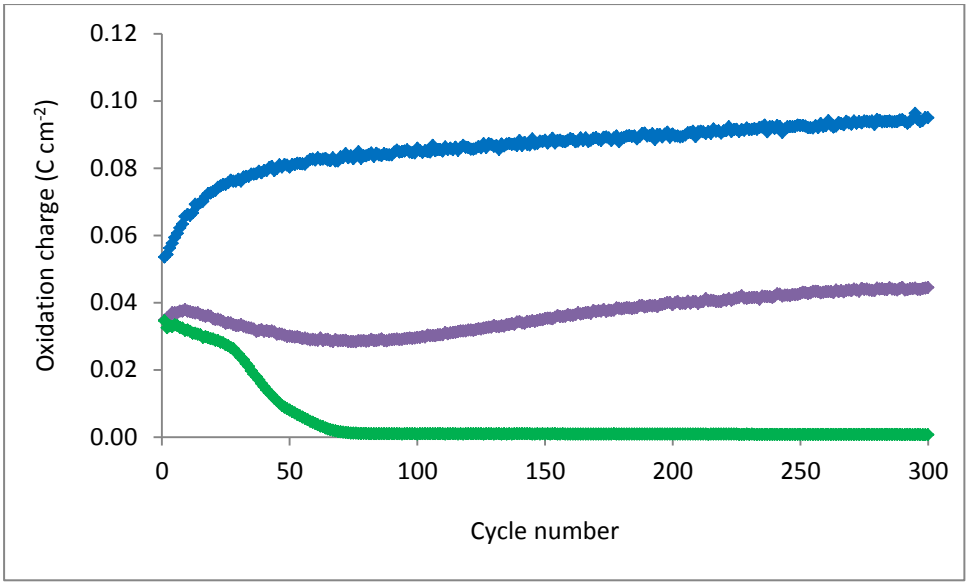

Figure 4.23: Oxidation charge plotted as a function of cycle number for PPy-Urs-SCD films cycled from -0.60 to 0.80 V vs. SCE, at 0.10 V s^{-1} in a phosphate buffer solution, 0.05 mol dm^{-3}, at a pH of 7.0 with approximate polymer thickness of — 26.20 µm, — 3.55 µm and — 0.60 µm.

4.3.6.2 Reusability of the PPy-Urs-SCD Polymer Films

The reusability of the PPy-Urs-SCD films was investigated by growing the polymer films at a constant potential of 0.70 V vs. SCE to a charge of 1.42 C cm^{-2} which corresponds to a thickness of approximately 3.55 µm. The electrode was rinsed well with distilled water to remove any excess monomer from the surface of the electrode and the electrode was placed into a background solution of 0.05 mol dm^{-3} phosphate buffer at a pH of 7.0. A cyclic voltammogram was obtained by cycling the polymer film from -0.60 to 0.80 V vs. SCE, for 10 cycles. Then the polymer film was transferred to a solution containing 0.003 mol dm^{-3} solution of urea in 0.05 mol dm^{-3} phosphate buffer at a pH of 7.0, and cycled in the same window. The oxidation charge was recorded and the background subtracted to obtain the true oxidation charge. This process was repeated a total of ten times and the corresponding data are presented in Figure 4.24, with the oxidation charge plotted as a function of the number of uses.

There is a clear loss in the oxidation charge with repeated use. Indeed, there is a 25% loss in the charge from the first to the second use. This indicates that the PPy-Urs-SCD polymer film is not suitable for re-use as the charge obtained decreases significantly with each use. This is comparable with studies done by Pandey, *et al.*[49] and Adeloju, *et al.*[50] on other polymer-based urea sensors, such as polyaniline, and polypyrrole. In contrast, Syu and Chang[8] reported excellent reusability of a polypyrrole based urea sensor with 80% of the signal remaining after 40 uses, while Osaka *et al.*[51] found a 10% loss from the first to the 10th use, again with a polypyrrole modified sensor.

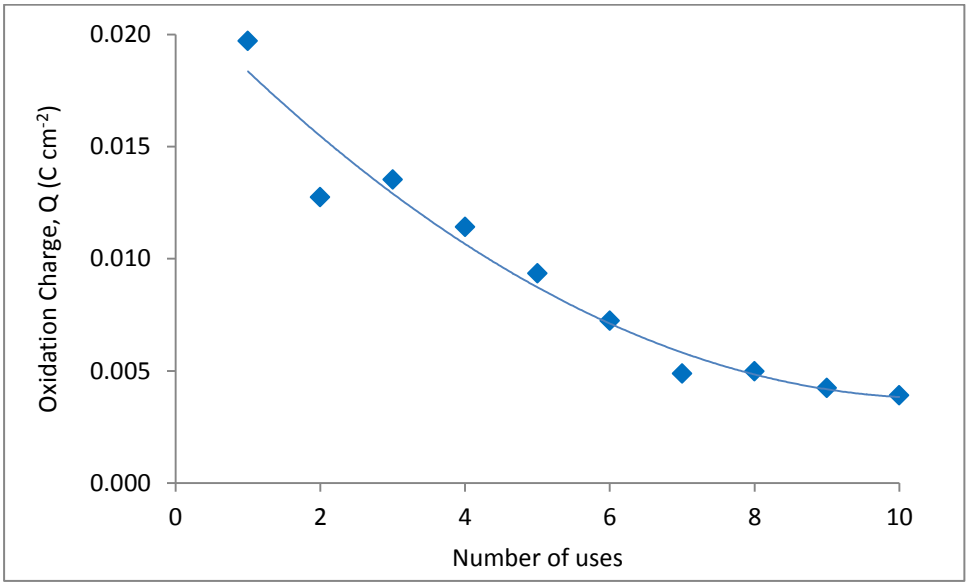

Figure 4.24: Oxidation charge of the PPy-Urs-SCD film recorded in 0.003 mol dm^{-3} urea plotted as a function of the number of uses.

4.3.6.3 Reproducibility of the PPy-Urs-SCD Polymer Films

The reproducibility of the PPy-Urs-SCD polymer films in the detection of urea was investigated by growing a number of polymer films and cycling them initially in the background solution of 0.05 mol dm^{-3} phosphate buffer solution, pH 7.0, and then in a 0.003 mol dm^{-3} urea in 0.05 mol dm^{-3} phosphate buffer solution, pH 7.0. The oxidation charge was computed and these charges are presented in Figure 4.25.

It is obvious from Figure 4.25 that the oxidation charges obtained for six different PPy-Urs-SCD polymer films are very similar, giving very good reproducibility. This compares very favourably with other urea sensors, such as those described by Dhawan, *et al.*[7], and Chen, *et al.*[3]; however, these materials are more prone to enzyme leaching and, consequently, this leads to a lack of reproducibility of the urea sensor[3]. This is not the case with the PPy-Urs-SCD sensor, Figure 4.25.

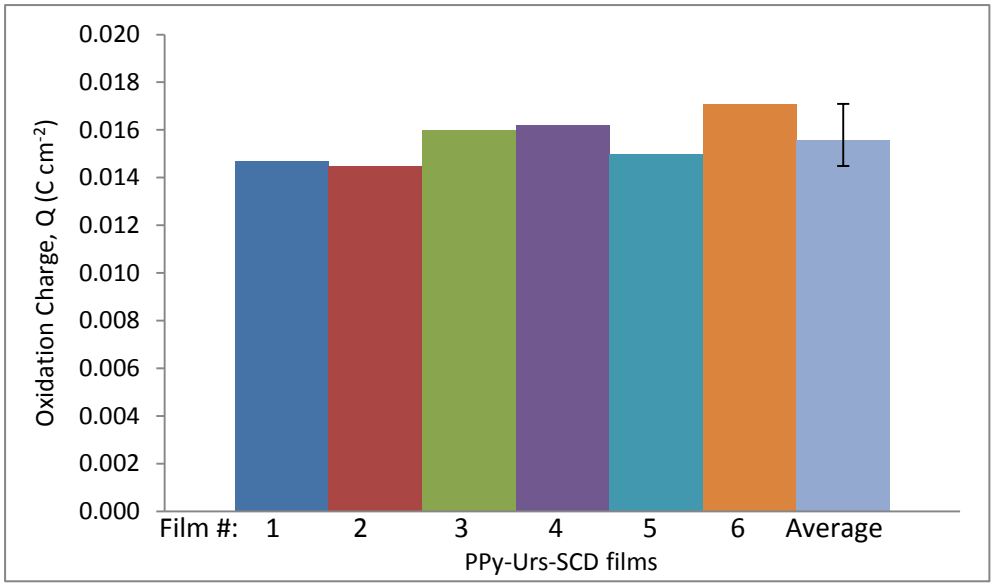

Figure 4.25: Oxidation charges obtained for six different PPy-Urs-SCD polymer films by cycling in a 0.003 mol dm^{-3} urea in 0.05 mol dm^{-3} phosphate buffer solution, pH 7.0, and subtracting the background oxidation charge.

4.3.6.4 Shelf-life of the PPy-Urs-SCD Polymer Films

The shelf-life of the PPy-Urs-SCD films was investigated by cycling a PPy-Urs-SCD film in a background 0.05 mol dm^{-3} phosphate buffer solution, pH 7.0, and then in a 0.003 mol dm^{-3} urea in 0.05 mol dm^{-3} phosphate buffer solution, pH 7.0. The oxidation charge was computed. The PPy-Urs-SCD film was then stored in a solution of pH 7.0, 0.05 mol dm^{-3} phosphate buffer for 10 weeks, after which it was cycled in the background solution again, followed by a 0.003 mol dm^{-3} urea in 0.05 mol dm^{-3} phosphate buffer solution, pH 7.0. The oxidation charge was obtained and recorded for the initial (Week 0) and final (Week 10) PPy-Urs-SCD films, and this is shown in Figure 4.26.

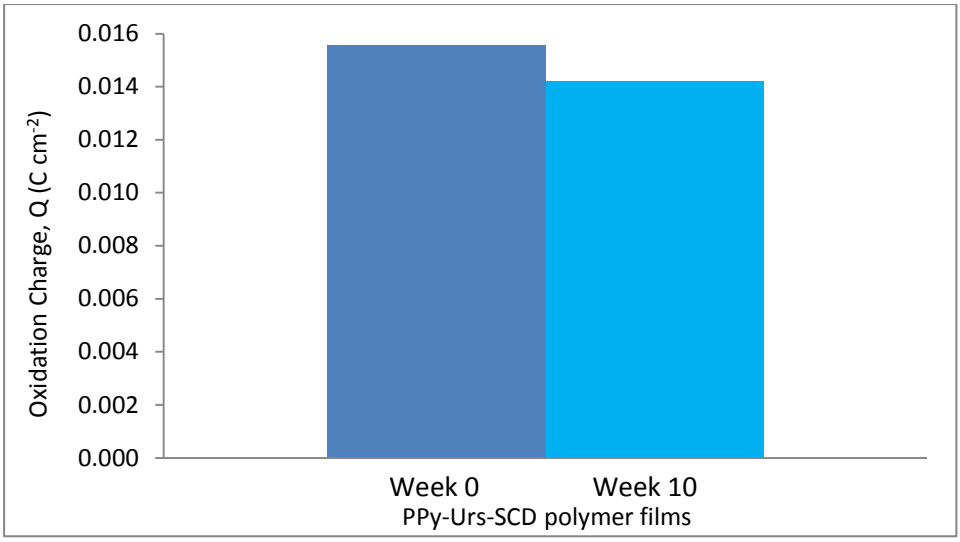

Figure 4.26: Oxidation charge of PPy-Urs-SCD films recorded on the initial (Week 0) and after the final (Week 10) in 0.003 mol dm^{-3} urea in 0.05 mol dm^{-3} phosphate buffer solution, pH 7.0.

It is evident from Figure 4.26 that storing the PPy-Urs-SCD film over 10 weeks has little effect on the oxidation charge. This indicates that the PPy-Urs-SCD polymer film is quite stable when stored in a solution of pH 7.0, 0.05 mol dm^{-3} phosphate buffer. Accordingly, the shelf-life of the polymer film is greater than 10 weeks. This is comparable to the work done by Singh, *et al.*[10] and Dhawan, *et al.*[7] who investigated the shelf life of various urea sensors and found a range of shelf life times from 24 h up to 99 days, depending on the mode of urease immobilisation.

4.3.6.5 Storage Conditions of the PPy-Urs-SCD Polymer Films

Finally, the storage conditions of the PPy-Urs-SCD polymer film were investigated by growing two polymer films as before. The PPy-Urs-SCD films were cycled in a background solution of 0.05 mol dm^{-3} phosphate buffer solution, pH 7.0, and then in a 0.003 mol dm^{-3} urea in 0.05 mol dm^{-3} phosphate buffer solution, pH 7.0. One of the polymer films was stored at room temperature, at approximately 25 °C, and the other in a refrigerator at 4 °C in identical solutions of pH 7.0, 0.05 mol dm^{-3} phosphate buffer. The polymer films were removed at weekly intervals and cycled in the background electrolyte and then in the urea-containing solution and the oxidation charge was computed. These results are highlighted in Figure 4.27.

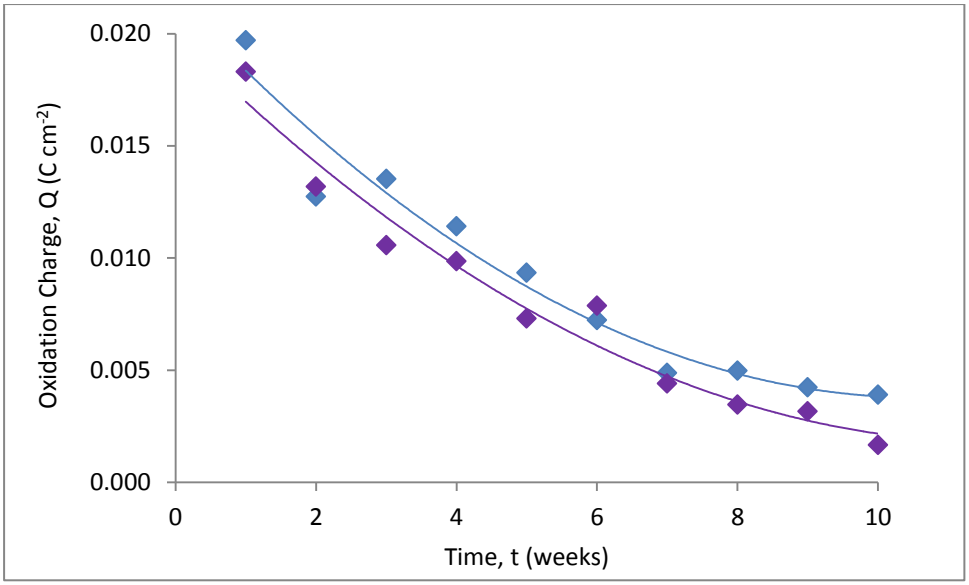

Figure 4.27: Oxidation charges obtained for the PPy-Urs-SCD polymer films stored at — 4 °C and — 25 °C.

It is obvious from Figure 4.27 that the oxidation charges decrease with increasing cycling of the polymer films. Indeed these data are similar to that presented in Figure 4.24, indicating that the loss in signal is related to cycling of the polymer films. However, it is also apparent from Figure 4.27 that the storage conditions have little effect. The loss in the charge is similar for the film stored at 4 and 25 °C. It is evident that the polymer film stored at 4 °C has a slightly higher oxidation charge compared to the film stored at 25 °C; however, this difference is negligible and it can be concluded that the storage temperature does not play a significant role in the stability of the sensor. Research reported by Dhawan and co-workers[7] implies that the temperature plays an important role on the stability and shelf-life of urea sensors. However, the work carried out by Singh and co-workers[10] and Chen *et al.*[52] shows little diminution in sensitivity while storing the urea sensors at a lower temperature, i.e., at 4 °C. However, a comparison at room temperature was not made. Rajesh, *et al.*[53], did present results on the storage conditions of a urea sensor at both 25 °C and at 4 °C and, found a loss of approximately 70 % of the initial enzyme activity within two weeks at 25 °C, compared to a retention of approximately 80% of the initial enzyme activity for over two months when the urea sensor was stored at 4 °C[54].

The effect of pH on the stability of the sensor was not investigated as the urease enzyme becomes denatured at pH values below 6.0 and above 8.0[50]. In addition, the polypyrrole film losses stability at very alkaline pH conditions[54,55,56,57]. Consequently, the pH of all the experiments described in this chapter was maintained at a pH of 7.0 using a pH 7.0, 0.05 mol dm^{-3} phosphate buffer solution[50].

4.3.7 Urea Detection using the PPy-SCD and PPy-Urs-SCD Polymers

The sensitivity of both the PPy-Urs-SCD and PPy-SCD films to a range of urea concentrations was investigated. In order to accurately determine the oxidation charge, the background charge recorded in the phosphate buffer solution was subtracted as mentioned previously. The resulting oxidation charge from the urea was then plotted against increasing urea concentration and a calibration curve was obtained, as shown in Figure 4.28 for the PPy-SCD and PPy-Urs-SCD films. The data recorded at the lower urea concentrations is highlighted again in Figure 4.29.

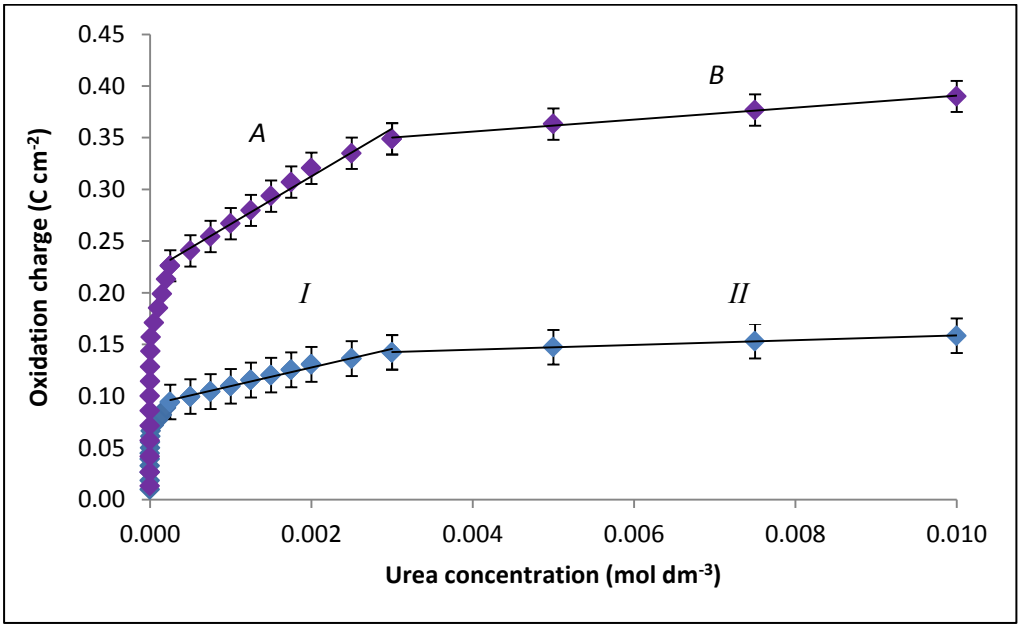

Figure 4.28: Calibration curve (n = 6) with the oxidation charge plotted as a function of the urea concentration for — PPy-Urs-SCD and — PPy-SCD films.

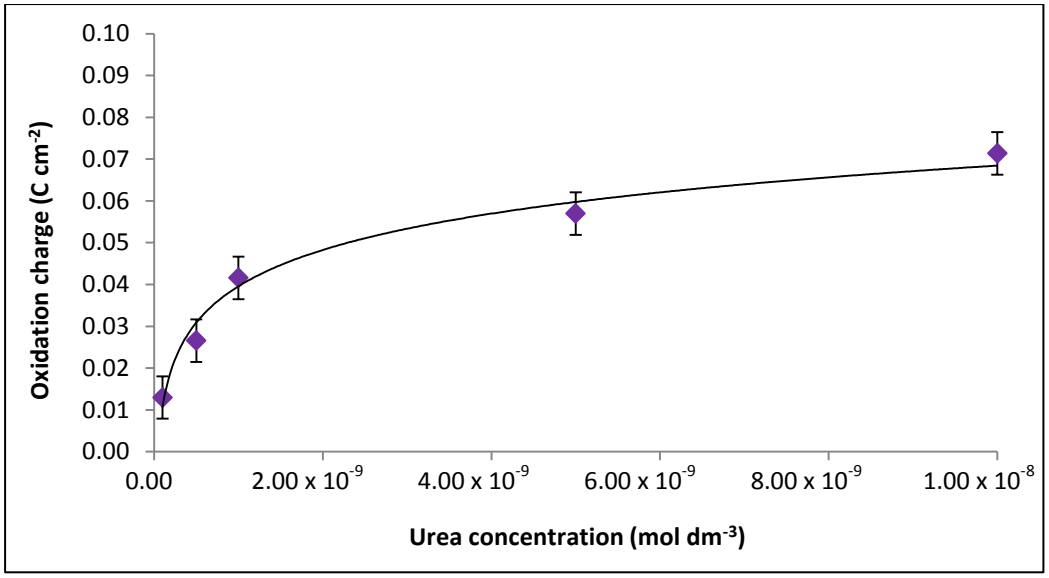

Figure 4.29: Calibration curve (n = 6) with the oxidation charge of the PPy-Urs-SCD film plotted as a function of the urea concentration for urea concentrations below 1.0 x 10^{-8} mol dm^{-3}.

It is evident from Figure 4.29 that the presence of the sulphonated cyclodextrin in the polypyrrole film greatly enhances the sensitivity of the sensor and in addition, it gives a better limit of detection (LOD). The LOD value for PPy-Urs-Cl was found to be 5.0 x 10^{-4} mol dm^{-3} urea, whereas the LOD for the PPy-SCD and PPy-Urs-SCD polymer films are in the region of 1.0 x 10^{-10} mol dm^{-3} urea.

Again, the calibration curve obtained for the detection of urea using the sulphonated cyclodextrin polymers has two linear regions. The slopes of these linear regions were obtained for both the PPy-SCD and PPy-Urs-SCD polymer films. The linear region corresponding to the lower urea levels for the PPy-SCD polymer film (*I*) was found to have a slope of 18.04 C cm^{-2} mol^{-1} dm^{3}, whereas the same linear region for the PPy-Urs-SCD film (*A*) has a slope of 46.09 C cm^{-2} mol^{-1} dm^{3}. This can be equated to the sensitivity of these films, with the sensitivity of the PPy-SCD film at 18.04 µC $µM^{-1}$ and the PPy-Urs-SCD at 46.09 µC $µM^{-1}$. Clearly, these films have a better sensitivity than the PPy-Urs-Cl polymer, which has a sensitivity to urea of only 5.41 µC $µM^{-1}$.

The same analysis was applied to the second linear region, which is the region in which the normal blood urea levels lie. This region is very important in the biomedical industry as higher urea concentrations are indicative of renal failure. The

PPy-SCD film was found to have a higher sensitivity to urea of 2.29 µC µM^{-1} (*II*) compared to the PPy-Urs-Cl film which had a sensitivity of 0.76 µC µM^{-1}. Again, the PPy-Urs-SCD film has the best sensitivity of 5.79 µC µM^{-1} in this higher urea concentration region (*B*). A comparison of the sensitivity of the four polymer films at the higher urea concentrations is given in Figure 4.30, where it is evident that the PPy-Urs-SCD film yields the best sensitivity towards urea detection.

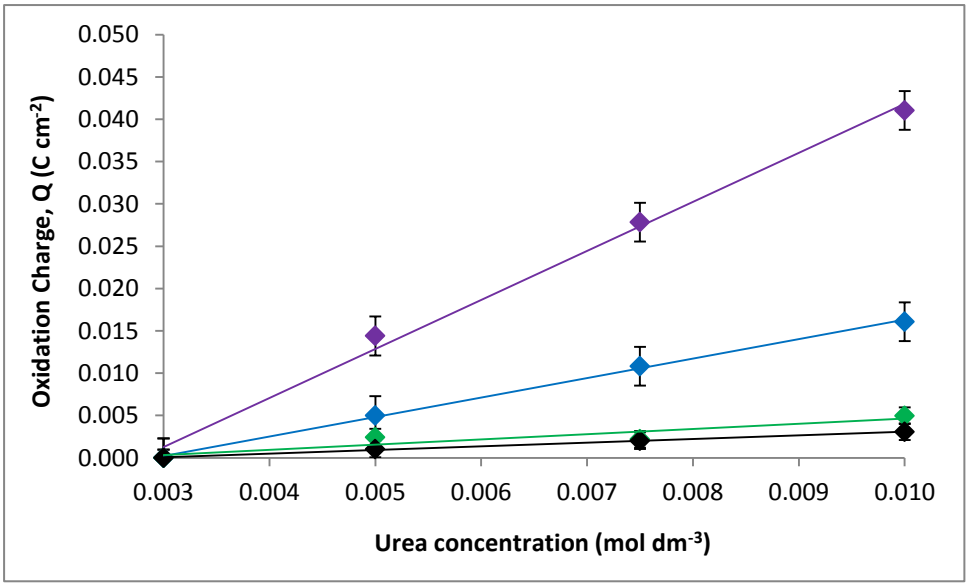

Figure 4.30: Calibration curve (n = 6) with the oxidation charge plotted as a function of the urea concentration for — PPy-Urs-SCD, — PPy-SCD, — PPy-Urs-Cl and — PPy-Cl films at the higher urea concentration levels.

It is evident that the slopes of the two linear regions change significantly with the increased urea concentration from the lower urea levels to the higher levels. For the lower urea concentrations, the slope of the linear region is much higher than that of the higher urea concentrations. It is also apparent that the anion used to dope the polymer film plays an important role in the sensitivity of the film towards the urea[58]. The anionic sulphonated group leads to better urea detection, even without the presence of the urease enzyme. Obviously, having the urea enzyme present increases the sensitivity of the polymer film to urea[59]. As a result, the PPy-Urs-SCD film was chosen for further detection of urea, as described in Chapter 5.

4.4 Conclusions

In summary, the urease enzyme was successfully incorporated within the polypyrrole-chloride matrix; this was characterised using SEM, EDX and cyclic voltammetry. The presence of the nickel in the EDX spectra is proof that the urease enzyme was included in the PPy-Urs-Cl polymer film. This film was then investigated as a coulombometric sensor for urea detection, along with the PPy-Cl film as a comparison. The addition of the urease greatly enhances the detection of the film, with detection in the region of 5.0 x 10^{-4} mol dm^{-3} for urea and a sensitivity of 5.41 µC μM^{-1} for the lower urea level region using the PPy-Urs-Cl film. In comparison, the PPy-Cl film exhibited a sensitivity of 2.68 µC μM^{-1} towards urea, with a limit of detection of 1.0 x 10^{-3} mol dm^{-3}. Although the PPy-Urs-Cl film exhibited reasonable sensitivity towards urea, the limit of detection was found to be poor in comparison to other techniques such as chromatography, which yields LODs in the region of 5.0 x 10^{-8} mol dm^{-3} for urea. Consequently, the dopant anion was changed to the sulphonated-β-cyclodextrin as increasing the ionic charge would possibly enhance the performance of the sensor in the detection of urea. Subsequently, the PPy-Urs-SCD film and the PPy-SCD film, as a comparison, were formed and used in the detection of urea. The PPy-Urs-SCD film had a good sensitivity of 46.09 µC μM^{-1} towards urea in the lower concentration regions and detection in the region of 1.0 x 10^{-10} mol dm^{-3}, whereas the PPy-SCD film had a sensitivity of 18.04 µC μM^{-1} towards urea and detection in the region of 1.0 x 10^{-10} mol dm^{-3}. Additionally, the PPy-Urs-SCD film has excellent sensitivity towards urea in the higher concentration regions, which correspond to the blood urea levels. Obviously, the anion used to dope the polymer film plays an important role in the sensitivity of the film towards urea, with the more anionic group leading to better detection, even in the absence of the urease enzyme. Additionally, an investigation into the stability, reusability, shelf life, storage conditions and reproducibility of the polymer films was carried out. It was found that the thin polymer films decay rapidly; however, good stability was observed on increasing the thickness of the polymer film. In addition, there was a clear loss in the oxidation charge with repeated use, implying that the PPy-Urs-SCD film is not suitable as a re-useable sensor. However, good reproducibility was obtained from different polymer films and, the polymer films have a shelf life greater than 10 weeks.

4.5 References

1 A. J. Taylor and P. Vadgama, *Annals of Clinical Biochemistry*, **29**, 245, (1992)

2 L. Della Cianna and G. Capho, *Clinical Chemistry*, **42**, 1079, (1996)

3 Y.-P. Chen, B. Liu, H.-T. Lian and X.-Y. Sun, *Electroanalysis*, **23**, (6), 1454, (2011)

4 D. Aronson, M. A. Mittleman and A. J. Burger, *American Journal of Medicine*, **116**, 466, (2004)

5 C. Ronco, R. Bellomo, P. Hommel, A. Brendolan, M. Dan, P. Piccinni and G, L. Greca, *Lancet*, **355**, 26, (2000)

6 M. Olszak-Humienik, *Thermochimica Acta*, **378**, 107, (2001)

7 G. Dhawan, G. Sumana and B. D. Malhotra, *Biochemical Engineering Journal*, **44**, 42, (2009)

8 M.-J. Syu and Y.-S. Chang, *Biosensors and Bioelectronics*, **24**, 2671, (2009)

9 Y.-C. Luo and J.-S. Do, *Biosensors and Bioelectronics*, **20**, 15, (2004)

10 M. Singh, N. Verma, A. K. Garg and N. Redhu, *Sensors and Actuators B*, **134**, 345, (2008)

11 G. G. Wallace, P. C. Dastoor, D. L. Officer and C. O. Too, *Journal of the American Chemical Society*, **30**, (1), 14, (2000)

12 E. Garfias-Garcia, M. Romero-Roma, M. T. Ramirez-Silva, J. Morales and M. Palomar-Pardave, *International Journal of Electrochemical Science*, **5**, 763, (2010)

13 S. B. Adeloju, S. J. Shaw and G. G. Wallace, *Analytica Chimica Acta*, **341**, 155, (1997)

14 T. Momma, M. Yamamoto, S. Komaba and T. Osaka, *Journal of Electroanalytical Chemistry*, **407**, 91, (1996)

15 S. Komaba, M. Seyama, T. Momma and T. Osaka, *Electrochimica Acta*, **42**, (3), 383, (1997)

16 A. Ramanavicius, A. Ramanaviciene and A. Malinauskas, *Electrochimica Acta*, **51**, 6025, (2006)

17 S. Sadki, P. Schottland, N. Brodie and G. Sabouraud, *Chemistry Society Reviews*, **29**, 283, (2000)

18 T. Yuan, Y. Huang, S. Dong, T. Wang and M. Xie, *Polymer Testing*, **21**, 641, (2002)

19 T. Ahuja, I. A. Mir, D. Kumar and Rajesh, *Sensors and Actuators: B. Chemical*, **134** (1), 140, (2008)

20 T. *de* J. Licona-Sanchez, G, A. Alvarez-Romero, M. Palomar-Pardave, C. A. Galan-Videl, M. E. Paez-Hernandez, M. T. Ramirez Silva and M. Romero-Romo, *International Journal of Electrochemical Science*, **6**, 1537, (2011)

21 G. G. Wallace, G. M. Spinks, L. A. P. Kane-Maguire and P. R. Teasdale, *Conductive Electroactive Polymers: Intelligent Materials Systems*, CRC Press, **237**, (2003)

22 G. Maia, R. M. Torresi, E. A. Ticianelli and F. C. Nart, *Journal of Physical Chemistry*, **100**, 15910, (1996)

23 A. L. Brisena, A. Baca, Q. Z. Zhou, R. Lai and F. M. Zhou, *Analytica Chimica Acta*, **441**, 123, (2001)

24 V. D. Patake, S. S. Joshi, C. D. Lokhande and O.-S. Joo, *Materials Chemistry and Physics*, **114**, 6, (2009)

25 F.-R. F. Fan and A. J. Bard, *Journal of the Electrochemical Society*, **133**, 301, (1986)

26 J. Bard and L. R. Faulkner, *Electrochemical Methods: Fundamentals and Applications*, John Wiley and Sons, Inc., 833 (2001)

27 L. Ozcan, Y. Sahin and H. Turk, *Biosensors and Bioelectronics*, **24**, 512, (2008)

28 M. D. Ingram, H. Staesche and K. S. Ryder, *Solid State Ionics*, **169**, 51, (2004)

29 S. Suematsu, Y. Oura, H. Tsujimoto, H. Kanno and K. Naoi, *Electrochimica Acta*, **45**, 3813, (2000)

30 S. Clark, P. S. Francis, X. A. Conlan and N. W. Barnett, *Journal of Chromatography A*, **1161**, 207, (2007)

31 A. L. Briseno, A. Baca, Q. Zhou, R. Lai and F. Zhou, *Analytica Chimica Acta*, **441**, 123, (2001)

32 G. Maia, R. M. Torresi, E. A. Ticianelli and F. C. Nart, *Journal of Physical Chemistry*, **100**, 15910, (1996)

33 G.-Z. Hu, D.-P. Zhang, W.-L. Wu and Z.-S. Yang, *Colloids and Surfaces B: Biointerfaces*, **62**, 199, (2008)

34 L. Zhang and X. Jiang, *Journal of Electroanalytical Chemistry*, **583**, 292, (2005)

35 A. A. Ensafi, M. Taei and T. Khayamian, *Journal of Electroanalytical Chemistry*, **633**, 212, (2009)

36 J.-M. Zen, J.-J. Jou and G. Ilangovan, *Analyst*, **123**, 1345, (1998)

37 E. M. M. Valle, *Process Biochemistry*, **39**, 1033, (2004)

38 J. Szejtli, *Chemical Reviews*, **98**, 1743, (1998)

39 G. Astray, C. Gonzalez-Barreiro, J. C. Mejuto, R. Rial-Otero and J. Simal-Gandara, *Food Hydrocolloids*, **23**, 1631, (2009)

40 D. A. Reece, S. F. Ralph and G. G. Wallace, *Journal of Membrane Science*, **249**, 9, (2005)

41 G. Bidan, C. Lopez, F. Mendes-Viegas and E. Vieil, *Biosensors and Bioelectronics*, **9**, 219, (1994)

42 K. R. Temsamani, H. B. Mark Jr, W. Kutner and A. M. Stalcup, *Journal of Solid State Electrochemistry*, **6**, 391, (2002)

43 T. *de* J. Licona-Sanchez, G, A. Alvarez-Romero, L. H. Mendoza-Huizar and C. A. Galan-Videl, *Journal of Physical Chemistry*, **114**, 9737, (2010)

44 M.-C. Shin and H.-S. Kim, *Biosensors and Bioelectronics*, **11**, 161, (1996)

45 N. H. Chou, J. C. Chou, T. P. Sun and S. K. Hsiung, *Sensors and Actuators B*, **130**, 359, (2008)

46 A. F. Diaz, J. I. Castillo, J. A. Logan and W. Y. Lee, *Journal of Electroanalytical Chemistry*, **129**, 115, (1981)

47 J. Tietje-Girault, C. Ponce De Leon and F. C. Walsh, *Surface and Coatings Technology*, **201**, 6025, (2007)

48 C. E. Schmidt, J. M. Fonner, L. Forciniti, H. Nguyen, J. D. Byrne, Y. F. Kou and J. Syeda-Nawaz, *Biomedical Materials*, **3**, (2008)

49 P. C. Pandey and G. Singh, *Talanta*, **55**, 773, (2001)

50 S. B. Adeloju, S. J. Shaw and G. G. Wallace, *Analytica Chimica Acta*, **323**, 107, (1996)

51 T. Osaka, S. Komaba, M. Seyama and K. Tanabe, *Sensors and Actuators B*, **35-36**, 463, (1996)

52 J. C. Chen, J. C. Chou, T. P. Sun and S. K. Hsiung, *Sensors and Actuators B: Chemical*, **91**, (1-3), 180, (2003)

53 Rajesh, V. Bisht, W. Takashima and K. Kaneto, *Biomaterials*, **26**, 3683, (2005)

54 M. Zhou and J. Heinze, *Journal of Physical Chemistry B*, **103**, 8443, (1999)

55 S. Asavapiriyanont, G. K. Chandler, G. A. Gunawardena and D. Pletcher, *Journal of Electroanalytical Chemistry*, **177**, 229, (1984)

56 S. Kuwabata, J. Nakamura and H. Yoneyama, *Journal of the Chemical Society-Chemical Communications*, 779, (1988)

57 S. Shimoda and E. Smela, *Electrochimica Acta*, **44**, 219, (1998)

58 R. Colle and A. J. Curioni, *Journal of the American Chemical Society*, 120, 4832, (1998)

59 M. Cortina, M. J. Esplandiu, S. Alegret and M. del Valle, *Sensors and Actuators B*, **118**, 84, (2006)

Chapter 5

An Investigation into the Effects of Interfering Compounds on the Detection of Urea

"Learning is finding out what you already know. Doing is demonstrating that you know it. Teaching is reminding others that they know just as well as you. We are all learners, doers, teachers."
- *Richard David Bach*

5.1 Introduction

One of the major difficulties in the detection of urea is the presence of a wide array of interfering compounds[1]. There are many interfering compounds in biological systems that are known to influence the detection of urea and a selection of these compounds was studied as potential interferants, and the results of this study are presented in this chapter. The chosen compounds include the main interfering compounds, ascorbic acid (AA), which was described in Chapter 3, Section 3.3.5, uric acid (UA) and creatinine (CR), as depicted in Figure 5.1. In addition, compounds that are structurally related to urea may interfere with urea detection and these include thiourea and hydroxyurea[1], as shown in Figure 5.2. Finally, the ammonium (NH_4^+) ion was also considered as a potential interfering species. The NH_4^+ ion, although not electroactive, is a product of the hydrolysis of urea and consequently, the detection of urea in the presence of NH_4^+ is important in the development of any urea sensor.

(a) (b) (c)

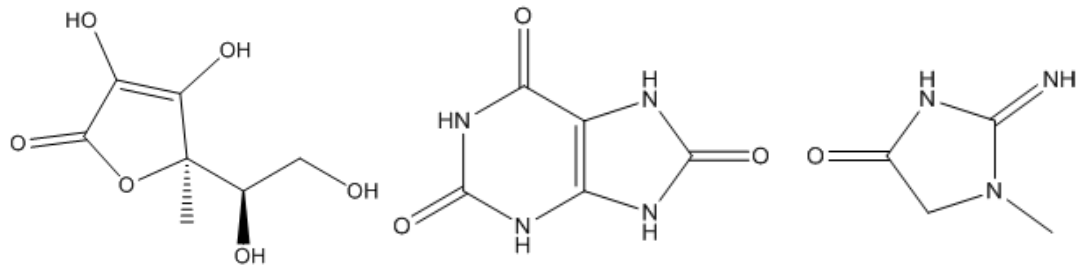

Figure 5.1: Common biological interfering compounds in urea detection: (a) ascorbic acid, (b) uric acid and (c) creatinine.

(a) (b)

Figure 5.2: Compounds that are structurally related to urea: (a) thiourea and (b) hydroxyurea.

5.2 Experimental

The instrumentation and software employed for the experiments detailed in this chapter are described in Section 2.3. All chemicals were purchased from Sigma-Aldrich or its subsidiary company, Fluka and were used as supplied, with the exception of pyrrole which was vacuum-distilled and stored in the dark at -20 °C prior to use. Solutions of 0.10 mol dm^{-3} NaCl and 0.02 mol dm^{-3} sulphonated-β-cyclodextrin, which were prepared using distilled water, were used to form the PPy-Urs films. All other solutions consisted of a 0.05 mol dm^{-3} phosphate buffer, pH 7.0, which was prepared using distilled water. All the solutions were prepared freshly before each experiment and were used at room temperature. A constant potential of 0.70 V vs. SCE was used to deposit the polypyrrole films and a fresh polymer film was formed for each experiment. The experimental conditions described in Chapter 4, Section 4.2 were used to prepare the PPy-Urs-SCD, PPy-Cl and PPy-Urs-Cl polymer films. The electrochemical response of the interfering compounds was initially studied using a glassy carbon electrode and then the response at the polymer-modified electrodes was recorded. The experiments were performed a minimum of six times (n = 6) and it is the average result that is presented in the figures, while error bars are provided for calibration curves.

5.3 Results and Discussion

The interfering compounds were selected based on their concentrations in biological systems, electroactivity, charge and structure in solution. Ascorbic acid (AA), uric acid (UA) and creatinine (CR) exist in relatively high concentrations in biological systems[1], while thiourea and hydroxyurea, although at lower concentrations, are structurally related to urea. Moreover, at a pH of 7.0 the interfering compounds range from neutral to anionic species in solution. As previously highlighted in Chapter 4, urea is important in both the medical and agricultural industries[2,3] and the influence of these potential interfering species on the detection of urea is important in the development of a urea sensor.

5.3.1 Ascorbic Acid as an Interfering Species

Ascorbic acid (AA), Figure 5.1(a), more commonly known as Vitamin C, is a major interfering compound in biological systems[4,5]. AA exists at concentrations of up to 1.0 x 10^{-4} mol dm^{-3} in the body[6,7]. It is also electrochemically active and can be easily oxidised between -100 and 400 mV vs. SCE on most solid electrodes[4]. Moreover, the products of the AA oxidation reaction have been shown to foul the electrode surface[8].

The electrochemical response of urea and AA at a glassy carbon electrode was initially investigated using cyclic voltammetry. The electrodes were cycled at 50 mV s^{-1} in a 0.05 mol dm^{-3} phosphate buffer solution, pH 7.0, from -0.60 to 0.80 V vs. SCE in the absence and presence of 0.01 mol dm^{-3} urea or 1.0 x 10^{-4} mol dm^{-3} AA. This electrochemical window was chosen as the PPy-Urs-SCD film is stable when cycled to 0.80 V vs. SCE, but at higher applied potentials, repeated cycling leads to overoxidation of the film, Section 4.3.2.2. Typical cyclic voltammograms, recorded in the phosphate buffer solution in the presence and absence of urea, are shown in Figure 5.3. In the presence of urea, there is a slight increase in the measured current between -0.10 and 0.80 V vs. SCE, indicating some oxidation of the urea. However, there is no evidence to support a significant oxidation reaction at the glassy carbon electrode. The oxidation of urea has been studied at several noble metal electrodes and the anodic oxidation is shown to depend on the applied potential, the composition of the electrolyte solution, the pH, urea concentration and the nature and properties of the electrode surface. Wang *et al.*[9], have shown that a large oxidation current, extending from about 1.00 to 1.20 V vs. SCE can be obtained for the oxidation of urea at a glassy carbon electrode modified with amino groups, however the signal at an un-modified glassy carbon electrode is much lower. The oxidation wave was explained in terms of the oxidation of the electroactive carbamic acid, which is produced during the hydrolysis of urea. The data presented in Figure 5.3 are in good agreement with the results presented by Wang *et al.*[9] at the un-modified glassy carbon electrode, showing some oxidation, but no significant oxidation wave.

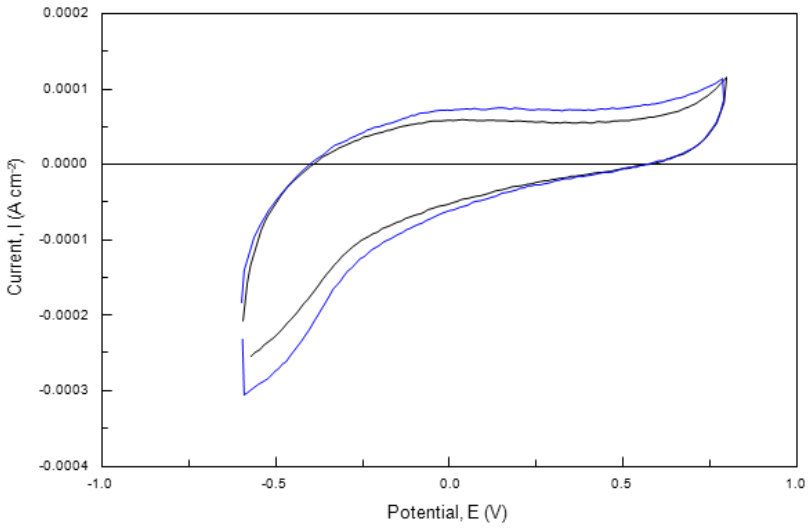

Figure 5.3: Cyclic voltammograms recorded at 50 mV s^{-1} at glassy carbon electrode in ▬ pH 7.0 phosphate buffer solution and ▬ 1.0 x 10^{-2} mol dm^{-3} urea in a pH 7.0, phosphate buffer solution.

The electroactivity of AA is shown in Figure 5.4. It is clearly evident that AA is oxidised readily, with a large oxidation wave observed between approximately 0.10 and 0.80 V vs. SCE. This is in good agreement with literature reports on the electrochemical oxidation of AA at noble metal electrodes[10]. On addition of the AA to a 1.0 x 10^{-2} mol dm^{-3} urea-containing phosphate solution, a considerable difference in the voltammograms is seen. This is shown in Figure 5.5, which compares the voltammograms recorded in the buffered urea-containing solution in the presence and absence of the AA. Clearly, the presence of AA in the urea-containing solution alters both the voltammetry of the AA, Figure 5.4, and the voltammograms recorded in the buffered urea solution. The currents are considerably higher, in the combined AA and urea solution compared to the urea solution. Furthermore, when compared to the voltammogram recorded for the AA solution, Figure 5.4, there is a considerable decrease in the AA oxidation wave. It is clear that the urea inhibits the oxidation of the AA. However, the addition of AA to the buffered urea solution also alters the voltammograms recorded for urea, with a significant increase in the current from approximately 0.10 V to 0.08 V vs. SCE, Figure 5.5. Based on these measurements, it is clear that AA is a potential interfering compound in the electrochemical detection of urea.

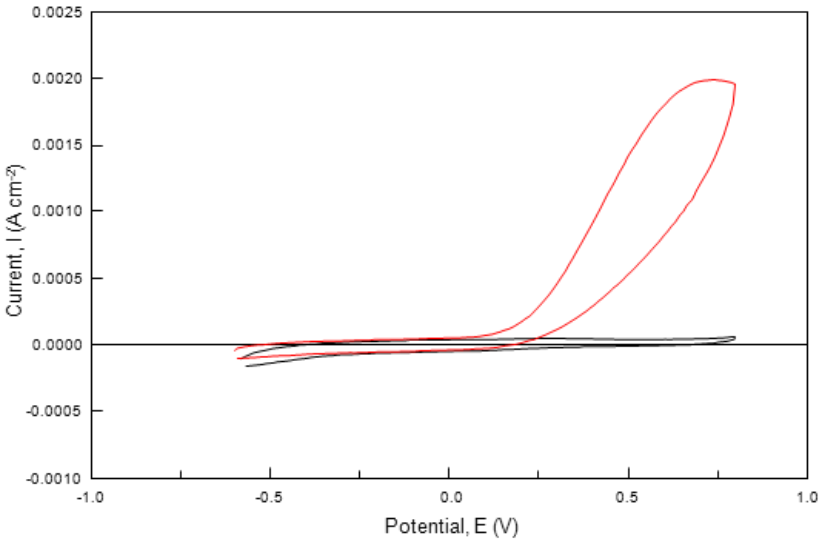

Figure 5.4: Cyclic voltammograms recorded by cycling the bare glassy carbon electrode in a pH 7.0 phosphate buffer solution in the ▬ absence and ▬ presence of 1.0 x 10^{-4} mol dm^{-3} AA.

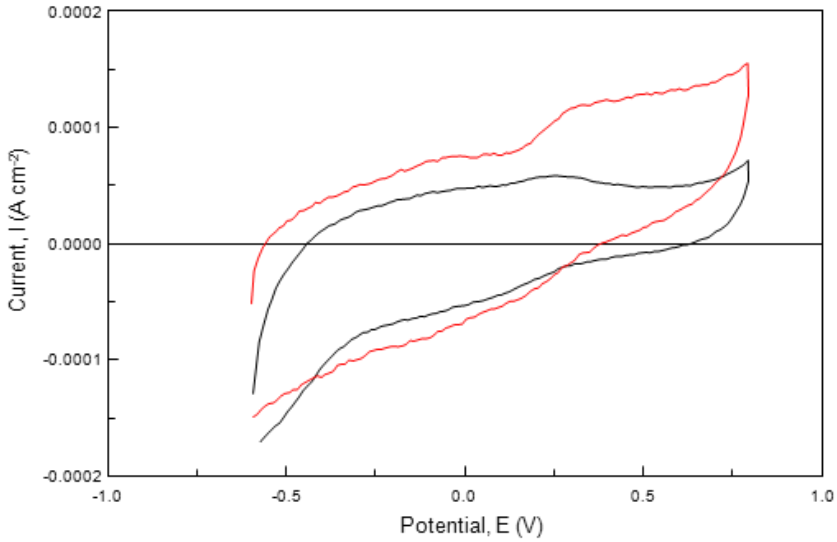

Figure 5.5: Cyclic voltammograms recorded by cycling the bare glassy carbon electrode in 1.0 x 10^{-2} mol dm^{-3} urea in a pH 7.0 phosphate buffer solution in the ▬ absence and ▬ presence of 1.0 x 10^{-4} mol dm^{-3} AA.

It was shown in Chapter 4, Section 4.3.7, that the PPy-Urs-SCD film had excellent sensitivity in the electrochemical detection of urea and this polymer film was chosen and used in an attempt to eliminate the interference from AA. Because SCD is a large anionic species[11], as discussed in Chapter 1, Section 1.4.2, this anionic character may be sufficient to repel the anionic ascorbate species[12]. Ascorbic acid has a p*K*a value of 4.10 and, at the pH of the phosphate buffer solution, dissociation of AA occurs to favour the ascorbate anion, as shown in Scheme 5.1[12]. Indeed, using Equation 5.1, where [AA^-] represents the concentration of the ascorbate anion, the plot in Figure 5.6 was obtained, which clearly shows that at pH values of 7.0 and slightly lower, it is the anionic species that is present in solution.

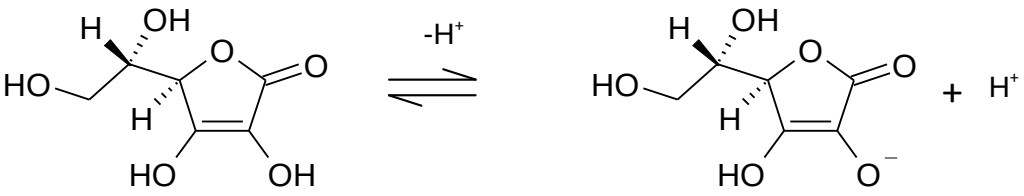

Scheme 5.1: The dissociation of AA.

% Anions $$AA^- = \frac{100}{1 + 10^{pK_a - pH}} \quad 5.1$$

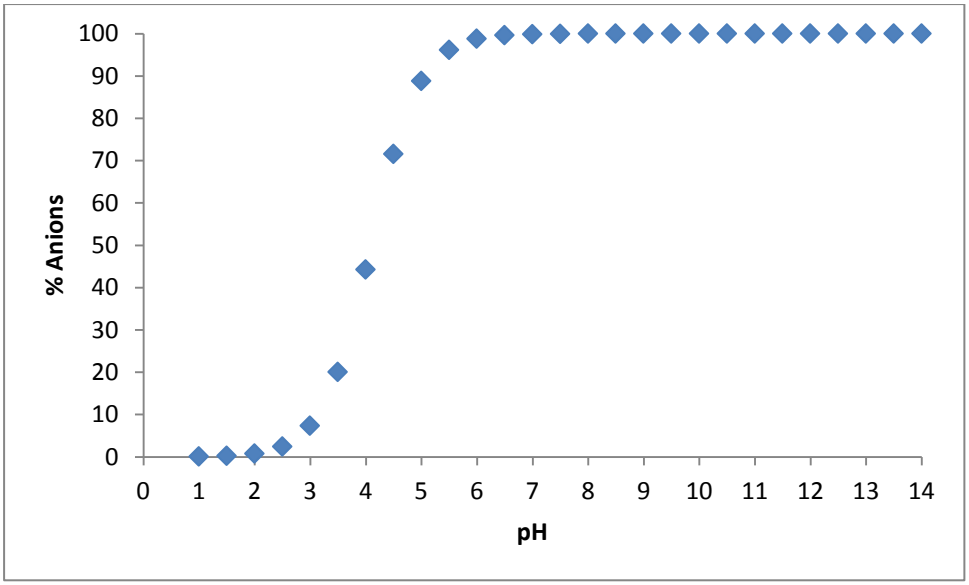

Figure 5.6: The percentage of anions as a function of pH for the AA molecule, which exists as the ascorbate anion at pH 7.0.

The PPy-Urs-SCD polymer was deposited as detailed in Chapter 4, Section 4.3.4 and cycled in a urea solution in the presence and absence of ascorbic acid, AA. The urea concentration was varied from 1.0 x 10^{-10} to 1.0 x 10^{-2} mol dm^{-3}, while a fixed concentration of 1.0 x 10^{-4} mol dm^{-3} AA was added to give AA/urea concentration ratios ranging from 1.0 x 10^{6} to 1.0 x 10^{-2}. As detailed in Section 4.3.7, the oxidation charge was computed. This charge was recorded in the urea solutions and then compared with the charge recorded in the mixed urea and AA solution. These data are summarised in Figure 5.7, while the influence of AA on the calibration curve at low urea concentrations is presented in Figure 5.8. It is clear from these data that the interference observed when adding AA to the urea solution at the glassy carbon electrode is eliminated at the PPy-Urs-SCD polymer films. The oxidation charges obtained from cycling the polymer in a urea solution in the absence of AA are similar to those obtained on cycling the polymer film in a urea solution in the presence of AA. Regardless of the ratio of AA to urea, which is in the vicinity of 1.0 x 10^{6} at the low concentrations of urea, there is no evidence of any interference from the added AA.

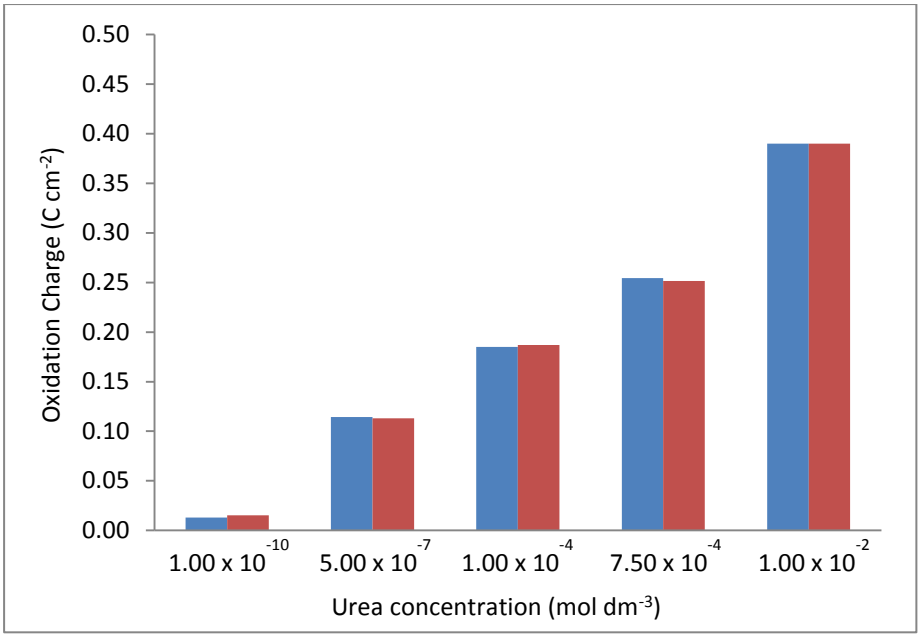

Figure 5.7: Charge plotted at different urea concentrations in the — absence and — presence of 1.0 x 10^{-4} mol dm^{-3} AA at the PPy-Urs-SCD polymer films.

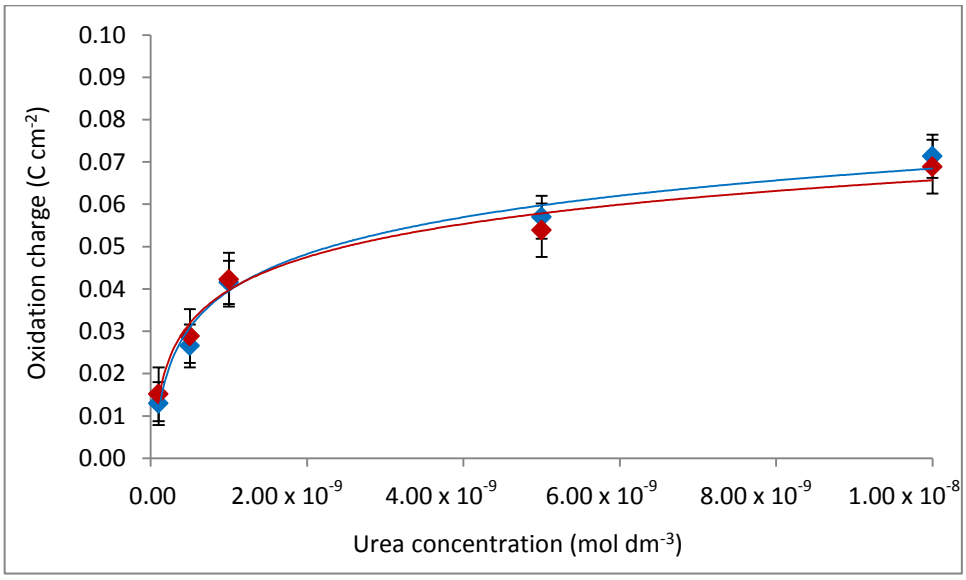

Figure 5.8: Calibration curve (n = 6) with the oxidation charge plotted as a function of the urea concentration in the — absence and — presence of 1.0 x 10^{-4} mol dm^{-3} AA, at the PPy-Urs-SCD polymer films.

These data can be explained in terms of the negative charges of the sulphonated groups on the β-cyclodextrin within the PPy-Urs-SCD film. Although the charge on the sulphonated groups may be balanced by an equal and opposite charge from the oxidised polypyrrole backbone (PPy^+), the $–SO_3^-$ pendants will provide a highly negative local charge. In addition, free $–SO_3^-$ groups are likely to exist at the PPy-

Urs-SCD surface[13]. It appears that the negatively charged sulphonated groups on the β-cyclodextrin are successful in repelling the anionic ascorbate from the surface of the electrode and hence, the urea can be detected without any interference from AA, as clearly shown in Figures 5.7 and 5.8.

5.3.2 Uric Acid

Uric acid, UA, Figure 5.1(b) exists in conjunction with urea at concentrations of up to 1.0 x 10^{-4} mol dm^{-3} in the body[1]. UA is the primary end product of purine metabolism in the human body[14] and abnormal levels of UA are indicators of several diseases including gout, hyperuricemia and Lesch-Nyan disease[15,16]. Increased ureate levels have also been linked with diseases such as leukaemia and pneumonia[17]. The existence of several tautomeric forms of UA, which are depicted in Scheme 5.2, has been widely researched in order to account for its physiochemical and biological behaviour[18]. UA is known to be electroactive with a range of $E_{½}$ values lying between 0.30 and 0.40 V vs. SCE on most solid electrodes and it can be irreversibly oxidised in aqueous solutions to produce allantoin[19,20]. Consequently, UA can interfere directly with urea detection as urea is also oxidised in this region. In order to investigate the effect of uric acid on urea detection, cyclic voltammograms were recorded for urea on a bare glassy carbon electrode in the presence and absence of uric acid. The voltammograms recorded were similar to the data shown for the AA system in Figure 5.4. An increase in the current from about 0.20 to 0.80 V vs. SCE was observed in the presence of UA, which can be attributed to the oxidation of UA. This shows that UA is indeed a potential interferant in the electrochemical detection of urea.

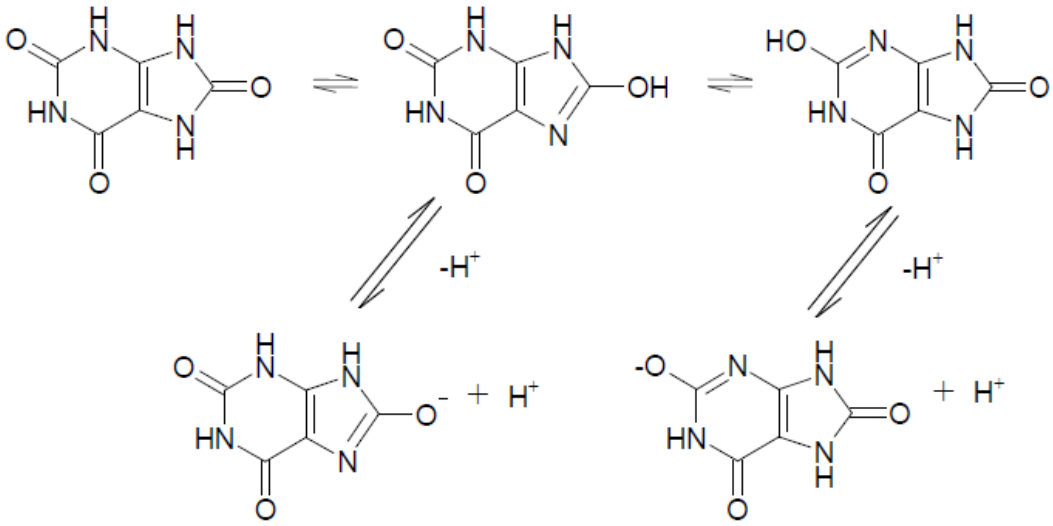

Scheme 5.2: The dissociation of UA.

In an attempt to overcome this potential interference, the PPy-Urs-SCD polymer was used. The polymer film was grown and cycled in a urea solution in the presence and absence of uric acid. Typical cyclic voltammograms recorded in a 1.0 x 10^{-2} mol dm^{-3} urea solution and in a solution containing both 1.0 x 10^{-2} mol dm^{-3} urea and 1.0 x 10^{-4} mol dm^{-3} UA are shown in Figure 5.9. A significant difference in the two voltammograms is evident, with higher currents measured in the presence of UA, particularly from about -0.10 to 0.80 V vs. SCE.

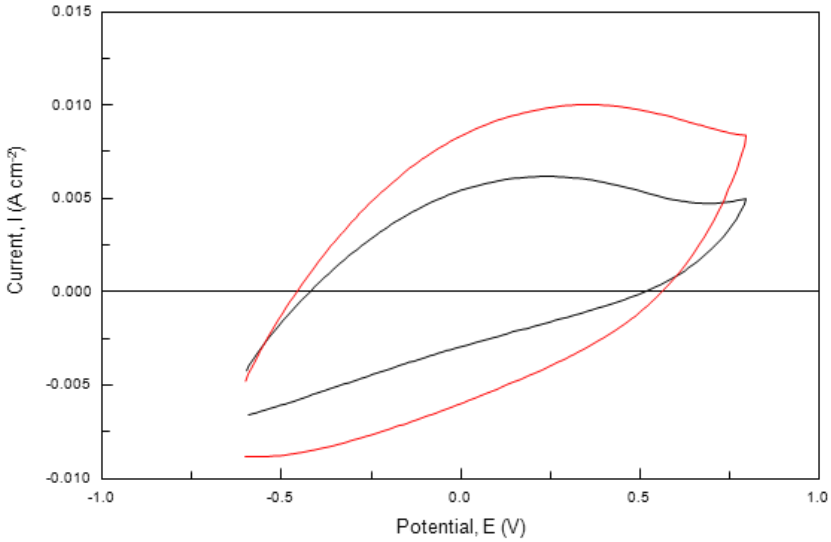

Figure 5.9: Cyclic voltammograms recorded by cycling the PPy-Urs-SCD polymer film in a 1.0 x 10^{-2} mol dm^{-3} urea solution in the ▬ absence and ▬ presence of 1.0 x 10^{-4} mol dm^{-3} uric acid.

It is clear that the current and the charge obtained from cycling the polymer in a urea solution are lower than that obtained from cycling the polymer film in a urea solution with uric acid present. Hence, the uric acid is indeed interfering with urea detection, even in the presence of the PPy-Urs-SCD polymer film. This is a surprising result given that uric acid, with a pK_a value of 5.4[21], is predominantly anionic at a pH of 7.0, as shown in Figure 5.10, where the % of anions is plotted as a function of the pH, using Equation 5.1. As discussed in Section 5.3.1, with the ascorbic acid/ascorbate anion, it is expected that the anionic nature of the SCD[22], incorporated within the PPy-Urs-SCD polymer film, would be sufficient to repel the uric acid/ureate anion from the electrode surface. However, this is clearly not the case, as shown in Figure 5.9.

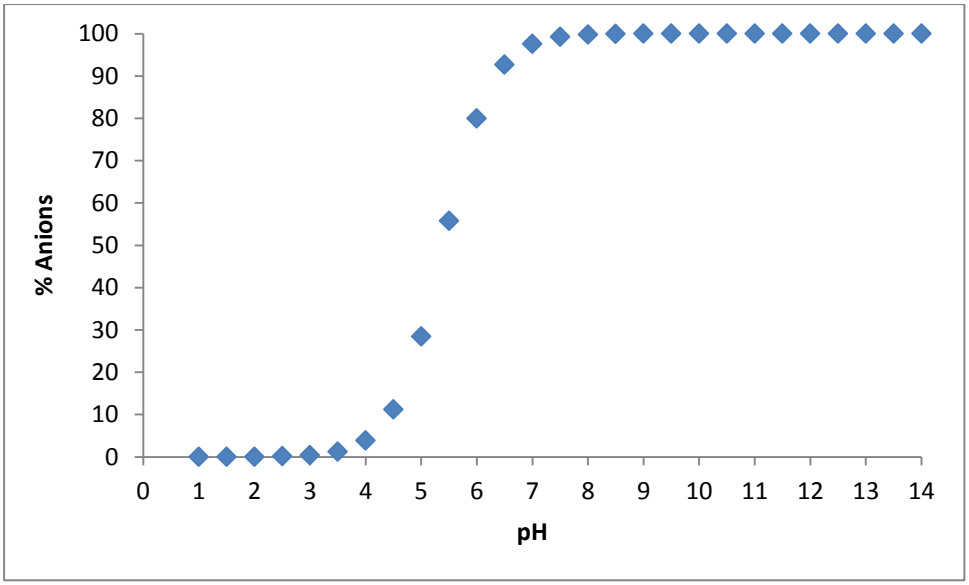

Figure 5.10: The percentage anions as a function of pH for the uric acid molecule, UA, which exists as the ureate anion at pH 7.0.

The oxidation charge plotted as a function of urea concentration in the absence and presence of a fixed concentration of UA, at 1.0 x 10^{-4} mol dm^{-3}, is shown in Figure 5.11. Again, it is clear that higher charges are recorded in the presence of UA, regardless of the urea concentration, or indeed the ratio of the UA to urea. When the concentration of urea is 1.0 x 10^{-2} mol dm^{-3} to give a concentration ratio of urea:UA of 1.00:0.01, the charge is increased from 0.40 C cm^{-2} to 0.48 C cm^{-2}, giving a 20% increase in the measured charge. This increase is maintained when the ratio of urea:UA is varied. For example, a 22% increase in the charge is observed when the concentration of urea is 5.0 x 10^{-7} mol dm^{-3} to give a urea:UA ratio of 1:10^{3}. This suggests that the observed increase in the charge is not connected with the concentration of urea, but is related to the uric acid only. This increase in the charge in the presence of UA is a surprising result since most interfering compounds tend to foul, adhere to and block the surface of the electrode[23]. As a result, the signal is lost or lowered significantly; however this is not the case as shown in Figures 5.9 and 5.11.

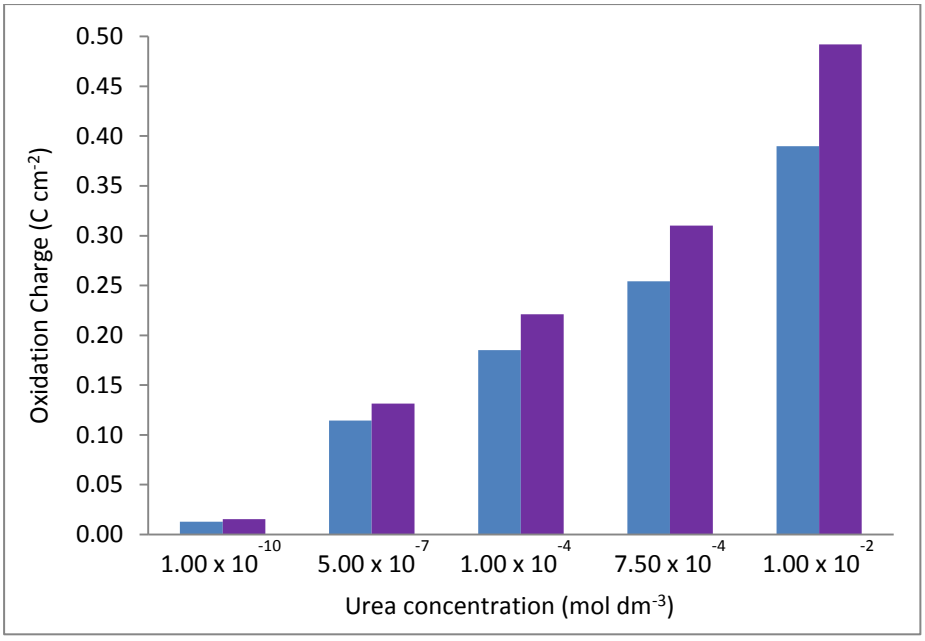

Figure 5.11: Charge plotted as a function of urea concentration in the — absence and — presence of 1.0 x 10^{-4} mol dm^{-3} UA.

One possible explanation to account for these observations is the diffusion of UA through the polymer film to the polymer-electrode interface, where oxidation of UA occurs. As detailed earlier, oxidation of UA occurs at the glassy carbon substrate and this oxidation reaction would contribute to the measured charges. This possibility was explored by using polymer films deposited to different thickness. For this study, PPy-Cl and PPy-Urs-Cl polymer films were chosen. The polymer films were deposited to different charges, ranging from 0.01 to 0.74 C cm^{-2}. Once deposited, the films were cycled in the buffered 0.01 mol dm^{-3} urea solution, in the absence and presence of 1.0 x 10^{-4} mol dm^{-3} UA. It was found that the thickness of the polymer film had a significant influence on the measured oxidation charge. When relatively thin PPy-Cl films were used, the charges recorded in the presence of UA were significantly higher, as shown in Figure 5.12. However, when the thickness of the PPy-Cl films was increased, the charges recorded in the urea solution were similar in the presence and absence of UA, as highlighted in Figure 5.13.

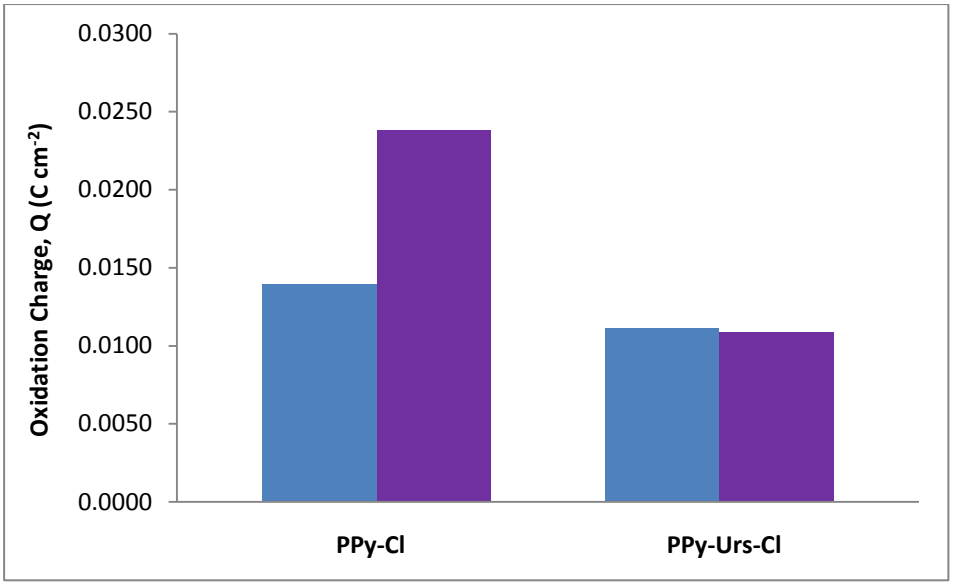

Figure 5.12: Charge recorded (5th cycle) for the PPy-Cl and PPy-Urs-Cl polymer films grown to a charge of 0.017 C cm^{-2} cycled in a 0.01 mol dm^{-3} solution of urea in the — presence and — absence of 1.0 x 10^{-4} mol dm^{-3} uric acid.

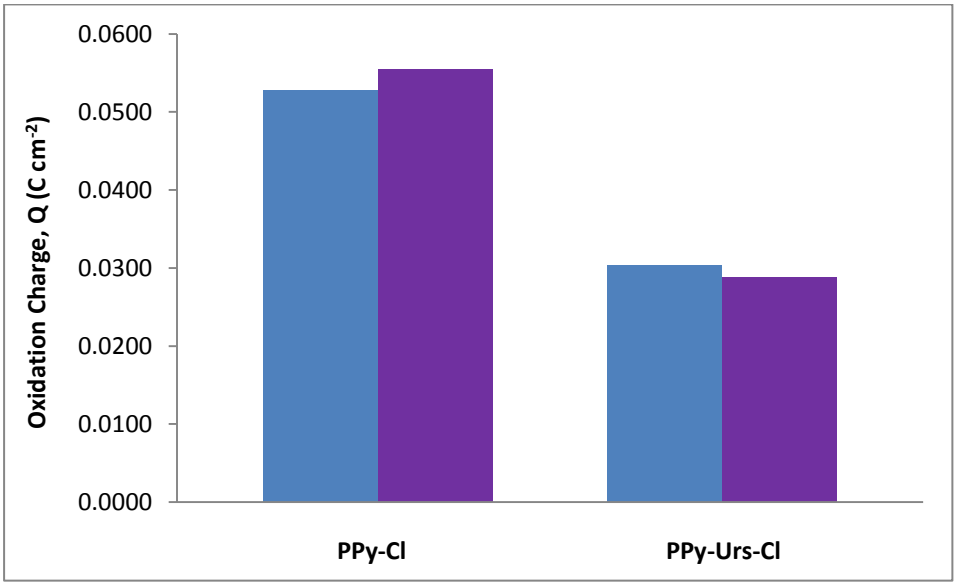

Figure 5.13: Charge recorded (5th cycle) for the PPy-Cl and PPy-Urs-Cl polymer films grown to a charge of 0.74 C cm^{-2} cycled in a 0.01 mol dm^{-3} solution of urea in the — presence and — absence of 1.0 x 10^{-4} mol dm^{-3} uric acid.

Interestingly, the PPy-Urs-Cl film, although grown to the same charge as the PPy-Cl film, does not allow the UA to reach the electrode surface as readily. This is clearly evident in Figure 5.12 where the presence of UA leads to a significant increase in the charge recorded at the PPy-Cl, but not at the PPy-Urs-Cl films. This may be related to the fibrous morphology observed for the PPy-Urs-Cl film, compared to the cauliflower-like morphology of the PPy-Cl film, Section 4.3.2.1. The pores in the PPy-Urs-Cl polymer film are blocked by the large enzyme and this may inhibit the diffusion of UA throughout the polymer film. However, the morphology of the PPy-Urs-SCD films is very different and more porous, enabling the diffusion of UA to the substrate interface.

This clearly shows that while the anionic charge provided by the SCD is important in eliminating interference from AA, the porosity of the polymer film is also significant. Although the PPy-Urs-SCD film gives the best sensitivity and detection limit and eliminates any interference from AA, the PPy-Urs-Cl film can eliminate interference from UA. Consequently, a combination of these two polymer films, with a first layer of PPy-Urs-Cl deposited to a charge of 0.017 C cm^{-2}, followed by the deposition of PPy-Urs-SCD is the ideal sensor, with excellent sensitivity, limit of detection and complete elimination of any interference from AA and UA.

5.3.3 Thiourea

Thiourea (TU), Figure 5.2(a), is a planar, organosulphur compound used as a reagent in organic synthesis. Thiourea is structurally related to urea, except with a sulphur atom present in the position of the oxygen atom on the urea compound[24]. Thiourea occurs in two tautomeric forms, a thione form and a thiol form, as shown in Figure 5.14. In aqueous solutions, the thione form predominates; however, with the thiol form, significant fouling of the sensor by the thiol group is likely. Thiourea is electroactive and is readily oxidised above 0.30 V vs. SCE to form formamidine disulphide[25,26]. However, upon electrochemical reduction of TU, sulphide ions are formed[27] which can lead to significant fouling of the electrode surface.

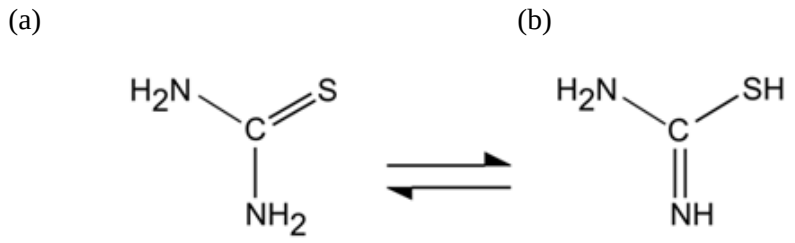

Figure 5.14: The two tautomeric forms of thiourea (TU): (a) the thione and (b) the thiol form.

In order to investigate the electroactivity of TU, cyclic voltammograms were recorded by cycling the bare glassy carbon electrode in a buffered 1.0 x 10^{-4} mol dm^{-3} TU solution from -0.60 to 0.80 V vs. SCE. The resulting voltammogram is presented in Figure 5.15. Shown for comparison is the voltammogram recorded in the buffer solution. It is evident that TU oxidises readily at the bare glassy carbon electrode as there is a significant increase in the current in the presence of TU. The oxidation of TU is observed from approximately 0.20 V to 0.80 V vs. SCE, as highlighted in Figure 5.15. However, there is no reduction wave observed, which is indicative of the formation of formamidine disulphide[25,26]. As TU is readily oxidised it is a potential interferant, but unlike AA and UA, it does not exist as an anionic species in the pH 7.0 phosphate buffer solution.

Again, the influence of TU on the electrochemical detection of urea was investigated at the PPy-Urs-SCD polymer film. The polymer was formed and cycled in a urea solution in the presence and absence of 1.0 x 10^{-4} mol dm^{-3} TU. The concentration of urea was varied, while the concentration of TU was fixed at 1.0 x 10^{-4} mol dm^{-3} to give TU/urea ratios ranging from 1.0 x 10^{6} to 1.0 x 10^{-2}. The charge was computed and this is shown in Figure 5.16 where the charge is plotted as a function of the urea concentration in the absence and presence of TU. At the lowest urea concentration of 1.0 x 10^{-10} mol dm^{-3}, there is no evidence of any interference, but at the higher urea concentrations it is clear that the presence of TU gives higher charges. The charge is increased by about 6 to 7% on addition of TU to the buffered solution. This increase is less significant than that observed with UA, Figure 5.11. Again, this could be due to the diffusion of TU throughout the porous polymer film and its oxidation at the substrate electrode. However, as discussed in Section 5.3.2, this

diffusion can be inhibited by increasing the film thickness and reducing the film porosity.

Interestingly, there is no evidence of any surface fouling due to the presence of the thiol group. Furthermore, there was no loss or reduction of the charge with continued cycling in the presence of TU. This is significant as sulphur-containing compounds, such as thiourea, are well known to foul the surface of the electrode[27].

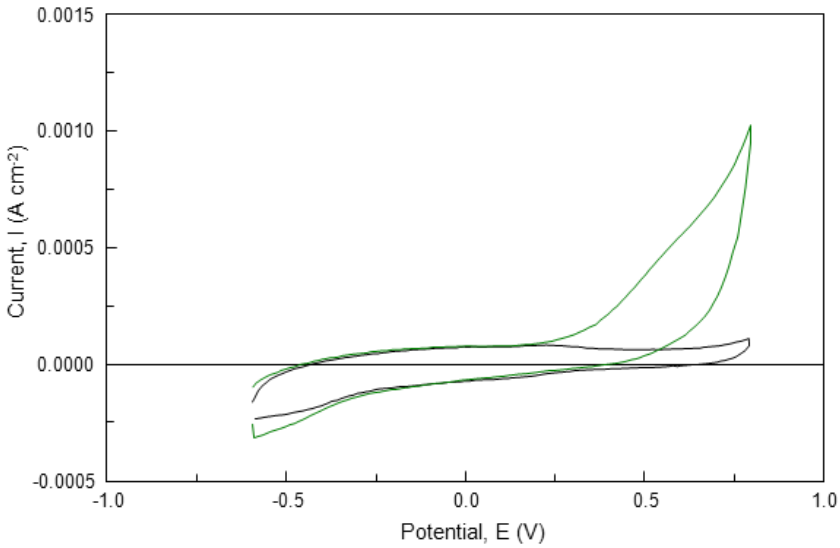

Figure 5.15: Cyclic voltammograms recorded by cycling glassy carbon in a pH 7.0 phosphate buffer solution in the ▬ absence and ▬ presence of 1.0 x 10^{-4} mol dm^{-3} TU.

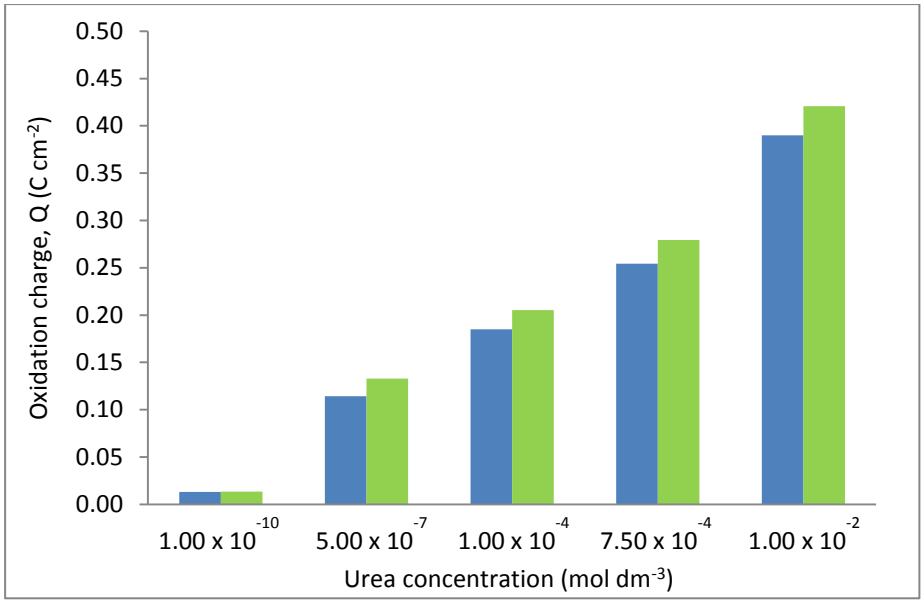

Figure 5.16: Charge plotted as a function of the urea concentration in the — absence and — presence of 1.0 x 10^{-4} mol dm^{-3} TU.

5.3.4 Hydroxyurea

Hydroxyurea, HU, Figure 5.2(b), also known as hydroxycarbamide, is an antineoplastic [28] and chemotherapy drug that is structurally similar to the urea compound. Hydroxyurea was first synthesised by Dresler and Stein in 1869[29], from the reaction of hydroxylamine and hydrogen cyanate. Hydroxyurea has found widespread use in the treatment of sickle cell disease[30] and as an anticancer agent[31]. Hydroxyurea increases the concentration of fetal haemoglobin[32] by increasing the nitric oxide levels in the treatment of sickle cell disease. It also inhibits the ribonucleotide reductase enzyme by scavenging tyrosyl free radicals which depletes the production of deoxyribonucleotides; hence its antiretroviral properties[33].

Hydroxyurea has been used primarily for the treatment of myeloproliferative diseases, which has an inherent risk of transforming to acute myeloid leukaemia[30]. There has been a longstanding concern that hydroxyurea itself carries a leukaemia risk, but a number of studies have shown that the risk is either absent or very small. Nevertheless, this concern has been a barrier for its wider use in patients with sickle-cell disease[30].

In order to investigate the electroactivity of HU, cyclic voltammograms were obtained by cycling the bare glassy carbon electrode in a phosphate buffer solution in the absence and presence of 1.0 x 10^{-4} mol dm^{-3} HU from -0.60 to 0.80 V vs. SCE. Typical voltammograms are presented in Figure 5.17. It is evident that HU oxidises readily at the bare electrode, with the oxidation of HU observed at approximately 0.25 V vs. SCE, as highlighted in Figure 5.17. These data are similar to that presented for TU in Figure 5.15, suggesting that HU is a likely interferant.

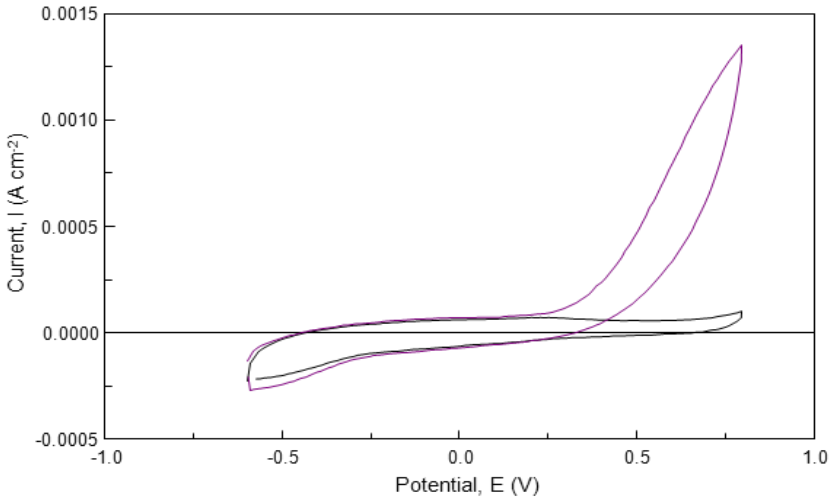

Figure 5.17: Cyclic voltammograms recorded by cycling glassy carbon in a pH 7.0 phosphate buffer solution in the ━ absence and ━ presence of 1.0 x 10^{-4} mol dm^{-3} HU.

Again, the PPy-Urs-SCD film was used in an attempt to eliminate the detection of hydroxyurea. The PPy-Urs-SCD polymer was deposited and cycled in a urea solution in the presence and absence of hydroxyurea. The concentration of urea was varied from 1.0 x 10^{-10} to 1.0 x 10^{-2} mol dm^{-3}, while the concentration of HU was fixed at 1.0 x 10^{-4} mol dm^{-3}, giving significant variations in the ratio of HU to urea. Representative data are shown in Figure 5.18, where the charge is plotted as a function of the urea concentrations in the absence and presence of HU. Again, it is clearly evident that the presence of HU gives rise to an increase in the charge. The relative increase in the charge is higher than that observed with the TU system. In Figure 5.18, the increase in charge on addition of HU to the urea-containing solution is close to 20%, indicating a higher degree of interference. On a comparison of the voltammograms recorded at the bare glassy carbon electrode for the TU and HU,

Figures 5.15 and 5.17, it is evident that higher currents are measured with the HU. This may be connected to the higher level of interference observed with HU, Figure 5.18.

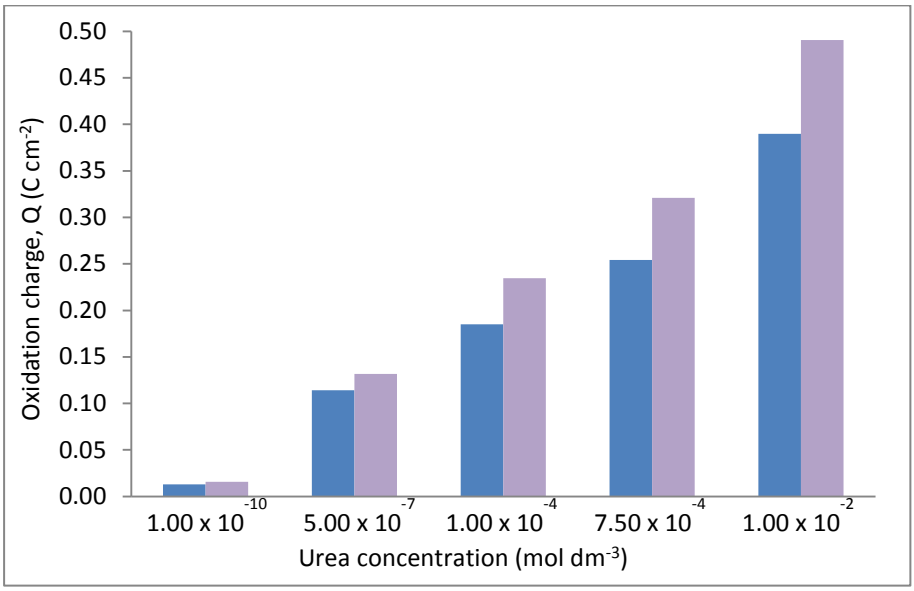

Figure 5.18: Charge plotted as a function of the urea concentration in the absence and presence of 1.0 x 10^{-4} mol dm^{-3} HU.

5.3.5 Creatinine

Creatinine, (CR), Figure 5.1(c), is a spontaneously formed cyclic derivative of creatine, and is a break-down product of creatine phosphate in muscle that is produced at a fairly constant rate within the body and released into the blood[34]. Several tautomers of creatinine exist and these are shown in Figure 5.19. The normal serum physiological concentration range of creatinine and creatine is approximately 35 x 10^{-6} to 140 x 10^{-6} mol dm^{-3}, while pathological values may rise to 1.0 x 10^{-3} mol dm^{-3} or higher [35,36]. Abnormal creatinine levels are indicative of renal, thyroid and muscle dysfunctions[37]. Creatinine is filtered out of the blood via the kidneys, with little to no reabsorption. In the case of renal deficiency or muscle disorder, the creatinine blood levels rise significantly[36], whereas low levels of creatinine are indicative of muscular dystrophy and myasthenia[38]. Creatinine levels in blood and urine may be used to calculate the creatinine clearance (CRCl), which reflects the glomerular filtration rate (the amount of fluid filtered per unit time), a measure of renal function[39].

A more complete estimation of renal function can be obtained when the blood plasma concentration of creatinine is compared to the urea concentration. The ratio of blood urea nitrogen to creatinine (the BUN-to-creatinine ratio) can indicate problems beyond those intrinsic to the kidney[40]. High levels of urea concentration compared to creatinine concentrations may indicate a pre-renal problem, such as volume depletion. It is important to note that diuretics, such as coffee and tea, cause more frequent urination, thus decreasing creatinine levels. In addition, greater muscle content[41] gives rise to higher concentrations of creatinine, while a decrease in muscle mass will cause a lower reading of creatinine[42].

Hence, like urea, creatinine is an important biological compound in the area of renal deficiency[43]. In contrast to urea, however, the concentration of creatinine in the body fluids is not influenced by protein intake and therefore, the creatinine concentration is a more reliable indicator of renal function[44]. Creatinine is generally present at lower concentrations than urea in biological systems. Creatinine is found at concentrations of up to 1.0 x 10^{-4} mol dm^{-3} in the body[1], whereas urea levels vary from 1.0 x 10^{-3} to 1.0 x 10^{-2} mol dm^{-3}. However, it is well known that creatinine can interfere with the detection of urea[45].

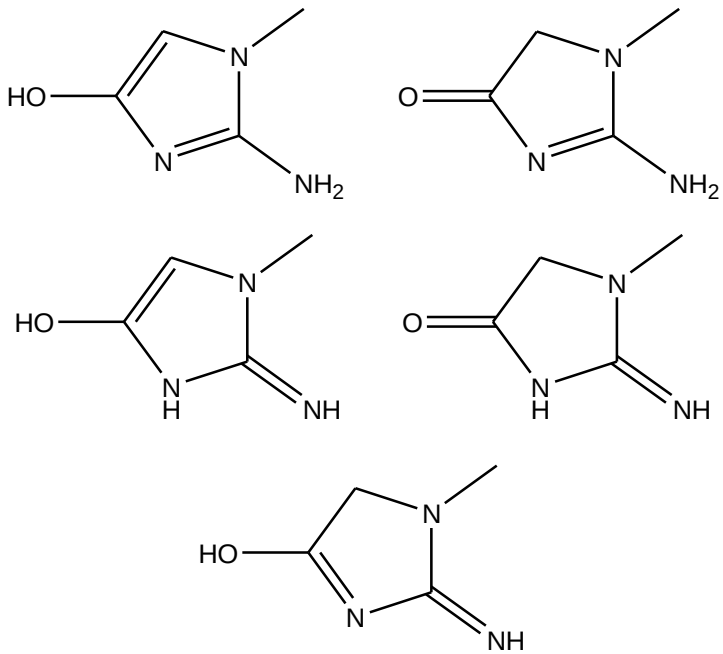

Figure 5.19: The structures of the contributing tautomers of creatinine.

The electroactivity of CR was investigated by cycling the bare glassy carbon electrode in 1.0 x 10^{-4} mol dm^{-3} CR in a phosphate buffer solution from -0.60 to 0.80 V vs. SCE, as shown in Figure 5.20. It is evident from these data that CR is oxidised to some extent at the bare glassy carbon electrode. Although there is no significant oxidation wave, there is a slight increase in the oxidation current in the presence of CR over the entire potential window, as highlighted in Figure 5.20. Again, this is in the region where the oxidation of urea occurs.

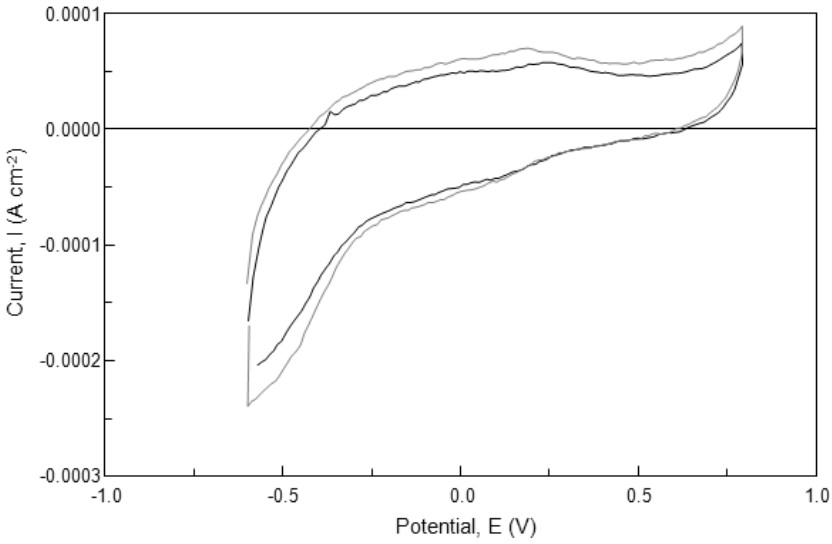

Figure 5.20: Cyclic voltammograms recorded at glassy carbon in a pH 7.0, phosphate buffer solution in the ━ absence and ━ presence of 1.0 x 10^{-4} mol dm^{-3} CR.

The data recorded for the PPy-Urs-SCD polymer film are shown in Figure 5.21. The PPy-Urs-SCD film was cycled in a urea solution in the presence of 1.0 x 10^{-4} mol dm^{-3} CR and the charge was computed and compared to the values recorded in the absence of CR. Again, a significant increase in the charge, close to 30%, is observed when CR is added to the urea-containing solution, indicating considerable interference. As detailed earlier, this may be related to the diffusion of CR to the substrate and oxidation at the substrate; however, as highlighted in Figure 5.20, the currents arising from the oxidation of CR at the glassy carbon electrode are relatively low.

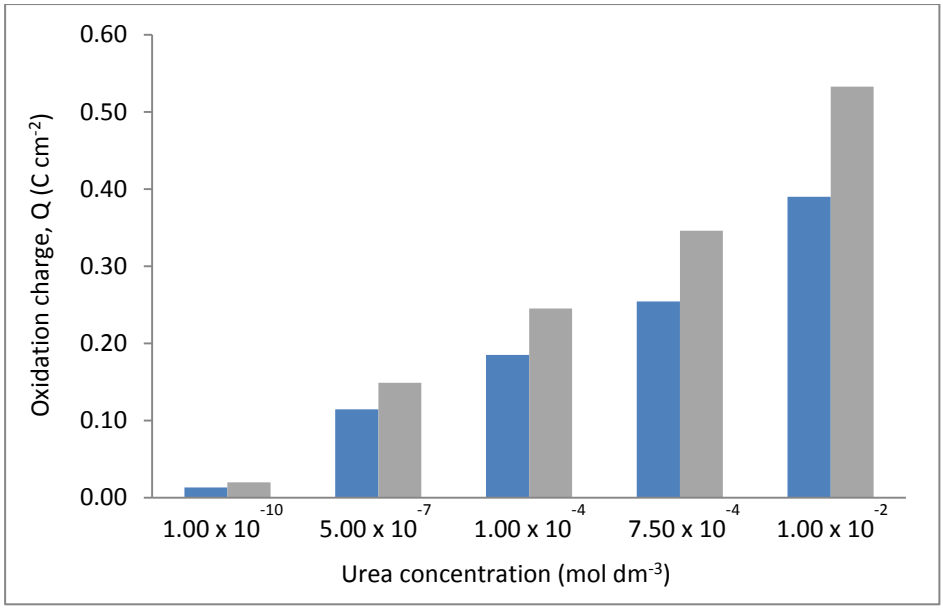

Figure 5.21: Charge plotted as a function of urea concentration in the — absence and — presence of 1.0 x 10^{-4} mol dm^{-3} CR.

5.3.6 Ammonium Chloride

Ammonium chloride, NH_4Cl, is a white, crystalline, inorganic compound; however, there are no reports in the literature to suggest that NH_4Cl is electroactive or oxidised. However, NH_4^+ is produced during the hydrolysis of urea and its influence on the electrochemical detection of urea is important in the development of a urea sensor. As expected, there is no evidence for the oxidation of NH_4Cl at the glassy carbon electrode, as shown in Figure 5.22. The voltammograms recorded in the phosphate buffer solution are identical to the voltammograms recorded in a 1.0 x 10^{-4} mol dm^{-3} NH_4Cl buffered solution.

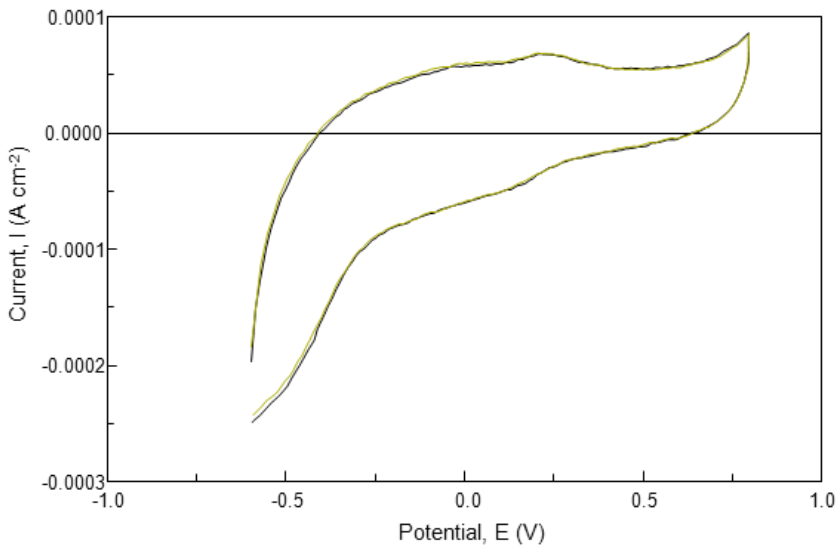

Figure 5.22: Cyclic voltammograms obtained by cycling the bare GC electrode in a pH 7.0, phosphate buffer solution in the ━ absence and ━ presence of 1.0 x 10^{-4} mol dm^{-3} NH_4Cl.

The PPy-Urs-SCD polymer film was cycled in a urea solution in the presence and absence of NH_4Cl and the charges were recorded and plotted, as shown in Figure 5.23. Clearly, there is no evidence of any interference from the NH_4Cl. Furthermore, there was no evidence of any surface fouling in the presence of NH_4Cl. These data clearly show that urea can be detected with the PPy-Urs-SCD film in the presence of NH_4^+ without any interference or surface fouling. This proves that the PPy-Urs-SCD polymer film not only enhances detection of urea compared to the bare glassy carbon electrode, as discussed in Chapter 4, but indeed, it also inhibits or eliminates fouling of the electrode by common biological salts, such as NH_4Cl.

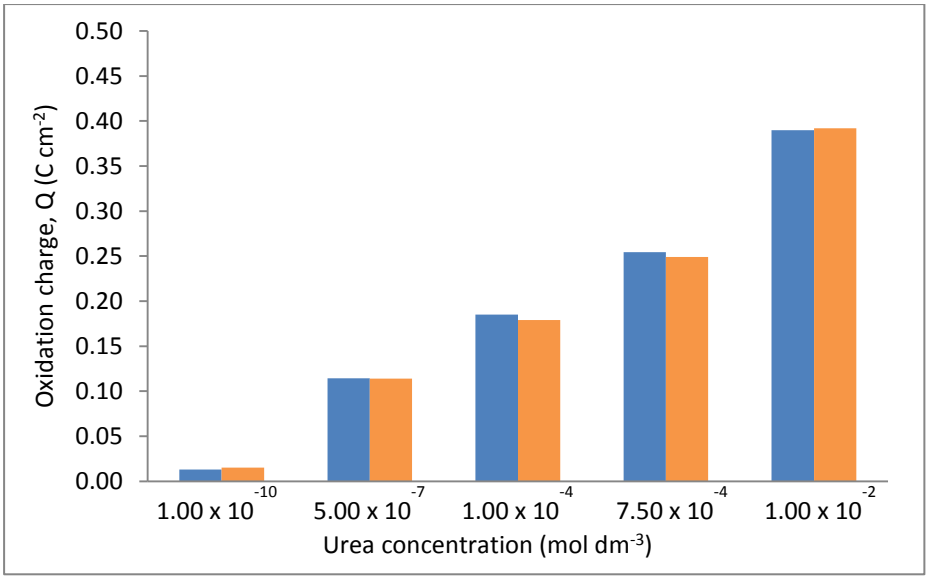

Figure 5.23: Charge plotted as a function of urea concentration in the absence and presence of 1.0 x 10^{-4} mol dm^{-3} NH_4Cl.

5.4 Conclusions

The PPy-Urs-SCD polymer film has proven to be successful in repelling the common interfering compound, ascorbic acid (AA), during the detection of urea, and is capable of detecting only urea in the presence of relatively high concentrations of AA, up to 1.0 x 10^{-4} mol dm^{-3}. It also successfully detects urea in the presence of 1.0 x 10^{-4} mol dm^{-3} NH_4Cl, without any interference or surface fouling. However, in the case of the other interfering compounds, an increase in the charge is observed in the presence of the interfering compounds. This is somewhat unusual as most interfering compounds tend to foul and block the surface of the electrode[23] and thus diminish the electrochemical signal from the target analyte.

This increase in charge was explained in terms of diffusion of the interfering species through the porous polymer film to the electrode surface and oxidation of the species at this surface. The interfering species are electroactive at the bare glassy carbon electrode and are relatively small, facilitating diffusion. This can be accounted for by the fact that the urease in the PPy-Urs-SCD film is a large, fibrous enzyme, while, the SCD is also large, to give a porous polymer network. Indeed, the SEM micrographs recorded for the PPy-Urs-SCD film show that this film is more porous than the PPy-SCD polymer film or, indeed, the PPy-Urs-Cl and PPy-Cl films,

Chapter 4. Interestingly, the interference from uric acid can be eliminated by increasing the thickness of the polymer film, clearly showing that the polymer thickness and porosity are important in the elimination of interfering species.

5.5 References

1 Y.-P. Chen, B. Liu, H.-T. Lian and X.-Y. Sun, *Electroanalysis*, **23**, (6), 1454, (2011)

2 A. J. Taylor and P. Vadgama, *Annals of Clinical Biochemistry*, **29**, 245, (1992)

3 L. Della Cianna and G. Capho, *Clinical Chemistry*, **42**, 1079, (1996)

4 G.-Z. Hu, D.-P. Zhang, W.-L. Wu and Z.-S. Yang, *Colloids and Surfaces B: Biointerfaces*, **62**, 199, (2008)

5 L. Zhang and X. Jiang, *Journal of Electroanalytical Chemistry*, **583**, 292, (2005)

6 G. Mihael and W. M. A. Damien, *Electrochimica Acta*, **49**, 4743, (2004)

7 J. Zheng and X. Zhou, *Bioelectrochemistry*, **70**, 408, (2007)

8 U. E. Majewska, K. Chmurski, K. Biesiada, A. R. Olszyna and R. Bilewicz, *Electroanalysis*, **18**, 1463, (2006)

9 X. Wang, H. Watanabe, N. Sekioka, H. Hamana and S. Uchiyama, *Electroanalysis*, **19**, 1300, (2007)

10 S. Yilmaz, M. Sadikoglu, G. Sadikoglu, S. Yagmur and G. Askin, *International Journal of Electrochemical Science*, **3**, 1534, (2008)

11 A. Amini, T. Rundlof, M. B. G. Rydberg and T. Arvidsson, *Journal of Separation Science*, **27**, 1102, (2004)

12 H. Zhao, Y. Zhang and Z. Yuan, *Analytica Chimica Acta*, **441**, 117, (2001)

13 S. Suematsu, Y. Oura, H. Tsujimoto, H. Kanno and K. Naoi, *Electrochimica Acta*, **45**, 3813, (2000)

14 A. A. Ensafi, M. Taei and T. Khayamian, *Journal of Electroanalytical Chemistry*, **633**, 212, (2009)

15 S. Thiagarajan and S.-M. Chen, *Talanta*, **74**, 212, (2007)

16 V. S. E. Dutt and H. A. Mottola, *Analytical Chemistry*, **46**, 1777, (1974)

17 E. Miland, A. J. M. Ordieres, P. T. Blanco, M. R. Smyth and C. O. Fagain, *Talanta*, **43**, 785, (1996)

18 V. Jimenez and J. B. Alderete, *Journal of Molecular Structure: THEOCHEM*, **755**, 209, (2005)

19 J. M. Zen and J. S. Tang, *Analytical Chemistry*, **67**, 1892, (1995)

20 L. Zhang and X. Lin, *Analyst*, **126**, 367, (2001)

21 J.-M. Zen, J.-J. Jou and G. Ilangovan, *Analyst*, **123**, 1345, (1998)

22 F. T. A. Chen, G. Shen and R. A. Evangelista, *Journal of Chromatography A*, **924**, 523, (2001)

23 R. Gifford, J. J. Kehoe, S. L. Barnes, B. A. Kornilayev, M. A. Alterman and G. S. Wilson, *Biomaterials*, **27**, 2587, (2006)

24 E. G. Ciapine, E. A. Carbonio, F. Colmati and E. R. Gonzalez, *Journal of Power Sources*, **175**, 18, (2008)

25 A. E. Bolzan, R. C. V. Piatti and A. J. Arvia, *Journal of Electroanalytical Chemistry*, **552**, 19, (2003)

26 T. Grownewald, *Journal of Applied Electrochemistry*, **5**, 71, (1975)

27 M. Quinet, F. Lallemand, L. Ricq, J.-Y. Hihn and P. Delobelle, *Surface and Coatings Technology*, **204**, 3108, (2010)

28 M. Jadrijevic-Mladar Takac, I. Kos, M. Birus, I. Butual and M. Gabricevic, *Journal of Molecular Structure*, **782**, 24, (2006)

29 W. F. C. Dressler and R. Stein, *Justus Liebigs Annalen der Chemie*, **150,** 242, (1869)

30 T. Kettani, F. Cotton, B. Gulbis, A. Ferster and A. Kumps, *Journal of Chromatography B*, **877**, 446, (2009)

31 S. Nussbaumer, P. Bonnabry, J.-L. Veuthey and S. Fleury-Souverain, *Talanta*, **85**, 2265, (2011)

32 F. H. Epstein, *The New England Journal of Medicine*, **337**, 762, (1997)

33 B. S. van Asbeck, N. A. Georgiou, T. van der Bruggen, M. Oudshoorn, H. S. L. M. Nottet and J. J. M. Marx, *Journal of Clinical Virology*, **20**, 141, (2001)

34 B. Khadro, C. Sanglar, A. Bonhomme, A. Errachid and N. Jaffrezic-Renault, *Procedia Engineering*, **5**, 371, (2010)

35 M. B. Madaras, I. C. Popescu, S. Ufer and R. P. Buck, *Analytica Chimica Acta*, **319**, 335, (1996)

36 G. F. Kahn and W. Wernet, *Analytica Chimica Acta*, **351**, 151, (1997)

37 T. N. Kumar, A. Ananthi, J. Mathiyarasu, J. Joseph, K. L. Pjani and V. Yegnaraman, *Journal of Electroanalytical Chemistry*, **661**, 303, (2011)

38 D. Laksmi, B. B. Prasad and P. S. Sharma, *Talanta*, **70**, 272, (2006)

39 D. A. Walsh and E. Dempsey, *Analytica Chimica Acta*, **459**, 187, (2002)

40 A. Radomska, R. Koncki, K. Pyrzynska and S. Glab, *Analytica Chimica Acta*, **523**, 193, (2004)

41 M. D. Guo and H. X. Guo, *Journal of Electroanalytical Chemistry*, **585**, 28, (2005)

42 K. M. Daniel and C. L. Cason, *The Journal for Nurse Practitioners*, (2007)

43 P. C. Pandey and A. P. Mishra, *Sensors and Actuators B*, **99**, 230, (2004)

44 S. Yadav, A. Kumar and C. S. Pundir, *Analytical Biochemistry*, **419**, 277, (2011)

45 J.-C. Chen, A. S. Kumar, H.-H. Chung, S.-H. Chien, M.-C. Kuo and J.-M. Zen, *Sensors and Actuators B*, **115**, 473, (2006)

Chapter 6

Complexation Studies

"I may not have gone where I intended to go, but I think I have ended up where I needed to be." - *Douglas Adams*

6.1 Introduction

It is evident from Chapter 4 that the PPy-Urs-SCD polymer gives the best sensitivity towards the electrochemical sensing of urea, with detection in the 1.0 x 10^{-10} mol dm^{-3} region, whereas the PPy-Urs-Cl polymer film has a limit of detection of 1.0 x 10^{-5} mol dm^{-3}. Obviously, the presence of the urease enzyme enhances the detection of urea. However, the SCD has an equally important role to play in enhancing the detection of urea.

Cyclodextrins are well known to act as hosts for a variety of guest molecules[1], as described in Chapter 1, Section 1.4.3. These guest molecules can be organic, inorganic or ionic; once they enter the cavity they can form non-covalent host-guest inclusion complexes[2,3]. This inclusion complexation depends on many factors including, but not limited to, the charge on the host and guest molecules and the size of the internal cavity of the host molecule. Upon the formation of host-guest inclusion complexes, the electronic and redox properties of both the host and the guest molecules may change. This allows the study of the host-guest interactions both spectroscopically and electrochemically[4,5,6].

This chapter is primarily concerned with an investigation into the formation of inclusion complexes between urea and the sulphonated-β-cyclodextrin (SCD). Additionally, an investigation into the formation of inclusion complexes between urea and the sulphonated-α-cyclodextrin, α-SCD, was carried out as a comparison. Finally, the inclusion complexation between the sulphonated-β-cyclodextrin and each of the interfering compounds, that were described in Chapter 5, was studied.

The complexation was investigated using cyclic voltammetry[7]. The binding stoichiometry was determined by a continuous variation method or Job's method[8] using voltammetry and this was also employed to evaluate the stability constant of the urea-SCD complex.

6.2 Experimental

The instrumentation and software employed for the experiments detailed in this chapter and their analyses are described in Chapter 2, Section 2.3. The chemicals used throughout this study were purchased from Sigma-Aldrich or its subsidiary company Fluka. All the solutions were made from a stock solution of 0.30 mol dm^{-3} NaCl in a 0.05 mol dm^{-3} phosphate buffer, pH 7.0, which was initially prepared using distilled water. The NaCl was added to the 0.05 mol dm^{-3} phosphate buffer in order to raise the conductivity of the solution, as the SCD has a very high conductivity of 21.40 mS, at room temperature, and an ionic strength of 2.25 mol dm^{-3} for a 0.05 mol dm^{-3} concentration. All the solutions were prepared freshly before each experiment. All experiments were performed at room temperature on a freshly polished glassy carbon (GC) electrode with a surface area of 0.125 cm^2. Cyclic voltammetry was chosen as the analytical technique to probe the complexation. The voltammograms were recorded at different scan rates, ranging from 300 to 5 mV s^{-1} and in solutions with increasing concentrations of sulphonated-β-cyclodextrin, SCD. Jobs plots were constructed using the voltammetry approach by recording the current measured at a fixed potential in solutions with different mole fractions of the sulphonated-β-cyclodextrin, SCD, and the guest molecule. Each experiment was performed a minimum of six times (n = 6) and the average was obtained. It is this average that is presented and discussed in Section 6.3.

6.3 Results and Discussion

The compounds investigated in this chapter were described in detail in Chapter 5 and include urea, ascorbic acid (AA), uric acid (UA), hydroxyurea (HU), thiourea (TU), and creatinine (CR). Results are presented and discussed on the possible interactions between each of these species, as guests, and the sulphonated-β-cyclodextrin, SCD, as the host. The data were recorded at a pH of 7.0, and at this pH the AA and UA exist predominantly as the anionic species. Additionally, an investigation into the formation of inclusion complexes between urea and the sulphonated-α-cyclodextrin, α-SCD, was carried out to determine if the size of the cavity influenced the formation of the inclusion complex.

6.3.1 Urea

6.3.1.1 Urea with SCD

Cyclic voltammetry is a technique that is commonly employed to investigate the interactions between a host and guest molecule, as long as either the host or guest is electroactive[9,10]. The electroactivity of urea is described in detail in Chapter 5, Section 5.3.1, where there is evidence for the oxidation of urea at the glassy carbon electrode[11]. This is shown again in Figure 6.1, where the cyclic voltammograms were recorded in the phosphate buffer solution in the absence and presence of 1.0 x 10^{-2} mol dm^{-3} urea. It is clearly evident that the oxidation of urea occurs over a very broad potential range and no significant oxidation or reduction peaks are observed. Although the peak oxidation or peak reduction currents cannot be plotted, the currents at a fixed potential may be recorded for the anodic and cathodic processes. The currents were obtained for both the anodic and cathodic reactions of 5.0 x 10^{-4} mol dm^{-3} urea in a pH 7.0 NaCl-phosphate buffer solution, at 0.30 V vs. SCE and, as shown in Figure 6.2, the currents are directly proportional to the square root of the scan rate.

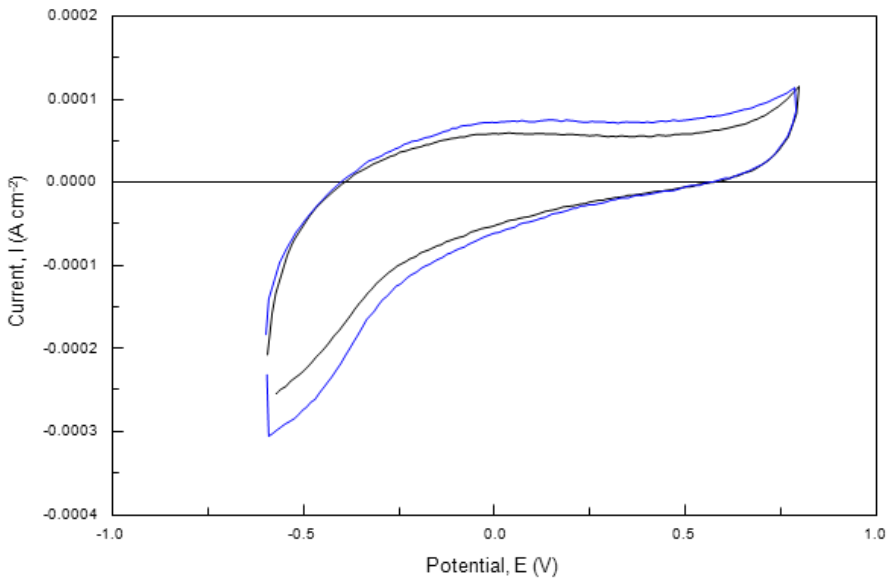

Figure 6.1: Cyclic voltammograms obtained by cycling a bare glassy carbon electrode in ▬ pH 7.0 phosphate buffer solution and ▬ 1.0 x 10^{-2} mol dm^{-3} urea made in a pH 7.0 phosphate buffer solution.

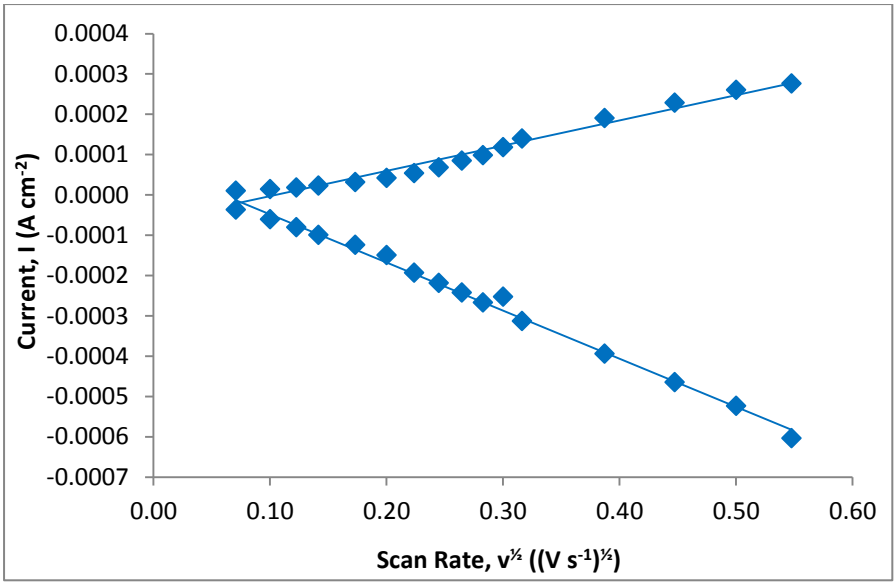

Figure 6.2: Plot of the currents recorded at 0.30 V vs. SCE as a function of the square root of the scan rate on a GC disc electrode in a NaCl-phosphate buffer solution, pH 7.0, for 5.0 x 10^{-4} mol dm^{-3} urea.

Very good linearity was achieved and R^2 values of 0.970 and 0.993 were obtained for the anodic and cathodic currents, respectively. Figure 6.2 shows that the reaction is diffusion controlled. This is significant as it has been reported in the literature that voltammetric methods, such as cyclic voltammetry and rotating disc voltammetry, are only suitable in the analysis of inclusion complexes if the guest is electroactive and under diffusion control[12]. Consequently, this electrochemical approach is ideal for probing the complexation between urea and the SCD[13]. Moreover, as the SCD is not electroactive, only the electrochemistry of the urea will be observed.

The stoichiometry of the urea and the SCD complex was investigated using the Job's plot or continuous variation method[14,15,16]. To carry this out, 0.01 mol dm^{-3} stock solutions of urea and SCD were made up in the NaCl-phosphate buffer and mixed together in different ratios in order to keep the total concentration constant while varying the mole fractions of urea from 0.0 to 1.0 in increments of 0.1. The volumes of each stock solution and mole fractions of urea employed for the Job's method are given in Table 6.1. In Figure 6.3 the cyclic voltammograms recorded in these solutions are presented. It can be seen that the currents increase with increasing mole fractions of urea. For example, the current recorded at a fixed potential of 0.30 V vs. SCE for the solution with a 0.10 mole fraction of urea is 2.96 x 10^{-5} A cm^{-2}, whereas this is increased to 3.42 x 10^{-5} A cm^{-2} at a mole fraction of 1.0.

Table 6.1: Volumes of the SCD and urea stock solutions and mole fractions of urea used for the Job's plot measurements, where the total volume is 10.0 mL.

Solution number	Volume of SCD (mL)	Volume of urea (mL)	Mole fraction of urea
1	10.0	0.0	0.0
2	9.0	1.0	0.1
3	8.0	2.0	0.2
4	7.0	3.0	0.3
5	6.0	4.0	0.4
6	5.0	5.0	0.5
7	4.0	6.0	0.6
8	3.0	7.0	0.7
9	2.0	8.0	0.8
10	1.0	9.0	0.9
11	0.0	10.0	1.0

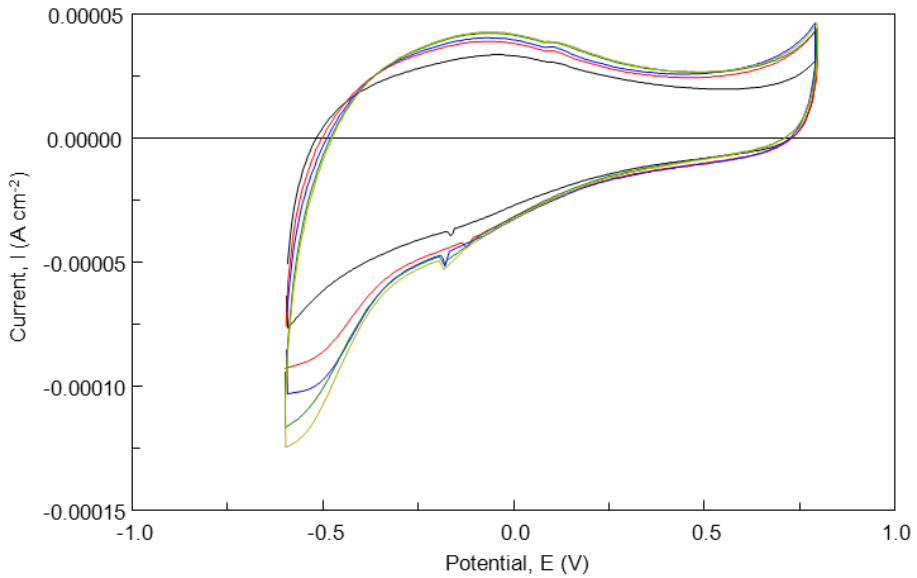

Figure 6.3: Cyclic voltammograms recorded at GC in the presence of urea and SCD in a NaCl-phosphate buffer solution, pH 7.0, for mole fractions of urea from 0.1 to 1.0 in increments of 0.1. Currents increase with increasing mole fraction.

To generate the Job's plot curve from the cyclic voltammograms, the currents recorded at a fixed potential were monitored and used to compute □*i* values, as shown in Equation 6.1[7].

$$\Delta i = i_0 - i_x \qquad 6.1$$

Here i_0 and i_x are the currents obtained at 0.30 V vs. SCE for urea in the absence and presence of SCD, respectively. These Δi values were then multiplied by the corresponding mole fraction (Δi*mole fraction) and the product was plotted as a function of the mole fraction of urea. Figure 6.4 shows the resulting Job's plot generated from the data presented in Figure 6.3. The Job's plot has the characteristic shape and reaches a maximum value at a mole fraction of 0.50. This provides evidence for the formation of an inclusion complex between the urea and the SCD with a 1:1 stoichiometry[17].

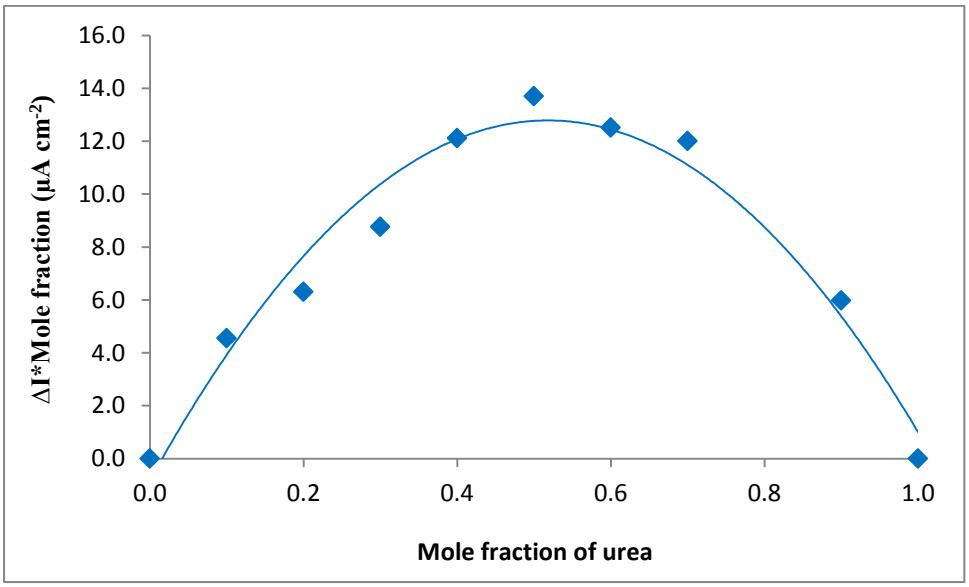

Figure 6.4: Job's plot curve where the change in the currents recorded at 0.30 V vs. SCE are plotted as a function of the mole fraction of urea in a urea and SCD solution in a NaCl-phosphate buffer, at a pH of 7.0.

In order to further investigate the formation of an inclusion complex between urea and the SCD, cyclic voltammograms were recorded at varying scan rates for 5.0 x 10^{-4} mol dm^{-3} urea in the absence and presence of 2.0 x 10^{-2} mol dm^{-3} SCD in the buffer solution. The currents recorded at 0.30 V vs. SCE were plotted as a function of the square root of the scan rate, and the resulting plots are presented in Figure 6.5. Again, these plots show very good linearity with correlation coefficients of 0.988 and 0.970 for urea in the absence and presence of SCD, respectively, for the anodic currents. The diffusion coefficients were evaluated from the slopes of these plots using the Randles-Sevcik equation, Equation 6.2.

$$I = k\, n^{3\ 2} D^{1\ 2}\, c\, v^{1\ 2} \qquad 6.2$$

Here, k has a value of 2.69 x 10^5, I represents the current density recorded at a fixed potential of 0.30 V vs. SCE, c is the concentration of urea in mol cm^{-3} and v is the scan rate in V s^{-1}. It is clear from this equation that I is directly proportional to both the bulk concentration, c, of the electroactive species and the square root of the scan rate, $v^{1\ 2}$.

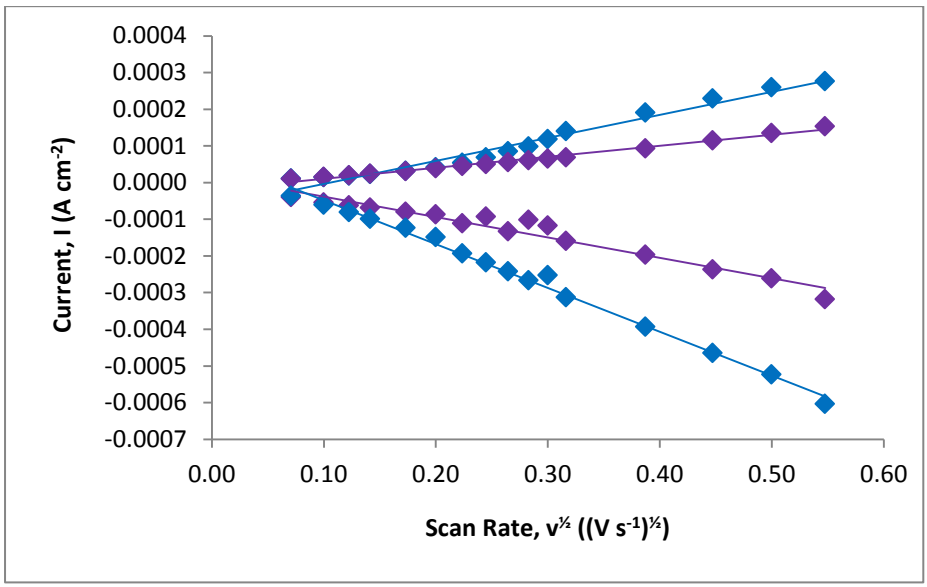

Figure 6.5: Plot of the current, I, recorded at 0.30 V vs. SCE as a function of $v^{1/2}$ on a GC disc electrode in a NaCl-phosphate buffer solution, pH 7.0, for 5.0 x 10^{-4} mol dm^{-3} urea in the — absence and — presence of 2.0 x 10^{-2} mol dm^{-3} SCD.

From the linear relationships observed in Figure 6.5, it can be seen that the slopes of the linear plots are very different in the presence and absence of the SCD. Although the anionic cyclodextrin may give rise to an increase in the viscosity of the solution, according to the literature, no significant change in the cyclodextrin viscosity is detected for concentrations up to 1.0 x 10^{-2} mol dm^{-3} SCD[18,19]. Therefore, these data are consistent with a decrease in the diffusion coefficient of urea in the presence of the SCD. This decrease can be attributed to the formation of an inclusion complex between urea and the SCD. The sulphonated cyclodextrin is very large and bulky compared to urea and this will influence the diffusion of urea when urea is confined within the cavity of the cyclodextrin. Indeed, it has been clearly shown that the diffusion coefficient of a guest molecule is reduced when included inside the cavity of a cyclodextrin[18].

The diffusion coefficients of urea were calculated for the oxidation of urea using an *n* value of 2[20] in the absence and presence of SCD using the Randles-Sevcik equation, Equation 6.2. These data are shown in Table 6.2, and are in reasonably good agreement with the values of 3.70 to 8.30 x 10^{-6} cm^2 s^{-1} reported in the literature[21,22,23].

Table 6.2: The diffusion coefficients obtained for the oxidation of urea in the absence and presence of SCD using the Randles-Sevcik equation.

	Slope (A cm^{-2} $V^{-1/2}s^{1/2}$)	**Diffusion coefficient (cm^2 s^{-1})**
Urea	6.27 x 10^{-4}	2.72 x 10^{-6}
Urea + SCD	3.02 x 10^{-4}	6.30 x 10^{-7}

Further evidence to support the formation of an inclusion complex was obtained by adding an excess concentration of the SCD to the urea-containing solution. Figure 6.6 shows the cyclic voltammograms recorded for 1.0 x 10^{-4} mol dm^{-3} urea in the presence of increasing concentrations of SCD, up to a large excess of 2.0 x 10^{-2} mol dm^{-3}. There is a considerable reduction in the current with increasing concentrations of the SCD, and this effect is more clearly shown in Figure 6.7. These data indicate that the urea is more difficult to oxidise in the presence of the SCD, and again this

points to the formation of an inclusion complex. In particular, the significant decrease in the recorded currents is consistent with the change in the diffusion coefficient of urea, where a lower diffusion coefficient is obtained when a guest in included within the host cavity[18,24].

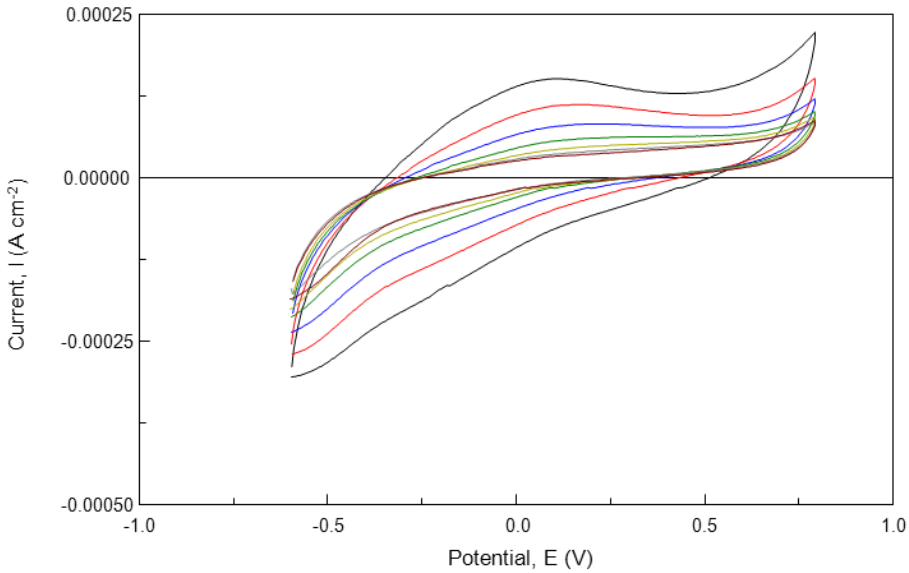

Figure 6.6: Cyclic voltammograms recorded for 1.0 x 10^{-4} mol dm^{-3} urea in the ▬ absence and presence of increasing concentrations of SCD: ▬ 1.0 x 10^{-4}, ▬ 5.0 x 10^{-4}, ▬ 1.0 x 10^{-3}, ▬ 5.0 x 10^{-3}, ▬ 1.0 x 10^{-2} and ▬ 2.0 x 10^{-2} mol dm^{-3}.

The current recorded at a fixed potential of 0.30 V vs. SCE is plotted as a function of the SCD concentration in Figure 6.7. Again, there is a significant decay in the current as the concentration of the SCD is initially increased. Then the current reaches a near constant value when a large excess of the SCD is added to the solution. A similar trend was observed for the current recorded at potentials ranging from -0.25 to 0.80 V vs. SCE. Again this is consistent with the formation of an inclusion complex and indicates that the urea is included within the cavity when an excess of the SCD is present in the solution.

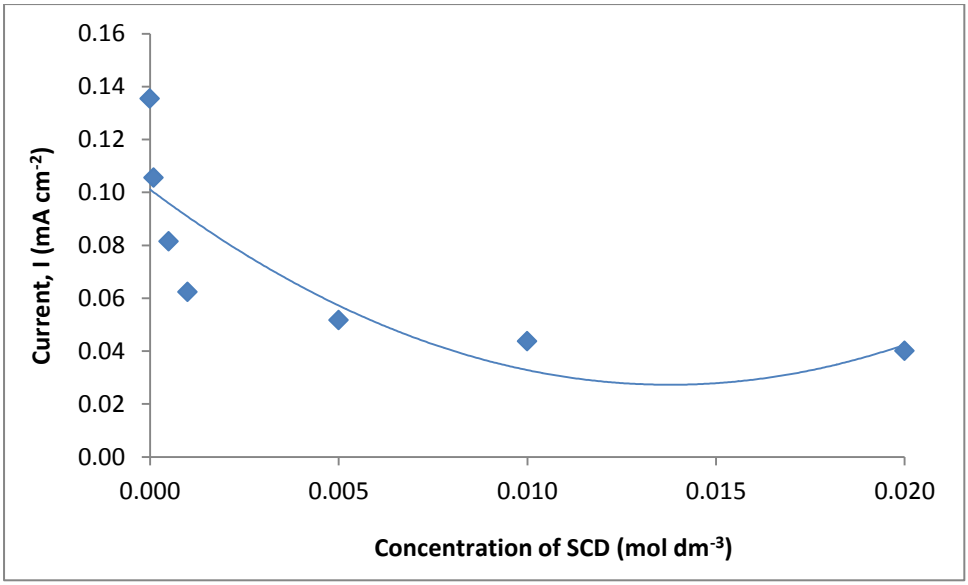

Figure 6.7: Oxidation current for urea, recorded at 0.30 V vs. SCE, as a function of the SCD concentration.

The K_f value for the inclusion complex was calculated from the cyclic voltammetry data using Equation 6.3.

$$\frac{1}{[SCD]} = K_f \frac{(1-A)}{1-\frac{i}{i_0}} - K_f \qquad 6.3$$

Here, i_o represents the current obtained in the absence of the SCD, i represents the currents recorded in the presence of the SCD, [SCD] is the concentration of the SCD, and K_f corresponds to the stability constant for the inclusion complex. A linear plot, with an R^2 value of 0.986, was obtained when the inverse of the SCD concentration was plotted as a function of $1/(1-i/i_o)$, as shown in Figure 6.8. This linear relationship not only confirms the existence of a 1:1 inclusion complex but can also be used to calculate the stability constant[8,25]. Accordingly, the K_f value for the inclusion complex was calculated as 2745.27 ± 299.56 mol^{-1} dm^3. This is quite high compared to stability constants ranging from 250 to 350 as found in the literature for inclusion complexes formed between β-cyclodextrins and other guest molecules[5].

It is clear from the data presented in Figures 6.4, 6.5, 6.6, 6.7 and 6.8 and the diffusion coefficients provided in Table 6.2 that an inclusion complex is indeed formed between the urea and the SCD.

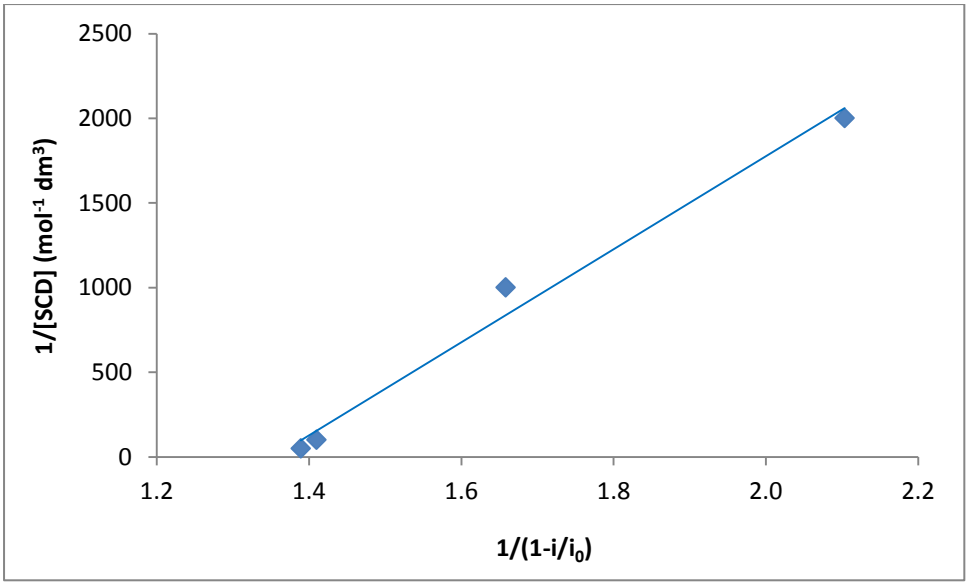

Figure 6.8: Plot of 1/[SCD] as a function of $1/(1-i/i_0)$, for the evaluation of the stability constant, K_f, for urea in a NaCl-phosphate buffer solution at pH 7.0.

6.3.1.2 Urea with α-SCD

It is clear from Section 6.3.1.1 that an inclusion complex is indeed formed between urea and the sulphonated-β-cyclodextrin, SCD. In order to investigate the effects of cavity size on the formation of this inclusion complex, the sulphonated-α-cyclodextrin was used instead of the sulphonated-β-cyclodextrin as this has a much smaller diameter[26,27]. Cyclic voltammograms were obtained for 1.0 x 10^{-4} mol dm^{-3} urea in the absence and presence of increasing concentrations of α-SCD ranging from 1.0 x 10^{-4} to 2.0 x 10^{-2} mol dm^{-3}. The resulting cyclic voltammograms are given in Figure 6.9 and a plot of the oxidation current, recorded at a fixed potential of 0.30 vs. SCE, plotted as a function of the α-SCD concentration is presented in Figure 6.10. It is clearly evident from Figures 6.9 and 6.10 that the increasing α-SCD concentrations do not have a significant effect on the oxidation current recorded at a fixed potential for urea. This is very different to the corresponding data recorded with the sulphonated-β-cyclodextrin, SCD, Figures 6.6 and 6.7. These data presented for the α-SCD indicate little or no interaction between the α-SCD and the urea[28,29]. Indeed, the measured current increases slightly as the concentration of the α-SCD is increased. In order to verify this further, a Job's plot analysis was carried out with increasing mole fractions of urea in α-SCD. The characteristic curve, which

is evident in Figure 6.4, was not obtained. Instead, there was no obvious relationship between the Δi and the mole fractions of urea. This analysis, although not shown here, provides further evidence that an inclusion complex is not formed between urea and the smaller α-SCD.

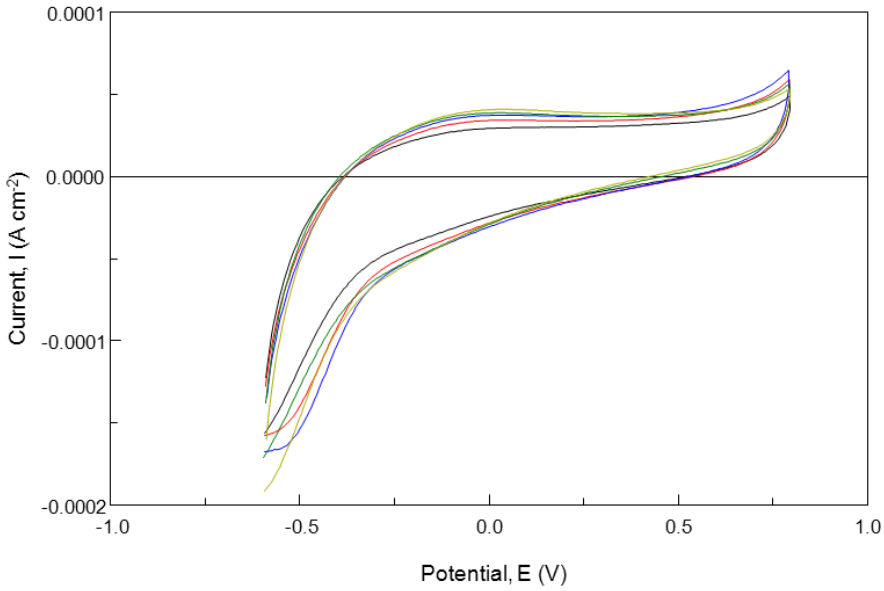

Figure 6.9: Cyclic voltammograms recorded for 1.0 x 10^{-4} mol dm^{-3} urea in the ▬ absence and presence of increasing concentrations of α-SCD: ▬ 1.0 x 10^{-4}, ▬ 1.0 x 10^{-3}, ▬ 1.0 x 10^{-2} and ▬ 2.0 x 10^{-2} mol dm^{-3}.

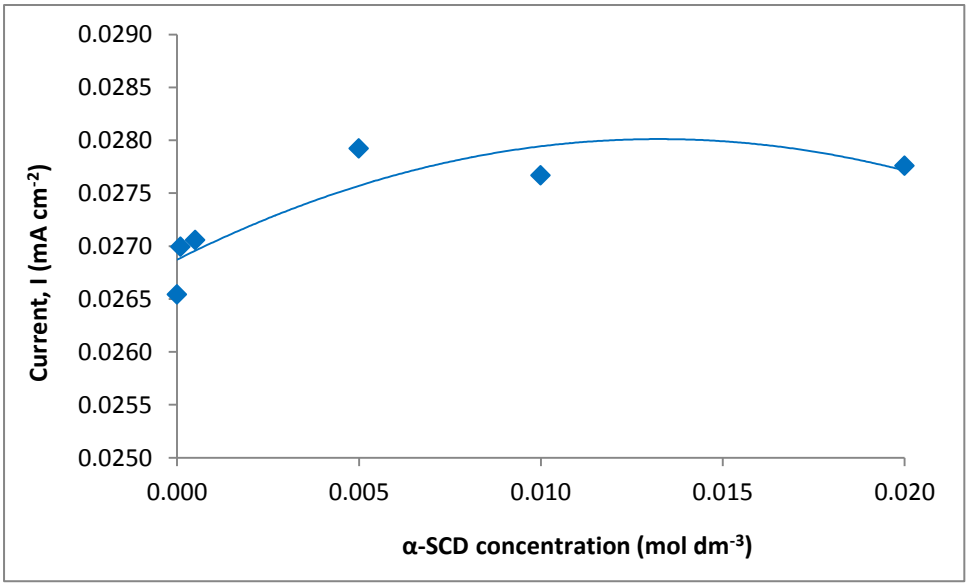

Figure 6.10: Oxidation current recorded for urea, at 0.30 V vs. SCE, in the presence of increasing concentrations of α-SCD.

The diameter of urea was calculated in order to investigate if it would structurally be able to fit inside the cavity of the α-SCD, as the α-CD has a cavity diameter of only 4.70 Å compared to 6.00 Å for the β-CD[25,30]. The diameter was calculated using density functional theory (DFT), which is a quantum mechanical calculation. This considers the electron density at a point and thus optimises the geometry from which the diameter can be calculated. An illustration of the geometry of urea is shown in Figure 6.11[31]. The diameter between the two furthest points on the urea molecule was calculated as 4.03 Å. This is illustrated in Figure 6.11. Theoretically, as the diameter of the urea is smaller than that recorded for the cavity of α-CD, the urea should fit inside the cavity of the α-SCD.

However, the diameter of the urea is quite close to the diameter of the cavity of the α-SCD. In addition, this diameter is recorded for the neutral α-CD so there is the possibility that the sulphonated groups on the rim of the α-SCD are orientated in such a way that the diameter of the α-SCD is smaller than 4.70 Å. As a result, the urea molecule may not be able to fit inside the cavity of the α-SCD. This seems to be a reasonable explanation for the lack of any inclusion complex between urea and the α-SCD.

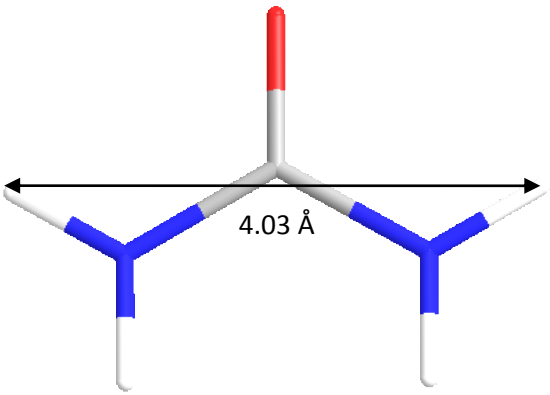

Figure 6.11: Illustration of the urea molecule and the intramolecular distance between its two furthest points.

6.3.2 Ascorbic Acid

The same analysis was applied using ascorbic acid (AA) as the potential guest molecule. Cyclic voltammograms were recorded for a 1.0 x 10^{-4} mol dm^{-3} ascorbic acid solution in the absence and presence of increasing concentrations of SCD, ranging from 1.0 x 10^{-4} to 2.0 x 10^{-2} mol dm^{-3}. Again, the NaCl-phosphate buffer solution was employed and under these conditions the AA exists as the anionic species, as shown in Section 5.3.1, Chapter 5. The current was recorded at 0.30 V vs. SCE and this current is plotted as a function of the SCD concentration in Figure 6.12.

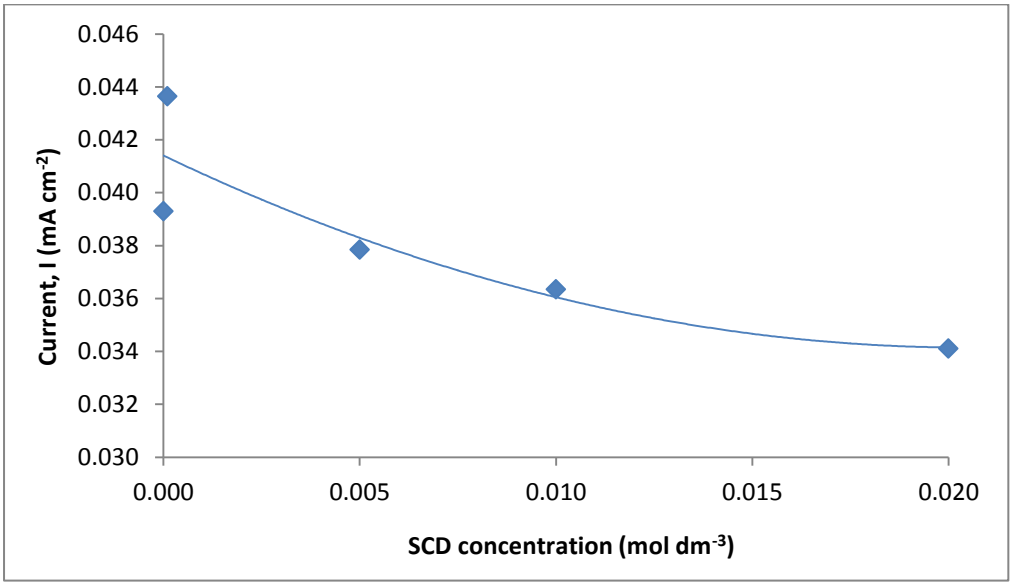

Figure 6.12 Oxidation current for AA, recorded at 0.30 V vs. SCE, as a function of the SCD concentration.

It is evident from Figure 6.12 that the increasing SCD concentration has little or no effect on the currents obtained for ascorbic acid at a fixed potential of 0.30 V vs. SCE. This indicates that there is no complexation occurring between the AA and SCD.

This is not surprising as ascorbic acid is anionic at the pH of this experiment, pH 7.0 and, as such, it should repel the highly anionic SCD because of the presence of the negatively charged sulphonated groups. This is in good agreement with Harley[32], who found that no inclusion complex was formed between AA and the SCD. To the best of our knowledge, there are no further reports on the formation of an inclusion complex between AA and SCD. However, there have been reports of an inclusion

complex between AA and the neutral-β-cyclodextrin, β-CD. For example, Manzanares *et al.*[33] found that there was an inclusion complex formed between the β-CD and both the neutral and negatively charged AA, with the anionic AA having less affinity for the β-CD. However, this is in contrast to the findings of Terekhova *et al.*[34], who observed no inclusion complex between the β-CD and AA, despite the fact that the interaction of β-CD is favourable from an enthalpy point of view[35].

6.3.3 Uric Acid

A similar analysis was carried out with uric acid (UA) as the potential guest molecule. Again, cyclic voltammograms were recorded in solutions containing 1.0 x 10^{-4} mol dm^{-3} uric acid and increasing concentrations of SCD, ranging from 1.0 x 10^{-4} to 2.0 x 10^{-2} mol dm^{-3}. The resulting plot of the oxidation current, recorded at a fixed potential of 0.30 V vs. SCE, plotted as a function of the SCD concentration is presented in Figure 6.13.

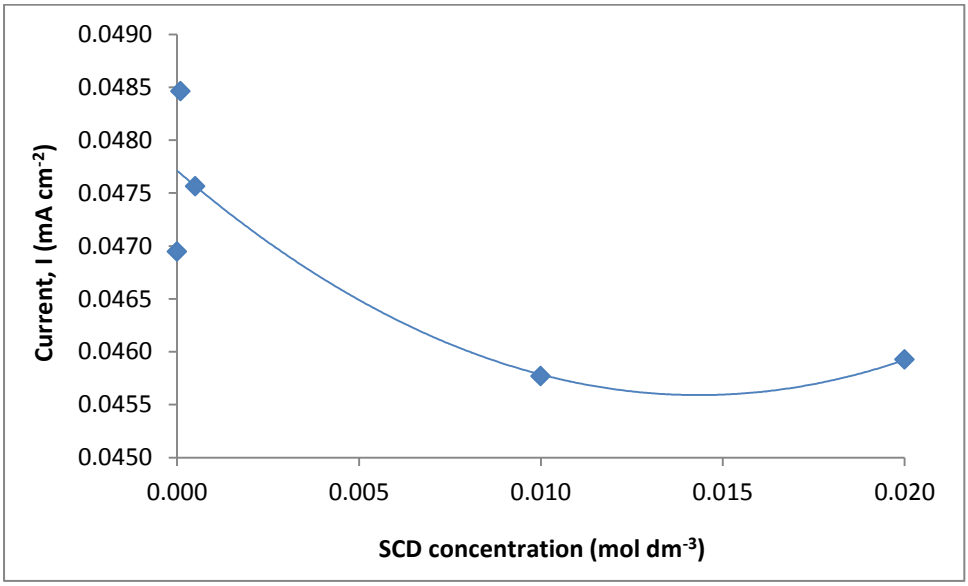

Figure 6.13: Oxidation current for UA, recorded at 0.30 V vs. SCE, as a function of the concentration of SCD.

It is clear from Figure 6.13 that the increasing SCD concentrations have little effect on the measured currents for uric acid. This is consistent with the ascorbic acid system. At the pH of the experiment, the uric acid is essentially anionic (almost 100 % anionic at a pH of 7.0) as shown in Section 5.3.2, Chapter 5 and it will be repelled from the anionic SCD. A Job's plot was carried out with increasing mole fractions of uric acid in the presence of the SCD in order to verify that no inclusion complex is formed. As expected, the characteristic curve, indicating the formation of an inclusion complex, was not obtained. Although the data are not shown here, this study provides additional evidence that an inclusion complex between uric acid and the SCD is not formed.

To the best of our knowledge, there have been no reports on the formation of an inclusion complex between uric acid and SCD. However, there are reports in the literature which show the formation of inclusion complexes between uric acid and the neutral-β-cyclodextrin, β-CD[36,37,38]. Ramirez-Berriozabal *et al.*[36] found that the selective detection of uric acid was improved by the formation of an inclusion complex between uric acid and β-CD, which is in agreement with Wu and co-workers[38] who found that a 250-fold excess of ascorbic acid did not interfere with the determination of uric acid.

6.3.4 Hydroxyurea

Similar experiments were carried out with hydroxyurea as a potential guest molecule. A 1.0 x 10^{-4} mol dm^{-3} concentration of hydroxyurea was prepared in the NaCl-phosphate buffer solution and cyclic voltammograms were recorded in the absence and presence of SCD. The SCD concentration was varied from 1.0 x 10^{-4} to 2.0 x 10^{-2} mol dm^{-3} to give solutions with a large excess of the SCD. The current measured at a fixed potential of 0.30 V vs. SCE was then plotted as a function of the SCD concentration and the resulting plot is given in Figure 6.14.

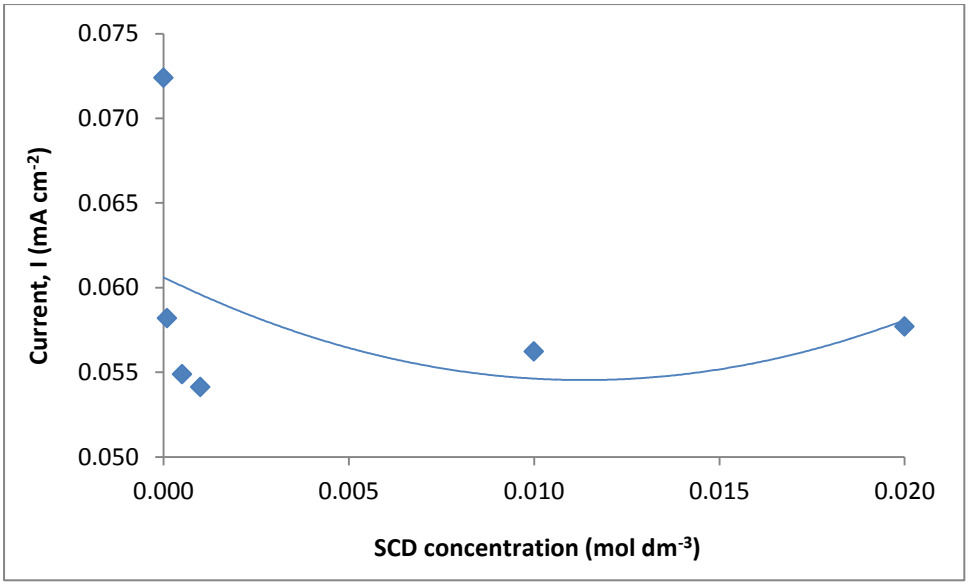

Figure 6.14: Oxidation current for HU, recorded at 0.30 V vs. SCE, plotted as a function of the SCD concentration.

Again, it is clearly evident from Figure 6.14 that the currents are essentially independent of the SCD concentration. This is very different to the data presented in Figure 6.7 for the urea system, and provides direct evidence that an inclusion complex is not formed between hydroxyurea and the SCD. To the best of our knowledge, there are no literature reports that propose the formation of an inclusion complex between hydroxyurea and cyclodextrins. However, cyclodextrins have previously been applied as sensor ionophores for potentiometric ion-selective electrodes for the determination of hydroxyurea[39].

6.3.5 Thiourea

Thiourea was also considered as a potential guest molecule. Again, cyclic voltammograms of 1.0 x 10^{-4} mol dm^{-3} thiourea in the absence and presence of increasing concentrations of SCD were obtained. The resulting plot of the oxidation current recorded at a fixed potential of 0.30 V vs. SCE as a function of the increasing SCD concentration is given in Figure 6.15.

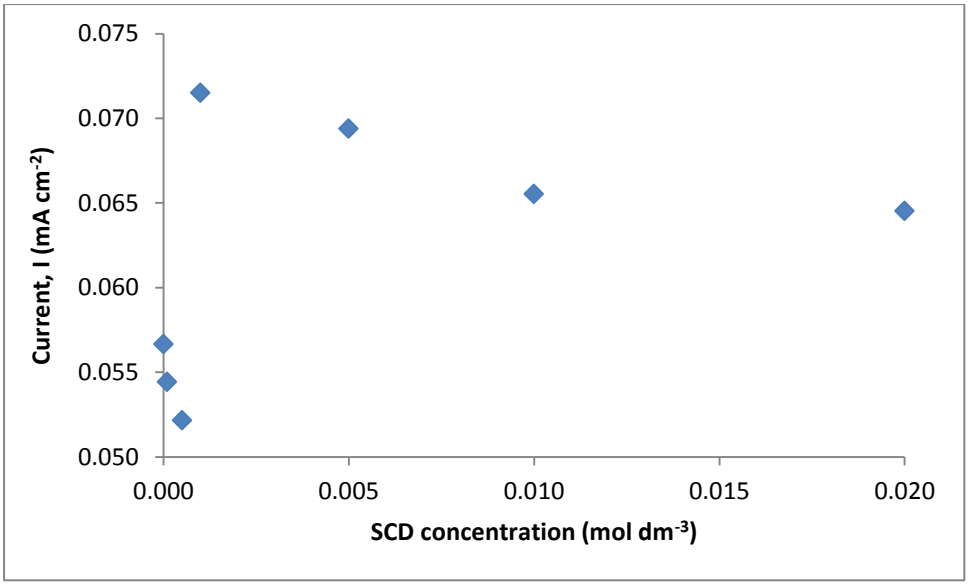

Figure 6.15: Oxidation current for TU recorded at 0.30 V vs. SCE as a function of the SCD concentration.

As evident from Figure 6.15, the currents have little or no relationship with the SCD concentration. There is an initial drop in the current, but then with increasing concentrations of the SCD the current increases, indicating higher currents when the SCD concentration is in excess. Again, there is no evidence to support the formation of an inclusion complex between thiourea and the SCD. Indeed, the Job's plot analysis confirmed that an inclusion complex was not formed.

There are no reports in the literature on the formation of inclusion complexes between thiourea and SCD, or indeed between thiourea and the neutral β-cyclodextrin. However, an inclusion complex has been reported between sym-diphenyl-thiourea and neutral β-CD, where the phenyl groups form a 2:1 inclusion complex within the β-CD cavity[40]. Additionally, β-CD has been used as a catalyst for the asymmetric Michael addition of thiourea and other thiol groups to chalcones[41].

6.3.6 Creatinine

Finally, the potential interactions between creatinine and the SCD were studied. Similar experiments were carried out with a 1.0 x 10^{-4} mol dm^{-3} solution of creatinine and increasing concentrations of SCD, ranging from 1.0 x 10^{-4} to 2.0 x

10^{-2} mol dm^{-3}. Cyclic voltammograms were recorded and the resulting plot of the oxidation current recorded at 0.30 V vs. SCE as a function of the increasing SCD concentration is given in Figure 6.16. Again, there is no significant change in the current with the increasing SCD concentrations. Hence, it can be concluded that an inclusion complex is not formed between the SCD and the creatinine molecule.

There has been some evidence in the literature to support a weak binding between creatinine and β-cyclodextrins. This is thought to arise via non-covalent interactions between the amide hydrogen of the creatinine molecule and the glucopyranose oxygen atom in the β-cyclodextrin[42]. Additionally, β-cyclodextrins have been used for the specific binding of creatinine over creatine as shown by Tsai and Syu[43] and, as with the hydroxyurea, they have been used as ionophores for the detection of creatinine[44]. However, none of these studies show direct evidence to support the formation of an inclusion complex between creatinine and the cyclodextrin and, to the best of our knowledge, there is no evidence of complexation between the sulphonated-β-cyclodextrin, SCD, and these molecules.

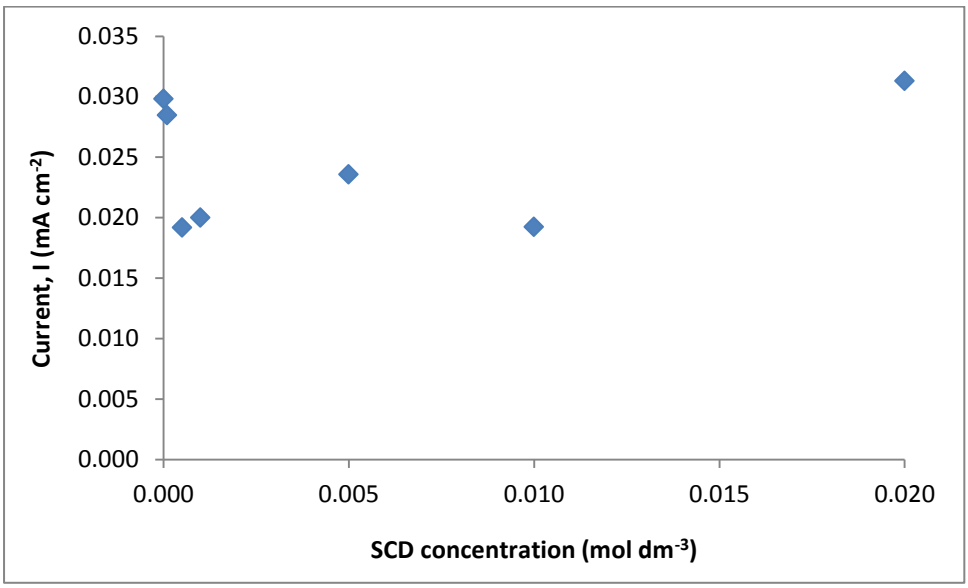

Figure 6.16: Oxidation current for CR, recorded at 0.30 V vs. SCE, as a function of the SCD concentration.

6.4 Conclusions

It has been clearly shown that the sulphonated-β-cyclodextrin, SCD, forms a 1:1 inclusion complex with urea. However, the sulphonated-α-cyclodextrin does not form inclusion complexes with urea. This indicates that the diameter of the cyclodextrin cavity is important in determining what guest molecules can interact with the cyclodextrin to form inclusion complexes. In addition, an investigation into the formation of inclusion complexes between the sulphonated-β-cyclodextrin and the interfering compounds was carried out. Job's plot analyses was done for increasing mole fractions of each of the interfering compounds in the presence of SCD; however, none of the interfering compounds appear to form inclusion complexes with the SCD.

6.5 References

1 T. Loftsson and D. Duchene, *International Journal of Pharmaceutics*, **329**, 1, (2007)

2 K. L. Larsen and W. Zimmermann, *Journal of Chromatography A*, **836**, 3, (1999)

3 J. M. Lehn, *Angewandte Chemie-International Edition in English*, **27**, 89, (1988)

4 A. Bernini, O. Spiga, A. Ciutti, M. Scarselli, G. Bottoni, P. Mascagni and N. Niccolai, *European Journal of Pharmaceutical Sciences*, **22**, 445, (2004)

5 X.-J. Dang, M.-Y. Nie, J. Tong and H.-L. Li, *Journal of Electroanalytical Chemistry*, **448**, 61, (1998)

6 J.-F. Bergamini, M. Belabbas, M. Jouini, S. Aeiyach, J.-C. Lacroix, K. I. Chane-Ching and P.-C. Lacaze, *Journal of Electroanalytical Chemistry*, **482**, 156, (2000)

7 G.-C. Zhao, J.-J. Zhu, J.-J. Zhang and H.-Y. Chen, *Analytica Chimica Acta*, **394**, 337, (1999)

8 J. Szejtli, *Chemical Reviews*, **98**, 1743, (1998)

9 H. Dodziuk, *Cyclodextrins and their Complexes: Chemistry, Analytical Methods, Applications*, Wiley-VCH, 489, (2006)

10 M. S. Ibrahim, I. S. Shehatta and A. A. Al-Nayeli, *Journal of Pharmaceutical and Biomedical Analysis*, **28**, 217, (2002)

11 X. Wang, H. Watanabe, N. Sekioka, H. Hamana and S. Uchiyama, *Electroanalysis*, **19**, 1300, (2007)

12 P. M. Bersier, J. Bersier and B. Klingert, *Electroanalytical Chemistry*, **3**, 443, (1991)

13 C. Yanez, L. J. Nunez-Vergara and J. A. Squella, *Electroanalytical Chemistry*, **15**, 1771, (2003)

14 A. Dimitrovska, B. Andonovski and K. Stojanoski, *International Journal of Pharmaceutics*, **134**, 213, (1996)

15 C. Y. Huang, R. X. Zhou, D. C. H. Yang and P. B. Chock, *Biophysical Chemistry*, **100**, 143, (2003)

16 A. Sayago, M. Boccio and A. G. Asuero, *International Journal of Pharmaceutics*, **295**, 29, (2005)

17 S. Letellier, B. Maupas, J. P. Gramond, F. Guyon and P. Gareil, *Analytica Chimica Acta*, **315**, 357, (1995)

18 T. Matsue, D. H. Evans, T. Osa and N. Kobayashi, *Journal of the American Chemical Society*, **107**, 3411, (1985)

19 Z. N. Gao, X. L. Wen and H. L. Li, *Polish Journal of Chemistry*, **76**, 1001, (2002)

20 Q. G. Nehring, J. W. Hightower and J. L. Anderson, *Journal of Analytical Chemistry*, **58**, 2777, (1986)

21 H. Demircigolu, H. Beyenal, A. Tanyolac and N. Hasirci, *Polymer*, **23**, (21), 4091, (1995)

22 H. Miyama, T. Kobayashi and Y. Nosaka, *Biotechnology and Bioengineering*, **24**, 2757, (1982)

23 B. Krajewska, M. Lezski and W. Zaborska, *Journal of Chemical Technology and Biotechnology*, **48**, 337, (1990)

24 X. J. Dang, J. Tong and H. L. Li, *Journal of Inclusion Phenomena and Macrocyclic Chemistry*, **24**, 275, (1996)

25 G. Astray, C. Gonzalez-Barreiro, J. C. Mejuto, R. Rial-Otero and J. Simal-Gandara, *Food Hydrocolloids*, **23**, 1631, (2009)

26 J. Szejtli, *Cyclodextrins and Their Inclusion Complexes*, Akademiai Kiado: Budapest, (1982)

27 J. W. Steed and J. L. Atwood, *Supramolecular Chemistry*, J. Wiley and Sons: Chicester: New York, (2000)

28 Z. Gao and H. Li, *Acta Physico-Chimica Sinica*, **15**, 1009, (1999)

29 A.-E. Radi and S. Eissa, *Electroanalysis*, **22**, (24), 2991, (2010)

30 A.-E. Radi and S. Eissa, *The Open Chemical and Biomedical Methods Journal*, **3**, 74, (2010)

31 D. A. Dixon and N. Matsuzawa, *Journal of Physical Chemistry*, **98**, 3967, (1994)

32 C. Harley, PhD, NUI Maynooth, (2009)

33 M. I. Manzanares, V. Solis and R. H. de Rossi, *Journal of Electroanalytical Chemistry*, **407**, 141, (1996)

34 I. V. Terekhova, O. V. Kulikov, R. S. Kumeev, M. Y. Nikiforov and G. A. Al'per, *Russian Journal of Coordination Chemistry*, **31**, 218, (2005)

35 I. V. Terekhova and N. A. Obukhova, *Mendeleev Communications*, **15**, (1), 38, (2005)

36 M. Ramirez-Berriozabal, L. Galicia, S. Gutierrez-Granados, J. S. Cortes and P. Herrasti, *Electroanalysis*, **20**, 1678, (2008)

37 Z. H. Wang, Y. M. Wang and G. Luo, *Analyst*, **127**, 1353, (2002)

38 S. Wu, T. Wang, Z. Gao, H. Xu, B. Zhou and C. Wang, *Biosensors and Bioelectronics*, **23**, 1776, (2008)

39 A. M. El-Kosasy, *Journal of Association of Official Analytical Chemists, International*, **86**, (1), 15, (2003)

40 H. Yao, T. B. Wei, W. X. Xu and Y. M. Zhang, *Guang Pu Xue Yu Guang Pu Fen Xi*, **26**, (9), 1664, (2006)

41 P. Suresh and K. Pitchumani, *Tetrahedron: Asymmetry*, **19**, 2037, (2008)

42 T. N. Kumar, A. Ananthi, J. Mathiyarasu, J. Joseph, K. L. Phani and V. Yegnaraman, *Journal of Electroanalytical Chemistry*, **661**, 303, (2011)

43 H. Tsai and M. Syu, *Biomaterials*, **26**, 2759, (2005)

44 R. Kataky, P. M. Kelly, D. Parker and A. F. Patti, *Journal of the Chemical Society, Perkin Transactions 2*, **19**, 2381, (1994)

Chapter 7

Conclusions

"That's what learning is. You suddenly understand something you understood all your life, but in a new way." - *Doris Lessing*

7.1 General Conclusions

The objective of this thesis was to develop a polypyrrole based sensor for the detection of urea. Although the pyrrole monomer is a known toxin, the corresponding polymer form, polypyrrole (PPy), is a highly biologically compatible polymer matrix[1], which has led to its use in a broad number of biomedical fields including biosensors[2,3], tissue engineering[4,5] and implantable biodevices[6]. Another interesting and prominent property of PPy is its ability to switch its redox behaviour, which has resulted in the design of ion-selective electrodes, electrochromic displays, solar cells, drug delivery systems and actuators. The focus of this thesis, however, was to develop a sensor by incorporating biological molecules within the polypyrrole matrix.

The results obtained in Chapter 3 describe the formation and characterisation of a polypyrrole film with a large protein, bovine serum albumin (BSA), incorporated within the polymer matrix. These PPy-BSA films were fabricated on a platinum electrode, from a solution of pyrrole, BSA and NaCl using a potentiostatic mode of electropolymerisation. In general, an oxidation potential of 0.70 V vs. SCE was applied to the electrode until a fixed charge was reached. The presence of the BSA in the polymer films was confirmed using EDX analysis, while SEM micrographs showed that the films had the cauliflower morphology consistent with that of polypyrrole doped with a simple anion such as chloride.

The kinetics of the electropolymerisation reactions showed that the partial order of the reaction with respect to the monomer concentration, α_1, was found to be 0.99 in the absence of BSA, while a somewhat higher value of 1.38 was obtained for the partial order of the reaction for the monomer concentration, α_2, in the presence of BSA. The partial order close to unity calculated for the growth of the film in the absence of BSA is in good agreement with previous literature values[7]. The higher value of 1.38 computed in the presence of BSA shows that the addition of BSA to the electropolymerisation solution has a significant influence on the rate-determining step, giving a higher dependence on the pyrrole concentration. Furthermore, the value of the partial order of the reaction with respect to the BSA concentration was found to be negative, indicating a complex electropolymerisation process whereby the BSA inhibits the electropolymerisation process and decreases the rate of

electropolymerisation. The optimum growth parameters for the PPy-BSA polymer film were determined; these were then used as a basis for incorporating the urease enzyme into the polypyrrole matrix for the detection of urea.

In Chapter 4, the PPy-Urs films were fabricated on a platinum electrode, from a solution of pyrrole, urease and sulphonated-β-cyclodextrin (SCD) using a potentiostatic mode of electropolymerisation. In general, an oxidation potential of 0.70 V vs. SCE was applied to the electrode until a fixed charge was reached. The presence of the SCD and urease in the polymer films was confirmed using EDX measurements. The presence of sulphur in the EDX spectra proves that the SCD was indeed incorporated into the polymer films, while the presence of nickel in the EDX spectra confirms the incorporation of the urease enzyme. Additionally, the urease-containing polymer films had a very fibrous morphology compared to the films formed in the absence of urease.

The PPy-Urs-Cl film exhibited reasonable sensitivity towards urea, however, the limit of detection was found to be poor in comparison to other techniques such as chromatography, which yields LODs in the region of 5.0×10^{-8} mol dm^{-3} for urea. Consequently, the PPy-Urs-SCD film and the PPy-SCD film, as a comparison, were formed and used in the detection of urea. The PPy-Urs-SCD film displayed excellent sensitivity of 46.09 μC μM^{-1} towards urea and detection in the region of 1.0×10^{-10} mol dm^{-3}, whereas the PPy-SCD film had a sensitivity of 18.04 μC μM^{-1} towards urea and detection in the region of 1.0×10^{-10} mol dm^{-3} also. At the higher urea concentrations, the PPy-Urs-SCD film was found to have superior sensitivity towards urea compared to the other films investigated.

Chapter 5 discusses how the presence of the SCD also aids in eliminating or reducing the effects of interfering compounds as SCD contains between 7 and 11 negatively charged sulphonated groups. The PPy-Urs-SCD polymer film was successful in repelling the common interfering compound, ascorbic acid (AA), during the detection of urea, and is capable of detecting only urea in the presence of relatively high concentrations of AA, up to 1.0×10^{-4} mol dm^{-3}. This is attributed to the fact that AA is also negatively charged at the pH of the experiments, pH 7.0. The PPy-Urs-SCD film also successfully detects urea in the presence of 1.0×10^{-4} mol dm^{-3} NH_4Cl, without any interference or surface fouling. However, the urease in the

PPy-Urs-SCD film is a large, fibrous enzyme, while, the SCD is also large, which gives rise to a porous polymer network. Thus, interference was observed with the other interfering compounds, giving rise to an increase in the oxidation charge. This is somewhat unusual as most interfering compounds tend to foul and block the surface of the electrode[8] and thus diminish the electrochemical signal from the target analyte. This increase in charge was explained in terms of diffusion of the interfering species through the porous polymer film to the electrode surface and oxidation of the species at this surface.

The excellent sensing ability of the PPy-SCD film compared to the PPy-Urs-Cl film was attributed to the fact that a 1:1 host-guest complex is formed between the SCD and the urea. This was confirmed using cyclic voltammetry in Chapter 6, whereby a decrease in the oxidation current was observed with increasing SCD concentrations. This is a common feature of inclusion complexes; the urea becomes more difficult to oxidise when inside the SCD cavity and thus a decrease in the diffusion coefficient is observed in the presence of SCD. Indeed, the diffusion coefficients for urea were found to be 2.72×10^{-6} cm^2 s^{-1} and 6.30×10^{-7} cm^2 s^{-1} in the absence and presence of SCD, respectively. In addition, Job's plot analysis confirmed the formation of a 1:1 inclusion complex between urea and SCD, with a maximum of the curve obtained at 0.5 and a formation constant of 2745.27 ± 299.56 mol^{-1} dm^3.

7.2 Future Work/Potential Applications

There are a number of potential applications that this urea sensor could be used for; however, the most promising application would be in the area of dialysis. Currently, there are over 400 people in Ireland successfully receiving dialysis treatment and over half of these must attend major city hospitals to receive haemodialysis. The remainder filter their blood at home through the use of peritoneal dialysis. Depending on the severity of the renal failure, patients receive dialysis between three times per week to daily, with each session lasting a number of hours or potentially overnight. Presently, the time frame for a dialysis session is based on the weight, height and gender of the patient, rather than an accurate measurement of the concentration of urea and toxins that are removed from the body.

The urea sensor described in this thesis is quite sensitive to urea concentrations over a wide concentration range, including much lower levels than typically found in biological systems and higher concentrations which correspond to elevated urea levels, typically found in patients suffering from renal disease and undergoing dialysis.

Although the urea sensor described has not been tested in blood or serum; if it was to be applied to the area of dialysis, the solution of dialysate is free from proteins or large biomolecules which would tend to foul the sensor. In addition, it is possible to enhance the sensitivity of the urea sensor in the higher concentration regions by dampening the sensitivity at the lower urea concentrations. This could be done in a number of ways but typically, using more compact/thicker films or applying a semi-porous membrane to the sensor to decrease the rate of diffusion, would be advised. Additionally, the PPy-SCD sensor in the absence of urease has excellent sensitivity towards urea, which leads to the possibility of an enzyme-free biosensor which would be less expensive to form, readily available and not prone to enzyme leaching which diminishes the sensitivity of a biosensor.

The pH at which the urea experiments were carried out was at pH 7.0, which is close to biological pH. In addition, the interference from the main biological interfering compounds, ascorbic acid and uric acid, which are anionic at pH 7.0 and above, can be eliminated by applying a compact layer of PPy-Urs-Cl followed by a thicker layer of the negatively charged SCD-containing film, which repels the anionic interfering compounds.

7.3 Conference Presentations

- Anita Hamilton and Carmel Breslin, "The formation of a novel urea sensor using polypyrrole as a conducting matrix", 63rd Chemistry colloquium, University College Dublin, Ireland, 24th 06th 2011 [Oral presentation]

- Anita Hamilton and Carmel Breslin, "The development of a novel urea sensor using polypyrrole as a conducting matrix" 3rd Eirelec Conference, Adare, Co. Limerick, Ireland, 16th 05th 2011 [Poster presentation]

- Anita Hamilton and Carmel Breslin, "Entrapment of biological entities into a conducting polymer matrix" 61st ISE Conference, Nice, France, 27th 09th 2010 [Poster presentation]

- Anita Hamilton and Carmel Breslin, "The fabrication of a novel biosensor that can detect amino acids in vitro" 216th ECS Conference, Vienna, Austria, 05th 10th 2009 [Poster presentation]

- Anita Hamilton and Carmel Breslin, "Creating a unique biosensor using polypyrrole as a binding matrix" Intel European Research and Innovation Conference, Intel, Leixlip, Co. Kildare, Ireland, 08th 09th 2009 [Poster presentation]

- Anita Hamilton and Carmel Breslin, "The formation and characterisation of polypyrrole with bovine serum albumin immobilised onto its surface" Electroanalytical Chemistry DRHEA Module, NUI Maynooth, Maynooth, Co. Kildare, Ireland, 16th 06th 2009 [Poster presentation]

7.4 Papers in Preparation/Submitted

- The incorporation of biological entities into conducting polymers in one simple step.

- A novel urea sensor using polypyrrole as a conducting matrix.

- The influence of the dopant anion of the sensitivity of urea sensors.

- Complexation studies of urea and sulphonated-β-cyclodextrin using electrochemical techniques.

7.5 References

1 S. Geetha, C. R. K. Rao, M. Vijayan and D. C. Trivedi, *Analytica Chimica Acta*, **568**, 119, (2006)

2 J. Wang and M. Musameh, *Analytica Chimica Acta*, **539**, 209, (2005)

3 K. Ghanbari, S. Z. Bathaie and M. F. Mousavi, *Biosensors and Bioelectronics*, **23**, 1825, (2008)

4 J. H. Collier, J. P. Camp, T. W. Hudson and C. E. Schmidt, *Journal of Biomedical Materials Research*, **50**, 574, (2000)

5 M. Martina and D. W. Hutmacher, *Polymer International*, **56**, 145, (2007)

6 P. M. George, A. W. Lyckman, D. A. LaVan, A. Hegde, Y. Leung, R. Avasare, C. Testa, P. M. Alexander, R. Langer and M. Sur, *Biomaterials*, **26**, 3511, (2005)

7 J. O. Iroh and G. A. Wood, *European Polymer Journal*, **33**, 107, (1997)

8 R. Gifford, J. J. Kehoe, S. L. Barnes, B. A. Kornilayev, M. A. Alterman and G. S. Wilson, *Biomaterials*, **27**, 2587-2598, (2006)

“I wanted a perfect ending. Now I've learned, the hard way, that some poems don't rhyme, and some stories don't have a clear beginning, middle, and end. Life is about not knowing, having to change, taking the moment and making the best of it, without knowing what's going to happen next. Delicious Ambiguity.” - *Gilda Radner*